Dipl.-Ing. Christoph AUGUSTIN

Classical and All-floating FETI Methods with Applications to Biomechanical Models

DISSERTATION

zur Erlangung des akademischen Grades eines Doktors der technischen Wissenschaften

Doktoratsstudium der Technischen Wissenschaften im Rahmen der Doktoratsschule "Mathematik und Wissenschaftliches Rechnen"

Technische Universität Graz

Betreuer:
Univ.-Prof. Dr. Olaf STEINBACH

Mitberichter:
Univ.-Prof. Dr. Gerhard A. HOLZAPFEL
Univ.-Prof. Dr. Arnd MEYER

Institut für Numerische Mathematik

Graz, im Juni 2012

Eidesstattliche Erklärung

Ich erkläre an Eides statt, dass ich die vorliegende Arbeit selbständig verfasst, andere als die angegebenen Quellen/Hilfsmittel nicht benutzt, und die den benutzten Quellen wörtlich und inhaltlich entnommenen Stellen als solche kenntlich gemacht habe.

Graz, am ....

(Unterschrift)

Abstract

This thesis deals with domain decomposition solvers, more precisely the finite element tearing and interconnecting (FETI) approach, to simulate the elastic behavior of cardiovascular tissues, such as the myocardium or the artery. These biological materials are characterized by anisotropic and nonlinear material properties due to preferential orientations of collagen and muscle fibers in the tissue. The high complexity of the underlying nonlinear equations as well as the fine mesh structures of the cardiovascular components demand fast solving algorithms, where one possibility is the mentioned FETI method. This approach shows high performance and enables a natural parallelization to solve the nonlinear elasticity problem.

The strategy of the FETI method is to decompose the computational domain into a finite number of non-overlapping subdomains. Therein the corresponding local problems can be handled efficiently by direct solvers. The reduced global system, that is related to discrete Lagrange multipliers on the interface of the subdomains, is then solved with a parallel Krylov space method to deduce the desired solution, in the case of elasticity the displacement. For the global Krylov space method we need suitable preconditioning. In this thesis we consider the simple lumped preconditioner, the optimal Dirichlet preconditioner and, in addition to that, a in this kind of applications new BEM based preconditioner, formed by local hypersingular boundary integral operators. This type of preconditioning works, since the hypersingular operator approximates the Steklov–Poincaré operator, which is the basis for the optimal Dirichlet preconditioning. A variant of the classical FETI method is all-floating FETI where, in contrast to the classical approach, the Dirichlet boundary acts as a part of the interface. The in this application to nonlinear and orthotropic biological materials for the first time used all-floating FETI approach shows advantages in the implementation and in most times improves the convergence of the global iterative method for the considered problems.

Finally, we include numerical examples where we compare the classical and the all-floating FETI approach and the different preconditioning techniques.

Zusammenfassung

Die vorliegende Arbeit beschäftigt sich mit Gebietszerlegungsmethoden, genauer gesagt mit der „finite element tearing and interconnecting“– Methode (FETI), zur Simulation des elastischen Verhaltens von kardiovaskulärem Gewebe. Beispiele hierfür sind der Herzmuskel oder die Arterie. Diese biologischen Materialien zeichnen sich durch anisotrope und nichtlineare Materialeigenschaften aus, die durch eine bevorzugte Orientierung von Kollagen- und Muskelfasern im Gewebe verursacht werden. Die dadurch entstehende hohe Komplexität der zugrunde liegenden nichtlinearen Gleichungen, sowie die feinen Strukturen der Herz–Kreislauf–Komponenten erfordern schnelle und effiziente Lösungsalgorithmen. Eine Möglichkeit hierfür ist die oben genannte FETI–Methode. Dieser Ansatz ermöglicht eine natürliche Parallelisierung des nichtlinearen Elastizitätsproblems, wobei der Kommunikationsaufwand zwischen den einzelnen Prozessen relativ gering gehalten wird.

Die Grundidee der FETI–Methode ist es, das Rechengebiet in eine endliche Anzahl von nicht-überlappenden Teilgebieten zu zerlegen. In diesen Teilgebieten können die kleineren lokalen Probleme effizient durch direkte Löser behandelt werden. Die globale Lösung, im Falle der Elastizität die globale Verschiebung, wird durch ein reduziertes globales System, das mit einem parallelen Krylovraum–Verfahren gelöst wird, rekonstruiert. Für das globale Krylovraum–Verfahren werden geeignete Vorkonditionierungsstrategien benötigt. In dieser Arbeit betrachten wir in diesem Zusammenhang den einfachen „lumped“–Vorkonditionierer, den optimalen Dirichlet–Vorkonditionierer und einen, in dieser Anwendung neuen, auf Randelementverfahren basierenden BEM–Vorkonditionierer. Dieser wird mit dem aus Randelementverfahren bekannten hypersingulären Integraloperator gebildet. Diese Art der Vorkonditionierung funktioniert aufgrund der Spektraläquivalenz der lokalen hypersingulären Operatoren mit den lokalen Steklov–Poincaré–Operatoren. Diese bilden die Grundlage für den optimalen Dirichlet–Vorkonditionierer.

Eine Variante des klassischen FETI-Ansatzes ist „Allfloating“–FETI, wo im Gegensatz zur klassischen Formulierung der Dirichlet–Rand als Teil des Koppelrandes betrachtet wird. Das in der Simulation von nichtlinearen orthotropen biologischen Materialien erstmals angewendete „Allfloating“–FETI Verfahren vereinfacht die Implementierung und verbessert in vielen Fällen die Konvergenz der globalen iterativen Methode.

Schließlich betrachten wir numerische Beispiele, wo wir die klassische Formulierung mit dem „Allfloating“–Ansatz und die verschiedenen Vorkonditionierungstechniken vergleichen.

Preface

In this thesis I present results that where obtained within my research at the Institute of Computational Mathematics at the Graz University of Technology. I gratefully acknowledge the support by the Austrian Science Fund (FWF) within the SFB Mathematical Optimization and Applications in Biomedical Sciences.

First and foremost, I would like to thank my supervisor Olaf Steinbach for his encouragement, support, guidance and patience throughout the creation of this thesis. At the same time my gratitude goes to Gerhard Holzapfel and Arnd Meyer for assisting me in my research and for co-refereeing this thesis.

I am deeply indebted to Clemens Pechstein and Günther Of without whom my work and especially the numerical experiments would have been a considerably more daunting task.

Special thanks go to Gernot Plank for showing so much interest in my results and the possibility to continue my research in his group.

Additionally, I would like to thank the TU Wien and the TU Graz for the permission to use the high end cluster VSC2 for many of my numerical experiments.

Maybe my thesis would not have come to an end, but for sure it would have been a much more dreary undertaking, without the fruitful discussions, the coffee breaks and the support by my colleagues and friends Günther Of, Lorenz John, Martin Neumüller, Arno Kimeswenger, Elias Karabelas, Markus Windisch, Sarah Engleder, Peter Urthaler, Barbara Pöltl and Gerhard Unger.

For keeping me busy in my spare time and hence for distracting me in times when this thesis bothered me, I want to thank all my friends.

Last but no least, I would like to express my sincere thanks to my family, my parents for their love and support through all the years, my grandparents for their unwavering confidence in me, Peter for being a supportive brother as well as a pleasant flatmate and my girlfriend Anita for her love and understanding and for being just the way she is.

Thank you all!

Graz, June 2012 Christoph Augustin

Contents

1. Introduction

Motivation

According to a very recent report, published by the World Health Organization (WHO) in 2011, cardiovascular diseases, such as atherosclerosis or heart diseases, "are the leading causes of death and disability in the world" [99]. Hence the understanding of the underlying pathological processes is a very important topic in many different fields of science.

In the areas of applied mathematics the interest lies, e.g., in the simulation of electrochemical processes in the heart, in the modeling of the blood flow through the human body, resulting in fluid structure interaction problems, and many others. In this thesis we investigate the mechanical behavior of the organs involved in the cardiovascular system, such as arteries or the myocardium of the heart. This is of interest since in silico simulations of arterial tissues which are exposed to boundary forces, may help to improve surgical methods such as angioplasty or artery stenting. The elastomechanical modeling of the myocardium and especially the modeling of the coupling of the mechanics with electrochemical processes in the heart is still in its infancy. Nonetheless, work in this field will give the possibility to study cardiac diseases without open surgery and maybe comprehend activities in the heart that are not yet understood.

Partial Differential Equations and Finite Element Methods

The basis for the numerical simulation of biological tissues are partial differential equations (PDE) that appear throughout in the modeling of the physics of natural processes. In this work, where we regard tissues as elastic materials, we are concerned with the stationary equilibrium equations

$$\operatorname{div} \sigma(\boldsymbol{u}, \boldsymbol{x}) + \boldsymbol{f}(\boldsymbol{x}) = \boldsymbol{0} \quad \text{for } \boldsymbol{x} \in \Omega,$$

with the stress tensor σ that depends on the unknown displacement field $\boldsymbol{u}$, the source term $\boldsymbol{f}$ and the computational domain $\Omega \subset \mathbb{R}^3$. In order to formulate boundary conditions, the boundary $\Gamma = \partial\Omega$ is decomposed into disjoint parts so that $\Gamma = \overline{\Gamma}_D \cup \overline{\Gamma}_N$. To embed forces that act on the boundary of the domain, like tension, traction or pressure, we formulate Neumann boundary conditions $\sigma(\boldsymbol{u}, \boldsymbol{x})\boldsymbol{n}(\boldsymbol{x}) = \boldsymbol{g}_N(\boldsymbol{x})$ on Γ_N, where $\boldsymbol{n}(\boldsymbol{x})$ is the exterior normal vector. Dirichlet boundary conditions $\boldsymbol{u}(\boldsymbol{x}) = \boldsymbol{g}_D(\boldsymbol{x})$ on Γ_D correspond to a prescribed displacement field, that is enforced component-by-component.

The modeling of different elastic materials is realized by using a so-called strain energy function Ψ included in a constitutive equation for the stress tensor

$$\sigma = \det(\mathsf{F})^{-1}\mathsf{F}\frac{\partial\Psi(\mathsf{C})}{\partial\mathsf{C}}\mathsf{F}^{\top},$$

where F is the deformation gradient and $\mathsf{C} = \mathsf{F}^{\top}\mathsf{F}$ is the right Cauchy-Green tensor. For a comprehensive overview and mathematical theory on elastic deformations, compare [25, Ciarlet (1988)], [112, Ogden (1997)] and [59, Holzapfel (2000)] for example. A well established model for arterial tissues is discussed in [63, Gasser, Holzapfel and Ogden (2000)]. An adequate model for the myocardium can be found in a recent publication of Holzapfel and Ogden [65].

In almost every practical application, an analytical solution of the PDE is not possible. Hence we use the finite element method (FEM) as a powerful numerical tool to find an approximate solution of the equilibrium equations. The analytical framework for the finite element method is discussed in an overwhelming amount of books including the classic works [24, Ciarlet (1978)], [159, Zienkiewicz (1971)] and more recent [17, Brenner and Scott (1994)] and [14, Braess, 2007]. In addition, for explanations on the solvability of the governing equations, especially for linear and nonlinear elasticity see [25, Ciarlet (1988)] and [29, Dacorogna (2008)].

Due to preferential orientations of fibers such as collagen, the modeling of biological tissues leads to an anisotropic and highly nonlinear material model. In order to apply the finite element method to this problem we use Newton's method and a linearized form of the variational problem. For a detailed elaboration of the linearization for nonlinear elastic models cf. [60, Holzapfel (2003)].

Domain Decomposition Methods

The fine mesh structure to model cardiovascular organs normally yields a very large number of degrees of freedom. The combination with the high complexity of the underlying partial differential equations demand fast solving algorithms and, conforming to up-to-date computer hardware architectures, parallel methods. One possibility to achieve these specifications are domain decomposition (DD) methods. The first reference to these numerical techniques was the alternating Schwarz method, already mentioned in the early work [136, Schwarz (1870)]. In the last three decades several overlapping as well as non-overlapping DD methods were developed. They all work according to the same principle: the domain Ω is subdivided into a set of (overlapping or non-overlapping) subdomains Ω_i. DD algorithms now decompose the large global problem into a set of smaller local problems on the subdomains. This yields a natural parallelization of the underlying problem. In addition to well established standard DD methods,

other examples for more advanced domain decomposition methods are hybrid methods [146, Steinbach (2003)], mortar methods [95, Maday et al. (1989)], [155, Wohlmuth (2000)], [13, Bernardi et al. (1994)] and tearing and interconnecting methods, i.e. the FETI method [41, Farhat and Roux (1991)] for the finite element approach and the BETI method [91, Langer and Steinbach (2003)] for boundary elements. Commendable compendia on domain decomposition methods are [117, Quarteroni and Valli (1999)] and [148, Toselli and Widlund (2005)].

In this thesis we will focus on the FETI method. A modification of the classical finite element tearing and interconnecting approach, the dual-primal FETI (FETI–DP) method, cf., e.g., [39, Farhat et al. (2001)] and [85, Klawonn and Widlund (2001)], was already applied to model arterial tissues, see [84, Klawonn and Rheinbach (2010)], [118, Rheinbach (2009)] and references therein. In contrast to this we use another variant, the all-floating tearing and interconnecting method (AF–FETI), introduced independently for the boundary element method in [109,110, Of (2006, 2008)], [111, Of and Steinbach (2009)] and as the Total–FETI (TFETI) method for finite elements in [37, Dostál et al. (2006)]. For a mathematical analysis of FETI methods, including convergence proofs for the classical one-level FETI method we refer to [96, Mandel and Tezaur (1996)] and [85,86, Widlund and Klawonn (2000,2001)].

The underlying principle of all FETI methods is a non-overlapping domain decomposition

$$\overline{\Omega} = \bigcup_{i=1}^{p} \overline{\Omega}_i \quad \text{with } \Omega_i \cap \Omega_j = \emptyset \quad \text{for } i \neq j, \quad \Gamma_i = \partial\Omega_i.$$

The local interfaces are given by $\Gamma_{ij} := \Gamma_i \cap \Gamma_j$. The global coupling boundary Γ_C is the union of all these local interfaces. Instead of the global problem, in our case the equilibrium equations, we now consider local subproblems to find the local restrictions $\boldsymbol{u}_i = \boldsymbol{u}_{|\Omega_i}$ satisfying partial differential equations

$$\operatorname{div}(\sigma(\boldsymbol{u}_i, \boldsymbol{x})) + \boldsymbol{f}(\boldsymbol{x}) = \boldsymbol{0} \quad \text{for } \boldsymbol{x} \in \Omega_i,$$

the Dirichlet and Neumann boundary conditions

$$\boldsymbol{u}_i = \boldsymbol{u}_D \text{ on } \Gamma_D \cap \Gamma_i, \quad \sigma(\boldsymbol{u}_i)\,\boldsymbol{n}_i = \boldsymbol{g}_N \text{ on } \Gamma_N \cap \Gamma_i,$$

and the transmission conditions

$$\boldsymbol{u}_i = \boldsymbol{u}_j, \quad \boldsymbol{t}_i + \boldsymbol{t}_j = \boldsymbol{0} \quad \text{on } \Gamma_{ij}.$$

Here $\boldsymbol{t}_i = \sigma(\boldsymbol{u}_i)\boldsymbol{n}_i$ is the local boundary stress and $\boldsymbol{n}_i$ is the exterior normal vector of the local subdomain boundary $\Gamma_i = \partial\Omega_i$. The FETI approach now leads to a reduced global system of equations that is related to discrete Lagrange multipliers on the coupling boundary Γ_C. This global system is then solved with a parallel Krylov space method with suitable preconditioning. A computationally efficient form of preconditioning, the lumped preconditioner, was already discussed in [41, Farhat and Roux (1991)]. A few

years later an optimal, so-called Dirichlet preconditioner was introduced [40, Farhat, Mandel and Roux (1994)]. In addition to that, we use a BEM based preconditioner, formed by local hypersingular boundary integral operators. This type of preconditioner works, since the hypersingular operator approximates the Steklov–Poincaré operator, which is the basis for the optimal Dirichlet preconditioning. Especially for large subdomains the application of the hypersingular operator should outperform the usage of the Steklov–Poincaré operator, since there we have the building of an inverse matrix involved. On the other hand, given the approximation properties of the hypersingular operator, the BEM preconditioner yields better condition numbers than the computationally efficient lumped preconditioner. For a comprehensive introduction to boundary integral equation methods see [98, McLean (2000)], [70, Hsiao and Wendland (2008)] and [147, Steinbach (2008)].

An essential part of FETI methods is solving the local subproblems. Challenges occur with so-called *floating subdomains* which have no contribution to the Dirichlet boundary. These cases correspond to local Neumann problems and are – in the case of elasticity – only unique up to the rigid body modes. One possibility to overcome this trouble is the before mentioned FETI-DP method. In this variant some specific degrees of freedom (DOF), called primal DOF, are fixed. This yields solvable systems for all subdomains. Choosing the primal DOF may be very sophisticated. For linear elasticity this issue is discussed in [83, 88, Klawonn and Widlund (2005,2006)]. The classical FETI method, as well as all-floating FETI, needs the construction of a Moore-Penrose pseudoinverse. This may be achieved using direct solvers with a sparsity preserving stabilization or stabilized iterative methods.

In contrast to the standard approach, using all-floating FETI, the Dirichlet boundary acts as a part of the coupling boundary. Dirichlet boundary conditions are incorporated by using discrete Lagrange multipliers. AF–FETI shows advantages in the implementation and, as we will see in the numerical examples, may improve the convergence of the global iterative method.

Outline of Contents

Subsequent to this introduction, we give a short overview on the histology of biological materials in the second chapter. Furthermore, the mechanical properties of arteries as well as the myocardium are discussed. Worth mentioning in this context are the layered structure and the composition of elastin and reinforced collagen and muscle fibers. Due to this we may treat biological tissues as anisotropic elastic materials. This complex structure will lead to a highly nonlinear material model. Another important issue is that we are concerned with almost incompressible materials.

The third chapter starts with a general introduction to continuum mechanics. We ex-

plain two important settings, the reference and the current configuration, and show transformations from one to the other. The major tensors, needed for the material models, are introduced. Amongst others we have the deformation gradient and the right and the left Cauchy–Green deformation tensor. We introduce the theory of stress including the fundamental *Cauchy stress theorem*. Using this, we set up the main equations which result in partial differential equations for quasi-stationary elasticity problems. Subsequently, we discuss specific elastic models ranging from linear elasticity to general nonlinear elasticity models. The latter requires the introduction of a so-called strain energy function, which enables us to construct constitutive equations for nonlinear elasticity models. To conclude this chapter we outline in detail the construction of material models for the artery and the myocardium. We show the specific representation of the energy function and, using this functional, calculate the tensors needed for the implementation of the numerical methods.

In the forth chapter we present the variational formulation for the elasticity problems as considered in this thesis. This formulation is the basis for the finite element approach which is discussed in detail in chapter five. Nonlinear problems demand the use of a linearization technique, in our case we use the well-known *Newton method* in Banach spaces. We discuss the basic ideas of this approach for the particular case of nonlinear elasticity and outline the main steps that lead to a linearized version of the variational formulation. Incompressible and nearly incompressible elastic materials may cause some numerical problems, so-called locking effects, which must be taken into account. We show possibilities to overcome this problem for linear and nonlinear elastic problems. For nonlinear elasticity we use the so-called *mean dilatation technique* which is based on a decoupled formulation of the weak form. Furthermore, we discuss existence theorems of the equilibrium problem. We show unique solvability of linear elasticity problems using *Korn's inequalities*. To show that nonlinear elasticity problems have at least one solution we introduce a variety of convexity concepts. In the following we outline existence theorems for general nonlinear elasticity problems, which include the artery and the myocardium model. In contrast to linear elasticity we are not able to show uniqueness of a solution in the general case.

Subsequently, we treat the discretization of the variational formulation in the fifth chapter. We outline the main ideas of the *finite element method* which will be used to find an approximate solution of the classical boundary value problem. Since the numerical solution of nonlinear operator equations involves function and derivative approximations we have to apply *inexact Newton methods*. We give a short overview on the convergence analysis of this linearization procedure and to the assembling of the involved stiffness matrices. Moreover, we discuss different types of solvers for the system of linear equations, that arises from the finite element method. Some direct solver packages are presented and we outline the main iterative methods, including the conjugate gradient (CG) and the generalized minimal residual (GMRES) method. At last, we give a short overview to time stepping schemes.

The sixth chapter comprises a general introduction to domain decomposition methods. We start with a short historical review and present the basic concepts that are suitable for all DD methods. Subsequently, we concentrate on the finite element tearing and interconnecting approach. The main steps from the general finite element to the FETI formulation are given. This results in a split-up of the global problem in particular local problems, which may be solved in parallel, and a global parallel iterative method. We present diverse preconditioning techniques for this global iterative method, including the well known Dirichlet and lumped preconditioners as well as a new BEM-based preconditioner using the hypersingular boundary integral operator. We also present a modification of classical FETI, the all-floating FETI approach. We conclude this chapter with an overview on the implementation, including the construction of the main operators and the pseudo-inverse matrices.

In the seventh chapter we present some numerical examples to all described methods. First we test the FETI implementation for linear elasticity problems. There we are able to compare the computed results to a given exact solution, which enables us to show the correctness of our implementation. We compare the different preconditioning techniques and present differences between the classical FETI and the all-floating FETI approach. Following to this we do the same for nonlinear elasticity models, i.e. the anisotropic artery and myocardium model. At the end we present examples with realistic geometries. Here we apply the anisotropic artery model to a tube consisting of two layers and the orthotropic myocardium model to the myocardium of a rabbit heart.

We conclude in the last chapter with a short overview and an outlook to upcoming perspectives and open questions.

2. Histology of Biological Materials

In this chapter we give a general introduction to the histology and the mechanical properties of biological tissues. We take a closer look on arteries and the cardiac muscle (myocardium) as representatives for this huge class of elastic materials. For more informations on the histology and these tissues confer, e.g., [72, 73, Humphrey (1995,1999)] for arteries and [93, 94, Le Grice et al. (1995,1997)], [158, Young et al. (1998)] and [129, Sands et al. (2005)] for the heart.

2.1. Histology of Arteries

Arteries are vessels that transport blood from the heart to the organs. In vivo the artery is a prestretched elastic material under an internal pressure load. In this work we concentrate on the in vitro passive behavior of healthy arteries. Hence in vivo effects such as the vasa vasorum[1] etc. are neglected. In general, arteries are subdivided into two types: *elastic* and *muscular* arteries. The elastic ones have large diameters and are located close to the heart (proximal arteries). One example for an artery with elastic behavior would be the aorta. In contrast the muscular vessels are located within the periphery of the body (distral arteries). Here an example would be the small cerebral arteries in the brain. These arteries show a pronounced viscoelastic behavior with hysteresis. However, some arteries exhibit morphological structures of both types.

Healthy arterial walls consist of three primary layers: the intima, the media and the adventitia. For a diagrammatic model of the major components of a healthy elastic artery see Fig. 2.1.

The *intima* is the innermost layer of the artery. It consists solely of a single layer of endothelial cells which serve as an interface between elastic material and blood.

The middle layer of an artery is called *media*. In contrast to the intima it is a complex 3D network of muscle cells, elastin and collagen fibers. The media shows a high ability to resist loads in both the longitudinal and circumferential direction. In healthy arteries it is the most significant layer from the mechanical perspective, cf. [63, Holzapfel et al. (2000)].

At last the outermost layer of an artery is the so-called *adventitia*. It consists of

[1] network of small blood vessels that supply the outer tissues of larger ones (e.g. the aorta).

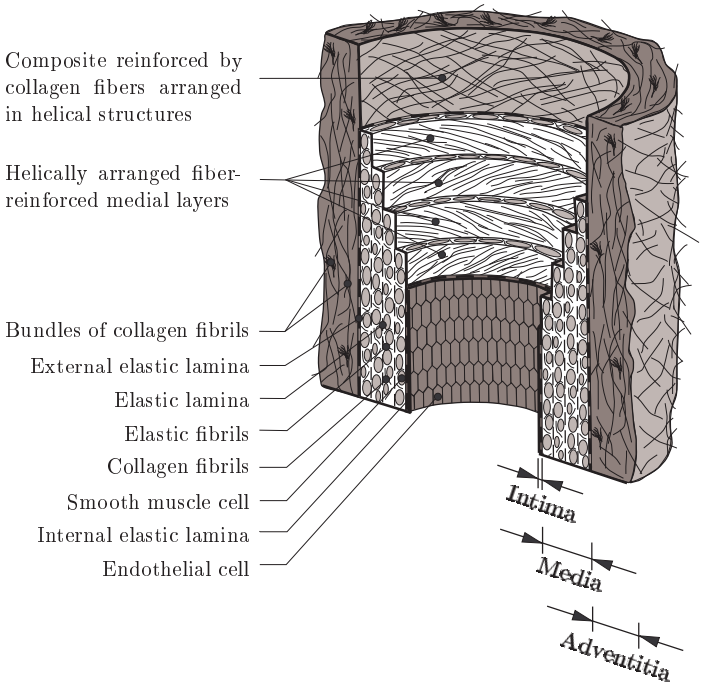

Figure 2.1. – Diagrammatic model of the major components of a healthy elastic artery, from [63, Holzapfel et al. (2000)].

histological ground substance and thick bundles of collagen fibers. At higher levels of pressure the adventitia behaves like a stiff 'jacket-like' tube, [135, Schulze-Bauer et al. (2002)].

2.2. Typical Mechanical Behavior of Arterial Walls

As mentioned before, proximal arteries behave like an elastic material, while distral arteries behave like an viscoelastic or pseudo-elastic material. Healthy arteries are highly deformable composite structures and show a non-linear stress-strain response with a typical stiffening effect at higher pressures. Reasons for this are the embedded collagen fibers which lead to an *anisotropic* mechanical behavior of arterial walls, see Fig. 2.2.

An important observation is that arteries do not change their volume within the physiological range of deformation [63, Holzapfel et al. (2000)]. Thus they are treated as a nearly incompressible material. Other properties are certain in vivo prestretches in longitudinal direction. That means that a segment of a vessel shortens on removal from the body. In circumferential direction a load-free arterial ring contains residual stresses.

So it will spring open when one cuts it in a radial direction. More information on the histology of arterial walls can be found in [72,73, Humphrey (1995,1999)], [63, Holzapfel et al. (2000)], [62, Holzapfel (2008)] or [127, Rhodin (1980)]. Nice illustrations of the prestretches and residual stresses one can find in [68, Holzapfel et al. (2007)], the modeling of such a problem is discussed in [67, Holzapfel et al. (2010)] and [20, Bustamente et al.].

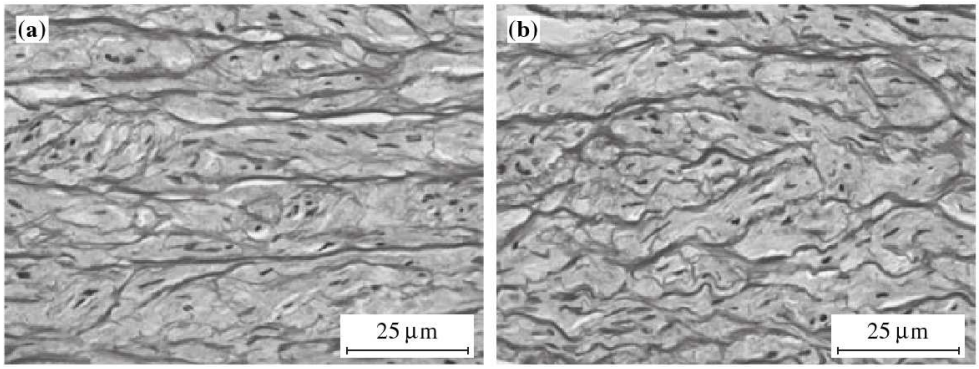

Figure 2.2. – Histological images of collagen in the media of an human aorta: (a) stretched and (b) unstretched sample, from [62, Holzapfel 2008].

2.3. Histology of the Human Heart

The heart consists of four chambers, the right and the left atria and the right and the left ventricle. Here the ventricles serve to pump blood around the body while the atria receive the blood again. The heart wall thickness varies a lot over these different parts and as well through the cardiac cycles.

Like the arterial wall the heart wall consists of different layers. The inner layer is called the *endocardium*, which serves as an interface between elastic media and blood. The *epicardium*, the outermost layer, serves as a protective membrane. Like the endocardium it is just a thin layer with an approximate wall thickness of $100\mu m$, [65, Holzapfel and Ogden (2009)].

The middle layer, the *myocardium* is the cardiac muscle. As we will use the proposed model of [65, Holzapfel and Ogden (2009)], we focus the attention on the myocardium of the left ventricle. The cardiac muscle consists of myocardiocyteal muscle cells and it is the most significant part for the modeling of the elastic behavior of the heart wall. The cardiac myocytes[2] are arranged in parallel in different sheets within the myocardium. Although this is the predominant fiber type in that layer, we have also collagen that

[2] in this context muscle fibers

is arranged in a spatial network that connects the muscle fibers. Characteristic for the myocytes is a layered organization of the fibers which can be described by a right-handed orthonormal set of basis vectors (cf. Fig. 2.3). This set consists of a vector field $\boldsymbol{f}_0$ that coincides with the main direction of the muscle fibers. In the literature it is referred to as the *fiber axis*. The second basis vector is the so-called *sheet axis* $\boldsymbol{s}_0$ which is defined to be perpendicular to $\boldsymbol{f}_0$ in the plane of the layer. This direction coincides with the collagen fiber orientation (cf. Fig. 3.4). The orthonormal set is completed by the *sheet-normal axis* $\boldsymbol{n}_0$.

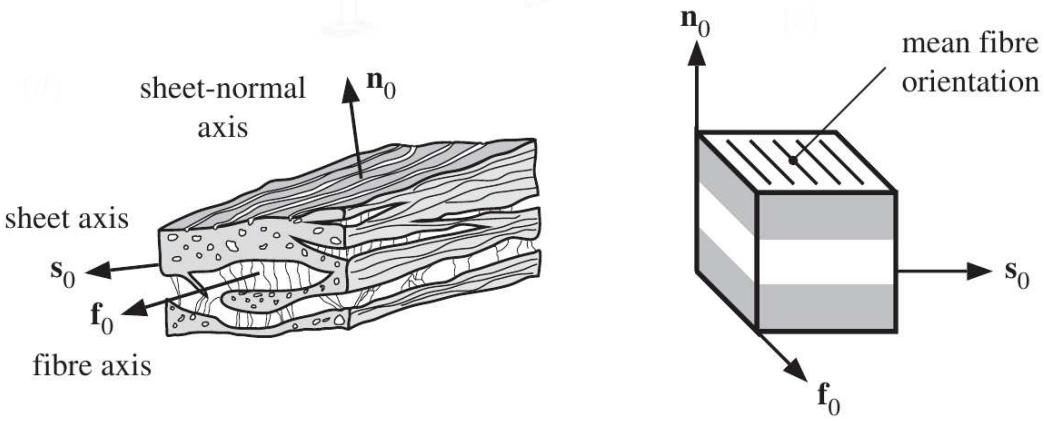

Figure 2.3. – to the left: indication of the layered organization of the muscle fibers in the myocardium with a right-handed orthonormal coordinate system where $\boldsymbol{f}_0$ is the fiber axis, $\boldsymbol{s}_0$ is the sheet axis and $\boldsymbol{n}_0$ is the sheet-normal axis; to the right: a schematic cube of the layered tissue which serves as a basis for the constitutive model, from [65, Holzapfel and Ogden (2009)].

2.4. Mechanical Behavior of Heart Walls

As arterial walls and many other biological tissues we can treat the myocardium as an incompressible material [153, Vossoughi et al. (1980)]. It shows a highly nonlinear and, due to the myocytes, an anisotropic behavior. The characteristic property of the myocardium, that the muscle fibers have a layered organization with an orthogonal basis, was shown in experiments by [36, Dokos et al. (2002)]. They also did shear tests on a cube of myocardial specimen in the direction of the three different orthogonal planes. From these experiments it was observed that the ventricular myocardium is most resistant to shear deformations in the plane built by the vector fields $\boldsymbol{f}_0$ and $\boldsymbol{s}_0$ (fs-plane). High resistance was also shown in the fn-plane. In all other directions the resistance to simple shear deformations was considerably smaller. More details concerning the mechanics of the myocardium can be found in [65, Holzapfel and Ogden (2009)] and references therein.

3. Modeling the Nonlinear Behavior of Biological Tissues

The aim of this chapter is to describe the highly nonlinear material properties of biological tissues by a model that will be capable of large elastic deformations. The following is related to the descriptions in [59, Holzapfel (2000)], [112, Ogden (1997)] and [25, Ciarlet]. The mathematical model for arterial walls is discussed in detail in [63, Holzapfel et al. (2000)] and [66, Holzapfel and Ogden (2010)].

3.1. Preliminaries

A *body* $\mathcal{B}$ is a set with elements that correspond to points of a region Ω in the three-dimensional Euclidean space. We call the elements of $\mathcal{B}$ *particles* and Ω the *configuration* of $\mathcal{B}$. If the body moves then this configuration changes with time $t \in \mathbb{R}^+$. For each t a unique configuration Ω_t is associated. For $t = 0$ the body $\mathcal{B}$ occupies an arbitrary but fixed configuration Ω_0 which is called the *reference* or *undeformed configuration*. Here each particle P of the body may be specified by its position vector $\boldsymbol{X}$ in Ω_0 relative to some origin. For an arbitrary time t the body occupies the con-

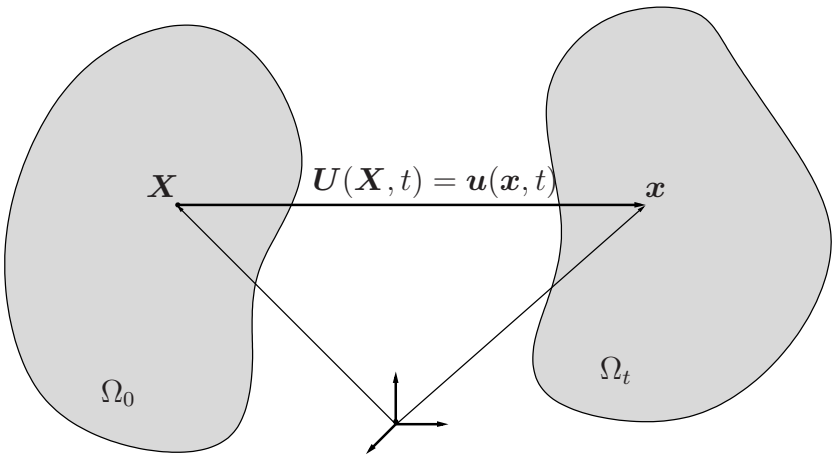

Figure 3.1. – Deformation of an elastic body.

figuration Ω_t which we identify as the *current* or *deformed configuration*. Let $\boldsymbol{x}$ be the position vector of the particle P in the current configuration. The vector $\boldsymbol{X}$ describes

the *material* or *referential* coordinates of a point, while $\boldsymbol{x}$ describes the *spatial* or *current* coordinates. Since both Ω_0 and Ω_t are configurations of $\mathcal{B}$ there exists a bijective mapping $\chi : \Omega_0 \mapsto \Omega_t$ such that

$$\boldsymbol{x} = \chi(\boldsymbol{X}, t) \quad \text{for all } \boldsymbol{X} \in \Omega_0,\ t \in \mathbb{R}^+. \tag{3.1}$$

The mapping χ is called the *motion* or *deformation* of the body $\mathcal{B}$ from Ω_0 to Ω_t. We assume that $\chi(\boldsymbol{X}, t)$ is twice continuously differentiable with respect to position and time. Its inverse $\chi^{-1}(\boldsymbol{x}, t)$ is uniquely defined as

$$\boldsymbol{X} = \chi^{-1}(\boldsymbol{x}, t) \quad \text{for all } \boldsymbol{x} \in \Omega_t,\ t \in \mathbb{R}^+.$$

The terminologies *Lagrangian* and *Eulerian description* are also used with respect of Ω_0 and Ω_t respectively. The vector fields $\boldsymbol{u}(\boldsymbol{x}, t) = \boldsymbol{x} - \boldsymbol{X}(\boldsymbol{x}, t)$ and $\boldsymbol{U}(\boldsymbol{X}, t) = \boldsymbol{x}(\boldsymbol{X}, t) - \boldsymbol{X}$ represent the *displacement field* of a particle. One can easily show that

$$\boldsymbol{u}(\boldsymbol{x}, t) = \boldsymbol{u}(\chi(\boldsymbol{X}, t)) = \boldsymbol{U}(\boldsymbol{X}, t). \tag{3.2}$$

Let Grad denote the gradient operator in the reference configuration, i.e. with respect to $\boldsymbol{X}$. Then we define the *deformation gradient* F by

$$\mathsf{F}(\boldsymbol{X}, t) = \operatorname{Grad} \chi(\boldsymbol{X}, t). \tag{3.3}$$

With the definition of the displacement field this can be re-written as

$$\mathsf{F}(\boldsymbol{X}, t) = \mathsf{I} + \operatorname{Grad} \boldsymbol{U}(\boldsymbol{X}, t), \tag{3.4}$$

with I being the identity.

Remark 3.1.1. *From the bijective mapping χ it follows that the deformation gradient F is non-singular. This fits with the observation that $\mathsf{F}\,\mathrm{d}\boldsymbol{X} \neq 0$ if $\mathrm{d}\boldsymbol{X} \neq 0$ which means that a line element cannot be annihilated by the deformation process.*

We define the *right* and *left Cauchy–Green deformation tensors* as

$$\mathsf{C} := \mathsf{F}^\top \mathsf{F} \quad \text{and} \quad \mathsf{B} := \mathsf{F}\mathsf{F}^\top \tag{3.5}$$

which are both symmetric and positive definite.

3.2. Transformations between Reference and Current Configuration

Let $\mathrm{d}\boldsymbol{x}$ and $\mathrm{d}\boldsymbol{X}$ be the infinitesimal line elements in the current and reference configuration, respectively. From the definition of the deformation gradient we can deduce the following fundamental relation

$$\mathrm{d}\boldsymbol{x} = \mathsf{F}(\boldsymbol{X}, t)\,\mathrm{d}\boldsymbol{X}, \tag{3.6}$$

which has the inverse

$$\mathrm{d}\boldsymbol{X} = \mathsf{F}^{-1}(\boldsymbol{x}, t)\,\mathrm{d}\boldsymbol{x}. \tag{3.7}$$

Let $\mathrm{d}v$ and $\mathrm{d}V$ be the infinitesimal volume elements in the current and reference configuration respectively. The transformation of a volume element between the reference and the current configuration is done by the relation

$$\mathrm{d}v = \det(\mathsf{F}(\boldsymbol{X}, t))\,\mathrm{d}V. \tag{3.8}$$

We denote $J(\boldsymbol{X}, t) := \det(\mathsf{F}(\boldsymbol{X}, t))$ as the *Jacobian determinant* which is also known as volume ratio. It describes the change of volume under the deformation. Since $\mathsf{F}(\boldsymbol{X}, t)$ is non-singular and by the convention that volume elements have positive measure it can be stated that

$$J(\boldsymbol{X}, t) \equiv \det(\mathsf{F}(\boldsymbol{X}, t)) > 0. \tag{3.9}$$

If we have a deformation without any change of volume then this deformation is called *isochoric* and

$$J(\boldsymbol{X}, t) \equiv \det(\mathsf{F}(\boldsymbol{X}, t)) = 1. \tag{3.10}$$

An *incompressible material* is a material for which (3.10) holds for all deformations.

In the following, we will omit the arguments of the quantities to enhance readability.

Theorem 3.1 (Nanson's Formula)**.** *Let* $\mathrm{d}s$ *and* $\mathrm{d}S$ *be infinitesimal surface elements on the current and reference configuration respectively. Then it holds that*

$$\boldsymbol{n}\,\mathrm{d}s = J\mathsf{F}^{-\top}\boldsymbol{N}\,\mathrm{d}S, \tag{3.11}$$

with F *the deformation gradient,* $J = \det\mathsf{F}$ *and* $\boldsymbol{n}$ *and* $\boldsymbol{N}$ *the normal vectors in the current and reference configuration.*

Proof. For the proof, e.g., cf. [112, Ogden (1997)]. □

Let $\mathrm{Grad} = \mathrm{Grad}_X$ be the gradient defined in the reference configuration, and let $\mathrm{grad} = \mathrm{grad}_x$ be the gradient defined in the current configuration. By the chain rule we get the following useful properties

$$\mathrm{Grad}\,\phi = \mathsf{F}^{\top}\,\mathrm{grad}\,\phi \tag{3.12}$$

for a scalar function ϕ and

$$\mathrm{Grad}\,\boldsymbol{w} = (\mathrm{grad}\,\boldsymbol{w})\,\mathsf{F} \tag{3.13}$$

for a vector field $\boldsymbol{w}$. For the divergence operators Div in the reference configuration and div in the current configuration, and a tensor field A we get

$$\mathrm{Div}\,\mathsf{A} = (\mathrm{div}\,\mathsf{A})\,\mathsf{F}^{\top}. \tag{3.14}$$

For the proofs of these useful relations see, e.g., [59, Holzapfel (2000), Ch. 2.4].

3.3. Decomposition of the Deformation Gradient

In the following theorem we decompose the deformation gradient F into a pure stretch and a pure rotation.

Remark 3.3.1 (Polar Decomposition Theorem)**.** *Let* F *be a second-order tensor with* $\det F > 0$*. Then there exist unique, positive definite, symmetric tensors,* U *and* V*, and a unique orthogonal tensor* R *such that*

$$\mathsf{F} = \mathsf{RU} = \mathsf{VR}. \tag{3.15}$$

U *and* V *are called the right and left stretch tensor,* R *represents a rotation.*

For the right and left stretch tensor it holds that

$$\mathsf{U}^2 = \mathsf{F}^\top\mathsf{F} = \mathsf{C} \quad \text{and} \quad \mathsf{V}^2 = \mathsf{F}\mathsf{F}^\top = \mathsf{B}$$

which is a result of the *square-root theorem* [52, Gurtin (1981)].

3.4. Stretch and Strain

Strain is measured locally by changes in the lengths of line elements. In contrast a material is said to be *unstrained* if no line element changes length, i.e.

$$|\mathrm{d}\boldsymbol{x}|^2 - |\mathrm{d}\boldsymbol{X}|^2 = 0.$$

Let $\hat{\boldsymbol{X}}$ and $\hat{\boldsymbol{x}}$ be the unit vectors along $\mathrm{d}\boldsymbol{X}$ and $\mathrm{d}\boldsymbol{x}$ in the reference and current configuration respectively. Then we can write $\mathrm{d}\boldsymbol{X} = \hat{\boldsymbol{X}}\,|\mathrm{d}\boldsymbol{X}|$ and $\mathrm{d}\boldsymbol{x} = \hat{\boldsymbol{x}}\,|\mathrm{d}\boldsymbol{x}|$. With (3.6) we get $\hat{\boldsymbol{x}}\,|\mathrm{d}\boldsymbol{x}| = \mathsf{F}\hat{\boldsymbol{X}}\,|\mathrm{d}\boldsymbol{X}|$ and

$$|\mathrm{d}\boldsymbol{x}|^2 = (\mathsf{F}\hat{\boldsymbol{X}}) \cdot (\mathsf{F}\hat{\boldsymbol{X}})\,|\mathrm{d}\boldsymbol{X}|^2 = \left(\mathsf{F}^\top\mathsf{F}\hat{\boldsymbol{X}}\right) \cdot \hat{\boldsymbol{X}}\,|\mathrm{d}\boldsymbol{X}|^2\,. \tag{3.16}$$

Hence

$$\frac{|\mathrm{d}\boldsymbol{x}|}{|\mathrm{d}\boldsymbol{X}|} = \left|\mathsf{F}\hat{\boldsymbol{X}}\right| = \left[\hat{\boldsymbol{X}} \cdot (\mathsf{F}^\top\mathsf{F}\hat{\boldsymbol{X}})\right]^{1/2} =: \lambda(\hat{\boldsymbol{X}}). \tag{3.17}$$

The value $\lambda(\hat{\boldsymbol{X}})$ has the physical interpretation of the *stretch* in direction of $\hat{\boldsymbol{X}}$ at $\boldsymbol{X}$ and we can easily see that $0 < \lambda(\hat{\boldsymbol{X}}) < \infty$ for all unit vectors $\hat{\boldsymbol{X}}$. The equation (3.17) motivates the names stretch tensors for U and V, introduced in Section 3.3.1, since $\mathsf{U}^2 = \mathsf{F}^\top\mathsf{F}$ and $\mathsf{V}^2 = \mathsf{F}\mathsf{F}^\top$.

From (3.16) we can describe the change of a line element length from the reference to the current configuration by

$$|\,\mathrm{d}\boldsymbol{x}|^2 - |\,\mathrm{d}\boldsymbol{X}|^2 = \mathrm{d}\boldsymbol{X} \cdot \left(\mathsf{F}^\top \mathsf{F} - \mathsf{I}\right) \mathrm{d}\boldsymbol{X}. \tag{3.18}$$

As mentioned earlier, strain is measured by changes in the lengths of line elements. Thus we can see from (3.18) that the tensor $\mathsf{F}^\top \mathsf{F} - \mathsf{I}$ is a measure of strain. Hence we define the so-called *Green strain tensor* as

$$\mathsf{E} := \frac{1}{2}\left(\mathsf{F}^\top \mathsf{F} - \mathsf{I}\right) = \frac{1}{2}\left(\mathsf{C} - \mathsf{I}\right). \tag{3.19}$$

One can see from (3.18) that $\mathsf{E} = 0$ coincides with no change of the line length and thus with no strain.

From the definition of the deformation gradient we can express the Green strain tensor in terms of the gradient as

$$\mathsf{E}(\boldsymbol{U}) = \frac{1}{2}\left(\operatorname{Grad}\boldsymbol{U} + (\operatorname{Grad}\boldsymbol{U})^\top + (\operatorname{Grad}\boldsymbol{U})^\top \operatorname{Grad}\boldsymbol{U}\right). \tag{3.20}$$

The strain tensors C and E are used in the reference configuration while the left Cauchy–Green tensor B is used in the current configuration.

3.5. The Concept of Stress

To introduce the theory of stress we consider a continuous and deformable body $\mathcal{B}$ which occupies the region Ω at time t. The boundary of this body we denote as $\partial\Omega$. The forces which act on the boundary surface are called *external* or *contact forces*; examples can be pressure or friction. Those forces which act on the particles of the body we call *internal* or *body forces*. The latter may arise due to gravity or thermal fields, for example. The body force is denoted by $\boldsymbol{b}$. For a mathematical description of the contact forces we rely on *Cauchy's stress principle*. This axiom states that the action over a closed surface $\partial\Omega$ is represented by a vector field $\boldsymbol{t}(t, \boldsymbol{x}, \boldsymbol{n})$, defined on $\partial\Omega$. This vector is called *stress vector* and its physical interpretation is the force measured per unit area. With these definitions we may formulate the following fundamental theorem, see, e.g., [112, Ogden (1997)]:

Theorem 3.2 (Cauchy's Stress Theorem)**.** *Let $\boldsymbol{b}$ and $\boldsymbol{t}(t, \boldsymbol{x}, \boldsymbol{n})$ be the body and contact forces for a body $\mathcal{B}$ during a motion. Then there exists a unique and symmetric second-order tensor field σ, such that for each unit vector $\boldsymbol{n}$*

$$\boldsymbol{t}(t, \boldsymbol{x}, \boldsymbol{n}) = \sigma^\top(\boldsymbol{x})\boldsymbol{n}, \tag{3.21}$$

where σ is independent of $\boldsymbol{n}$ and satisfies

$$\sigma^\top = \sigma. \tag{3.22}$$

Furthermore, σ satisfies Cauchy's equation of motion

$$\rho \frac{\partial^2}{\partial t^2}\boldsymbol{u} - \operatorname{div}\sigma = \rho \boldsymbol{b}, \tag{3.23}$$

where ρ is the mass density of the material composing $\mathcal{B}$. σ is called Cauchy's stress tensor.

From (3.21) we get with the use of Nanson's formula (3.11)

$$\boldsymbol{t}\,\mathrm{d}s = \sigma \boldsymbol{n}\,\mathrm{d}s = J\sigma \mathsf{F}^{-\top}\boldsymbol{N}\,\mathrm{d}S \tag{3.24}$$

where we define the so-called *first Piola–Kirchhoff stress tensor* by

$$\mathsf{P} := J\sigma \mathsf{F}^{-\top}. \tag{3.25}$$

P measures the *force per unit reference area* while σ measures the *force per unit deformed area*. Note that in general P is not symmetric. To provide a symmetric stress tensor in the reference configuration as well, we define the *second Piola–Kirchhoff stress tensor* by

$$\mathsf{S} := \mathsf{F}^{-1}\mathsf{P} = J\mathsf{F}^{-1}\sigma \mathsf{F}^{-\top}. \tag{3.26}$$

Remark 3.5.1 (Piola Transformation)**.** S *is the so-called Piola transformation of σ. With this transformation a correspondence between quantities defined over the current and reference configuration is established.*

Corollary 3.1. *An equivalent version of Cauchy's equation of motion in the reference configuration can be re-casted in terms of S by*

$$\rho_0 \frac{\partial^2}{\partial t^2}\boldsymbol{U} - \operatorname{Div}(\mathsf{FS}) = \rho_0 \boldsymbol{b}_0 \tag{3.27}$$

with ρ_0 the mass density and $\boldsymbol{b}_0$ the body force, each in the reference configuration . It holds $\rho = J^{-1}\rho_0$.

For more details and the derivation of the latter corollary compare, e.g., [112, Ogden (1997), Ch. 3.4].

3.6. General Problem Formulation

We want to find the displacement field $\boldsymbol{u}(\boldsymbol{x}, t)$ that satisfies Cauchy's equation of motion (3.21), i.e.

$$\rho(\boldsymbol{x}, t)\frac{\partial^2}{\partial t^2}\boldsymbol{u}(\boldsymbol{x}, t) - \operatorname{div}\sigma(\boldsymbol{x}, t) = \rho(\boldsymbol{x}, t)\boldsymbol{b}(\boldsymbol{x}, t) \quad \text{for all } \boldsymbol{x} \in \Omega,\ t \geq 0. \tag{3.28}$$

$\boldsymbol{b}$, the body force per unit volume, acts on a particle of the region Ω and it is considered to be a prescribed (given) force. The inertia force per unit volume is characterized by $\rho\,\partial^2 u/\partial t^2$, with ρ the spatial mass density of the material.

In order to formulate boundary conditions, $\partial\Omega$ is decomposed into disjoint parts so that

$$\partial\Omega = \overline{\Gamma}_D \cup \overline{\Gamma}_N \qquad \text{with} \qquad \Gamma_D \cap \Gamma_N = \emptyset.$$

Dirichlet boundary conditions on Γ_D correspond to a given displacement field $\boldsymbol{u} = \boldsymbol{u}_D$, which is enforced component-wise. Neumann boundary conditions on Γ_N are identified physically with a given surface traction $\sigma(\boldsymbol{x},t)\boldsymbol{n}(\boldsymbol{x}) = \boldsymbol{t}_N(\boldsymbol{x},t)$.

Finally, we require initial conditions. The displacement field and the velocity field at initial time $t = 0$ are specified as

$$\boldsymbol{u}(\boldsymbol{x},t)|_{t=0} = \boldsymbol{u}_0(\boldsymbol{X}), \qquad \dot{\boldsymbol{u}}(\boldsymbol{x},t)|_{t=0} := \frac{\partial}{\partial t}\boldsymbol{u}(\boldsymbol{x},t)|_{t=0} = \boldsymbol{u}_1(\boldsymbol{X}).$$

If we consider a stress-free reference configuration Ω_0 at time $t = 0$ the initial values are assumed to be zero.

Combining the above-mentioned relations, this leads to the following classical formulation of the boundary value problem of interest:
let Ω be a bounded domain with a sufficiently smooth boundary $\Gamma = \partial\Omega$. We have a disjunct decomposition of the boundary of the form $\Gamma = \overline{\Gamma}_D \cup \overline{\Gamma}_N$. Given a continuous body force $\boldsymbol{b}$, boundary and initial conditions, the density $\rho > 0$, find the displacement field $\boldsymbol{u}$ such that

$$\left.\begin{aligned} \rho(\boldsymbol{x},t)\frac{\partial^2}{\partial t^2}\boldsymbol{u}(\boldsymbol{x},t) - \operatorname{div}\sigma(\boldsymbol{u},\boldsymbol{x},t) &= \rho(\boldsymbol{x},t)\,\boldsymbol{b}(\boldsymbol{x},t) && \text{in } \Omega, t>0,\\ \boldsymbol{u}(\boldsymbol{x},t) &= \boldsymbol{u}_D(\boldsymbol{x},t) && \text{on } \Gamma_D, t>0,\\ \sigma(\boldsymbol{u},\boldsymbol{x},t)\,\boldsymbol{n}(\boldsymbol{x}) &= \boldsymbol{t}_N(\boldsymbol{x},t) && \text{on } \Gamma_N, t>0,\\ \boldsymbol{u}(\boldsymbol{x},t) &= \boldsymbol{u}_0(\boldsymbol{X}) && \text{for } t=0,\\ \dot{\boldsymbol{u}}(\boldsymbol{x},t) &= \boldsymbol{u}_1(\boldsymbol{X}) && \text{for } t=0. \end{aligned}\right\} \tag{3.29}$$

For the modeling of biological tissues the second time derivative on the left hand side is of practically negligible order (cf. [154, Whiteley and al. (2007)]). Additionally we set the body force to zero. Thus we concentrate on the simplified problem: find the displacement field $\boldsymbol{u}$ such that

$$\left.\begin{aligned} -\operatorname{div}\sigma(\boldsymbol{u},\boldsymbol{x},t) &= \boldsymbol{0} && \text{in } \Omega, t>0,\\ \boldsymbol{u}(\boldsymbol{x},t) &= \boldsymbol{u}_D(\boldsymbol{x},t) && \text{on } \Gamma_D, t>0,\\ \sigma(\boldsymbol{u},\boldsymbol{x},t)\,\boldsymbol{n}(\boldsymbol{x}) &= \boldsymbol{t}_N(\boldsymbol{x},t) && \text{on } \Gamma_N, t>0, \end{aligned}\right\} \tag{3.30}$$

with initial conditions. For a time-stepping scheme this leads to a quasi-stationary approach, as proposed in [60, Holzapfel (2003)] for biological tissues.

To specify a similar form of this boundary value problem in terms of the reference configuration we use (3.27). With this we get for the stationary boundary value problem in the reference configuration

$$\left.\begin{aligned} -\operatorname{Div}[\mathsf{FS}(\boldsymbol{u},\boldsymbol{X})] &= \mathbf{0} && \text{in } \Omega_0, \\ \boldsymbol{u}(\boldsymbol{X}) &= \boldsymbol{u}_D(\boldsymbol{X}) && \text{on } \Gamma_D, \\ \mathsf{FS}(\boldsymbol{u},\boldsymbol{X})\boldsymbol{N}(\boldsymbol{X}) &= \boldsymbol{t}_N(\boldsymbol{X}) && \text{on } \Gamma_N. \end{aligned}\right\} \tag{3.31}$$

In this case it is important to take a closer look at the embedding of the traction forces, i.e. the Neumann boundary conditions. If the applied surface force $\boldsymbol{t}_N(\boldsymbol{X})$ in the reference configuration is independent of the deformation gradient F then we consider a *dead load*. This case is a simplification and is seldom usable to model actual applied forces. For the modeling of biological tissue we need to apply *pressure loads* on the boundary of the domain; for example the pressure loads applied to the myocardium in the ventricles of the heart. In the current configuration an applied surface force is a pressure load if it is of the form

$$\boldsymbol{t}_N(\boldsymbol{x}) = -p\boldsymbol{n}(\boldsymbol{x}), \tag{3.32}$$

where p is referred to as the hydrostatic pressure. In the reference configuration the surface load then depends on the deformation and is of the form

$$t_N(\boldsymbol{X}) = \hat{t}_N(\boldsymbol{X},\mathsf{F}) = -p(\det(\mathsf{F}))\mathsf{F}^{-\top}\boldsymbol{N}(\boldsymbol{X}). \tag{3.33}$$

For a more detailed discussion on displacement dependent pressure loads cf. [25, Ciarlet (1988), Sect. 2.6 and 5.1] or [137, Schweizerhof and Ramm (1984)].

3.7. Linear Elasticity

For *small deformations* it is justified not to distinguish between the Eulerian and Lagrangian description and to replace the strain tensor E by the linearized strain tensor $\varepsilon(\boldsymbol{u})$, defined by

$$\varepsilon_{ij}(\boldsymbol{u}) = \frac{1}{2}\left(\frac{\partial u_j}{\partial x_i} + \frac{\partial u_i}{\partial x_j}\right). \tag{3.34}$$

A material is called linear elastic if it can be modeled using *Hooke's Law* which describes a linear relationship between stress and strain. It states

$$\sigma = \mathbb{C} : \varepsilon, \quad \sigma_{ij} = \sum_{kl} C_{ijkl}\varepsilon_{kl}. \tag{3.35}$$

The *elasticity tensor* $\mathbb{C}$ is formed by so-called elastic coefficients and it satisfies the symmetry conditions

$$C_{ijkl} = C_{klij} \quad \text{and} \quad C_{ijkl} = C_{jikl} = C_{jilk}.$$

An important special case are homogeneous, isotropic linear elastic materials which are called *linear St. Venant–Kirchhoff materials*. In this case

$$\sigma = \frac{E\nu}{(1+\nu)(1-2\nu)}\,\mathrm{tr}(\varepsilon)\mathsf{I} + \frac{E}{(1+\nu)}\varepsilon \tag{3.36}$$

with Young's modulus $E > 0$, measured normally in Gigapascal (GPa), and Poisson's ratio $\nu \in (0, 0.5)$. E quantifies the stiffness of an elastic material. The range of Young's modulus is from $E = 0.01$ GPa, e.g. for some types of rubber, to values around 1000 GPa, e.g. for diamond we have $E = 1220$ GPa. ν is a dimensionless parameter and a measure of compressibility. For the incompressible limit we have $\nu = 0.5$, e.g., rubber; for very compressible materials like cork ν is very near to zero. Since biological tissues are considered as rubber-like materials we have Young's modulus around 1 GPa and a Poisson's ratio close to 0.5. This is consistent with the assumption of nearly incompressibility.

We define the so-called Lamé coefficients λ and μ as

$$\lambda := \frac{E\nu}{(1+\nu)(1-2\nu)}, \quad \mu := \frac{E}{2(1+\nu)}. \tag{3.37}$$

Lamé's second parameter $\mu > 0$ is also known as the shear modulus. It spans between 0 GPa for rubber and 478 GPa for diamond. Lamé's first parameter λ has no physical interpretation and is also measured in Gigapascal. With these two constants we can write the elasticity tensor for a linear St. Venant–Kirchhoff material as

$$C_{ijkl} = \lambda\delta_{ij}\delta_{kl} + \mu(\delta_{ik}\delta_{jl} + \delta_{il}\delta_{jk}). \tag{3.38}$$

For the incompressible limit we have

$$\nu \to 0.5 \quad \text{or} \quad \lambda \to \infty. \tag{3.39}$$

In the classical literature there exist many treatments of the theory of linear elastic materials. Amongst others see the works of [51, Gurtin (1972)] or [107, Nečas and Hlaváček (1980)]. Matters of solvability of the boundary value problem and uniqueness of an eventual solution are discussed in Sect. 4.3.

3.8. Constitutive Equations for Nonlinear Elasticity

Considering the study of the hyper-elastic properties of biological tissues we have to deal with a nonlinear relationship between stress and strain and with large deformations. Since a linear elasticity model is not adequate to treat such a complex behavior we have to take a look at the more general concept of nonlinear elasticity. Here we model the non-linear stress-strain response via a constitutive equation that links the stress

to a derivative of a so-called *strain energy function*. This scalar-valued function $W(\mathsf{F})$ represents the elastic stored energy per unit reference volume. It takes one tensor variable F as argument and we assume it to be continuous.

The *total strain energy* (or the *internal potential energy*) can be described as the integral of $W(\mathsf{F})$ over the domain Ω_0.

In this work we will concentrate on *perfectly elastic materials*. These are by definition materials which produce locally no entropy and thus the internal dissipation[1] equals zero. In other words we exclude plastic deformations as well as damaging or viscous mechanisms.

Theorem 3.3 (Constitutive Equation). *Given a strain energy function W, the first Piola–Kirchhoff stress tensor P and the deformation gradient F are linked by the constitutive equation*

$$\mathsf{P} = \frac{\partial W(\mathsf{F})}{\partial \mathsf{F}}. \tag{3.40}$$

Proof. Cf. for example [25, Ciarlet (1988)] or [112, Ogden (1997)]. □

Remark 3.8.1. *$W(\mathsf{F})$ is also referred to as the Helmholtz free-energy function.*

Remark 3.8.2. *It is important to note that we use the convention*

$$\left(\frac{\partial W(\mathsf{F})}{\partial \mathsf{F}}\right)_{ij} := \frac{\partial W(\mathsf{F})}{\partial F_{ij}},$$

as in [59, Holzapfel (2000)] and in [25, Ciarlet (1988)]. In the literature the definition

$$\left(\frac{\partial W(\mathsf{F})}{\partial \mathsf{F}}\right)_{ij} := \frac{\partial W(\mathsf{F})}{\partial F_{ji}}.$$

is also common, e.g. in [112, Ogden (1997)]. In this case the constitutive equation above holds for $\mathsf{P}^\top$.

In the following, we denote the strain energy function as $W(\mathsf{F})$ if it depends on the deformation gradient F. In case it depends on the right Cauchy–Green tensor C we denote it as $\Psi(\mathsf{C})$. At times we may need an energy function depending on the Green–Lagrange strain tensor E. Since E may be expressed in terms of C, see (3.19), we write $\Psi(\mathsf{E})$ as well.

Since all three functions describe the same behavior of a considered material we can write

$$W(\mathsf{F}) = \Psi(\mathsf{C}) = \Psi(\mathsf{E}). \tag{3.41}$$

[1] dissipative system: a dynamical system loses energy over time due to a conversion into thermal energy; processes in such a system are irreversible and the entropy in it rises.

Remark 3.8.3 (Normalization Conditions). *For convenience we require that W and Ψ vanish in the reference configuration Ω_0. So we get the following so-called normalization conditions*

$$W(\mathsf{I}) = 0, \quad \Psi(\mathsf{I}) = 0. \tag{3.42}$$

Moreover, from a physical observation we require that the free-energy function increases with a deformation, that it is finite for a finite deformation and that it tends to infinity if the displacement $\boldsymbol{u}$ tends to infinity, i.e.

$$W(\mathsf{F}) \geq 0, \quad W(\mathsf{F}) < \infty \quad \textit{if} \quad |\boldsymbol{u}| < \infty \quad \textit{and} \lim_{\boldsymbol{u}\to\infty} W(\mathsf{F}) = \infty.$$

These requirements hold for $\Psi(\mathsf{C})$ and $\Psi(\mathsf{E})$ as well.

Lemma 3.4. *For the different representations of the strain energy functions $W(\mathsf{F})$, $\Psi(\mathsf{C})$ and $\Psi(\mathsf{E})$ it holds:*

$$\frac{\partial W(\mathsf{F})}{\partial \mathsf{F}} = 2\frac{\partial \Psi(\mathsf{C})}{\partial \mathsf{C}}\mathsf{F}^\top = \frac{\partial \Psi(\mathsf{E})}{\partial \mathsf{E}}\mathsf{F}^\top, \tag{3.43}$$

with the deformation gradient F, the right Cauchy–Green tensor C and the Green–Lagrange strain tensor E.

Proof. The proof follows from (3.41) and the chain rule. □

In the following corollary we collect the constitutive equations for the different stress tensors.

Corollary 3.2. *The first Piola–Kirchhoff stress tensor may be expressed in terms of the deformation gradient and a strain energy function as*

$$\mathsf{P} = \frac{\partial W(\mathsf{F})}{\partial \mathsf{F}} = 2\frac{\partial \Psi(\mathsf{C})}{\partial \mathsf{C}}\mathsf{F}^\top = \frac{\partial \Psi(\mathsf{E})}{\partial \mathsf{E}}\mathsf{F}^\top. \tag{3.44}$$

For the second Piola–Kirchhoff stress tensor we get

$$\mathsf{S} = \mathsf{F}^{-1}\left(\frac{\partial W(\mathsf{F})}{\partial \mathsf{F}}\right)^\top = 2\frac{\partial \Psi(\mathsf{C})}{\partial \mathsf{C}} = \frac{\partial \Psi(\mathsf{E})}{\partial \mathsf{E}}, \tag{3.45}$$

and for the Cauchy stress tensor the constitutive equations

$$\sigma = J^{-1}\mathsf{F}\left(\frac{\partial W(\mathsf{F})}{\partial \mathsf{F}}\right)^\top = 2J^{-1}\mathsf{F}\frac{\partial \Psi(\mathsf{C})}{\partial \mathsf{C}}\mathsf{F}^\top = J^{-1}\mathsf{F}\frac{\partial \Psi(\mathsf{E})}{\partial \mathsf{E}}\mathsf{F}^\top \tag{3.46}$$

hold.

Proof. The different constitutive equations follow immediately from the constitutive equation for P in Theorem 3.3, the Piola transformations (3.25) and (3.26), Lemma 3.4 and the symmetry of σ and S. □

3.9. Modeling of (Nearly) Incompressible Elastic Materials

As mentioned in Chapter 2 we treat biological tissues as nearly incompressible elastic materials. This goes back to observations in [153, Vossoughi et al. (1980)]. To get a realistic model for such materials, where $J = \det(\mathsf{F})$ gets very close to 1, we have to adapt the constitutive equations slightly. In the following two sections, we will introduce two different approaches, one of them to model the myocardium (Sect. 3.9.1), the other one to treat nearly incompressible arterial materials (Sect. 3.9.2).

In this section we will need the derivatives

$$\frac{\partial J}{\partial \mathsf{C}} = \frac{J}{2}\mathsf{C}^{-1} \quad , \quad \frac{\partial J^{-2/3}}{\partial \mathsf{C}} = -\frac{1}{3}J^{-2/3}\mathsf{C}^{-1}, \tag{3.47}$$

cf. [59, Holzapfel (2000)]. Additionally, to simplify matters, we introduce the deviatoric operators:

Definition 3.5. *We define the deviatoric operator in the current configuration as*

$$\mathrm{dev}(\bullet) = (\bullet) - \frac{1}{3}\,\mathrm{tr}(\bullet)\mathsf{I}. \tag{3.48}$$

The deviatoric operator in the Lagrangian description reads

$$\mathrm{Dev}(\bullet) = (\bullet) - \frac{1}{3}\,[(\bullet) : \mathsf{C}]\,\mathsf{C}^{-1}, \tag{3.49}$$

with the right Cauchy–Green tensor $\mathsf{C} = \mathsf{F}^{\top}\mathsf{F}$.

3.9.1. Adaptation of the Strain Energy Function

For incompressible materials, with $J = \det \mathsf{F} = 1$, the following form of a strain energy function is proposed

$$W = W(\mathsf{F}) - p(J-1), \quad \Psi = \Psi(\mathsf{C}) - p(J-1), \tag{3.50}$$

see, e.g., [59, Holzapfel (2000), Ch. 6.3]. The unknown p is the so-called hydrostatic pressure and serves as a Lagrange multiplier to guarantee the side condition that J equals 1.

With $(3.47)_1$ and the formulas of Corollary 3.2 we get for the first and the second Piola–Kirchhoff stress tensor for an incompressible material

$$\mathsf{P} = -p\mathsf{F}^{-\top} + \frac{\partial W(\mathsf{F})}{\partial \mathsf{F}}, \quad \mathsf{S} = -p\mathsf{C}^{-1} + 2\frac{\partial \Psi(\mathsf{C})}{\partial \mathsf{C}}. \tag{3.51}$$

For the Cauchy stress tensor we obtain

$$\sigma = -p\mathsf{I} + \mathsf{F}\left(\frac{\partial W(\mathsf{F})}{\partial \mathsf{F}}\right)^{\top} = -p\mathsf{I} + 2\mathsf{F}\frac{\partial \Psi(\mathsf{C})}{\partial \mathsf{C}}\mathsf{F}^{\top}. \tag{3.52}$$

3.9.2. Decoupling of the Deformation

An approach to handle nearly incompressible materials, with $J = \det \mathsf{F}$ close to one, is the decoupling of the deformation into a *volumetric* (i.e. volume changing) and an *isochoric* (i.e. volume preserving) part. This method was already considered in [43, Flory (1961)] and it is proposed for the artery model in the papers [63, Holzapfel et al. (2000)] and [60, Holzapfel (2003)]. In [38, Eriksson et al. (2012)] the authors suggest this approach for the myocardium model as well.

A multiplicative factorization of the deformation gradient F is performed by

$$\mathsf{F} = (J^{1/3}\mathsf{I})\,\overline{\mathsf{F}} \qquad \text{with} \qquad \det \overline{\mathsf{F}} = 1, \tag{3.53}$$

where I denotes the second-order unit tensor. This is motivated by the property of the determinant such that

$$\det(J^{1/3}\overline{\mathsf{F}}) = J \det(\overline{\mathsf{F}}) = J = \det(\mathsf{F}).$$

Hence with (3.5) we obtain an analogous multiplicative factorization for the left and the right Cauchy–Green strain tensor:

$$\mathsf{C} = J^{2/3}\overline{\mathsf{C}} \quad \text{and} \quad \mathsf{B} = J^{2/3}\overline{\mathsf{B}}. \tag{3.54}$$

Using this we can postulate a unique decoupled form of the strain energy function $\Psi(\mathsf{C})$ with the specific representation

$$\Psi(\mathsf{C}) = U(J) + \overline{\Psi}(\overline{\mathsf{C}}), \tag{3.55}$$

where $U(J)$, the so-called *volumetric elastic response*, is a strictly convex function with the unique minimum at $J = 1$. $\overline{\Psi}(\overline{\mathsf{C}})$ is called the *isochoric elastic response*.

We require

$$\begin{aligned} U(J) &= 0, \quad \text{if and only if } J = 1, \\ \overline{\Psi}(\overline{\mathsf{C}}) &= 0, \quad \text{if and only if } \overline{\mathsf{C}} = \mathsf{I} \end{aligned}$$

to fulfill the normalization conditions (3.42).

One possibility for the volumetric elastic response $U(J)$ is

$$U(J) = \frac{\kappa}{2}(J-1)^2 \tag{3.56}$$

with $\kappa > 0$ being the bulk modulus. In terms of Lamé's coefficients λ and μ , see (3.37), and the elasticity module E and Poisson's ratio ν respectively, κ may be expressed as

$$\kappa = \lambda + \frac{2\mu}{3} = \frac{E}{3(1-2\nu)}. \tag{3.57}$$

There are several other possible choices for $U(J)$. If not mentioned otherwise, we will use (3.56) for this function in the following.

We define the constitutive equation of the hydrostatic pressure as

$$p := \frac{\mathrm{d}U(J)}{\mathrm{d}J}, \tag{3.58}$$

cf. [59, Holzapfel (2000), Ch. 6.4].

Theorem 3.6 (Decoupling of the Cauchy stress tensor). *A decomposition of the energy function* $\Psi(\mathsf{C})$ *into a volumetric and an isochoric part*

$$\Psi(\mathsf{C}) = U(J) + \overline{\Psi}(\overline{\mathsf{C}}) \tag{3.59}$$

yields

$$\sigma = \sigma_{vol} + \sigma_{iso} \tag{3.60}$$

with

$$\sigma_{vol} = p\mathsf{I}, \quad \textit{and} \quad \sigma_{iso} = 2J^{-1}\,\mathrm{dev}\left(\overline{\mathsf{F}}\frac{\partial\overline{\Psi}(\overline{\mathsf{C}})}{\partial\overline{\mathsf{C}}}\overline{\mathsf{F}}^{\top}\right). \tag{3.61}$$

Proof. The main ingredients of the proof are (3.47), Theorem 3.3 and the chain rule. For more details compare [59, Holzapfel (2000)]. □

In an analogous way a decomposition for the stress tensor in the Lagrangian description S may be derived.

Corollary 3.3 (Decoupling of the second Piola–Kirchhoff stress tensor). *A decomposition of the energy function* $\Psi(\mathsf{C})$ *as in* (3.59) *yields*

$$\mathsf{S} = \mathsf{S}_{vol} + \mathsf{S}_{iso} \tag{3.62}$$

with

$$\mathsf{S}_{vol} = Jp\mathsf{C}^{-1}, \quad \textit{and} \quad \mathsf{S}_{iso} = 2J^{-2/3}\,\mathrm{Dev}\left(\frac{\partial\overline{\Psi}(\overline{\mathsf{C}})}{\partial\overline{\mathsf{C}}}\right). \tag{3.63}$$

A decoupling of the stress tensors in a form that was discussed in combination with the properties (3.56) and (3.58), leads to the following stationary boundary value problem:

$$\begin{aligned} -\operatorname{div}[p(\boldsymbol{u},\boldsymbol{x})\mathsf{I} + \sigma_{\mathrm{iso}}(\boldsymbol{u},\boldsymbol{x})] &= \mathbf{0} \quad \text{in } \Omega, \\ p(\boldsymbol{u},\boldsymbol{x}) &= \kappa(J(\boldsymbol{u},\boldsymbol{x})-1), \end{aligned} \tag{3.64}$$

with the hydrostatic pressure p and the corresponding Dirichlet and Neumann boundary conditions. The corresponding version of (3.64) in the reference configuration would be

$$\begin{aligned} -\operatorname{Div}[\mathsf{F}(\boldsymbol{U},\boldsymbol{X})((J(\boldsymbol{U},\boldsymbol{X})p(\boldsymbol{U},\boldsymbol{X})\mathsf{C}(\boldsymbol{U},\boldsymbol{X}) + \mathsf{S}_{\mathrm{iso}}(\boldsymbol{U},\boldsymbol{X})] &= \mathbf{0} \quad \text{in } \Omega_0, \\ p(\boldsymbol{U},\boldsymbol{X}) &= \kappa(J(\boldsymbol{U},\boldsymbol{X})-1), \end{aligned} \tag{3.65}$$

with the definitions from above and by using the right Cauchy–Green tensor C. Note that $\boldsymbol{u} = \boldsymbol{U}$ due to (3.2).

3.10. The Strain Energy Function in Terms of Invariants

In the following, we discuss the structure of the strain energy function. We introduce the concept of invariants and then express the strain energy function in terms of the principal invariants of its tensor-valued argument. For a compendium on the theory of invariants cf. [143, Spencer (1971)].

Definition 3.7 (Principle scalar invariants of a tensor)**.** *Let* A *be a given* 3×3 *second-order tensor. Then the characteristic polynomial of* A *is given by*

$$p(\lambda) = \det(\mathsf{A} - \lambda \mathsf{I}) = (\lambda_1 - \lambda)(\lambda_2 - \lambda)(\lambda_3 - \lambda) = -\lambda^3 + I_1\lambda^2 - I_2\lambda + I_3. \tag{3.66}$$

Here λ_i *are the eigenvalues and* $I_i, i = 1, 2, 3$ *are the so-called principal scalar invariants of* A*.*

From this definition we can easily derive the following corollary:

Corollary 3.4. *The invariants of a* 3×3 *second-order tensor* A *are*

$$\begin{aligned} I_1(\mathsf{A}) &= \operatorname{tr}(\mathsf{A}) = \lambda_1 + \lambda_2 + \lambda_3, \\ I_2(\mathsf{A}) &= \frac{1}{2}\left(\operatorname{tr}(\mathsf{A})^2 - tr(\mathsf{A}^2)\right) = \lambda_1\lambda_2 + \lambda_1\lambda_3 + \lambda_2\lambda_3, \\ I_3(\mathsf{A}) &= \det(\mathsf{A}) = \lambda_1\lambda_2\lambda_3. \end{aligned}$$

In the theory of mechanics the eigenvalues of the left and right stretch tensors U and V, introduced in Sect. 3.3.1, may be regarded as stretches in the principal directions. This is due to the coherence described in (3.17). They have the following property:

Corollary 3.5. U *and* V *have the same eigenvalues* $\lambda_i > 0$*.* λ_i *are called the principal stretches.*

As we consider the definition of the invariants in Corollary 3.4 we can state that $I_1(\mathsf{U})$ and $I_2(\mathsf{U})$ can be interpreted as a measure of stretch while $I_3(\mathsf{U})$ is a measure of volume change.

Consequently, if we consider an incompressible material the deformation gradient must satisfy the internal constraint

$$J \equiv \det(\mathsf{F}) = \det(\mathsf{U}) = I_3(\mathsf{U}) = 1. \tag{3.67}$$

If we have no stretch, i.e. $\lambda_i = 1$ for $i = 1, 2, 3$, then

$$I_1(\mathsf{U}) = I_2(\mathsf{U}) = 3. \tag{3.68}$$

For the two Cauchy–Green deformation tensors $\mathsf{C} = U^2$ and $\mathsf{B} = V^2$ the eigenvalues of both are the squares of the principal stretches. Thus we have for the invariants

$$\begin{aligned} I_1(\mathsf{C}) &= I_1(\mathsf{B}) = \lambda_1^2 + \lambda_2^2 + \lambda_3^2, \\ I_2(\mathsf{C}) &= I_2(\mathsf{B}) = \lambda_1^2\lambda_2^2 + \lambda_1^2\lambda_3^2 + \lambda_2^2\lambda_3^2, \\ I_3(\mathsf{C}) &= I_3(\mathsf{B}) = \lambda_1^2\lambda_2^2\lambda_3^2. \end{aligned}$$

Hence the same constraints (3.67) and (3.68) are valid for these tensors. Thus we can state that if we have no deformation, i.e. $\mathsf{C} = \mathsf{I}$ then there is consequently no strain, stretch, stress or volume change of the body involved. This fits perfectly well with the physical understanding of elastic materials.

Theorem 3.8 (Representation Theorem for Invariants)**.** *Let $f(\mathsf{A})$ be a scalar-valued tensor function. If f is invariant under rotations, it may be expressed in terms of the principal invariants of its argument* A*:*

$$f(\mathsf{A}) = f[I_1(\mathsf{A}), I_2(\mathsf{A}), I_3(\mathsf{A})]. \tag{3.69}$$

Proof. For a proof of this fundamental theorem see [52, Gurtin (1981), p. 231] or [151, Truesdell and Noll (1992), Sect. 10]. □

In the literature this theorem is also referred to as the *Rivlin–Ericksen representation theorem*.

3.11. Specific Strain Energy Functions for Elastic Materials

3.11.1. Isotropic Materials

In the following, we restrict the structure of the strain energy function of interest by the property that the material is *isotropic*, i.e. homogeneous in all directions. If that is the case then the strain energy function is invariant with respect to rotations. Thus

$$\Psi(\mathsf{C}) = \Psi(\mathsf{R}\mathsf{C}\mathsf{R}^\top) \tag{3.70}$$

holds for all symmetric tensors C and orthogonal rotation tensors R. For a more detailed discussion see, for example, [59, Holzapfel (2000), Ch. 6.2] or [25, Ciarlet (1988), Ch. 3.6]. Since $\Psi(\mathsf{C})$ fulfills the requirements of Theorem 3.8 we may write

$$\Psi(\mathsf{C}) = \Psi[I_1(\mathsf{C}), I_2(\mathsf{C}), I_3(\mathsf{C})], \tag{3.71}$$

where the principal invariants of the right Cauchy–Green tensor C are (cf. Corollary 3.4)

$$\begin{aligned} I_1(\mathsf{C}) &= \mathrm{tr}\mathsf{C}, \\ I_2(\mathsf{C}) &= \frac{1}{2}[(\mathrm{tr}\mathsf{C})^2 - \mathrm{tr}\mathsf{C}^2)], \\ I_3(\mathsf{C}) &= \det\mathsf{C}. \end{aligned}$$

For the stress-free reference configuration $\mathsf{C} = \mathsf{I}$, the strain-energy function (3.71) must satisfy the normalization condition $\Psi(\mathsf{I}) = 0$, i.e. $\Psi = 0$ for $I_1 = I_2 = 3$ and $I_3 = 1$.

Subject to the regularity assumption that Ψ is infinitely many times continuously differentiable with respect to I_1, I_2, I_3, Ogden [112, Ch. 4] proposed the following polynomial approximation for a strain-energy function

$$\Psi(I_1, I_2, I_3) = \sum_{p,q,r=0}^{\infty} c_{pqr}(I_1 - 3)^p (I_2 - 3)^q (I_3 - 1)^r, \tag{3.72}$$

with $c_{000} = 0$ and $c_{100} + 2c_{010} + c_{001} = 0$ to satisfy the normalization condition.

If we set $I_3 = 1$, which would be valid for an incompressible material, then we obtain

$$\Psi(I_1, I_2) = \sum_{p,q=0}^{\infty} c_{pq}(I_1 - 3)^p (I_2 - 3)^q$$

with $c_{00} = 0$.

To simplify this expression we make note of the special case

$$\Psi(I_1, I_2) = c_{10}(I_1 - 3) + c_{01}(I_2 - 3), \tag{3.73}$$

which is referred to as the *Mooney–Rivlin* strain-energy function. This important model to cover the behavior of an isotropic elastic material was proposed independently by Melvin Mooney and Ronald Rivlin; see [103, Mooney (1940)] and [121–123, Rivlin (1948, 1949)].

Finally, with $c_{01} = 0$ and $c_{10} = \mu/2$ this reduces to the *Neo–Hookean* model

$$\Psi(I_1) = \frac{\mu}{2}(I_1 - 3), \tag{3.74}$$

where $\mu > 0$ is a stress-like material parameter.

Another way to motivate the strain energy function (3.74) is through *statistical theory*; see [59, Holzapfel (2000), Ch. 7.2] for a brief discussion.

(3.74) just relies on one parameter and offers a simple way to describe the nonlinear deformation behavior of isotropic rubber-like materials. This model may be seen as the nonlinear counterpart of Hooke's law (cf. Sect 3.7) and goes back to R. Rivlin in [120, Rivlin (1948)].

Another candidate for a response function, and indeed a very famous one, was proposed independently by A.J.-C.B. Saint Venant in 1844 and G.R. Kirchhoff in 1852 and is thus named after these two physicists:

Definition 3.9 (St. Venant–Kirchhoff material)**.** *The strain energy function associated with the St. Venant–Kirchhoff model is defined by*

$$\Psi(\mathsf{E}) = \frac{\lambda}{2}(\operatorname{tr}\,\mathsf{E})^2 + \mu\,\operatorname{tr}(\mathsf{E}^2), \tag{3.75}$$

where the constants $\lambda > 0, \mu > 0$ are the Lamé parameters.

Although this kind of a function is not polyconvex (cf. Sect. 4.4.6), existence results were shown in [29, Dacorogna (2008)]. However, this kind of models brings some other drawbacks. These are, for example, so-called eversion problems, which means that large strains are possible although the stress is small [3, Antman (1979)], [150, Truesdell (1978)]. Another disadvantage is that $J = det(\mathsf{F})$ could possibly approach zero or even become negative. More details to these drawbacks and other shortcomings of the St. Venant–Kirchhoff model are described in [25, Ciarlet (1988), Sect. 3.9].

Hence we will use exclusively the Neo–Hookean and the Mooney–Rivlin models as a basis for modeling anisotropic materials.

3.11.2. Almost Incompressible Isotropic Materials

In Sect. 3.11.1 we already mentioned some possibilities to model isotropic materials. In this section we consider nearly incompressible materials, like most of the biological tissues. Hence a unique decoupled representation of the energy function is proposed as in Sect. 3.9.2.

We formulate the decoupled version of the strain energy function for isotropic materials as

$$\Psi(C) = U(J) + \overline{\Psi}(\overline{\mathsf{C}}), \tag{3.76}$$

where the function $U(J)$ is motivated mathematically and serves as a penalty function within the numerical analysis. It denotes Lagrange multiplier terms which vanish for the incompressible limit.

The function $\overline{\Psi}(\overline{\mathsf{C}})$ can also be written in terms of the invariants of $\overline{\mathsf{C}}$

$$\overline{\Psi}(\overline{\mathsf{C}}) = \overline{\Psi}[\overline{I}_1(\overline{\mathsf{C}}), \overline{I}_2(\overline{\mathsf{C}}), \overline{I}_3(\overline{\mathsf{C}})]$$

as already discussed in (3.71). Since $\overline{I}_3(\overline{\mathsf{C}}) = \det(\overline{\mathsf{C}}) = 1$ we can neglect this invariant and write

$$\overline{\Psi}(\overline{\mathsf{C}}) = \overline{\Psi}[\overline{I}_1(\overline{\mathsf{C}}), \overline{I}_2(\overline{\mathsf{C}})].$$

We formulate the decoupled version of (3.74) in the following definition:

Definition 3.10 (Almost Incompressible Neo–Hooke Material)**.** *The strain energy function to model nearly incompressible Neo–Hookean materials is defined by*

$$\Psi(J, \overline{I}_1) = U(J) + \frac{\mu}{2}(\overline{I}_1 - 3), \tag{3.77}$$

where the material parameter μ may be interpreted as the shear modulus. By definition this value is positive, i.e. $\mu > 0$.

For this simple model we can calculate the explicit formulation for the stress tensors in both the Lagrangian and Eulerian description using the formulas given in Sect. 3.9.2:

$$\begin{aligned} \mathsf{S} &= pJ\mathsf{C}^{-1} + cJ^{-2/3}\left(\mathsf{I} - \frac{1}{3}\operatorname{tr}(\overline{\mathsf{C}})\overline{\mathsf{C}}^{-1}\right), \\ \sigma &= p\mathsf{I} + cJ^{-5/3}\operatorname{dev}(\mathsf{B}). \end{aligned}$$

Analogous we obtain for the decoupled version of (3.73):

Definition 3.11 (Mooney–Rivlin Material)**.** *An elastic material is a Mooney–Rivlin material if its strain energy function is of the form*

$$\Psi(J, \overline{I}_1, \overline{I}_2) = U(J) + c_1(\overline{I}_1 - 3) + c_2(\overline{I}_2 - 3), \tag{3.78}$$

with material constants $c_1, c_2 > 0$.

In the following, we will concentrate on the Neo–Hookean and the Mooney–Rivlin model. Nonetheless one can formulate similar decoupled strain energy functions for all Ogden-type materials as given in (3.72).

3.11.3. First Steps to an Anisotropic Material Model

As mentioned in Chapter 2, many biological tissues consist of an isotropic ground substance, in the case of arteries elastin, and collagen fibers which lead to an anisotropic behavior of these materials. The modeling of such a complex structure goes back

to [44, Fung (1967)] where the author proposed a very influential constitutive model. From experiments he observed a linear relation between stiffness $\mathrm{d}\mathsf{P}/\mathrm{d}\lambda$ and the first Piola–Kirchhoff stress P, as seen in Fig. 3.2. He fitted this linear behavior according to

$$\frac{\mathrm{d}\mathsf{P}}{\mathrm{d}\lambda} = k_1 + k_2\mathsf{P}, \tag{3.79}$$

where $k_1 > 0$ is a stress-like and $k_2 > 0$ is a dimensionless parameter. λ is the stretch ratio in the direction of the applied load. By solving the differential equation (3.79) we obtain

$$\mathsf{P} = c\exp(k_2\lambda) - \frac{k_1}{k_2}.$$

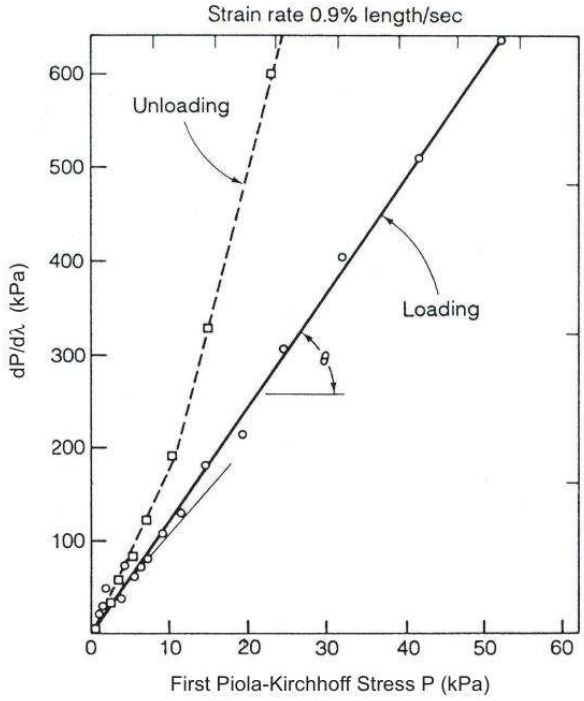

Figure 3.2. – Linear relationship between stiffness $\mathrm{d}\mathsf{P}/\mathrm{d}\lambda$ and stress P (from [45, Fung 1971] in a modification from [74, Humphrey 2002]).

If $\lambda = 1$, i.e. there is no stretch, one has consequently that the stress is zero: $\mathsf{P} = 0$. From this normalization condition the constant c may be determined and we conclude the following exponential constitutive relation

$$\mathsf{P} = \frac{k_1}{k_2}\left\{\exp[k_2(\lambda - 1)] - 1\right\}, \tag{3.80}$$

known as the 'Fung-Elastic' material model. This exponential function is widely used in the field of biomechanics to model soft tissues. In [63, Holzapfel et al. (2000)]

the authors now combine the Neo–Hookean response function for the isotropic ground substance with Fung's proposal for the collagen fibers and suggest a strain energy function to model a fiber-reinforced material according to

$$\Psi = \frac{\mu}{2}(I_1 - 3) + \frac{k_1}{k_2}\left\{\exp[k_2(I_4 - 1)^2] - 1\right\}. \tag{3.81}$$

Here the parameters μ, k_1 and k_2 come from the Neo–Hookean model (3.77) and the Fung model (3.80), respectively. To guarantee a stiffening in fiber direction, as observed in the histology of the arterial wall, we set $k_1 > 0$ and $k_2 > 0$. The shear modulus μ is positive by definition, cf. (3.77). $I_4 > 1$ is an invariant and can be seen as the stretch in fiber direction. This proposal gives rise to the well known artery model of Holzapfel et al. [63] which will be treated in the next section.

3.12. A Multi-Layer Model for Arterial Walls

In this section a potential is discussed that models each layer of the artery as a fiber-reinforced composite. The anisotropic model was first proposed in [63, Holzapfel et al. (2000)]. The reader is also referred to [64, Holzapfel et al. (2004)] and [66, Holzapfel and Ogden (2010)] for a more detailed discussion of arterial models. Recent issues like modeling with respect to residual stresses is neglected in this work but is discussed in [67, Holzapfel and Ogden (2010)].

Since the artery is a nearly incompressible tissue the free-energy function is decoupled into a purely volumetric and a purely isochoric contribution

$$\Psi(\mathsf{C}, \mathsf{A}_1, \dots, \mathsf{A}_n) = \underbrace{U(J)}_{\text{volumetric}} + \underbrace{\overline{\Psi}(\overline{\mathsf{C}}, \mathsf{A}_1, \dots, \mathsf{A}_n)}_{\text{isochoric}}, \tag{3.82}$$

with $\mathsf{C} = J^{-2/3}\overline{\mathsf{C}}$, $\det(\overline{\mathsf{C}}) = 1$ and the Jacobian $J = \det(\mathsf{F})$, see Sect. 3.1.

The set $\{\mathsf{A}_\alpha \mid \alpha = 1, \dots, n\}$ of second order tensors is employed to describe the hyper-elastic stress response of anisotropic biological tissues. In case of arterial walls, where we have an anisotropy due to collagen bundles with two main directions $\boldsymbol{a}_{01}, \boldsymbol{a}_{02}$, two such structure tensors are incorporated. These are defined as the cross product of the two reference direction vectors

$$\mathsf{A}_i := \boldsymbol{a}_{0i} \otimes \boldsymbol{a}_{0i}, \quad \text{with } |\boldsymbol{a}_{0i}| = 1 \text{ for } i = 1, 2. \tag{3.83}$$

From this definition it is clear that A_1 and A_2 are both symmetric.

A second split of the isochoric strain-energy function $\overline{\Psi}$ into an isotropic part $\overline{\Psi}_{\text{iso}}$ and an anisotropic part $\overline{\Psi}_{\text{aniso}}$ leads to the following response function

$$\overline{\Psi}(\overline{\mathsf{C}}, \mathsf{A}_1, \mathsf{A}_2) = \overline{\Psi}_{\text{iso}}(\overline{\mathsf{C}}) + \overline{\Psi}_{\text{aniso}}(\overline{\mathsf{C}}, \mathsf{A}_1, \mathsf{A}_2). \tag{3.84}$$

A two-term potential of that type was already proposed in [69, Holzapfel and Weizsäcker (1998)]. In formula (3.84) the isotropic part is associated with the non-collagenous ground substance elastin and $\overline{\Psi}_{\text{aniso}}$ is associated with anisotropic deformations arising from the collagen fibers.

To formulate the strain energy function in terms of invariants we need the integrity basis of $\overline{\mathsf{C}}, \mathsf{A}_1, \mathsf{A}_2$. According to [63, Holzapfel et al. (2000)] and [144, Spencer(1984)]) this basis consists of the following nine invariants

$$\begin{aligned}
&\overline{I}_1(\overline{\mathsf{C}}) = \operatorname{tr}\overline{\mathsf{C}}, && \overline{I}_2(\overline{\mathsf{C}}) = \frac{1}{2}\left((\operatorname{tr}\overline{\mathsf{C}})^2 - \operatorname{tr}\overline{\mathsf{C}}^2\right), && \overline{I}_3(\overline{\mathsf{C}}) = \det\overline{\mathsf{C}} = 1,\\
&\overline{I}_4(\overline{\mathsf{C}}, \mathsf{A}_1) = \overline{\mathsf{C}} : \mathsf{A}_1, && \overline{I}_5(\overline{\mathsf{C}}, \mathsf{A}_1) = \overline{\mathsf{C}}^2 : \mathsf{A}_1, && \overline{I}_6(\overline{\mathsf{C}}, \mathsf{A}_2) = \overline{\mathsf{C}} : \mathsf{A}_2,\\
&\overline{I}_7(\overline{\mathsf{C}}, \mathsf{A}_2) = \overline{\mathsf{C}}^2 : \mathsf{A}_2, && \overline{I}_8(\overline{\mathsf{C}}, \mathsf{A}_1, \mathsf{A}_2) = (\boldsymbol{a}_{01} \cdot \boldsymbol{a}_{02})\, \boldsymbol{a}_{01} \cdot \overline{\mathsf{C}}\boldsymbol{a}_{02}, && \overline{I}_9(\overline{\mathsf{C}}, \mathsf{A}_1, \mathsf{A}_2) = (\boldsymbol{a}_{01} \cdot \boldsymbol{a}_{02})^2.
\end{aligned}$$

The invariants $\overline{I}_3$ and $\overline{I}_9$ are omitted since they are constants. The invariants $\overline{I}_4$ and $\overline{I}_6$ have a clear physical interpretation: they are the squares of the stretches in the directions of $\boldsymbol{a}_{01}$ and $\boldsymbol{a}_{02}$ respectively, so that they are stretch measures for the two families of fibers.

To ease the fitting to experimental data, the number of material parameters should be reduced. When using the classical Neo–Hookean model for the isotropic response we can leave the second invariant $\overline{I}_2$ out:

$$\overline{\Psi}_{\text{iso}}(\overline{I}_1) = \frac{c}{2}(\overline{I}_1 - 3), \tag{3.85}$$

where $c > 0$ is a stress-like material parameter (cf. Sect. 3.11.1). Since $\overline{I}_4$ and $\overline{I}_5$ describe both similar physical properties the latter invariant is omitted. If the same is done for the second fiber direction and interactions ($\overline{I}_8$) between the two fiber families are neglected, we have the reduced model

$$\overline{\Psi}(\overline{\mathsf{C}}) = \overline{\Psi}_{\text{iso}}(\overline{I}_1) + \overline{\Psi}_{\text{aniso}}(\overline{I}_4, \overline{I}_6). \tag{3.86}$$

Holzapfel et al. [63] now propose for the anisotropic part of this strain energy

$$\overline{\Psi}_{\text{aniso}}(\overline{I}_4, \overline{I}_6) = \frac{k_1}{2k_2} \sum_{i=4,6} \left\{\exp[k_2(\overline{I}_i - 1)^2] - 1\right\}. \tag{3.87}$$

In summary we have the following strain energy function to model the anisotropic behavior of arterial walls

$$\Psi(\mathsf{C}) = \Psi(\overline{I}_1, \overline{I}_4, \overline{I}_6) = U(J) + \frac{c}{2}(\overline{I}_1 - 3) + \frac{k_1}{2k_2} \sum_{i=4,6} \left\{\exp[k_2(\overline{I}_i - 1)^2] - 1\right\}, \tag{3.88}$$

where

$$\overline{I}_1(\overline{\mathsf{C}}) = \operatorname{tr}\overline{\mathsf{C}}, \quad \overline{I}_4(\overline{\mathsf{C}}, \boldsymbol{a}_{01}) = \overline{\mathsf{C}} : \mathsf{A}_1, \quad \overline{I}_6(\overline{\mathsf{C}}, \boldsymbol{a}_{02}) = \overline{\mathsf{C}} : \mathsf{A}_2, \tag{3.89}$$

and all material parameters c, k_1 and k_2 are positive, see (3.81). To obtain these parameters they are fitted to the experimentally observed response of the arterial layers, i.e. they are to be determined from mechanical tests of the tissue.

An important condition in dealing with this model is that the anisotropic response $\overline{\Psi}_{\text{aniso}}$ only contributes if

$$\overline{I}_i > 1 \text{ for } i = 4, 6, \tag{3.90}$$

i.e. if there is a stretch in a fiber direction. This condition is explained with the wavy structure of the collagen fibers (see Fig. 2.2), which are hence regarded as not being able to support compressive stresses. Thus the fibers are assumed to be active in extension ($\overline{I}_i > 1$) and inactive in compression ($\overline{I}_i < 1$). This assumption is not only based on physical reasons but it is also essential for reasons of stability, see [64, Holzapfel et al. (2004)].

Another consequence of the wavy structure of the collagen fibers is that they are not active at low pressures and if the material behaves isotropic. At high pressures the collagen fibers straighten and then they govern the resistance to stretch of the material. This behavior of collagen was already discussed in [125, Roach and Burton (1957)] and is fully covered by the artery model (3.88). The described strong stiffening effect at higher pressures also motivates the use of the exponential function in the anisotropic response of the strain energy Ψ.

3.12.1. The Artery Modeled as a Two-Layer Thick-Walled Tube

As already mentioned in Section 2.1, arteries are composed of three layers, the intima, the media and the adventitia. For the case of an healthy young artery the innermost layer, the intima, is not of mechanical interest. We model each of the remaining layers with a separate strain-energy function. We assume that the media as well as the adventitia respond with similar mechanical characteristics and therefore we use the same form of strain-energy functions. To capture the specifics of each layer we use different sets of material parameters.

Hence we can write the energy functions for the two-layer problem using the Holzapfel artery model (3.88) as

$$\begin{aligned}
\overline{\Psi}_{\text{med}} &= \frac{c_{\text{M}}}{2}(\overline{I}_1 - 3) + \frac{k_{1\text{M}}}{2k_{2\text{M}}} \sum_{i=4,6} \left\{ \exp[k_{2\text{M}}(\overline{I}_{i\text{M}} - 1)^2] - 1 \right\}, \\
\overline{\Psi}_{\text{adv}} &= \frac{c_{\text{A}}}{2}(\overline{I}_1 - 3) + \frac{k_{1\text{A}}}{2k_{2\text{A}}} \sum_{i=4,6} \left\{ \exp[k_{2\text{A}}(\overline{I}_{i\text{A}} - 1)^2] - 1 \right\}
\end{aligned} \tag{3.91}$$

for the media and adventitia, respectively.

The invariants used in this formulation are defined by

$$\overline{I}_{4\,j} = \mathsf{A}_{1j} : \overline{\mathsf{C}}, \quad \overline{I}_{6\,j} = \mathsf{A}_{2j} : \overline{\mathsf{C}}, \quad j = \mathrm{M}, \mathrm{A}, \tag{3.92}$$

with

$$\mathsf{A}_{1j} = \boldsymbol{a}_{01\,j} \otimes \boldsymbol{a}_{01\,j}, \quad \mathsf{A}_{2j} = \boldsymbol{a}_{02\,j} \otimes \boldsymbol{a}_{02\,j}.$$

If we regard the simplified configuration of an artery as a tube we can describe the components of the direction vectors in cylindrical polar coordinates. Hence the vectors $\boldsymbol{a}_{01\,j}$ and $\boldsymbol{a}_{02\,j}$ have, in matrix notation, the forms

$$[\boldsymbol{a}_{01\,j}] = \begin{pmatrix} 0 \\ \cos\,\beta_j \\ \sin\,\beta_j \end{pmatrix}, \quad [\boldsymbol{a}_{02\,j}] = \begin{pmatrix} 0 \\ \cos\,\beta_j \\ -\sin\,\beta_j \end{pmatrix}, \quad j = \mathrm{M}, \mathrm{A}, \tag{3.93}$$

where β_j are the angles between the collagen fibers and the circumferential direction for $j = \mathrm{M}, \mathrm{A}$. This angle is indicated in Fig. 3.3. There one can find exemplary values for the material and geometrical data for a carotid artery from a rabbit as well.

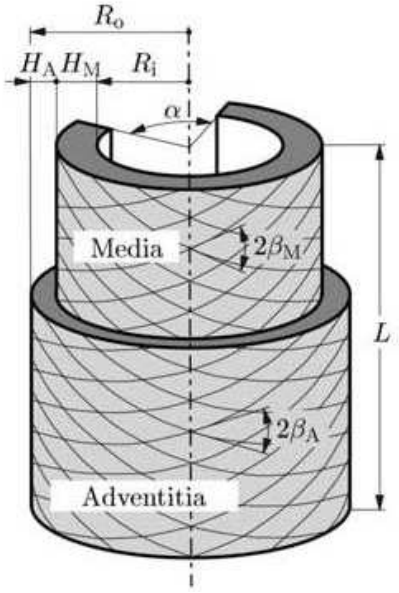

$R_i = 0.71$ [mm] for $\alpha = 0.0°$
$R_i = 1.43$ [mm] for $\alpha = 160.0°$

	Material	Geometry
Media	$c_\mathrm{M} = 3.0000$ [kPa] $k_{1\,\mathrm{M}} = 2.3632$ [kPa] $k_{2\,\mathrm{M}} = 0.8393$ [–]	$H_\mathrm{M} = 0.26$ [mm] $\beta_\mathrm{M} = 29.0°$
Adventitia	$c_\mathrm{A} = 0.3000$ [kPa] $k_{1\,\mathrm{A}} = 0.5620$ [kPa] $k_{2\,\mathrm{A}} = 0.7112$ [–]	$H_\mathrm{A} = 0.13$ [mm] $\beta_\mathrm{A} = 62.0°$

Figure 3.3. – Material parameters for a segment of a carotid artery from a rabbit (from [63, Holzapfel (2000)] using data from [23, Chuong and Fung (1983)]).

More experimental data and material and geometrical parameters fitted to the human aorta one may find in [61, Holzapfel (2006)].

3.12.2. Modeling with Respect to Fiber Dispersion

In Section 3.12.1 the existing dispersion of the collagen fibers is ignored. Nonetheless, this model works well for the media, where the collagen fibers are arranged in two helically distributed families with a small pitch and very little dispersion in their orientation. By contrast, in the adventitial and intimal layers the orientation of the collagen fibers is dispersed. Thus an additional measure of the dispersion of collagen fibers is proposed in [47, Gasser et al. (2006)] and [62, Holzapfel (2008)]. Both approaches are concerned with an extension of the model (3.87) to incorporate an isotropic behavior as a special case. In [62, Holzapfel (2008)] this is achieved by multiplying the anisotropic function $\exp[c_2(\overline{I}_i - 1)^2]$ with the isotropic function $\exp[c_1(\overline{I}_1 - 3)^2]$, where c_1, c_2 are two constants. This leads to

$$\overline{\Psi}_{\text{aniso}}(\overline{I}_1, \overline{I}_4, \overline{I}_6) = \frac{k_1}{2k_2} \sum_{i=4,6} \Big(\exp\{k_2[(1-\rho)(\overline{I}_1 - 3)^2 + \rho(\overline{I}_i - 1)^2]\} - 1 \Big) \tag{3.94}$$

with the dimensionless and stress-like parameters $k_2, k_1 > 0$ and a weighting factor $\rho \in [0, 1]$. For the limit $\rho = 1$ we get the anisotropic model (3.87), and for $\rho = 0$ an isotropic model is obtained. A similar model to the latter was already suggested by [33, Demiray (1972)].

Another approach was proposed by [47, Gasser et al. (2006)]. Therein an additional structure parameter ρ^* is introduced that characterizes the dispersed collagen orientation. As the first dispersion model (3.94) this is an extension to the anisotropic model (3.87):

$$\left.\begin{aligned} \overline{\Psi}_{\text{aniso}}(\overline{I}_1, \overline{I}_4, \overline{I}_6) &= \frac{k_1}{2k_2} \sum_{i=4,6} \Big\{ \exp[k_2(\overline{I}_i^* - 1)^2] - 1 \Big\}, \\ \text{with} \quad \overline{I}_i^* &= \rho^* \overline{I}_1 + (1 - 3\rho^*)\overline{I}_i. \end{aligned} \right\} \tag{3.95}$$

This modification of the forth and the sixth invariants enables the representation of the dispersion of the collagen fibers through the dispersion parameter $\rho^* \in [0, 1/3]$. For $\rho^* = 0$ the anisotropic model without dispersion (3.87) is obtained, the choice $\rho^* = 1/3$ leads to an isotropic distribution very similar to that proposed by [33, Demiray (1972)].

A more detailed overview concerning models with respect to fiber dispersion can be found in [62, Holzapfel (2008)].

3.12.3. Specific Representation Formulas of the Stress Tensors

In the following, we give specific representations of the stress tensors σ and S. For this we make use of the representation formulas (3.61) and (3.63) as derived in Section 3.9.2.

There we need the derivative of the isochoric strain energy function with respect to $\overline{\mathsf{C}}$. If we apply the chain rule we get

$$\frac{\partial\overline{\Psi}(\overline{\mathsf{C}})}{\partial\overline{\mathsf{C}}} = \frac{\partial\overline{\Psi}(\overline{I}_1,\overline{I}_4,\overline{I}_6)}{\partial\overline{\mathsf{C}}} = \frac{\partial\overline{\Psi}}{\partial\overline{I}_1}\frac{\partial\overline{I}_1}{\partial\overline{\mathsf{C}}} + \frac{\partial\overline{\Psi}}{\partial\overline{I}_4}\frac{\partial\overline{I}_4}{\partial\overline{\mathsf{C}}} + \frac{\partial\overline{\Psi}}{\partial\overline{I}_6}\frac{\partial\overline{I}_6}{\partial\overline{\mathsf{C}}}. \tag{3.96}$$

The derivative with respect to the invariants yields for the artery model (3.88)

$$\begin{aligned}
\frac{\partial\overline{\Psi}}{\partial\overline{I}_1} &= \frac{\partial\overline{\Psi}_{\text{iso}}}{\partial\overline{I}_1} = \frac{c}{2},\\
\frac{\partial\overline{\Psi}}{\partial\overline{I}_4} &= \frac{\partial\overline{\Psi}_{\text{aniso}}}{\partial\overline{I}_4} = k_1(\overline{I}_4-1)\exp[k_2(\overline{I}_4-1)^2],\\
\frac{\partial\overline{\Psi}}{\partial\overline{I}_6} &= \frac{\partial\overline{\Psi}_{\text{aniso}}}{\partial\overline{I}_6} = k_1(\overline{I}_6-1)\exp[k_2(\overline{I}_6-1)^2].
\end{aligned}$$

Using the chain rule we compute

$$\begin{aligned}
\frac{\partial\overline{I}_1}{\partial\overline{\mathsf{C}}} &= \frac{\partial\,\mathrm{tr}\,\overline{\mathsf{C}}}{\partial\overline{\mathsf{C}}} = \frac{\partial(\mathsf{I}:\overline{\mathsf{C}})}{\partial\overline{\mathsf{C}}} = \mathsf{I},\\
\frac{\partial\overline{I}_4}{\partial\overline{\mathsf{C}}} &= \frac{\partial(\overline{\mathsf{C}}:\mathsf{A}_1)}{\partial\overline{\mathsf{C}}} = \mathsf{A}_1 : \frac{\partial\overline{\mathsf{C}}}{\partial\overline{\mathsf{C}}} = \mathsf{A}_1 : \mathbb{I} = \mathsf{A}_1,\\
\frac{\partial\overline{I}_6}{\partial\overline{\mathsf{C}}} &= \frac{\partial(\overline{\mathsf{C}}:\mathsf{A}_2)}{\partial\overline{\mathsf{C}}} = \mathsf{A}_2 : \frac{\partial\overline{\mathsf{C}}}{\partial\overline{\mathsf{C}}} = \mathsf{A}_2 : \mathbb{I} = \mathsf{A}_2.
\end{aligned}$$

Combining the above results leads to

$$\frac{\partial\overline{\Psi}(\overline{\mathsf{C}})}{\partial\overline{\mathsf{C}}} = \frac{c}{2}\mathsf{I} + k_1(\overline{I}_4-1)\exp[k_2(\overline{I}_4-1)^2]\mathsf{A}_1 + k_1(\overline{I}_6-1)\exp[k_2(\overline{I}_6-1)^2]\mathsf{A}_2. \tag{3.97}$$

Hence we obtain for the isochoric part of the Cauchy stress tensor

$$\sigma_{\text{iso}} = J^{-1}\,\mathrm{dev}\left(c\,\overline{\mathsf{B}} + 2k_1\sum_{i=4,6}\overline{\mathsf{F}}(\overline{I}_i-1)\exp[k_2(\overline{I}_i-1)^2]\mathsf{A}_i\overline{\mathsf{F}}^{\top}\right), \tag{3.98}$$

with $\overline{\mathsf{B}} = \overline{\mathsf{F}}\,\overline{\mathsf{F}}^{\top}$. We can simplify this formula with the definition of the direction vectors in the current configuration, $\boldsymbol{a}_1$ and $\boldsymbol{a}_2$. These are calculated by a push-forward operation of the contravariant direction vector fields in the reference configuration, $\boldsymbol{a}_{01}$ and $\boldsymbol{a}_{02}$, by

$$\boldsymbol{a}_1 := \overline{\mathsf{F}}\boldsymbol{a}_{01}, \quad \boldsymbol{a}_2 := \overline{\mathsf{F}}\boldsymbol{a}_{02}. \tag{3.99}$$

With this definition we can state that

$$\overline{\mathsf{F}}\mathsf{A}_1\overline{\mathsf{F}}^{\top} = \boldsymbol{a}_1\otimes\boldsymbol{a}_1, \quad \overline{\mathsf{F}}\mathsf{A}_2\overline{\mathsf{F}}^{\top} = \boldsymbol{a}_2\otimes\boldsymbol{a}_2, \tag{3.100}$$

since

$$\overline{\mathsf{F}}\mathsf{A}_i\overline{\mathsf{F}}^{\top} = \overline{\mathsf{F}}(\boldsymbol{a}_{0i}\otimes\boldsymbol{a}_{0i})\overline{\mathsf{F}}^{\top} = (\overline{\mathsf{F}}\boldsymbol{a}_{0i})\otimes(\overline{\mathsf{F}}\mathsf{a}_{0i}).$$

Thus the isochoric Cauchy stress tensor is

$$\sigma_{\text{iso}} = J^{-1} c\,\mathrm{dev}(\overline{\mathsf{B}}) + 2k_1 J^{-1} \sum_{i=4,6} (\overline{I}_i - 1) \exp[k_2(\overline{I}_i - 1)^2]\,\mathrm{dev}(\boldsymbol{a}_i \otimes \boldsymbol{a}_i).$$

By Theorem 3.6 we finally obtain with σ_{iso} from above the explicit representation for the Cauchy stress tensor σ in the current configuration:

$$\sigma = p\mathsf{I} + cJ^{-1}\,\mathrm{dev}(\overline{\mathsf{B}}) + 2k_1 J^{-1} \sum_{i=4,6} (\overline{I}_i - 1) \exp[k_2(\overline{I}_i - 1)^2]\,\mathrm{dev}(\boldsymbol{a}_i \otimes \boldsymbol{a}_i). \tag{3.101}$$

In a similar manner the representation form for the second Piola–Kirchhoff stress tensor S in the reference configuration is obtained via Corollary 3.3:

$$\mathsf{S} = Jp\mathsf{C}^{-1} + cJ^{-2/3}\,\mathrm{Dev}(\mathsf{I}) + 2k_1 J^{-2/3} \sum_{i=4,6} (\overline{I}_i - 1) \exp[k_2(\overline{I}_i - 1)^2]\,\mathrm{Dev}(\boldsymbol{a}_{0i} \otimes \boldsymbol{a}_{0i}). \tag{3.102}$$

Considering the artery models with respect to fiber dispersion the procedure of calculating a representation formula for the stress tensors stays the same, just the derivatives of the strain energy function with respect to the invariants change a bit.

3.13. Modeling of Passive Myocardium

The model of the myocardium that is discussed in this section was introduced by Holzapfel and Ogden in [65, Holzapfel and Ogden (2009)]. In the derivation of a form for the strain energy function Ψ for the cardiac tissue we mainly stick to the descriptions of this paper. Nonetheless there exist other constitutive models of the myocardium. The interested reader is referred to the early works of [156, Yin (1981)] and [75, Humphrey and Yin (1987)]. Other strain energy functions were proposed by [26, Costa et al. (2001)] and [133, 134, Schmid et al. (2006, 2008)].

As discussed in Section 2.4 we have a layered organization of the muscle fibers within the myocardium which can be described by a right-handed orthonormal set of basis vectors $\boldsymbol{f}_0$, $\boldsymbol{s}_0$ and $\boldsymbol{n}_0$. Hence we can write the strain energy function as

$$\Psi = \Psi(\mathsf{C}, \mathsf{A}_f, \mathsf{A}_s, \mathsf{A}_n). \tag{3.103}$$

As done in Section 3.12 we need the integrity basis of the involved four tensors to formulate the strain energy function in terms of invariants. In the following only the most important invariants are mentioned, see [144, Spencer (1984)] for more details. For the isotropic part of the strain energy function we have the invariants as described in Corollary 3.4. The invariants associated with the fiber, sheet and sheet-normal direction are defined as

$$I_{4f} := \boldsymbol{f}_0 \cdot (\mathsf{C}\boldsymbol{f}_0), \quad I_{4s} := \boldsymbol{s}_0 \cdot (\mathsf{C}\boldsymbol{s}_0) \;\text{ and }\; I_{4n} := \boldsymbol{n}_0 \cdot (\mathsf{C}\boldsymbol{n}_0). \tag{3.104}$$

Due to the fact that the three direction vectors are orthonormal, we can state

$$\sum_{i=f,s,n} I_{4i} = \mathsf{C} : (\boldsymbol{f}_0 \otimes \boldsymbol{f}_0 + \boldsymbol{s}_0 \otimes \boldsymbol{s}_0 + \boldsymbol{n}_0 \otimes \boldsymbol{n}_0) = \mathsf{C} : \mathsf{I} = I_1, \tag{3.105}$$

hence only three of these four invariants are independent.

Next we mention coupling invariants associated with the pairs of directions

$$I_{8fs} = I_{8sf} := \boldsymbol{f}_0 \cdot (\mathsf{C}\boldsymbol{s}_0),\ I_{8fn} = I_{8nf} := \boldsymbol{f}_0 \cdot (\mathsf{C}\boldsymbol{n}_0),\ I_{8sn} = I_{8ns} := \boldsymbol{s}_0 \cdot (\mathsf{C}\boldsymbol{n}_0). \tag{3.106}$$

The invariants

$$I_{5f} := \boldsymbol{f}_0 \cdot (\mathsf{C}^2\boldsymbol{f}_0), \quad I_{5s} := \boldsymbol{s}_0 \cdot (\mathsf{C}^2\boldsymbol{s}_0) \ \text{ and } \ I_{5n} := \boldsymbol{n}_0 \cdot (\mathsf{C}^2\boldsymbol{n}_0) \tag{3.107}$$

are expressible in terms of the other invariants and the orthogonality reduces the number by an additional one (for more details cf. [65, Holzapfel and Ogden (2009)]).

In total we end up with seven independent invariants and we can write the most general form of the free energy function as

$$\Psi = \Psi(I_1,\ I_3,\ I_{4f},\ I_{4s},\ I_{8fn},\ I_{8fs},\ I_{8sn}) \tag{3.108}$$

for a compressible material. For an incompressible material we can state that $I_3 = 1$ and hence we have only six independent invariants.

To reduce the number of invariants and hence the number of material parameters we discuss the interpretations of the invariants. To model the isotropic response of the underlying matrix-material we could use the Neo–Hookean model (3.85) as in the case of arteries. Holzapfel and Ogden proposed in the case of the myocardium the following exponential model, introduced by [33, Demiray (1972)],

$$\Psi_{\text{iso}} = \frac{a}{2b} \exp\left[b(I_1 - 3)\right], \tag{3.109}$$

where $a > 0$ is a stress-like and b a dimensionless material parameter. To guarantee that the stress response increases exponentially in the corresponding stretch we have to set $b > 0$. The requirement of a positive parameter a follows from the analysis of the strain energy function, see Lemma 4.23 for more details.

To model the transversely isotropic behavior and the stiffening effect in the muscle fiber direction $\boldsymbol{f}$ and in the collagen fiber direction $\boldsymbol{s}$ the same proposal with an exponential function as for the case of arterial walls is used; cf. (3.87). Thus we obtain for this part of the constitutive equation

$$\Psi_{\text{trans}}(I_{4f}, I_{4s}) = \frac{a_f}{2b_f} \Big\{\exp[b_f(I_{4f} - 1)^2] - 1\Big\} + \frac{a_s}{2b_s} \Big\{\exp[b_s(I_{4s} - 1)^2] - 1\Big\}, \tag{3.110}$$

where again this part only contributes if $I_{4f} > 1$ or $I_{4s} > 1$, i.e. we have a stretch in one of the fiber directions (cf. Fig. 3.4). All material parameters, the stress like a_i as well as the dimensionless b_i for $i = f, s$ are supposed to be positive. Using this setting of the parameters we guarantee a stiffening in fiber and sheet direction as observed in the histology of the myocardium.

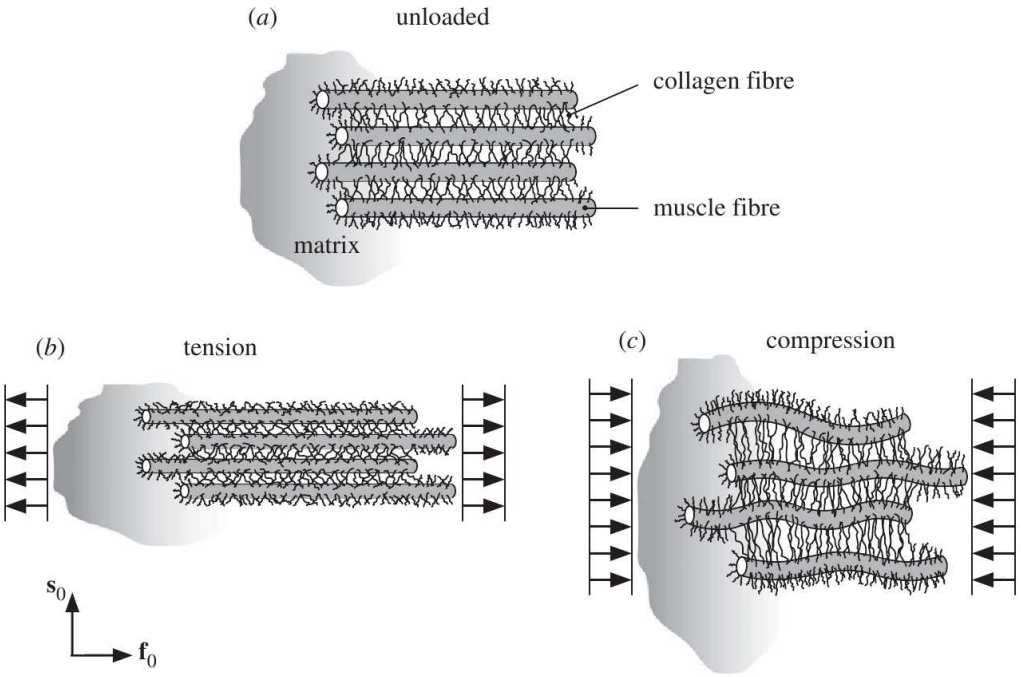

Figure 3.4. – Muscle and collagen fibers under tension and compression; $\boldsymbol{f}_0$ is the muscle fiber axis, $\boldsymbol{s}_0$ the sheet axis which corresponds to the direction of the collagen fibers. *(a)* unloaded configuration; *(b)* structure under tension in direction of $\boldsymbol{f}_0$ which results in a stretch of the muscle fibers; *(c)* compression is applied to the fiber network; this leads to a lateral extension of the collagen fibers while the myocytes are buckled (from [65, Holzapfel and Ogden 2009]).

Finally, the shear behavior as described in [36, Dokos et al. (2002)] and Section 2.4 is taken into consideration. Since the highest resistance was observed in the fs-plane and since it showed an exponential trend, Holzapfel and Ogden proposed to model this orthotropic part of the characterization in terms of the invariant I_{8fs} by

$$\Psi_{\text{ortho}}(I_{8fs}) = \frac{a_{fs}}{2b_{fs}} \left[\exp(b_{fs} I_{8fs}^2) - 1\right], \tag{3.111}$$

with $a_{fs} > 0$ a stress-like and $b_{fs} > 0$ a dimensionless material constant.

Summing up, we get the following strain energy function to model the passive myo-

cardium

$$\begin{aligned}\Psi(\mathsf{C}) = &\frac{a}{2b}\exp\left[b(I_1-3)\right] \\ &+ \sum_{i=f,s}\frac{a_i}{2b_i}\left\{\exp[b_i(I_{4i}-1)^2]-1\right\} + \frac{a_{fs}}{2b_{fs}}\left[\exp(b_{fs}I_{8fs}^2)-1\right].\end{aligned} \tag{3.112}$$

As discussed before, all of the eight material parameters are supposed to be positive and the transversely isotropic part only contributes if $I_{4f} > 1$ or $I_{4s} > 1$.

Using the constitutive equations for an incompressible material (3.51) and the chain rule of the form

$$\begin{aligned}\frac{\partial\Psi(\mathsf{C})}{\partial\mathsf{C}} &= \frac{\partial\Psi(I_1, I_{4f}, I_{4s}, I_{8fs})}{\partial\mathsf{C}} \\ &= \frac{\partial\Psi}{\partial I_1}\frac{\partial I_1}{\partial\mathsf{C}} + \frac{\partial\Psi}{\partial I_{4f}}\frac{\partial I_{4f}}{\partial\mathsf{C}} + \frac{\partial\Psi}{\partial I_{4s}}\frac{\partial I_{4s}}{\partial\mathsf{C}} + \frac{\partial\Psi}{\partial I_{8fs}}\frac{\partial I_{8fs}}{\partial\mathsf{C}}\end{aligned} \tag{3.113}$$

we get for the second Piola–Kirchhoff stress tensor

$$\begin{aligned}\mathsf{S} = &-p\mathsf{C}^{-1} + a\,\exp\left[b(I_1-3)\right]\mathsf{I} + 2a_f(I_{4f}-1)\exp[b_f(I_{4f}-1)^2]\boldsymbol{f}_0\otimes\boldsymbol{f}_0 \\ &+ 2a_s(I_{4s}-1)\exp[b_s(I_{4s}-1)^2]\boldsymbol{s}_0\otimes\boldsymbol{s}_0 \\ &+ a_{fs}I_{8fs}\exp(b_{fs}I_{8fs}^2)(\boldsymbol{f}_0\otimes\boldsymbol{s}_0 + \boldsymbol{s}_0\otimes\boldsymbol{f}_0).\end{aligned} \tag{3.114}$$

To get a representation for the Cauchy stress tensor as well we first introduce for the direction vectors in the current configuration the notation

$$\boldsymbol{f} := \mathsf{F}\boldsymbol{f}_0, \quad \boldsymbol{s} := \mathsf{F}\boldsymbol{s}_0. \tag{3.115}$$

By this and (3.26) we can express the Cauchy stress tensor in terms of the invariants as

$$\begin{aligned}\sigma = &-p\mathsf{I} + a\,\exp\left[b(I_1-3)\right]\mathsf{B} + 2a_f(I_{4f}-1)\exp[b_f(I_{4f}-1)^2]\boldsymbol{f}\otimes\boldsymbol{f} \\ &+ 2a_s(I_{4s}-1)\exp[b_s(I_{4s}-1)^2]\boldsymbol{s}\otimes\boldsymbol{s} \\ &+ a_{fs}I_{8fs}\exp(b_{fs}I_{8fs}^2)(\boldsymbol{f}\otimes\boldsymbol{s} + \boldsymbol{s}\otimes\boldsymbol{f}).\end{aligned} \tag{3.116}$$

To formulate the myocardium model in the form proposed in Section 3.9.2 we set

$$\Psi(\mathsf{C}) = U(J) + \overline{\Psi}(\overline{\mathsf{C}}) = U(J) + \overline{\Psi}_{\text{iso}}(\overline{I}_1) + \overline{\Psi}_{\text{trans}}(\overline{I}_{4\,f}, \overline{I}_{4\,s}) + \overline{\Psi}_{\text{ortho}}(\overline{I}_{8\,fs}), \tag{3.117}$$

where for the volumetric part we use

$$U(J) = \frac{\kappa}{2}\ln(J)^2 \tag{3.118}$$

as in [38, Eriksson et al. (2012)]. The expressions for the isotropic part (3.109), the transversely isotropic part (3.110) and the orthotropic part (3.111) stay the same,

except that the invariants are calculated only with the isochoric part of the Cauchy–Green strain tensor:

$$\overline{I}_1 := \mathrm{tr}(\overline{\mathsf{C}}), \quad \overline{I}_{4\,f} := \boldsymbol{f}_0 \cdot (\overline{\mathsf{C}}\boldsymbol{f}_0), \quad \overline{I}_{4\,s} := \boldsymbol{s}_0 \cdot (\overline{\mathsf{C}}\boldsymbol{s}_0), \quad \overline{I}_{8\,fs} := \boldsymbol{f}_0 \cdot (\overline{\mathsf{C}}\boldsymbol{s}_0). \tag{3.119}$$

This formulation leads to the stress tensors

$$\begin{aligned}\sigma = p\mathsf{I} + 2J^{-1}[\overline{\psi}_1 \,\mathrm{dev}(\overline{\mathsf{B}}) + \overline{\psi}_{4\,f} \,\mathrm{dev}(\overline{\boldsymbol{f}} \otimes \overline{\boldsymbol{f}}) + \overline{\psi}_{4\,s} \,\mathrm{dev}(\overline{\boldsymbol{s}} \otimes \overline{\boldsymbol{s}})] \\ + J^{-1}\overline{\phi}_{8\,fs} \,\mathrm{dev}(\overline{\boldsymbol{f}} \otimes \overline{\boldsymbol{s}} + \overline{\boldsymbol{s}} \otimes \overline{\boldsymbol{f}})\end{aligned} \tag{3.120}$$

in the reference configuration with

$$\overline{\boldsymbol{f}} = \overline{\mathsf{F}}\boldsymbol{f}_0, \quad \overline{\boldsymbol{s}} = \overline{\mathsf{F}}\boldsymbol{s}_0$$

and the derivatives with respect to the invariants

$$\overline{\psi}_i = \frac{\partial \Psi}{\partial \overline{I}_i}, \quad \text{for } i = 1, 4\,f, 4\,s, 8\,fs, \tag{3.121}$$

which are

$$\begin{aligned}\overline{\psi}_1 &= \frac{a}{2}\exp\left[b(\overline{I}_1 - 3)\right], & \overline{\psi}_{4\,f} &= a_f(\overline{I}_{4\,f} - 1)\exp\left[b_f(\overline{I}_{4\,f} - 1)^2\right], \\ \overline{\psi}_{4\,s} &= a_s(\overline{I}_{4\,s} - 1)\exp\left[b_s(\overline{I}_{4\,s} - 1)^2\right], & \overline{\psi}_{8\,fs} &= a_{fs}\overline{I}_{8\,fs}\exp\left[b_{fs}\overline{I}_{8\,fs}^2\right].\end{aligned}$$

The stress tensor in the reference configuration reads

$$\begin{aligned}\mathsf{S} = Jp\mathsf{C}^{-1} + 2J^{-2/3}[\overline{\psi}_1 \,\mathrm{Dev}(\mathsf{I}) + \overline{\psi}_{4\,f} \,\mathrm{Dev}(\boldsymbol{f}_0 \otimes \boldsymbol{f}_0) + \overline{\psi}_{4\,s} \,\mathrm{Dev}(\boldsymbol{s}_0 \otimes \boldsymbol{s}_0)] \\ + J^{-2/3}\overline{\psi}_{8\,fs} \,\mathrm{Dev}(\boldsymbol{f}_0 \otimes \boldsymbol{s}_0 + \boldsymbol{s}_0 \otimes \boldsymbol{f}_0).\end{aligned} \tag{3.122}$$

3.14. Elasticity Tensor

This section follows [59, Holzapfel (2000)] and [60, Holzapfel (2003)]. We provide an explicit symbolic expression for the so-called elasticity tensor $\mathbb{C}$. This will later be used to calculate a linearized form of the constitutive equation which we need for the application of Newton's method (cf. Sect. 4.4.1 ff.).

First, we postulate the existence of an energy function $\Psi(\mathsf{C})$.

Definition 3.12 (Elasticity Tensor). *The elasticity tensor $\mathbb{C}$ in the reference configuration is defined as the gradient of the nonlinear tensor-valued stress tensor S as*

$$\mathbb{C} := \frac{\mathsf{S}(\mathsf{E})}{\partial \mathsf{E}} = 2\frac{\partial \mathsf{S}(\mathsf{C})}{\partial \mathsf{C}} = 4\frac{\partial^2 \Psi(\mathsf{C})}{\partial \mathsf{C}^2}. \tag{3.123}$$

It measures the change in stress which is evoked through a change of strain.

Definition 3.13 (Elasticity tensor in spatial description). *The elasticity tensor in the spatial description, denoted by* $\mathbb{c}$ *is defined as the push-forward operation of* $\mathbb{C}$ *times a factor of* J^{-1}

$$c_{ijkl} = J^{-1} F_{ia} F_{jb} F_{kc} F_{le} C_{abcd}. \tag{3.124}$$

Remark 3.14.1 (Symmetry Properties). *The elasticity tensor* $\mathbb{C}$ *possesses minor symmetries in the following way*

$$C_{abcd} = C_{bacd} = C_{abdc}.$$

Using $(3.123)_3$*, we can show the major symmetries*

$$C_{abcd} = C_{cdab}.$$

This property holds for the elasticity tensor $\mathbb{c}$ *in Eulerian description as well, cf. [59, Holzapfel (2000), Ch. 6.6]).*

Remark 3.14.2 (Voigt notation). *A forth-order tensor* $\mathbb{C}$*, with the entries* C_{abcd} *for* $a, b, c, d = 1, 2, 3$*, satisfying minor symmetries may be represented as a* 6×6 *matrix* $\mathcal{C}$ *with* 36 *distinctive components. If additionally* $\mathbb{C}$ *is satisfying major symmetries then* $\mathcal{C}$ *is symmetric and has* 21 *distinctive components. It is written as*

$$\mathcal{C} = \begin{pmatrix} C_{1111} & C_{1122} & C_{1133} & C_{1112} & C_{1123} & C_{1113} \\ . & C_{2222} & C_{2233} & C_{2212} & C_{2223} & C_{2213} \\ . & . & C_{3333} & C_{3312} & C_{3323} & C_{3313} \\ . & . & . & C_{1212} & C_{1223} & C_{1213} \\ . & sym. & . & . & C_{2323} & C_{2313} \\ . & . & . & . & . & C_{1313} \end{pmatrix}.$$

Remark 3.14.3 (Positive definiteness). *For strict local strain energy functions* Ψ*, cf. Sect. 4.4.8, the elasticity tensor* C *and its representation in Voigt notation* $\mathcal{C}$ *are positive definite, cf. [63, Holzapfel (2000)], [112, Ogden (1997), Sect. 6.2]. This is a fundamental physical requirement that prevents material instabilities.*

In decoupled form we can write $\mathbb{C}$ as

$$\mathbb{C} = \mathbb{C}_{\text{vol}} + \mathbb{C}_{\text{iso}} \tag{3.125}$$

with the explicit expressions

$$\mathbb{C}_{\text{vol}} = 2\frac{\partial \mathsf{S}_{\text{vol}}(\mathsf{C})}{\partial \mathsf{C}} = 2\frac{\partial (Jp\mathsf{C}^{-1})}{\partial \mathsf{C}} \tag{3.126}$$

and

$$\mathbb{C}_{\text{iso}} = 2\frac{\partial \mathsf{S}_{\text{iso}}(\mathsf{C})}{\partial \mathsf{C}}. \tag{3.127}$$

Remark 3.14.4. *In Eulerian description the volumetric part of the elasticity tensor reduces to*

$$\mathbb{c}_{\text{vol}} = \left(p + J\frac{\mathrm{d}p}{\mathrm{d}J}\right)\mathsf{I}\otimes\mathsf{I} - 2p\mathbb{I}, \tag{3.128}$$

cf. [59, Holzapfel (2000), Ch. 6.6].

Corollary 3.6. *For the isochoric part of the elasticity tensor the following holds*

$$\mathbb{C}_{iso} = \mathbb{P} : \mathbb{C}^* : \mathbb{P}^\top + \frac{2}{3}(J^{-2/3}\mathsf{S}^* : \mathsf{C})\tilde{\mathbb{P}} - \frac{2}{3}\left(\mathsf{C}^{-1}\otimes\mathsf{S}_{iso} - \mathsf{S}_{iso}\otimes\mathsf{C}^{-1}\right). \tag{3.129}$$

The tensors involved in this equation are the isotropic part of the stress tensor in the reference configuration as described in Corollary 3.3, and the fictitious stress and elasticity tensors

$$\mathsf{S}^* = 2\frac{\partial\Psi_{iso}(\overline{\mathsf{C}})}{\partial\overline{\mathsf{C}}}, \quad \mathbb{C}^* = 2J^{-4/3}\frac{\partial\mathsf{S}^*}{\partial\overline{\mathsf{C}}} = 4J^{-4/3}\frac{\partial^2\Psi_{iso}(\overline{\mathsf{C}})}{\partial\overline{\mathsf{C}}^2}. \tag{3.130}$$

Moreover we have the forth-order projection tensor $\mathbb{P}^\top$ and the modified projection tensor $\tilde{\mathbb{P}}$ given by

$$\mathbb{P}^\top := \left(\mathbb{I} - \frac{1}{3}\mathsf{C}\otimes\mathsf{C}^{-1}\right), \quad \tilde{\mathbb{P}} = \mathsf{C}^{-1}\odot\mathsf{C}^{-1} - \frac{1}{3}\mathsf{C}^{-1}\otimes\mathsf{C}^{-1}, \tag{3.131}$$

where the tensor product $\odot$ is defined as

$$\left(\mathsf{C}^{-1}\odot\mathsf{C}^{-1}\right)_{ABCD} = \frac{1}{2}(C^{-1}_{AC}C^{-1}_{BD} + C^{-1}_{AD}C^{-1}_{BC}). \tag{3.132}$$

Proof. For the proof cf. [59, Holzapfel (2000), Example 6.8]. □

We still need a symbolic expression of the fictitious stress tensor S^* and elasticity tensor $\mathbb{C}^*$ which depend on the free energy function of the considered material. In the following, we give a representation of these tensors for the materials we will later deal with in the numerical analysis.

Incompressible Neo–Hookean Model: With the representation formulas in (3.130) one can easily see that

$$\mathsf{S}^* = c\mathsf{I}, \quad \mathbb{C}^* = \mathsf{0}. \tag{3.133}$$

Artery Model: For the modeling of the almost incompressible artery wall we can retrieve the desired tensors using (3.97) which leads to

$$\mathsf{S}^* = c\mathsf{I} + 2k_1 \sum_{i=4,6} (I_i - 1) \exp[k_2(I_i - 1)^2]\mathsf{A}_i, \tag{3.134}$$

and

$$\mathbb{C}^* = 4k_1 J^{-4/3} \sum_{i=4,6} (1 + 2k_2(\overline{I}_i - 1)^2) \exp[k_2(\overline{I}_i - 1)^2]\mathsf{A}_i^2. \tag{3.135}$$

Myocardium: For nearly incompressible cardiac tissue we obtain the tensors

$$\mathsf{S}^* = 2\overline{\psi}_1\mathsf{I} + 2\overline{\psi}_{4\,f}(\boldsymbol{f}_0 \otimes \boldsymbol{f}_0) + 2\overline{\psi}_{4\,s}(\boldsymbol{s}_0 \otimes \boldsymbol{s}_0) + \overline{\psi}_{8\,fs}(\boldsymbol{f}_0 \otimes \boldsymbol{s}_0 + \boldsymbol{s}_0 \otimes \boldsymbol{f}_0), \tag{3.136}$$

with $\overline{\psi}_i$, $i = 1, 4\,f, 4\,s, 8\,fs$ from (3.121), and

$$\begin{aligned} J^{4/3}\mathbb{C}^* = {} & 4b\,\overline{\psi}_1 + 4a_f(1 + 2b_f(\overline{I}_{4\,f} - 1)^2) \exp[b_f(\overline{I}_{4\,f} - 1)^2](\boldsymbol{f}_0 \otimes \boldsymbol{f}_0)^2 \\ & + 4a_s(1 + 2b_s(\overline{I}_{4\,s} - 1)^2) \exp[b_s(\overline{I}_{4\,s} - 1)^2](\boldsymbol{s}_0 \otimes \boldsymbol{s}_0)^2 \\ & + 2a_{fs}(1 + 2b_{fs}\overline{I}_{8\,fs}^2) \exp[b_{fs}\overline{I}_{8\,fs}^2](\boldsymbol{f}_0 \otimes \boldsymbol{s}_0 + \boldsymbol{s}_0 \otimes \boldsymbol{f}_0)^2. \end{aligned} \tag{3.137}$$

A more specific introduction to elasticity tensors one may find in [97, Marsden and Hughes (1994), Sect. 3] or [101, Miehe (1994)] and [102, Miehe and Stein (1992)].

4. Variational Formulation

In this chapter we will derive the variational formulation of the mixed boundary value problem as described in Section 3.6. This weak formulation will be the basis for the finite element method (FEM), cf. Section 5.1. In addition, we will also deal with the solvability of the models discussed in Chapter 3. We will see that for linear elasticity problems we can prove not only that there exists a solution, but also that this solution is unique. In contrast to this, it is not possible to give a similar statement for general nonlinear elasticity problems. Up to now there are no cogent arguments known that show uniqueness. At least we will give evidences when the resulting system is solvable. For more information on this topic refer to [14, Braess (2007)], [25, Ciarlet (1988)] and [29, Dacorogna (2008)].

For nonlinear problems, as for instance the tissue models discussed in Chapter 3, we have to apply Newton's method. This requires a linearization of the underlying variational formulation, cf. Section 4.4.3. A comprehensive monograph on Newton methods is [35, Deuflhard (2004)].

4.1. Preliminaries

In this section we present basic definitions and theorems that allow us to set up the theory of variational formulations. Definitions and tools to discuss the solvability of an abstract operator equation $Au = f$ are given. Finally, we introduce concepts for derivatives in Banach spaces, which will be used for the linearization of the nonlinear weak formulations.

Let X be a Hilbert space with the scalar product $\langle \cdot, \cdot \rangle_X$ and the corresponding induced norm $\|\cdot\|_X = \sqrt{\langle \cdot, \cdot \rangle_X}$. We denote by X' the dual space of X with the duality product $\langle \cdot, \cdot \rangle$ and with the norm

$$\|f\|_{X'} = \sup_{0 \neq v \in X} \frac{|\langle f, v \rangle|}{\|v\|_X} \quad \text{for all } f \in X'.$$

In the linear case we want to find the solution $u \in X$ of the *linear operator equation*

$$Au = f \tag{4.1}$$

with $A : X \to X'$ and $f \in X'$. Equivalent to this operator equation is the *variational formulation* to find $u \in X$, such that

$$\langle Au, v \rangle = \langle f, v \rangle \quad \text{for all } v \in X. \tag{4.2}$$

One can easily show that a solution of the variational formulation (4.2) is as well a solution of the operator equation (4.1), and vice versa.

The *bilinear form*

$$a(\cdot,\cdot) : X \times X \to \mathbb{R} \tag{4.3}$$

is induced by the operator $A : X \to X'$ through

$$a(u,v) := \langle Au, v\rangle \quad \text{for all } u, v \in X. \tag{4.4}$$

Definition 4.1 (boundedness). *The operator $A : X \to X'$ is called bounded if*

$$\|Av\|_{X'} \le c_2^A \|v\|_X \quad \textit{for all } v \in X$$

with a constant $c_2^A > 0$.

Definition 4.2 (X–ellipticity). *The operator A is called X–elliptic if*

$$\langle Av, v\rangle \ge c_1^A \|v\|_X^2 \quad \textit{for all } v \in X$$

with a constant $c_1^A > 0$

Theorem 4.3 (Lax–Milgram theorem). *Let the operator $A : X \to X'$ be bounded and X–elliptic. Then the operator equation $Au = f$ is uniquely solvable for every $f \in X'$. For the solution $u \in X$ it holds*

$$\|u\|_x \le \frac{1}{c_1^A} \|f\|_{X'}.$$

Proof. See, for example, [147, Steinbach (2008)] or [157, Yosida (1980]. □

Proposition 4.4 (Poincaré–Friedrich's inequality). *Let Ω be a subset of a cube in $\mathbb{R}^n$ with edge length c_F. Then*

$$\|v\|_{L_2(\Omega)} \le c_F |v|_{H^1(\Omega)} \quad \textit{for all } v \in H_0^1(\Omega).$$

Proof. Cf. [14, Braess (2007)]. □

From Proposition 4.4 it follows immediately that

$$\|\boldsymbol{v}\|^2_{[H^1(\Omega)]^3} \le (1 + c_F^2) |\boldsymbol{v}|^2_{[H^1(\Omega)]^d}, \quad \text{for all } \boldsymbol{v} \in [H_0^1(\Omega)]^3. \tag{4.5}$$

In the nonlinear case, we write in analogy to (4.1) the *nonlinear operator equation*

$$A(u) = f \tag{4.6}$$

with the equivalent variational formulation

$$\langle A(u), v\rangle = \langle f, v\rangle \quad \text{for all } v \in X. \tag{4.7}$$

For the linearization of the nonlinear variational formulations and the discussion of existence theorems, we need the following two definitions of derivatives in Banach spaces:

Definition 4.5 (Fréchet derivative). *Let X and Y be Banach spaces and G be an open subset of X. A function $f : G \subset X \to Y$ is called differentiable at $\xi \in G$, if there is a bounded linear operator $\Lambda : X \to Y$, such that for all $h \in X$*

$$f(\xi + h) - f(\xi) = \Lambda h + r(h) \quad \textit{with} \quad \lim_{h\to 0} \frac{r(h)}{\|h\|_X} = 0. \tag{4.8}$$

If the limit exists, then the uniquely defined operator Λ is called the Fréchet derivative of f at ξ and we denote it as $f'(\xi)$; e.g., cf. [56, Heuser (2008)].

Definition 4.6 (Gâteaux derivative). *Let X and Y be Banach spaces and G be an open subset of X. A function $f : X \to Y$ is called differentiable at $\xi \in G$ in the direction $h \in X$, if there is a bounded and linear operator $\Lambda : X \to Y$, such that*

$$\Lambda = \lim_{t\to 0} \frac{f(\xi + th) - f(\xi)}{t} \tag{4.9}$$

If the limit exists for every $h \in X$, then the operator Λ is called the Gâteaux derivative of f at ξ, and we denote it as $\Lambda = Df(\xi).h = f'_G(\xi)$; e.g., cf. [149, Tröltzsch (2010)].

Remark 4.1.1. *Every Fréchet differentiable function is Gâteaux differentiable and it holds*

$$f'(\xi) = f'_G(\xi).$$

With this we can calculate the particular Fréchet derivative using the definition of the Gâteaux derivative; e.g., cf. [149, Tröltzsch (2010)].

Remark 4.1.2 (Chain rule). *Let X, Y and Z be Banach spaces and $f : X \to Y$ and $g : V \to Z$ be Fréchet differentiable at ξ and $f(\xi)$, respectively, then*

$$e(\xi) = g(f(\xi))$$

is also Fréchet differentiable at ξ and

$$e'(\xi) = g'(f(\xi)) \circ f'(\xi);$$

e.g. cf. [76, Ioffe and Tichomirov (1979)].

In the following chapters, we consider $\Omega \subset \mathbb{R}^3$ and $\Omega_0 \subset \mathbb{R}^3$ to be open and bounded domains with Lipschitz-continuous boundaries $\partial\Omega = \Gamma$ and $\partial\Omega_0 = \Gamma_0$.

4.2. Variational Formulation for Elasticity Problems

First, we consider the classical formulation of the boundary value problem (3.30): given sufficiently smooth and continuous input data, find the displacement $\boldsymbol{u}$ such that

$$-\operatorname{div}\sigma(\boldsymbol{u},\boldsymbol{x}) = \boldsymbol{0} \quad \text{in } \Omega,$$

with the Dirichlet boundary conditions

$$\boldsymbol{u}(\boldsymbol{x}) = \boldsymbol{u}_D(\boldsymbol{x}) \quad \text{on } \Gamma_D,$$

and with the Neumann boundary conditions

$$\sigma(\boldsymbol{u},\boldsymbol{x})\boldsymbol{n}(\boldsymbol{x}) = \boldsymbol{t}_N(\boldsymbol{x}) \quad \text{on } \Gamma_N.$$

Let $\boldsymbol{u}$ be from some suitable space X with $\boldsymbol{u} = \boldsymbol{u}_D$ on Γ_D. Integration over Ω and multiplying component-wise with a test-function $\boldsymbol{v} \in X$ with $\boldsymbol{v} = \boldsymbol{0}$ on the Dirichlet boundary Γ_D leads to

$$\int_\Omega -\operatorname{div}\sigma(\boldsymbol{u},\boldsymbol{x}) \cdot \boldsymbol{v}(\boldsymbol{x}) \, \mathrm{d}\boldsymbol{x} = 0. \tag{4.10}$$

By using the identity, implied by the product rule,

$$\operatorname{div}\sigma \cdot \boldsymbol{v} = \operatorname{div}(\sigma\boldsymbol{v}) - \sigma : \operatorname{grad}\boldsymbol{v},$$

and the following formulation of the Gauss' divergence theorem

$$\int_\Omega \operatorname{div}(\sigma\boldsymbol{v}) \, \mathrm{d}\boldsymbol{x} = \int_\Gamma \boldsymbol{v} \cdot \sigma\boldsymbol{n} \, \mathrm{d}s_{\boldsymbol{x}},$$

equation (4.10) may be written as

$$\int_\Omega \sigma(\boldsymbol{u},\boldsymbol{x}) : \operatorname{grad}\boldsymbol{v}(\boldsymbol{x}) \, \mathrm{d}\boldsymbol{x} - \int_\Gamma \boldsymbol{v}(\boldsymbol{x}) \cdot \sigma\boldsymbol{n}(\boldsymbol{x}) \, \mathrm{d}s_{\boldsymbol{x}} = 0.$$

The symmetry of σ implies that

$$\sigma : \operatorname{grad}\boldsymbol{v} = \sigma : \frac{1}{2}\left(\operatorname{grad}\boldsymbol{v} + (\operatorname{grad}\boldsymbol{v})^\top\right) = \sigma : \varepsilon(\boldsymbol{v}). \tag{4.11}$$

With this and the fact that $\boldsymbol{v}$ vanishes on the part Γ_D of the boundary we may formulate the *weak form* of the *boundary-value problem* as

$$\int_\Omega \sigma(\boldsymbol{u},\boldsymbol{x}) : \varepsilon(\boldsymbol{v},\boldsymbol{x}) \, \mathrm{d}\boldsymbol{x} - \int_{\Gamma_N} \boldsymbol{t}_N(\boldsymbol{x}) \cdot \boldsymbol{v}(\boldsymbol{x}) \, \mathrm{d}s_{\boldsymbol{x}} = 0. \tag{4.12}$$

In summary, we get for the mixed boundary value problem with Dirichlet and Neumann boundary conditions the following variational formulation:
find $\boldsymbol{u} \in [H^1_D(\Omega, \Gamma_D)]^3 := \{\boldsymbol{u} \in [H^1(\Omega)]^3 : \boldsymbol{u} = \boldsymbol{u}_D \text{ on } \Gamma_D\}$ such that

$$\langle A(\boldsymbol{u}), \boldsymbol{v}\rangle = \langle \boldsymbol{f}, \boldsymbol{v}\rangle \tag{4.13}$$

for all test functions $\boldsymbol{v} \in [H^1_0(\Omega, \Gamma_D)]^3 := \{v \in [H^1(\Omega)]^3 : \boldsymbol{v} = \boldsymbol{0} \text{ on } \Gamma_D\}$ with

$$\langle A(\boldsymbol{u}), \boldsymbol{v}\rangle = \int_\Omega \sigma(\boldsymbol{u}, \boldsymbol{x}) : \varepsilon(\boldsymbol{v}, \boldsymbol{x})\, \mathrm{d}\boldsymbol{x} \tag{4.14}$$

and

$$\langle \boldsymbol{f}, \boldsymbol{v}\rangle = \int_{\Gamma_N} \boldsymbol{t}_N(\boldsymbol{x}) \cdot \boldsymbol{v}(\boldsymbol{x})\ \mathrm{d}s_{\boldsymbol{x}}. \tag{4.15}$$

In terms of the reference configuration we obtain, using similar procedures as above:
find $\boldsymbol{U} \in [H^1_D(\Omega_0, \Gamma_{0,D})]^3$ such that

$$\langle A(\boldsymbol{U}), \boldsymbol{V}\rangle := \int_{\Omega_0} \mathsf{FS}(\boldsymbol{U}, \boldsymbol{X}) : \operatorname{Grad} \boldsymbol{V}(\boldsymbol{X})\, \mathrm{d}\boldsymbol{X} = \langle \boldsymbol{f}, \boldsymbol{V}\rangle, \tag{4.16}$$

for all test functions $\boldsymbol{V} \in [H^1_0(\Omega_0, \Gamma_{0,D})]^3$. Note that the tensor FS is not necessarily symmetric.

Remark 4.2.1. *For a Neumann boundary value problem, i.e. $\Gamma = \Gamma_N$, we assume the following condition of solvability*

$$\int_\Omega \boldsymbol{r}_k(\boldsymbol{x})^\top \boldsymbol{f}(\boldsymbol{x})\, \mathrm{d}\boldsymbol{x} + \int_\Gamma \gamma_0^{int} \boldsymbol{r}_k(\boldsymbol{x})^\top \boldsymbol{t}_N(\boldsymbol{x})\, \mathrm{d}s_{\boldsymbol{x}} = 0 \quad \textit{for all } \boldsymbol{r}_k \in \mathcal{R}, \tag{4.17}$$

where $\boldsymbol{r}_k \in \mathcal{R}$ are the rigid body modes. In 3D we have

$$\mathcal{R} = \operatorname{span}\left\{ \begin{pmatrix}1\\0\\0\end{pmatrix}, \begin{pmatrix}0\\1\\0\end{pmatrix}, \begin{pmatrix}0\\0\\1\end{pmatrix}, \begin{pmatrix}-x_2\\x_1\\0\end{pmatrix}, \begin{pmatrix}0\\-x_3\\x_2\end{pmatrix}, \begin{pmatrix}x_3\\0\\-x_1\end{pmatrix} \right\}, \tag{4.18}$$

which describe rotations and translations of a rigid body.

4.3. Linear Elasticity

As mentioned before in Sect. 3.7, in the case of linear elasticity it is justified not to distinguish between the current and the reference configuration, since we are only considering small deformations. With Hooke's Law (3.35)

$$\sigma = \mathbb{C} : \varepsilon, \quad \sigma_{ij} = \sum_{kl} C_{ijkl}\varepsilon_{kl}, \quad C_{ijkl} = \lambda\delta_{ij}\delta_{kl} + \mu(\delta_{ik}\delta_{jl} + \delta_{il}\delta_{jk}),$$

we get the specific variational formulation for linear elasticity

$$\int_\Omega \mathbb{C}\,\varepsilon(\boldsymbol{u},\boldsymbol{x}) : \varepsilon(\boldsymbol{v},\boldsymbol{x})\,\mathrm{d}\boldsymbol{x} - \int_{\Gamma_N} \boldsymbol{t}_N(\boldsymbol{x})\cdot\boldsymbol{v}(\boldsymbol{x})\;\mathrm{d}s_{\boldsymbol{x}} = 0. \tag{4.19}$$

Hence, we write for the bilinear form

$$a(\boldsymbol{u},\boldsymbol{v}) = \int_\Omega \sum_{i,j,k,l=1}^{3} C_{ijkl}\,\varepsilon_{kl}(\boldsymbol{u},\boldsymbol{x}) : \varepsilon_{ij}(\boldsymbol{v},\boldsymbol{x})\,\mathrm{d}\boldsymbol{x} = \int_\Omega \mathsf{C}\,\varepsilon(\boldsymbol{u},\boldsymbol{x}) : \varepsilon(\boldsymbol{v},\boldsymbol{x})\,\mathrm{d}\boldsymbol{x}, \tag{4.20}$$

with C the constant elasticity tensor in Voigt notation.

To satisfy the conditions in the Lax–Milgram theorem 4.3 we need the famous Korn inequalities which were first formulated and named after Arthur Korn [89, Korn (1909)].

Lemma 4.7 (First Korn inequality). *For* $\boldsymbol{v} \in [H_0^1(\Omega,\Gamma_D)]^3$

$$\int_\Omega \sum_{i,j=1}^{3} [\varepsilon_{ij}(\boldsymbol{v},\boldsymbol{x})]^2\,\mathrm{d}\boldsymbol{x} \geq \frac{1}{2}|\boldsymbol{v}|^2_{H^1(\Omega)}.$$

Lemma 4.8 (Second Korn Inequality). *There exists a constant* $c = c(\Omega) > 0$ *such that*

$$\int_\Omega \sum_{i,j=1}^{3} [\varepsilon_{ij}(\boldsymbol{v},\boldsymbol{x})]^2\,\mathrm{d}\boldsymbol{x} + \|\boldsymbol{v}\|^2_{L_2(\Omega)} \geq c\|\boldsymbol{v}\|^2_{H^1(\Omega)}, \quad \textit{for all } \boldsymbol{v} \in [H^1(\Omega)]^3.$$

Proof. For proofs of these inequalities compare [108, Nitsche (1981)], [57, 58, Hlaváček and Nečas (1970)] and [147, Steinbach (2008)]. □

To fulfill the conditions of Theorem 4.3 (Lax–Milgram) the boundedness of the bilinear form (4.20) has to be shown. This is done via the following lemma:

Lemma 4.9 (Boundedness of the bilinear form). *For all* $\boldsymbol{u},\boldsymbol{v} \in [H^1(\Omega)]^3$ *it holds*

$$|a(\boldsymbol{u},\boldsymbol{v})| \leq \lambda_{max}(\mathsf{C})\,|\boldsymbol{u}|_{[H^1(\Omega)]^3}|\boldsymbol{v}|_{[H^1(\Omega)]^3}.$$

Proof. See, for example, [147, Steinbach (2008)]. □

To show $[H_0^1(\Omega,\Gamma_D)]^3$–ellipticity of the bilinear form (4.20) in the case that $\Gamma = \Gamma_D$ the first Korn inequality 4.7 is used. For all $\boldsymbol{v} \in [H_0^1(\Omega,\Gamma_D)]^3$ it holds

$$\begin{aligned} a(\boldsymbol{v},\boldsymbol{v}) &= \int_\Omega \mathsf{C}\varepsilon(\boldsymbol{v}.\boldsymbol{x}) : \varepsilon(\boldsymbol{v},\boldsymbol{x})\,\mathrm{d}\boldsymbol{x} \geq \lambda_{\min}(\mathsf{C}) \int_\Omega \sum_{i,j=1}^{3} [\varepsilon_{ij}(\boldsymbol{v},\boldsymbol{x})]^2\,\mathrm{d}\boldsymbol{x} \\ &\geq \lambda_{\min}(\mathsf{C})\frac{1}{2}|\boldsymbol{v}|^2_{[H^1(\Omega)]^3} \geq \lambda_{\min}(\mathsf{C})\frac{1}{2(1+c_F^2)}\|\boldsymbol{v}\|^2_{H^1(\Omega)}, \end{aligned}$$

where c_F denotes the constant from the Poincaré–Friedrich's inequality (4.5).

$[H_0^1(\Omega,\Gamma_D)]^3$–ellipticity for the mixed boundary value problem is shown using the second Korn inequality (Lemma 4.8), cf. [147, Steinbach (2008)].

We have shown boundedness and $[H_0^1(\Omega)]^3$–ellipticity for the Dirichlet and the mixed boundary value problem. With Theorem 4.3 the unique solvability of the linear elasticity problem follows.

For the Neumann boundary value problem with $\Gamma = \Gamma_N$ we assume the solvability conditions (4.17) and note that the solution is only unique up to the rigid body modes. These can be fixed using suitable scaling conditions. With the space

$$[H_*^1(\Omega)]^3 := \left\{ \boldsymbol{v} \in [H^1(\Omega)]^3 : \int_\Omega \boldsymbol{r}_k(\boldsymbol{x})^\top \boldsymbol{v}(\boldsymbol{x})\,\mathrm{d}x = 0 \text{ for all } \boldsymbol{r}_k \in \mathcal{R} \right\} \tag{4.21}$$

we can show $[H_*^1(\Omega)]^3$–ellipticity and hence unique solvability in $[H_*^1(\Omega)]^3$. For more information cf. [147, Steinbach (2008)].

4.3.1. Almost Incompressible Linear Materials

For almost incompressible materials it can happen that so-called *locking effects* occur. This means that the problem becomes very ill-conditioned and the calculated displacement field $\boldsymbol{u}$ is smaller than expected. For a more detailed exposition of locking effects the reader is referred to the works of [4, Arnold (1981)], [8, Babuška and Suri (1992)] and [14, Braess (2007), Ch. VI, § 4]. How to overcome these numerical difficulties is discussed in this section.

Without any loss of generality we can focus on homogeneous boundary conditions $\boldsymbol{u}_D = \boldsymbol{0}$. Furthermore, we introduce the spaces

$$\mathcal{X} := [H_0^1(\Omega,\Gamma_D)]^3, \quad \mathcal{M} := L_2(\Omega) := \{q \in L_2(\Omega) : \int_\Omega q\,\mathrm{d}\boldsymbol{x} = 0\}. \tag{4.22}$$

A possibility to prevent locking phenomena and to receive a better conditioned problem for almost incompressible linear elastic materials is a saddle point formulation of the boundary value problem. This yields a variational formulation that is similar to a Stokes problem. The main idea is to bring in a pressure term p which serves as a Lagrangian multiplier. A drawback of this method will be an increased number of degrees of freedom in the numerical simulation.

We start from the variational formulation for linear elasticity problems (4.19), which can be written, using the Lamé coefficients (3.37), as

$$2\mu \int_\Omega \varepsilon(\boldsymbol{u}) : \varepsilon(\boldsymbol{v}) \,\mathrm{d}\boldsymbol{x} + \lambda \int_\Omega \operatorname{div}(\boldsymbol{u}) \operatorname{div}(\boldsymbol{v}) \,\mathrm{d}\boldsymbol{x} - \int_{\Gamma_N} \boldsymbol{t}_N(\boldsymbol{x}) \cdot \boldsymbol{v}(\boldsymbol{x}) \,\mathrm{d}s_{\boldsymbol{x}} = 0. \tag{4.23}$$

We introduce the penalty variable p as

$$p = \lambda \operatorname{div} \boldsymbol{u}. \tag{4.24}$$

Note that for an incompressible material λ goes to infinity.

From (4.23) and the weak form of (4.24), we get the following saddle point problem: find $(\boldsymbol{u}, p) \in \mathcal{X} \times \mathcal{M}$, such that

$$\begin{aligned} a_0(\boldsymbol{u}, \boldsymbol{v}) \quad &+ b(\boldsymbol{v}, p) \quad &&= \langle \boldsymbol{f}, \boldsymbol{v} \rangle, \\ b(\boldsymbol{u}, q) \quad &- \lambda^{-1} c(p, q) \quad &&= 0, \end{aligned} \tag{4.25}$$

for all test functions $v \in \mathcal{X}$ and $q \in \mathcal{M}$ and

$$a_0(\boldsymbol{u}, \boldsymbol{v}) = \int_\Omega 2\mu \, \varepsilon(\boldsymbol{u}, \boldsymbol{x}) : \varepsilon(\boldsymbol{v}, \boldsymbol{x}) \,\mathrm{d}x, \quad b(\boldsymbol{v}, p) = \int_\Omega p \operatorname{div} \boldsymbol{v} \,\mathrm{d}\boldsymbol{x}, \quad c(p, q) = \int_\Omega pq \,\mathrm{d}\boldsymbol{x}.$$

The right-hand-side for elastostatics reads, disregarding body forces,

$$\langle \boldsymbol{f}, \boldsymbol{v} \rangle = \int_{\Gamma_N} \boldsymbol{t}_N(\boldsymbol{x}) \cdot \boldsymbol{v}(\boldsymbol{x}) \,\mathrm{d}s_{\boldsymbol{x}}.$$

For the limiting case $\lambda \to \infty$, i.e. for an incompressible material, we obtain: find $(\boldsymbol{u}, p) \in \mathcal{X} \times \mathcal{M}$ such that

$$\begin{aligned} a_0(\boldsymbol{u}, \boldsymbol{v}) + b(\boldsymbol{v}, p) \quad &= \langle \boldsymbol{f}, \boldsymbol{v} \rangle, \\ b(\boldsymbol{u}, q) \quad &= \boldsymbol{0}, \end{aligned} \tag{4.26}$$

for all test functions $(\boldsymbol{v}, q) \in \mathcal{X} \times \mathcal{M}$ and with the definitions from above.

Remark 4.3.1. *The saddle point problems* (4.25) *and* (4.26) *are uniquely solvable, e.g., cf. [14, Braess (2007), Ch. 6, §4].*

Remark 4.3.2. *For the case of a pure Dirichlet problem, i.e.* $\Gamma = \Gamma_D$*, we replace the ansatz space for the pressure* p*,* $\mathcal{M} = L_{2,0}(\Omega)$ *in* (4.22)*, by* $L_{2,0}(\Omega)/\mathbb{R}$*. This issue is also known for the Stokes problem, e.g., cf. [14, Braess (2007), Ch. 3].*

4.4. Nonlinear Elasticity

In this section we will derive a variational formulation for nonlinear elasticity models. We present a Newton method suitable for the linearization of the considered problem

and show the linearization procedure for an arbitrary elastic material that is modeled using a stress in the form (3.40). Here we follow the descriptions of Holzapfel in [59, Holzapfel (2000), Sect. 8.4] and [60, Holzapfel (2003)]. As proposed in these works we will perform the linearization in the reference configuration, since there we can interchange differentiation and integration. To get a linearized version of the constitutive equation in the current configuration we use tools that can be found in Section 3.2. We will also present the mean dilatation method that is used to treat nearly incompressible nonlinear materials. In the last part of this section we discuss existence theorems for nonlinear elasticity problems, following the results of Ball in the late 1970s [9,10].

4.4.1. Newton's Method

To obtain solutions of a nonlinear boundary value problem, iterative solution techniques of Newton type are often applied. This leads to a sequence of linearized problems. A great compendium on Newton's method is [35, Deuflhard (2004)].

We start with the nonlinear operator equation

$$F(x) = 0 \tag{4.27}$$

where $F : D \subset X \to Y$ for the Banach spaces X and Y. Given a starting guess x_0 for the unknown solution x^*, we obtain, using the technique of successive linearization, the general Newton method

$$F'(x^k)\Delta x^k = -F(x^k),\ x^{k+1} = x^k + \Delta x^k,\ k = 0, 1, \ldots. \tag{4.28}$$

Here F' is a derivative defined in Banach spaces, i.e. the Fréchet (Definition 4.5) or the Gâteaux derivative (Definition 4.6).

For the convergence analysis we give the fundamental Newton–Kantorovich theorem.

Theorem 4.10. *Let X and Y be Banach spaces and $D \subset X$ open and convex. Let $F : D \to Y$ be a continuously Fréchet differentiable operator and let $x^0 \in D$ be a starting point such that $F'(x^0)$ is invertible. Given that*

$$\|F'(x^0)^{-1}F(x^0)\| \leq \alpha \text{ and } \|F'(x^0)^{-1}(F'(y) - F'(\boldsymbol{x}))\| \leq \overline{\omega}_0\|y - x\|,$$

the sequence $\{x^k\}$, obtained from Newton's method (4.28) is well-defined and converges to a x^* with $F(x^*) = 0$. The convergence is quadratic for $h_0 := \alpha\overline{\omega}_0 < \frac{1}{2}$ and the sequence $\{x^k\}$ stays in the sphere $S(x^0, (1 - \sqrt{1 - 2h_0})/\overline{\omega}_0) \subset D$.

Proof. cf. [35, Deuflhard (2004)] and the classical work [78, Kantorovich (1948)]. □

For more information on convergence of the Newton method in Banach spaces cf. [35, Deuflhard (2004), Ch. 2.1]. In the case of numerical simulations we deal with discretizations and hence approximate solutions. Hence we have to deal with *inexact Newton methods*, cf. Sect. 5.2.

4.4.2. Mean Dilatation Technique for Almost Incompressible Nonlinear Elastic Materials

The first step of the mean dilatation technique is to introduce additional volumetric variables J and p by a decoupled formulation as described in Section 3.9.2. The main idea is now to penalize volumetric changes with the volumetric elastic response $U(J)$; e.g. by using

$$U(J) = \frac{\kappa}{2}(J-1)^2 \quad \text{with } \kappa \gg 1.$$

While the deformation $\boldsymbol{u}$ is continuous over the whole domain Ω, the volumetric variables are modeled to be discontinuous across element boundaries in the finite element formulation. Hence these variables can be eliminated at the element level, a procedure which is also known as *static condensation*. This results in a nonlinear problem in the unknown displacement field $\boldsymbol{u}$, that is solved using a Newton scheme.

This method goes back to [106, Nagtegaal et al. (1974)] and it has shown that it prevents locking effects when we deal with almost incompressible materials like biological tissue. For more information on this approach cf. [140, Simo et al. (1985)], [139, Simo (1998)], [60, Holzapfel (2003)] and [71, Hughes (2000)].

As a starting point we set up a variational formulation for the decoupled system discussed in Section 3.9.2 in the reference configuration. Analogous procedures as in Section 4.2 yield: find $\boldsymbol{U} \in [H_0^1(\Omega_0, \Gamma_{0,D})]^3$ such that

$$(A(\boldsymbol{U}), \boldsymbol{V}) = \int_{\Omega_0} F(\boldsymbol{U}) \left[J\, p \mathsf{C}^{-1} + \overline{\mathsf{S}} \right] (\boldsymbol{U}) : \operatorname{Grad} \boldsymbol{V} \, \mathrm{d}\boldsymbol{X} = \langle \boldsymbol{f}, \boldsymbol{V} \rangle \tag{4.29}$$

for all test functions $\boldsymbol{V} \in [H_0^1(\Omega_0, \Gamma_{0,D})]^3$.

In addition, we have a variational formulation for the volumetric variables J and p. Since we have defined the hydrostatic pressure p in Eq. (3.58) such that $p = \mathrm{d}U(J)/\mathrm{d}J$ it is sufficient to concentrate on the Jacobian J. Let $\overline{J}$ be a scalar variable that satisfies $\overline{J} = J$ in a weak sense, i.e.

$$\int_{\Omega_0} \left(\overline{J} - J(\boldsymbol{U}, \boldsymbol{X}) \right) q(\boldsymbol{X}) \, \mathrm{d}\boldsymbol{X} = 0, \quad \text{for all } q \in L_2(\Omega_0). \tag{4.30}$$

In this work we will focus on piecewise constant discontinuous ansatz-functions for the test function q. This leads to a Q_p–P_0–element for hexahedrons and a P_p–P_0–element

for tetrahedrons, with p the order of the base functions for the displacement field, see Section 5.1.4.

4.4.3. Linearization of the Standard Variational Formulation

In this section, we will perform the linearization of the variational formulation (4.16). As mentioned before, this is done in the reference configuration since there the integration domain Ω_0 is not dependent on the deformation $\boldsymbol{u}$ and hence we can interchange differentiation and integration. The loads are considered as independent of the deformation of the continuum body. Thus the linearization only affects the term

$$(A(\boldsymbol{U}), \boldsymbol{V}) := \int_{\Omega_0} (\mathsf{FS})(\boldsymbol{U}) : \operatorname{Grad}(\boldsymbol{V}) \, \mathrm{d}\boldsymbol{X}. \tag{4.31}$$

Hence to apply Newton's method (4.28), we use the scheme

$$(\boldsymbol{\Delta U}, A'(\boldsymbol{U}^k)\boldsymbol{V}) = \langle f, V \rangle - (A(\boldsymbol{U^k}), \boldsymbol{V}), \quad \boldsymbol{U}^{k+1} = \boldsymbol{U}^k + \boldsymbol{\Delta U}, \ k = 0, 1, \ldots.$$

with the Fréchet derivative $A'(\boldsymbol{U}^k)$. To simplify matters, we make use of Remark 4.1.1 and compute $A'(\boldsymbol{U}^k)$ as the Gâteaux derivative in direction of the increment $\boldsymbol{\Delta U}$. For better readability we omit the dependencies on the deformation $\boldsymbol{U}^k$ and denote by $(\bullet)' := D(\bullet).\boldsymbol{\Delta U}$ the Gâteaux derivatives. By interchanging differentiation and integration we obtain

$$(\boldsymbol{\Delta U}, A'\boldsymbol{V}) = \int_{\Omega_0} (\mathsf{FS})' : \operatorname{Grad} \boldsymbol{V} \, \mathrm{d}\boldsymbol{X} = \int_{\Omega_0} (\mathsf{F})'\mathsf{S} : \operatorname{Grad} \boldsymbol{V} \, \mathrm{d}\boldsymbol{X} + \int_{\Omega_0} \mathsf{F}(\mathsf{S})' : \operatorname{Grad} \boldsymbol{V} \, \mathrm{d}\boldsymbol{X}.$$

Using the chain rule we may write for the Gâteaux derivative of the stress tensor S

$$(\mathsf{S})' = \frac{\partial \mathsf{S}}{\partial \mathsf{C}}(\mathsf{C})' = 2\frac{\partial \mathsf{S}}{\partial \mathsf{C}}\frac{1}{2}(\mathsf{C})' = \mathbb{C}\frac{1}{2}(\mathsf{C})',$$

with $\mathbb{C}$ the elasticity tensor in the reference configuration and the tensor product (A.5).

For the Gâteaux derivative of the deformation gradient F we obtain with definitions (4.6) and (3.4)

$$D\,\mathsf{F}(\boldsymbol{U}).\boldsymbol{\Delta U} = \lim_{\tau \to \infty} \frac{\mathsf{I} + \operatorname{Grad}(\boldsymbol{U} + \tau \boldsymbol{\Delta U}) - \mathsf{I} - \operatorname{Grad}(\boldsymbol{U})}{\tau}.$$

Due to the linearity of the gradient we get

$$D\,\mathsf{F}(\boldsymbol{U}).\boldsymbol{\Delta U} = \lim_{\tau \to \infty} \frac{\tau \operatorname{Grad}(\boldsymbol{\Delta U})}{\tau} = \operatorname{Grad}(\boldsymbol{\Delta U}). \tag{4.32}$$

Hence we have for the tangent using $\mathsf{C}' = 2\mathsf{E}'$, cf. (3.19),

$$\begin{aligned}&(\boldsymbol{\Delta U}, A'(\boldsymbol{U}^k)\boldsymbol{V})\\ &= \int_{\Omega_0} \operatorname{Grad}(\boldsymbol{\Delta U})\,\mathsf{S}(\boldsymbol{U}^k) : \operatorname{Grad}\boldsymbol{V}\,\mathrm{d}\boldsymbol{X} + \int_{\Omega_0} \mathsf{F}(\boldsymbol{U}^k)\,(\mathbb{C}\,\mathsf{E}')\,(\boldsymbol{U}^k) : \operatorname{Grad}\boldsymbol{V}\,\mathrm{d}\boldsymbol{X}. \end{aligned} \tag{4.33}$$

To gain the formulation of the tangent in spatial quantities we use the identities $\mathrm{d}\boldsymbol{x} = J\,\mathrm{d}X$, $\operatorname{Grad}(\bullet) = \operatorname{grad}(\bullet)\,\mathsf{F}$ and the identity of all appearing vector valued variables in current and reference configuration, as mentioned in Sect. 3.2. So we get for the first part of (4.33)

$$\begin{aligned}\int_{\Omega_0} \operatorname{Grad}\boldsymbol{\Delta U}\,\mathsf{S} : \operatorname{Grad} v\,\mathrm{d}\boldsymbol{X} &= \int_{\Omega} \operatorname{grad}\boldsymbol{\Delta u}\mathsf{F}\,\mathsf{S} : \operatorname{grad}\boldsymbol{v}\,\mathsf{F}J^{-1}\,\mathrm{d}\boldsymbol{x}\\ &= \int_{\Omega} \operatorname{grad}\boldsymbol{\Delta u}\,(J^{-1}\mathsf{F}\mathsf{S}\mathsf{F}^{\top}) : \operatorname{grad}\boldsymbol{v}\,\mathrm{d}\boldsymbol{x} = \int_{\Omega} \operatorname{grad}\boldsymbol{\Delta u}\,\sigma : \operatorname{grad}\boldsymbol{v}\,\mathrm{d}\boldsymbol{x}.\end{aligned}$$

With the Gâteaux derivative of the left Cauchy–Green tensor

$$\begin{aligned}\mathsf{C}' &= (\mathsf{F}^{\top}\mathsf{F})' = (\mathsf{F}^{\top})'\mathsf{F} + \mathsf{F}^{\top}\mathsf{F}' = (\operatorname{Grad}\boldsymbol{\Delta U})^{\top}\mathsf{F} + \mathsf{F}^{\top}\operatorname{Grad}\boldsymbol{\Delta U}\\ &= \mathsf{F}^{\top}(\operatorname{grad}\boldsymbol{\Delta u})^{\top}\mathsf{F} + \mathsf{F}^{\top}\operatorname{grad}\boldsymbol{\Delta u}\mathsf{F} = \mathsf{F}^{\top}\left((\operatorname{grad}\boldsymbol{\Delta u})^{\top} + \operatorname{grad}\boldsymbol{\Delta u}\right)\mathsf{F} = 2\mathsf{F}^{\top}\varepsilon(\boldsymbol{\Delta u})\mathsf{F},\end{aligned}$$

the second part yields

$$\begin{aligned}\int_{\Omega_0} \mathsf{F}\left(\mathbb{C}\frac{1}{2}(\mathsf{C})'\right) : \operatorname{Grad}\boldsymbol{v}\,\mathrm{d}\boldsymbol{X} &= \int_{\Omega} \mathsf{F}\left(\mathbb{C}(\mathsf{F}^{\top}\varepsilon(\boldsymbol{\Delta u})\mathsf{F})\right) : \operatorname{grad}\boldsymbol{v}\,\mathsf{F}\,J^{-1}\,\mathrm{d}\boldsymbol{x}\\ &= \int_{\Omega} \mathbb{c}\,\varepsilon(\boldsymbol{\Delta u}) : \varepsilon(\boldsymbol{v})\,\mathrm{d}\boldsymbol{x}.\end{aligned}$$

Here we use the definition of the forth-order spatial elasticity tensor $\mathbb{c}$, see Def. 3.13, and its major and minor symmetry properties.

In total, the tangent in current configuration is

$$(\boldsymbol{\Delta u}, A'(\boldsymbol{u}^k)\boldsymbol{v}) = \int_{\Omega} \operatorname{grad}(\boldsymbol{\Delta u})\sigma(\boldsymbol{u}^k) : \operatorname{grad}\boldsymbol{v}\,\mathrm{d}\boldsymbol{x} + \int_{\Omega} \mathbb{c}(\boldsymbol{u}^k)\,\varepsilon(\boldsymbol{\Delta u}) : \varepsilon(\boldsymbol{v})\,\mathrm{d}\boldsymbol{x}. \tag{4.34}$$

4.4.4. Linearization of the Decoupled Variational Formulation

For nearly incompressible materials we have to perform the linearization of the decoupled variational formulation

$$(A(\boldsymbol{U}), \boldsymbol{V}) = \int_{\Omega_0} \mathsf{F}(\boldsymbol{U})[J(\boldsymbol{U})p(\boldsymbol{U})\mathsf{C}^{-1}(\boldsymbol{U}) + \mathsf{S}_{\mathrm{iso}}(\boldsymbol{U})] : \operatorname{Grad}(\boldsymbol{V})\,\mathrm{d}\boldsymbol{X}. \tag{4.35}$$

which is equivalent to (4.31). With a procedure analogous to Sect. 4.4.3, we compute the derivative in tangential direction by

$$
\begin{aligned}
(\boldsymbol{\Delta U}, A'(\boldsymbol{U}^k)\boldsymbol{V}) &= \int_{\Omega_0} \left[\mathsf{F}(Jp\mathsf{C}^{-1} + \mathsf{S}_{\text{iso}})\right]' : \operatorname{Grad} \boldsymbol{V} \, \mathrm{d}\boldsymbol{X} \\
&= \int_{\Omega_0} \mathsf{F}' \, (Jp\mathsf{C}^{-1} + \mathsf{S}_{\text{iso}}) : \operatorname{Grad} \boldsymbol{V} \, \mathrm{d}\boldsymbol{X} + \int_{\Omega_0} \mathsf{F}(Jp\mathsf{C}^{-1} + \mathsf{S}_{\text{iso}})' : \operatorname{Grad} \boldsymbol{V} \, \mathrm{d}\boldsymbol{X},
\end{aligned}
$$

where the dependencies on $\boldsymbol{U}^k$ are omitted and $(\bullet)'$ denote the Gâteaux derivatives with respect to the increment $\boldsymbol{\Delta U}$.

Now we take a look at the derivative of the stress tensor in particular:

$$
\begin{aligned}
(Jp\mathsf{C}^{-1} + \mathsf{S}_{\text{iso}})' &= p \, (J\mathsf{C}^{-1})' + p' J\mathsf{C}^{-1} + \mathsf{S}'_{\text{iso}} \\
&= p \frac{\partial}{\partial \mathsf{C}} (J\mathsf{C}^{-1}) \, \mathsf{C}' + p' J\mathsf{C}^{-1} + \frac{\partial}{\partial \mathsf{C}} \mathsf{S}_{\text{iso}} \, \mathsf{C}' \\
&= \left(2p \frac{\partial}{\partial \mathsf{C}} (J\mathsf{C}^{-1}) + 2 \frac{\partial}{\partial \mathsf{C}} \mathsf{S}_{\text{iso}} \right) \frac{1}{2} \mathsf{C}' + p' J\mathsf{C}^{-1}.
\end{aligned}
$$

Using tools of tensor calculus described in Sect. A.1 we obtain

$$
\begin{aligned}
(Jp\mathsf{C}^{-1} + \mathsf{S}_{\text{iso}})' &= \left(2p \frac{\partial J}{\partial \mathsf{C}} \otimes \mathsf{C}^{-1} + 2pJ \frac{\partial \mathsf{C}^{-1}}{\partial \mathsf{C}} + \mathbb{C}_{\text{iso}} \right) \frac{1}{2} \mathsf{C}' + p' J\mathsf{C}^{-1} \\
&= \left(Jp\mathsf{C}^{-1} \otimes \mathsf{C}^{-1} - 2Jp\mathsf{C}^{-1} \odot \mathsf{C}^{-1} + \mathbb{C}_{\text{iso}} \right) \frac{1}{2} \mathsf{C}' + p' J\mathsf{C}^{-1},
\end{aligned}
$$

where $\mathbb{C}_{\text{iso}}$ is the isochoric part of the elasticity tensor, cf. Cor. 3.6, and the tensor products are defined in (3.132) and (A.4). The Gâteaux derivative of the pressure term yields

$$
p' = D \, p(J).\boldsymbol{\Delta U} = \frac{\partial p(J)}{\partial J} D \, J.\boldsymbol{\Delta U} = \frac{\partial^2 U(J)}{\partial J^2} D \, J.\boldsymbol{\Delta U}.
$$

For the derivative of the Jacobian we obtain with the chain rule and Cor. A.2

$$
D \, J.\boldsymbol{\Delta U} = \frac{\partial J}{\partial \mathsf{F}} : D\mathsf{F}.\boldsymbol{\Delta U} = J\mathsf{F}^{-\top} : \operatorname{Grad}(\boldsymbol{\Delta U}).
$$

With $\mathsf{C}' = 2\mathsf{E}'$, cf. (3.19), and $\mathsf{F}' = \operatorname{Grad} \boldsymbol{\Delta U}$, cf. (4.32), we get for the complete linearized term

$$
\begin{aligned}
(\boldsymbol{\Delta U}, A'(\boldsymbol{U}^k)\boldsymbol{V}) = &\int_{\Omega_0} \operatorname{Grad} \boldsymbol{\Delta U} \, (Jp\mathsf{C}^{-1} + \mathsf{S}_{\text{iso}})(\boldsymbol{U}^k) : \operatorname{Grad} \boldsymbol{V} \, \mathrm{d}\boldsymbol{X} \\
&+ \int_{\Omega_0} \left[\mathsf{F} \left(Jp\mathsf{C}^{-1} \otimes \mathsf{C}^{-1} + 2Jp\mathsf{C}^{-1} \odot \mathsf{C}^{-1} + \mathbb{C}_{\text{iso}} \right) \mathsf{E}' \right] (\boldsymbol{U}^k) : \operatorname{Grad} \boldsymbol{V} \, \mathrm{d}\boldsymbol{X} \\
&+ \int_{\Omega_0} \frac{\partial^2 U(J)}{\partial J^2} \left[(J\mathsf{F}^{-\top})(\boldsymbol{U}^k) : \operatorname{Grad}(\boldsymbol{\Delta U}) \right] \left[(J\mathsf{F}^{-\top})(\boldsymbol{U}^k) : \operatorname{Grad} \boldsymbol{V} \right] \mathrm{d}\boldsymbol{X}.
\end{aligned}
\tag{4.36}
$$

The realization of the derivative in the current configuration is done by similar considerations as in Sect. 4.4.3. Additionally, we need

$$\mathsf{I} : \operatorname{grad}(\bullet) = \operatorname{div}(\bullet)$$

and tools from tensor calculus. For more details in this case cf. [59, Holzapfel (2000)] and [97, Marsden and Hughes (1994)]. Hence we obtain for the derivative in tangential direction in the current configuration

$$\begin{aligned}(\boldsymbol{\Delta u}, A'(\boldsymbol{u}^k), \boldsymbol{v}) &= (A'(\boldsymbol{u}^k), \boldsymbol{v})_{\text{geo}} + (A'(\boldsymbol{u}^k), \boldsymbol{v})_{\text{mat}} + (A'(\boldsymbol{u}^k), \boldsymbol{v})_{\text{pre}} \\ &= \int_\Omega \operatorname{grad} \boldsymbol{\Delta u}\, (p(\boldsymbol{u}^k)\mathsf{I} + \sigma_{\text{iso}}(\boldsymbol{u}^k)) : \operatorname{grad} \boldsymbol{v}\, \mathrm{d}\boldsymbol{x} \\ &+ \int_\Omega \left(p(\boldsymbol{u}^k)\mathsf{I} \otimes \mathsf{I} - 2p(\boldsymbol{u}^k)\mathbb{I} + \mathbb{C}_{\text{iso}(\boldsymbol{u}^k)}\right) \varepsilon(\boldsymbol{\Delta u}) : \varepsilon(\boldsymbol{v})\, \mathrm{d}\boldsymbol{x} \\ &+ \int_\Omega \frac{\partial^2 U(J)}{\partial J^2} \operatorname{div}(\boldsymbol{\Delta u}) \operatorname{div}(\boldsymbol{v})\, \mathrm{d}\boldsymbol{x}.\end{aligned} \tag{4.37}$$

Note that the piecewise constant volumetric variables $J(\boldsymbol{u}^k)$ and $p(\boldsymbol{u}^k)$ are elmininated at the element level (static condensation).

Remark 4.4.1. *It is obvious that we can find a starting point $\boldsymbol{u}_0$ that satisfies the requirements of Theorem 4.10 for the derivative of the variational formulations in Sections 4.4.3 and 4.4.4. This is due to the properties of the strain energy function described in Remark 3.8.3 (Normalization Conditions). A possible choice would be the solution of the linear elasticity problem.*

4.4.5. Linearized Elasticity

In this section we treat the linearized variational formulations in the current configuration as described in Sect. 4.4.3 and Sect. 4.4.4.

Remark 4.4.2 (Self-adjointness)**.** *The operator $A'(\boldsymbol{u}^k)$ in Eqs.* (4.34) *and* (4.37) *is self-adjoint. This is due to the symmetry properties of the elasticity tensor, compare to Remark 3.14.1, and the symmetry of the stress tensor σ.*

We define the bilinear and the linear forms

$$a_0'(\boldsymbol{\Delta U}, \boldsymbol{V}) := (\boldsymbol{\Delta U}, A'(\boldsymbol{U}^k)\boldsymbol{V}), \quad \langle \boldsymbol{F}_0, \boldsymbol{V}\rangle := \langle \boldsymbol{f}, \boldsymbol{V}\rangle - (A(\boldsymbol{U}^k), \boldsymbol{V})$$

and

$$a'(\boldsymbol{\Delta u}, \boldsymbol{v}) := (\boldsymbol{\Delta u}, A'(\boldsymbol{u}^k)\boldsymbol{v}), \quad \langle \boldsymbol{F}, \boldsymbol{v}\rangle := \langle \boldsymbol{f}, \boldsymbol{v}\rangle - (A(\boldsymbol{u}^k), \boldsymbol{v}).$$

Thus, in each Newton step we have to solve the linear systems

$$\begin{aligned} \text{find } \boldsymbol{\Delta u} \in [H_0^1(\Omega,\Gamma_D)]^3: &\quad a'(\boldsymbol{\Delta u},\boldsymbol{v}) = \langle \boldsymbol{F},\boldsymbol{v}\rangle, &&\text{for all } \boldsymbol{v}\in[H_0^1(\Omega,\Gamma_D)]^3 \text{ or}\\ \text{find } \boldsymbol{\Delta U} \in [H_0^1(\Omega_0,\Gamma_{0,D})]^3: &\quad a_0'(\boldsymbol{\Delta U},\boldsymbol{V}) = \langle \boldsymbol{F}_0,\boldsymbol{V}\rangle, &&\text{for all } \boldsymbol{V}\in[H_0^1(\Omega_0,\Gamma_{0,D})]^3, \end{aligned}$$

respectively.

In the following, we will show boundedness and ellipticity of the bilinear form $a'(\boldsymbol{\Delta u},\boldsymbol{v})$. Since the formulations in the reference and the current configuration are equivalent, similar estimates also hold for $a_0'(\boldsymbol{\Delta U},\boldsymbol{V})$.

Lemma 4.11 (Boundedness of the bilinear form). *For all $\boldsymbol{\Delta u},\boldsymbol{v}\in[H^1(\Omega)]^3$ it holds*

$$|a'(\boldsymbol{\Delta u},\boldsymbol{v})| \le (c_2^g + c_2^m)\,|\boldsymbol{\Delta u}|_{[H^1(\Omega)]^3}|\boldsymbol{v}|_{[H^1(\Omega)]^3},$$

with positive constants c_2^g and c_2^m.

Proof. We have to show the boundedness of

$$a'(\boldsymbol{\Delta u},\boldsymbol{v}) = \int_\Omega \operatorname{grad}(\boldsymbol{\Delta u})\,\sigma(\boldsymbol{u}^k) : \operatorname{grad}\boldsymbol{v}\,\mathrm{d}\boldsymbol{x} + \int_\Omega \mathbb{C}(\boldsymbol{u}^k)\,\varepsilon(\boldsymbol{\Delta u}) : \varepsilon(\boldsymbol{v})\,\mathrm{d}\boldsymbol{x}.$$

Inside a Newton step the values $\sigma(\boldsymbol{u}^k)$ and $\mathbb{C}(\boldsymbol{u}^k)$ may be treated as constants. Hence, with the boundedness of the bilinear form of linear elasticity, cf. Lemma 4.9, and the boundedness of the vectorial potential equation, cf. [147, Steinbach (2008)], it follows

$$\begin{aligned} |a'(\boldsymbol{\Delta u},\boldsymbol{v})| &\le \left|\int_\Omega \operatorname{grad}(\boldsymbol{\Delta u})\sigma(\boldsymbol{u}^k) : \operatorname{grad}\boldsymbol{v}\,\mathrm{d}\boldsymbol{x}\right| + \left|\int_\Omega \mathbb{C}(\boldsymbol{u}^k)\,\varepsilon(\boldsymbol{\Delta u}) : \varepsilon(\boldsymbol{v})\,\mathrm{d}\boldsymbol{x}\right|\\ &\le 3\|\sigma\|_{L_\infty}\,|\boldsymbol{\Delta u}|_{[H^1(\Omega)]^3}|\boldsymbol{v}|_{[H^1(\Omega)]^3} + |\lambda_{\max}(\mathsf{C})||\boldsymbol{\Delta u}|_{[H^1(\Omega)]^3}|\boldsymbol{v}|_{[H^1(\Omega)]^3}, \end{aligned}$$

where $\|\sigma\|_{L_\infty} := \max_{i,j=1,2,3}|\sigma_{ij}(\boldsymbol{u}^k)|$ and $\lambda_{\max}(\mathsf{C})$ is the largest eigenvalue of $\mathsf{C}(\boldsymbol{u}^k)$ which is the elasticity tensor $\mathbb{C}(\boldsymbol{u}^k)$ in Voigt notation.

Due to the equivalence of the standard and the decoupled formulation, we get the same result for the decoupled formulation with $\sigma = p\mathsf{I} + \sigma_{\text{iso}}$ and $\mathbb{C}=\mathbb{C}_{\text{vol}}+\mathbb{C}_{\text{iso}}$. □

We know that the stress tensor σ and the elasticity tensor C in Voigt notation, cf. Remark 3.14.2, are both symmetric.

Remark 4.4.3. *The eigenvalues of σ are called principal stresses and may be calculated by*

$$\sigma_i = J^{-1}\lambda_i\frac{\partial\Psi}{\partial\lambda_i}, \quad \text{for } i=1,2,3,$$

with $\Psi(\mathsf{C}) = \Psi(\lambda_1,\lambda_2,\lambda_3)$ the strain energy function and $\lambda_i > 0$ the principal stretches, cf. Cor. 3.5.

Then we get, using results of Sect. 4.3, for all $\boldsymbol{v} \in [H_0^1(\Omega)]^3$

$$\begin{aligned} a'(\boldsymbol{v},\boldsymbol{v}) &\geq \lambda_{\min}(\sigma(\boldsymbol{u}^k)) \sum_{i,j=1}^{3} \int_\Omega \left[\frac{\partial}{\partial x_j} v_i(\boldsymbol{x})\right]^2 \mathrm{d}\boldsymbol{x} + \lambda_{\min}(\mathsf{C}) \frac{1}{2(1+c_F^2)} \|\boldsymbol{v}\|^2_{[H^1(\Omega)]^3} \\ &= \lambda_{\min}(\sigma(\boldsymbol{u}^k)) |\boldsymbol{v}|^2_{[H^1(\Omega)]^3} + \lambda_{\min}(\mathsf{C}) \frac{1}{2(1+c_F^2)} \|\boldsymbol{v}\|^2_{[H^1(\Omega)]^3} \\ &= \frac{1}{2(1+c_F^2)} (2\lambda_{\min}(\sigma(\boldsymbol{u}^k)) + \lambda_{\min}(\mathsf{C})) \|\boldsymbol{v}\|^2_{[H^1(\Omega)]^3} \\ &= \frac{1}{2(1+c_F^2)} (2 \min_{i=1,2,3}(\sigma_i)) + \lambda_{\min}(\mathsf{C})) \|\boldsymbol{v}\|^2_{[H^1(\Omega)]^3} \end{aligned}$$

where c_F denotes the constant from the Poincaré–Friedrich's inequality (4.5) and σ_i are the principal stresses of $\sigma(\boldsymbol{u}^k)$. With the normalization conditions for the strain energy function, cf. Remark 3.8.3, and the positive definiteness of the elasticity tensor, cf. Remark 3.14.3, we can find a $c > 0$ such that

$$a'(\boldsymbol{v},\boldsymbol{v}) \geq \frac{1}{2(1+c_F^2)} (2 \min_{i=1,2,3}(\sigma_i)) \|\boldsymbol{v}\|^2_{[H^1(\Omega)]^3} = c\|\boldsymbol{v}\|^2_{[H^1(\Omega)]^3}.$$

Hence we obtain $[H_0^1(\Omega, \Gamma_D)]^3$–ellipticity of the bilinear form for the Dirichlet and the mixed boundary value problem, given the strain energy function fulfills the normalization conditions and is convex, cf. Sect. 4.4.8.

Similar to Sect. 4.3, we can show $[H_*^1(\Omega)]^3$–ellipticity for the Neumann case.

With these ellipticity results and Lemma 4.11 the unique solvability of the linearized elasticity equations in the appropriate spaces follows.

4.4.6. Convexity Concepts

In the following, we will introduce convexity concepts for vectorial functions.

Definition 4.12. *Let $f : \mathbb{R}^{m\times n} \to \mathbb{R}$ a function.*

1. *The function f is said to be convex if*

$$f(\lambda\mathsf{A} + (1-\lambda)\mathsf{B}) \leq \lambda f(\mathsf{A}) + (1-\lambda) f(\mathsf{B})$$

   for every $\mathsf{A}, \mathsf{B} \in \mathbb{R}^{m\times n}$, $\lambda \in [0,1]$.

2. *The function f is said to be polyconvex if there exists $F : \mathbb{R}^{\tau(n,m)} \to \mathbb{R}$ convex, such that*

$$f(\mathsf{A}) = F(T(\mathsf{A})).$$

Here $T : \mathbb{R}^{m\times n} \to \mathbb{R}^{\tau(n,m)}$ *is defined such that*

$$T(\mathsf{A}) = (\mathsf{A}, \operatorname{adj}_2 \mathsf{A}, \dots, \operatorname{adj}_{\min\{m,n\}} \mathsf{A})$$

where $\operatorname{adj}_s \mathsf{A}$, $2 \le s \le \min\{n, m\}$, *is the matrix of all* $s \times s$ *minors of the matrix* A. *Furthermore*

$$\tau(n, m) = \sum_{s=1}^{\min\{n,m\}} \binom{m}{s}\binom{n}{s}.$$

3. *The function* f *is said to be* quasiconvex *if it is Borel measurable and locally bounded and satisfies*

$$f(\mathsf{A}) \le \frac{1}{\operatorname{meas} D} \int_D f(\mathsf{A} + \nabla\varphi(\boldsymbol{x}))\,\mathrm{d}\boldsymbol{x}$$

for all open and bounded sets $D \subset \mathbb{R}^n$, *for all* $\mathsf{A} \in \mathbb{R}^{m\times n}$ *and for all* $\varphi \in W_0^{1,\infty}(D;\mathbb{R}^m)$.

4. *The function* f *is said to be* rank one convex *if*

$$f(\lambda\mathsf{A} + (1-\lambda)\mathsf{B}) \le \lambda f(\mathsf{A}) + (1-\lambda) f(\mathsf{B})$$

for every $\lambda \in [0, 1]$, $\mathsf{A}, \mathsf{B} \in \mathbb{R}^{m\times n}$ *with* $\operatorname{rank}(\mathsf{A} - \mathsf{B}) \le 1$.

Theorem 4.13 (Connection of the Convexity Concepts)**.** *Let* $f : \mathbb{R}^{m\times n} \to \mathbb{R}$ *be a function.*

1. *The convexity concepts are linked by the implications*

$$f \text{ convex} \Rightarrow f \text{ polyconvex} \Rightarrow f \text{ quasiconvex} \Rightarrow f \text{ rank-one convex}$$

The converse implications are in general not true.

2. *If* $\min\{m, n\} = 1$, *then all of the convexity concepts are equivalent.*

3. *If* $f \in \mathcal{C}^2(\mathbb{R}^{m\times n})$, *then rank one convexity is equivalent to the* Legendre–Hadamard condition

$$\sum_{i,j=1}^{m}\sum_{\alpha,\beta}^{n} \frac{\partial^2 f(\mathsf{A})}{\partial A_{i,\alpha}\partial A_{j,\beta}} \lambda_i\lambda_j\mu_\alpha\mu_\beta \ge 0$$

for all $\underline{\lambda} \in \mathbb{R}^m$, $\underline{\mu} \in \mathbb{R}^n$ *and* $\mathsf{A} \in \mathbb{R}^{m\times n}$.

Proof. Cf. [29, Dacorogna (2008)]. □

Subsequently, we denote by $D_{\mathsf{A}} f(\cdot).\mathsf{H}$ the Gâteaux derivative with respect to A in the direction of H.

Lemma 4.14. *Let K be a convex set and let $f : K \to \mathbb{R}$ be two times differentiable. Then the following statements are equivalent.*

$$\begin{aligned} &(i)\ f \text{ is convex} \\ &(ii)\ D^2_{\mathsf{A}} f(\mathsf{A}).(\mathsf{H},\mathsf{H}) \geq 0 \quad \text{for all } \mathsf{A} \in K \text{ and for all } \mathsf{H} \in \operatorname{span}(K). \end{aligned}$$

Proof. See [126, Rockafellar (1972)]. □

It is easy to see, using the definition of the derivative of a second-order tensor valued function cf. Eq. (A.20), that the condition in Lemma 4.14 implies Legendre Hadamard ellipticity (see Theorem 4.13_3), cf. [11, Balzani et al. (2006), p. 6067].

4.4.7. Existence Theorems in Nonlinear Elasticity

In this section we will give existence theorems for nonlinear elasticity problems using convexity concepts. Here we follow the fundamental results of Ball (1976/1977) [9,10], the compendia [28,29, Dacorogna (1989,2008)] and [25, Ciarlet (1988)].

To prove the existence of a solution for nonlinear elasticity problems we first have to introduce some tools from variational calculus.

Definition 4.15 (lower semicontinuity)**.** *A functional $\mathcal{I} : X \to \mathbb{R} \cup \{\infty\}$ is said to be lower semicontinuous in a Banach space X, if for every sequence $u_n \to u^*$ in X it holds that*

$$\liminf_{n\to\infty} \mathcal{I}(u_n) \geq \mathcal{I}(u^*).$$

Definition 4.16 (weak lower semicontinuity)**.** *A functional $\mathcal{I} : X \to \mathbb{R} \cup \{\infty\}$ is said to be weakly lower semicontinuous in a Banach space X, if for every sequence $u_n \rightharpoonup u^*$ in X it holds that*

$$\liminf_{n\to\infty} \mathcal{I}(u_n) \geq \mathcal{I}(u^*).$$

Definition 4.17 (coercivity)**.** *A functional $\mathcal{I} : X \to \mathbb{R} \cup \{\infty\}$ is called coercive in a Banach space X, if for every sequence $u_n \subset X$ with $\|u_n\|_X \to \infty$ it holds that $\mathcal{I}(u_n) \to \infty$.*

With these definitions we can state the fundamental theorem:

Theorem 4.18. *Let X be a reflexive Banach space and let the functional $\mathcal{I} : X \to \mathbb{R} \cup \{\infty\}$ be weakly lower semicontinuous and coercive over X. Assume that there exists $\tilde{u} \in X$ with $\mathcal{I}(\tilde{u}) < \infty$, then the minimization problem*

$$\mathcal{I}(u) = \inf\{\mathcal{I}(v) : v \in X\}$$

has at least one solution $u^* \in X$.

Proof. This theorem is due to [104,105, Morrey (1952,1966)] and [100, Meyers (1965)]. For the proof and more information, e.g., see [29, Dacorogna (2008), Ch. 8]. □

This theorem allows us to show the existence of a solution for minimization problems if we have weakly lower semicontinuous functionals $\mathcal{I}$. Since this rather abstract concept is hard to show for concrete examples, we will give two propositions which link the convexity principles, see Sect. 4.4.6, with weak lower semicontinuity. For the proofs of both theorems cf. [28, Dacorogna (1989)].

Proposition 4.19. *Let X be Banach space and let the functional $\mathcal{I} : X \to \mathbb{R} \cup \{\infty\}$ be convex and lower semicontinuous, then $\mathcal{I}$ is weakly lower semicontinuous.*

Proposition 4.20. *Let $\Omega \subset \mathbb{R}^d$ be a bounded Lipschitz domain and $f : \mathbb{R}^{d\times d} \mapsto [0, \infty]$ polyconvex and continuous. Then*

$$\begin{aligned} \mathcal{I} : W^{1,p}(\Omega) &\to [0, \infty], \\ u &\mapsto \int_\Omega f(\nabla u)\, \mathrm{d}\boldsymbol{x} \end{aligned}$$

is weakly lower semicontinuous over $W^{1,p}(\Omega)$ for all $p > d$.

To apply the above mentioned theorems to the case of nonlinear elasticity we have to reformulate the equilibrium equations as a minimization problem.

Let $\Omega \subset \mathbb{R}^3$ be a domain with a Lipschitz boundary $\partial\Omega = \overline{\Gamma}_D \cup \overline{\Gamma}_N$ as considered in Sect. 3.6. In the following, we restrict ourselves to the case of vanishing body forces $\boldsymbol{b} = \boldsymbol{0}$. Note that the existence results also hold for sufficiently regular $\boldsymbol{b} \neq \boldsymbol{0}$.

We define the functional

$$\mathcal{I}(\boldsymbol{U}, \boldsymbol{X}) := \int_\Omega W(\mathsf{F}, \boldsymbol{X})\, \mathrm{d}\boldsymbol{X} - \int_{\Gamma_N} \boldsymbol{t}_N(\boldsymbol{U}, \boldsymbol{X})\, \mathrm{d}S_{\boldsymbol{X}}, \tag{4.38}$$

where $W(\mathsf{F}, \boldsymbol{X})$ is the Helmholtz free-energy function and $\boldsymbol{t}_N(\boldsymbol{X})$ is the surface traction on Γ_N. Now we consider the minimization problem

$$\inf\{\mathcal{I}(\boldsymbol{U}) : \boldsymbol{U} \in \mathcal{W}\}, \tag{4.39}$$

with the space

$$\mathcal{W} = \mathcal{W}_{\boldsymbol{U}_D} := \left\{ \boldsymbol{U} \in W^{1,p}(\Omega, \mathbb{R}^3) : \boldsymbol{U}(\boldsymbol{X}) = \boldsymbol{U}_D(\boldsymbol{X}) \text{ on } \Gamma_D \right\}. \tag{4.40}$$

Note that we have $\det \mathsf{F} > 0$ for the considered elasticity problems, see Chapter 3.

Proposition 4.21. *Let $\boldsymbol{U}^*$ be sufficiently regular and a solution of* (4.39)*. Let the free-energy function W be twice continuously differentiable, then $\boldsymbol{U}^*$ satisfies the weak system of the equilibrium equations* (4.16)

$$\int_{\Omega_0} \mathsf{FS}(\boldsymbol{U}^*, \boldsymbol{X}) : \operatorname{Grad} \boldsymbol{V}(\boldsymbol{X}) \, \mathrm{d}\boldsymbol{X} - \int_{\Gamma_N} \boldsymbol{t}_N(\boldsymbol{U}^*, \boldsymbol{X}) \cdot \boldsymbol{V}(\boldsymbol{X}) \, \mathrm{d}S_{\boldsymbol{X}} = 0,$$

for all $\boldsymbol{V}(\boldsymbol{X}) \in \mathcal{W}_0$.

Proof. We show the equivalence of the minimization problem and the weak system of the equilibrium equations by using the first variation of $\mathcal{I}(\boldsymbol{U})$, i.e.

$$\phi(s) := \mathcal{I}(\boldsymbol{U}^* + s\boldsymbol{V})$$

for an arbitrary $\boldsymbol{V} \in \mathcal{W}_0$. $\mathcal{I}(\boldsymbol{U}^*) = 0$ is fulfilled if $\phi(s)$ has a local extremal value at $s = 0$. Hence we calculate the stationary point of the first variation, which yields

$$\nabla_s \mathcal{I}(\boldsymbol{U}^* + s\boldsymbol{V})|_{s=0} \overset{!}{=} 0. \tag{4.41}$$

The chain rule yields

$$\begin{aligned} \nabla_s \mathcal{I}(\boldsymbol{U}^* + s\boldsymbol{V}) = &\int_{\Omega} \frac{\partial W(\mathsf{F})}{\partial \mathsf{F}}(\boldsymbol{U}^* + s\boldsymbol{V}) : \frac{\partial \mathsf{F}(\boldsymbol{U}^* + s\boldsymbol{V})}{\partial s} \, \mathrm{d}\boldsymbol{X} \\ &- \int_{\Gamma_N} \boldsymbol{t}_N(\boldsymbol{U}^* + s\boldsymbol{V}) \cdot \boldsymbol{V} \, \mathrm{d}S_{\boldsymbol{X}}. \end{aligned}$$

Due to the linearity of the gradient we get

$$\nabla_s \mathcal{I}(\boldsymbol{U}^* + s\boldsymbol{V})|_{s=0} = \int_{\Omega} \frac{\partial W(\mathsf{F})}{\partial \mathsf{F}}(\boldsymbol{U}^*) : \operatorname{Grad} \boldsymbol{V} \, \mathrm{d}\boldsymbol{X} - \int_{\Gamma_N} \boldsymbol{t}_N(\boldsymbol{U}^*) \cdot \boldsymbol{V} \, \mathrm{d}S_{\boldsymbol{X}},$$

With (4.41), Theorem 3.3 and (3.26) we get the desired result. □

Remark 4.4.4. *Since the formulation of the weak form of the equilibrium equations in the reference and the current configuration are equivalent, a similar result to Proposition 4.21 is also valid for*

$$\int_{\Omega} \sigma(\boldsymbol{u}, \boldsymbol{x}) : \varepsilon(\boldsymbol{v}, \boldsymbol{x}) \, \mathrm{d}\boldsymbol{x} - \int_{\Gamma_N} \boldsymbol{t}_N(\boldsymbol{x}) \cdot \boldsymbol{v}(\boldsymbol{x}) \, \mathrm{d}s_{\boldsymbol{x}} = 0,$$

with $\boldsymbol{u} \in \mathcal{W}$ and $\boldsymbol{v} \in \mathcal{W}_0$.

Remark 4.4.5. *A similar result to Proposition 4.21 holds also for incompressible and nearly incompressible elasticity models as described in Sect. 3.9 and Sect. 4.4.2, cf. [28, Dacorogna (1989), Ch. A.1.2].*

Hence we have to show the convexity of the strain energy function $W(\mathsf{F})$, which is used to model the elastic material. Using Theorem 4.13 we get the polyconvexity of $W(\mathsf{F})$ which yields a weakly lower semicontinuous functional $\mathcal{I}(\boldsymbol{U})$, see Proposition 4.20 and Eq. (4.38). The minimization problem to find the infimum of $\mathcal{I}(\boldsymbol{U})$ with $\boldsymbol{U} \in \mathcal{W}$ is equivalent to the weak form of the equilibrium equations, cf. Proposition 4.21. With Theorem 4.18 we get the existence of a solution. To summarize we fomulate the following theorem, known as John Ball's existence result in the spaces $W^{1,p}(\Omega), p \geq 2$.

Theorem 4.22 (John Ball's Existence Result)**.** *Let $\Omega \subset \mathbb{R}^3$ be a bounded Lipschitz domain. Let the strain energy function $W : \mathbb{R}^{3\times 3} \to [0, \infty]$ be polyconvex, coercive and*

$$\lim_{\det \mathsf{F} \to 0} W(\mathsf{F}, \boldsymbol{x}) = +\infty.$$

Let the traction force $\boldsymbol{t}_N(\boldsymbol{x})$ be such that the linear form $\langle \boldsymbol{f}, \boldsymbol{v} \rangle$ is well defined and continuous. Let the Dirichlet boundary conditions $\boldsymbol{u}_D(\boldsymbol{x}) : \Gamma_0 \to \mathbb{R}^3$ be a measurable function on $\Gamma_D \neq \emptyset$ such that

$$\mathcal{W} = \left\{ \boldsymbol{u} \in W^{1,p}(\Omega, \mathbb{R}^3) : \boldsymbol{u}(\boldsymbol{x}) = \boldsymbol{u}_D(\boldsymbol{x}) \text{ on } \Gamma_D \text{ and } \det \mathsf{F} > 0 \right\} \neq \emptyset.$$

Let there exist $\tilde{\boldsymbol{u}} \in \mathcal{W}$ such that $\mathcal{I}(\tilde{\boldsymbol{u}}) < \infty$, with

$$\mathcal{I}(\boldsymbol{u}) = \int_\Omega W(\mathsf{F}, \boldsymbol{x}) \, \mathrm{d}\boldsymbol{x} - \int_{\Gamma_N} \boldsymbol{t}_N(\boldsymbol{u}, \boldsymbol{x}) \, \mathrm{d}s_{\boldsymbol{x}}.$$

Then there exists at least one $\boldsymbol{u}^* \in \mathcal{W}$ which satisfies

$$\mathcal{I}(\boldsymbol{u}^*) \leq \mathcal{I}(\boldsymbol{u}) \quad \text{for all } \boldsymbol{u} \in \mathcal{W}$$

and hence solves the equilibrium equations.

Proof. Following [10, Ball (1977), Thm. 7.3, Thm. 7.6], e.g., see [25, Ciarlet (1988), Sect. 7.7] and [28, Dacorogna (1989), Sect. A.1]. □

Remark 4.4.6. *The coercivity and the assumption $W(\mathsf{F}, \boldsymbol{x}) \to +\infty$ for $\det \mathsf{F} \to 0$ reflect the property that large deformations must accompany large strains.*

Remark 4.4.7. *The linear form $\langle \boldsymbol{f}, \boldsymbol{v} \rangle$ is well defined and continuous if the traction force $\boldsymbol{t}_N \in H^{-1/2}(\Gamma_N)$.*

Remark 4.4.8. *It is worth to mention that the solution is not necessarily unique. Physical examples of non-uniqueness one may find, e.g., in [25, Ciarlet (1988), Sect. 5.8].*

4.4.8. Convexity of the Specific Nonlinear Elasticity Models

A large class of materials are the so-called *Ogden materials*, see Sect. 3.11.1. A subclass of Ogden materials are *Mooney–Rivlin* (3.73) and *Neo–Hookean materials* (3.74).

Remark 4.4.9. *Ogden material models give rise to a polyconvex stored energy function W and in the case of Neo–Hookean materials this function is even convex, cf. [29, Dacorogna (2008)].*

Remark 4.4.10. *If the material is nearly incompressible we use a decomposition of the energy function in a volume deserving and a volume dilating part, see Sect. 3.9.2. This decomposition can be written as*

$$W(\mathsf{F}) = \overline{W}\left(\frac{\mathsf{F}}{\det(\mathsf{F})^{1/3}}\right) + U(\det(\mathsf{F})) \tag{4.42}$$

For the polyconvexity of such a W see [22, Charrier et al. (1988)].

Lemma 4.23. *The strain energy function for the artery model*

$$\Psi(\mathsf{C}) = \frac{c}{2}(I_1 - 3) + \frac{k_1}{2k_2}\sum_{i=4,6}\left\{\exp[k_2(I_i - 1)^2] - 1\right\},$$

see Sect. 3.12 and the strain energy function for the myocardium model

$$\Psi(\mathsf{C}) = \frac{a}{2b}\exp\left[b(I_1 - 3)\right] + \sum_{i=f,s}\frac{a_i}{2b_i}\left\{\exp[b_i(I_{4i} - 1)^2] - 1\right\} + \frac{a_{fs}}{2b_{fs}}\left[\exp(b_{fs}I_{8fs}^2) - 1\right],$$

see Sect. 3.13, are convex if all involved constants are positive.

Proof. Due to Lemma 4.14 the convexity of the strain energy functions follows, if

$$D_{\mathsf{C}}^2\Psi(\mathsf{C}).(\mathsf{H},\mathsf{H}) \geq 0$$

holds for all $H \in \mathbb{R}^{3x3}$. Since the sum of convex functions remains convex, we show this constraint for each summand in the strain energy function $\Psi(\mathsf{C})$. As one can easily see later, a strict inequality cannot be achived as H is arbitrary. For the convexity of the isotropic part of the artery model, which is nothing else than the Neo–Hooke model, cf. 4.4.9. For the isotropic part of the myocardium model we have, using the chain rule,

$$\begin{aligned} &D_{\mathsf{C}}^2\left(\frac{a}{2b}\exp[b(I_1(\mathsf{C}) - 3)]\right).(\mathsf{H},\mathsf{H}) = \frac{a}{2}D_{\mathsf{C}}\left\{\exp[b(I_1(\mathsf{C}) - 3)]\left(D_{\mathsf{C}}I_1(\mathsf{C}).\mathsf{H}\right)\right\}.\mathsf{H} \\ &= \frac{a}{2}\exp[b(I_1(\mathsf{C}) - 3)]\left[b\left(D_{\mathsf{C}}I_1(\mathsf{C}).\mathsf{H}\right)^2 + D_{\mathsf{C}}^2I_1(\mathsf{C}).(\mathsf{H},\mathsf{H})\right]. \end{aligned}$$

With $I_1(\mathsf{C}) = \mathrm{tr}(\mathsf{C})$ and the definition of the Gâteaux derivative 4.6 we get

$$D_{\mathsf{C}}^2\left(\frac{a}{2b}\exp[b(I_1(\mathsf{C}) - 3)]\right).(\mathsf{H},\mathsf{H}) = \frac{ab}{2}\exp[b(I_1(\mathsf{C}) - 3)](\mathrm{tr}\,\mathsf{H})^2.\mathsf{H}$$

which has to hold for all H. Hence we require that $a > 0$ and $b > 0$. Note that this holds by definition, see (3.109).

The terms corresponding to stretches in fiber directions have the structure

$$\frac{c_1}{2c_2}\left\{\exp[c_2(I(\mathsf{C},\boldsymbol{a})-1)^2]-1\right\} := \psi(\mathsf{C}),$$

where c_1, c_2 are constants and $\boldsymbol{a} \in \mathbb{R}^3$ is a constant vector, i.e a fiber direction. The second Gâteaux derivative of this exponential function yields

$$\begin{aligned} D^2_{\mathsf{C}}\,\psi(\mathsf{C}).(\mathsf{H},\mathsf{H}) &= c_1 D_{\mathsf{C}}\left(\exp[c_2(I(\mathsf{C},\boldsymbol{a})-1)^2]\,(I(\mathsf{C},\boldsymbol{a})-1)\,D_{\mathsf{C}}I(\mathsf{C},\boldsymbol{a}).\mathsf{H}\right).\mathsf{H} \\ &= c_1\exp[c_2(I(\mathsf{C},\boldsymbol{a})-1)^2]\left\{2c_2(I(\mathsf{C},\boldsymbol{a})-1)^2\,(D_{\mathsf{C}}I(\mathsf{C},\boldsymbol{a}).\mathsf{H})^2 + (D_{\mathsf{C}}I(\mathsf{C},\boldsymbol{a}).\mathsf{H})^2\right. \\ &\quad \left.+(I(\mathsf{C},\boldsymbol{a})-1)D^2_{\mathsf{C}}I(\mathsf{C},\boldsymbol{a}).(\mathsf{H},\mathsf{H})\right\}. \end{aligned}$$

In the case of stretches along a fiber or sheet direction, we have $I(\mathsf{C},\boldsymbol{a}) > 1$, where $\boldsymbol{a}$ is either $\boldsymbol{a}_{04}$, $\boldsymbol{a}_{06}$, $\boldsymbol{f}_0$ or $\boldsymbol{s}_0$. This holds since the anisotropic parts only contribute given a stretch in fiber direction, i.e. the corresponding invariants are larger than one; cf. Eqs. (3.90) and (3.110). With Lemma A.2 we can write the invariants I_4, I_6, I_{4s} and I_{4f} in the form $I(\mathsf{C},\boldsymbol{a}) = \mathrm{tr}(\mathsf{C}(\boldsymbol{a}\otimes\boldsymbol{a})) = \boldsymbol{a}^\top(\mathsf{C}\boldsymbol{a})$ and hence we obtain, using the Gâteaux derivative, that

$$2c_2(I(\mathsf{C},\boldsymbol{a})-1)^2 + 1 \geq 0$$

has to hold to guarantee convexity of $\psi(\mathsf{C})$. Hence we have to set $c_1 > 0$ and

$$c_2 > -\frac{1}{2(I(\mathsf{C},\boldsymbol{a})-1)^2},$$

which is trivially fulfilled for $c_2 > 0$. The requirement that all constants, i.e. k_1, k_2, a_f, b_f, a_s and b_s, are positive, fits with the histology of the biological materials, cf. Eqs. (3.81) and (3.110).

To show convexity of the myocardium model we calculate the second Gâteaux derivative of the orthotropic part with $I_{8fs} = I_{8fs}(\mathsf{C},\boldsymbol{f}_0,\boldsymbol{s}_0)$

$$\begin{aligned} D^2_{\mathsf{C}}\left(\frac{a_{fs}}{2b_{fs}}\left\{\exp(b_{fs}I^2_{8fs})-1\right\}\right).(\mathsf{H},\mathsf{H}) &= a_{fs}D_{\mathsf{C}}\left(\exp(b_{fs}I^2_{8fs})\,I_{8fs}\,D_{\mathsf{C}}I_{8fs}.\mathsf{H}\right).\mathsf{H} \\ = a_{fs}\exp(b_{fs}I^2_{8fs})\left(2b_{fs}I^2_{8fs}(D_{\mathsf{C}}I_{8fs}.\mathsf{H})^2 + (D_{\mathsf{C}}I_{8fs}.\mathsf{H})^2 + I_{8fs}D^2_{\mathsf{C}}I_{8fs}.(\mathsf{H},\mathsf{H})\right). \end{aligned}$$

With the definition that $I_{8fs} = \boldsymbol{f}_0.(\mathsf{C}\,\boldsymbol{s}_0)$, we need $a_{fs} > 0$ and

$$b_{fs} > -\frac{1}{2I^2_{8fs}}$$

for the convexity of the orthotropic part. Hence we have shown convexity of each summand of both strain energy functions which proves the lemma. □

It is easy to see that for $\boldsymbol{U} = \mathbf{0}$ it holds that $\mathsf{C} = \mathsf{I}$ and hence $\Psi(\mathsf{I}) < \infty$. Using Definition 4.38 we get $\mathcal{I}(\mathbf{0}) < \infty$ for a bounded Lipschitz domain Ω. Thus we fulfill the requirements of Theorem 4.22 and obtain the existence of a solution for the system of equations arising from the artery and the myocardium model. With Remark 4.4.5 and 4.4.10 we have the same for the incompressible and nearly incompressible case.

5. Discretization

In almost every practical application an exact solution of the variational formulations discussed in Chapter 4 is not possible. Hence we use discretization techniques, in particular the finite element method (FEM), see Sect. 5.1, as powerful numerical tools to find an approximate solution of the equilibrium equations.

To apply an inexact Newton method, see Sect. 5.2, we take a closer look at the discretization of the linearized variational formulations arising from nonlinear elasticity and the assembling of the corresponding stiffness matrices, see Sect. 5.3.

The resulting series of linear systems of equations may contain, especially for practical applications, a very high number of degrees of freedom. Hence we need elaborate algorithms to solve such a system. In Section 5.5 we outline the most common direct and iterative solution methods.

5.1. Galerkin Discretizations and Finite Element Method

We consider the bounded and X–elliptic operator A, satisfying the variational formulation (4.13):

$$\boldsymbol{u} \in X : \quad \langle A(\boldsymbol{u}), \boldsymbol{v} \rangle = \langle \boldsymbol{f}, \boldsymbol{v} \rangle \quad \text{for all } \boldsymbol{v} \in X.$$

For $M \in \mathbb{N}$ let

$$X_M := \operatorname{span} \{\varphi_k\}_{k=1}^{M} \subset X \tag{5.1}$$

be a conforming ansatz space. With

$$\boldsymbol{u}_M := \sum_{k=1}^{M} \boldsymbol{u}_k \varphi_k \in X_M$$

we formulate an approximate solution of the *Galerkin–Bubnov variational formulation* to find

$$\boldsymbol{u}_M \in X_M : \quad \langle A(\boldsymbol{u}_M), \boldsymbol{v}_M \rangle = \langle \boldsymbol{f}, \boldsymbol{v}_M \rangle \quad \text{for all } \boldsymbol{v}_M \in X_M. \tag{5.2}$$

For stability and error estimates of this approximation we refer to the following *Céa's Lemma* and the *Lemmas of Strang*. For more information, e.g., cf. [147, Steinbach (2008)].

Theorem 5.1 (Céa's Lemma). *Let $a : X \times X' \to \mathbb{R}$ be a bounded and X–elliptic bilinear form. Moreover let f be a bounded linear form in X and $X_h \subset X$ be a finite dimensional ansatz space. Then the discrete version of the variational formulation*

$$a(\boldsymbol{u}_h, \boldsymbol{v}_h) = \langle \boldsymbol{f}, \boldsymbol{v}_h \rangle \quad \text{for all } \boldsymbol{v}_h \in X_h$$

is uniquely solvable. For the discrete solution $u_h \in X_h$ the following stability estimate

$$\|\boldsymbol{u}_h\|_X \leq \frac{1}{c_1^A} \|\boldsymbol{f}\|_{X'}$$

and the error estimate

$$\|\boldsymbol{u} - \boldsymbol{u}_h\|_X \leq \frac{c_2^A}{c_1^A} \inf_{\boldsymbol{v}_h \in X_h} \|\boldsymbol{u} - \boldsymbol{v}_h\|_X$$

hold.

Proof. See for example [147, Steinbach (2008)]. □

For the nonlinear case we may apply Céa's Lemma to the discrete version of the linearized bilinear form $a'(\boldsymbol{\delta u}_h, \boldsymbol{v})$ with $\boldsymbol{\delta u}_h \in X$ the approximation of $\boldsymbol{\Delta u}$, see Sect. 4.4.5 and Sect. 5.2.

To find an approximate solution of the variational problem (4.13), we will use the finite element method (FEM). This numerical technique goes back to [130, Schellbach (1851)], [119, Ritz (1908)] and [46, Galerkin (1915)]. For this we will construct finite-dimensional ansatz spaces V_h, typically containing piecewise polynomial functions of degree k, and then find an approximate solution $\boldsymbol{u}_h \in V_h$. In the following, the parameter h indicates that we have a finite-dimensional approximation. Under appropriate assumptions we can estimate the approximation error by

$$\inf_{\boldsymbol{v}_h \in V_h} \|\boldsymbol{u}^* - \boldsymbol{v}_h\|_{H^1(\Omega)} \leq c h^k \|\boldsymbol{u}^*\|_{H^{k+1}(\Omega)},$$

with $\boldsymbol{u}^*$ the unique exact solution of the variational formulation.

For further information on the finite element method the interested reader is referred to the classical works [159, Zienkiewicz (1971)] and [24, Ciarlet (1978)]. From the almost overwhelming amount of more recent publications we want to mention the monographs [147, Steinbach (2008)], [14, Braess (2007)], [77, Jung and Langer (2001)] and [17, Brenner and Scott (1994)].

For the pure displacement problem in elastostatics we have as starting point for the finite element formulation the primal variational problem (4.13). In using Galerkin's principle of discretization we choose an appropriate finite-dimensional subspace $V_h \subset$

$[H^1_D(\Omega, \Gamma_D)]^3$. Hence we want to compute the approximate solution $\boldsymbol{u}_h \in V_h$ of the finite-dimensional variational problem

$$a(\boldsymbol{u}_h, \boldsymbol{v}_h) = \langle \boldsymbol{f}, \boldsymbol{v}_h \rangle, \tag{5.3}$$

for the finite-dimensional test functions $\boldsymbol{v}_h \in V^0_h \subset [H^1_0(\Omega, \Gamma_D)]^3$. In the nonlinear case we want to solve

$$a'(\boldsymbol{\delta u}_h, \boldsymbol{v}_h) = \langle \boldsymbol{F}, \boldsymbol{v}_h \rangle \tag{5.4}$$

in each Newton step for $\boldsymbol{\delta u}_h \in V_h$ and $\boldsymbol{v}_h \in V^0_h$.

Inhomogeneous and homogeneous Dirichlet boundary conditions are included using standard homogenization techniques. For more information, e.g., cf. [77, Jung and Langer (2001), Ch. 4.5].

5.1.1. Discretization in Finite Elements

Let $\Omega \subset \mathbb{R}^3$ be a bounded domain which is subdivided into N *finite elements* τ_l such that

$$\overline{\Omega}_h = \bigcup_{l=1}^{N} \overline{\tau}_l \ , \quad \text{with } \overline{\Omega}_h \to \ \overline{\Omega} \ , \quad \text{for } h \to 0. \tag{5.5}$$

Our choice for the finite elements in $\mathbb{R}^3$ are polyhedral tetrahedrons and hexahedrons. To approximate the fine structures on the surface of arterial and cardiac tissues a discretization in tetrahedrons shows the best results.

For each finite element τ_l we define the volume Δ_l and the local mesh size h_l as

$$\Delta_l := \int_{\tau_l} \mathrm{d}\boldsymbol{x} \quad \text{and} \quad h_l := \Delta_l^{1/3}. \tag{5.6}$$

With this we can define the *global mesh size* as

$$h := \max_{l=1,\cdots,N} h_l \ .$$

In our case all elements of our discretized mesh can be derived from one specific element the so-called *reference element* τ. In the case of tetrahedrons the reference element is given through

$$\tau = \left\{ \boldsymbol{\xi} \in \mathbb{R}^3 : 0 \le \xi_1 \le 1, 0 \le \xi_2 \le 1 - \xi_1, 0 \le \xi_3 \le 1 - \xi_1 - \xi_2 \right\}. \tag{5.7}$$

For an arbitrary $\boldsymbol{x} \in \tau_l$ we then have the following representation

$$\boldsymbol{x} = \boldsymbol{x}_{l_1} + \sum_{i=1}^{3} \boldsymbol{\xi}(\boldsymbol{x}_{l_{i+1}} - \boldsymbol{x}_{l_1}) = \boldsymbol{x}_{l_1} + J_l \boldsymbol{\xi} \quad \text{for } \boldsymbol{\xi} \in \tau$$

with the Jacobian matrix

$$J_l = \begin{pmatrix} x_{l_2,1} - x_{l_1,1} & x_{l_3,1} - x_{l_1,1} & x_{l_4,1} - x_{l_1,1} \\ x_{l_2,2} - x_{l_1,2} & x_{l_3,2} - x_{l_1,2} & x_{l_4,2} - x_{l_1,2} \\ x_{l_2,3} - x_{l_1,3} & x_{l_3,3} - x_{l_1,3} & x_{l_4,3} - x_{l_1,3} \end{pmatrix} .$$

With a simple calculation we get for the volume

$$\Delta_l = \frac{1}{6} |\det J_l| . \tag{5.8}$$

In case of hexahedrons we have the unit cube as reference element and we can formulate similar relations as for tetrahedrons; cf., e.g., [77, Jung and Langer (2001),Ch. 4.5.2].

For an arbitrary function $v(\boldsymbol{x})$ we then have the representation

$$v(\boldsymbol{x}) = v(\boldsymbol{x}_{l_1} + J_l \boldsymbol{\xi}) = \tilde{v}_l(\boldsymbol{\xi}) \quad \text{for } \boldsymbol{\xi} \in \tau .$$

and for the gradient

$$\nabla_{\boldsymbol{x}} v(\boldsymbol{x}) = J_l^{-\top} \nabla_{\boldsymbol{\xi}} \tilde{v}_l(\boldsymbol{\xi}) , \quad \nabla_{\boldsymbol{\xi}} \tilde{v}_l(\boldsymbol{\xi}) = J_l^{\top} \nabla_{\boldsymbol{x}} v(\boldsymbol{x}) .$$

5.1.2. Shape Functions

We now define ansatz spaces for the discretization Ω_h, (5.5). These spaces are constructed by piecewise polynomial functions, called shape functions. They are locally defined on the specific finite elements τ_l.

A simple possibility to discretize the variational formulations described in Section 4.2 are to use piecewise linear shape functions for each component of the displacement field $\boldsymbol{u}$. Unless otherwise indicated, we will use this kind of shape functions for our numerical simulations. The other type that is used are piecewise quadratic shape functions, which show advantages for the simulation of nearly incompressible materials.

Example 5.1. *For tetrahedrons the linear shape functions for the displacement field are given with*

$$\varphi_1^1(\boldsymbol{\xi}) := 1 - \xi_1 - \xi_2 - \xi_3, \ \varphi_2^1(\boldsymbol{\xi}) := \xi_1, \ \varphi_3^1(\boldsymbol{\xi}) := \xi_2, \ \varphi_4^1(\boldsymbol{\xi}) := \xi_3, \ \textit{for } \boldsymbol{\xi} \in \tau.$$

Let τ_l be an arbitrary tetrahedral finite element with the nodes $x_{l_1}, x_{l_2}, x_{l_3}, x_{l_4}$. Then we have for a linear function, given in τ_l, the following representation:

$$v_h(\boldsymbol{x}) = v_h(\boldsymbol{x}_{l_1} + J_l \boldsymbol{\xi}) = \sum_{k=1}^{4} v_{l_k} \varphi_k^1(\boldsymbol{\xi}) \quad \textit{for } \boldsymbol{x} \in \tau_l, \boldsymbol{\xi} \in \tau , \tag{5.9}$$

with coefficients v_{l_k}.

Cf. [77, Jung and Langer (2001)] or [14, Braess (2007)] for higher-order shape functions and shape functions on many different elements.

From the discrete variational formulation (5.3) we get with the basis representation for the wanted solution vector $\boldsymbol{u}_h = \sum_i \boldsymbol{u}_i \varphi_i$ the linear system of equations

$$\mathsf{K}_h \underline{u} = \underline{b}, \tag{5.10}$$

where $\underline{u} \in \mathbb{R}^m$ is the vector consisting of the coefficients $\boldsymbol{u}_i$, $\mathsf{K}_h \in \mathbb{R}^{m \times m}$ the stiffness matrix, $\underline{b} \in \mathbb{R}^m$ the right hand side vector and m the number of degrees of freedom. The entries of the stiffness matrix are determined by $\mathsf{K}_h = [a(\varphi_j, \varphi_i)]_{i,j \in \omega_h}$ with ω_h the node-indices of nodes on $\Omega \cup \Gamma_N$. The right hand side vector by $\underline{b} = [\langle \boldsymbol{f}, \varphi_i \rangle]_{i \in \omega_h}$. For the nonlinear case see (5.19).

5.1.3. Discretization of the Saddle Point Formulation

In this section we will sketch two possible choices of finite elements that can be used to treat saddle point problems (cf. 4.3.1). For additional information and other finite elements that may be of interest we refer to [14, Braess (2007)] and [27, Crouzeix and Raviart (1973)].

Let $\mathcal{X}_h$ and $\mathcal{M}_h$ the discrete version of the spaces defined in (4.22).

$\mathcal{Q}_k$–$\mathcal{P}_0$–element For this hexahedral element we use ansatz functions of polynomial degree $k \geq 1$ for the displacement $\boldsymbol{u}$ and piecewise constant functions for the pressure p, i.e.

$$\begin{aligned} \mathcal{X}_h &:= \{\boldsymbol{v} \in C^0(\overline{\Omega})^3 : \ \boldsymbol{v}|_\tau \in \mathcal{Q}_k \text{ for } \tau \in \Omega_h, k \geq 1\} \ , \\ \mathcal{M}_h &:= \{q \in L_{2,0}(\Omega) : \ q|_\tau \in \mathcal{P}_0 \text{ for } \tau \in \Omega_h\} \ . \end{aligned}$$

Concerning the saddle point system arising from nearly incompressible linear elasticity this element does not fulfill the LBB-condition, or *inf-sup-condition*, from [90, Ladyshenskaya (1969)], [7, Babuška (1973)] and [18, Brezzi (1974)]. Nonetheless it can be stabilized, see [82, Klawonn and Pavarino (1998)] and [81, Kechkar and Silvester (1992)]. To the best of our knowledge no stability proofs for nonlinear elasticity are yet known.

$\mathcal{P}_k$–$\mathcal{P}_0$–element: the tetrahedral counterpart of the $\mathcal{Q}_k$–$\mathcal{P}_0$–element.

Taylor–Hood–element In contrast to the $\mathcal{Q}_1$–$\mathcal{P}_0$–element the Taylor–Hood–element fulfills the inf-sup-condition for the case of almost incompressible linear elasticity is therefore considered as stable. We use quadratic ansatz functions for the displacement $\boldsymbol{u}$ and linear ansatz functions for the pressure p, i.e.

$$\mathcal{X}_h := \{\boldsymbol{v}_h \in C(\overline{\Omega})^3 \cap H_0^1(\Omega)^3 : \ \boldsymbol{v}_h|_\tau \in \mathcal{P}_2 \text{ for } \tau \in \Omega_h\},$$
$$\mathcal{M}_h := \{q_h \in C(\Omega) \cap L_{2,0}(\Omega) : q_h|_\tau \in \mathcal{P}_1 \text{ for } \tau \in \Omega_h\}.$$

For the proof of the inf-sup-condition we refer to [152, Verfürth (1984)] and [48, Girault and Raviart (1986)].

In the case of domain decomposition approaches, the usage of Taylor–Hood–elements is not straightforward and the continuity of the pressure across the interface imposes difficulties especially concerning preconditioning and the scalability of the parallel algorithms, see, e.g., [21, Calgaro and Laminie (2000)], [12, Benhassine and Bendali (2011)] and [141, Šístek et al. (2011)]. Thus, we concentrate on standard finite elements ($\mathcal{P}_k$) and the $\mathcal{P}_k$–$\mathcal{P}_0$–element in this theses. Hexahedral elements are neglected since they showed the same results as tetrahedral elements and due to the fact that the meshes for practical applications were given with a triangulation in tetrahedrons.

The difference in the order of the displacement and the pressure in all introduced elements is motivated by the differential operators that appear. For the displacement we have derivatives up to second order, while for the pressure we have to compute the gradient of p, hence first order.

5.1.4. Mean Dilatation Technique

In Sect. 4.4.2 we described the variational formulation of the decoupled boundary value problem to handle the case of incompressible and nearly incompressible nonlinear elastic materials. Here we introduced the scalar-valued volumetric variable $\overline{J}$ which has to satisfy $\overline{J} = J$ in a weak sense. This leads to the additional equation

$$\int_{\Omega_0} \left(\overline{J} - J(\boldsymbol{U}, \boldsymbol{X})\right) q(\boldsymbol{X}) \, \mathrm{d}\boldsymbol{X} = 0, \quad \text{for all } q \in L_2(\Omega_0). \tag{5.11}$$

The idea of the mean dilatation method is to eliminate this volumetric variable elementwise (static condensation). This may be achieved in using discontinuous ansatz functions, where we will concentrate on piecewise constants (as already mentioned in Sec. 4.4.2). Let $\tau_0 \subset \Omega_0$ be an arbitrary finite element. We choose q_h, such that it is constant over the element domain τ_0 and zero elsewhere. Hence, the discretized version of (5.11) in the element domain τ_0 reads

$$\int_{\tau_0} \overline{J}_h - J(\boldsymbol{U}, \boldsymbol{X}) \, \mathrm{d}\boldsymbol{X} = 0.$$

Since the element-wise constant $\overline{J}_h$ does not depend on $\boldsymbol{X}$ in τ_0, we obtain

$$\overline{J}_h \int_{\tau_0} \mathrm{d}\boldsymbol{X} - \int_{\tau_0} J(\boldsymbol{U}, \boldsymbol{X}) \, \mathrm{d}\boldsymbol{X} = 0.$$

Let $\mathrm{vol}(\tau_0)$ and $\mathrm{vol}(\tau)$ be the volumes of the domain τ_0 in the reference configuration and in the current configuration, respectively. Using (3.8) we get

$$\overline{J}_h = \frac{\mathrm{vol}(\tau)}{\mathrm{vol}(\tau_0)}. \tag{5.12}$$

With this we may calculate the discretized version $\overline{p}_h$ of the hydrostatic pressure p using (3.58). In the arbitrary domain τ_0, where both volumetric functions are constant, we can state

$$\overline{p}_h = \left. \frac{\mathrm{d}U(\overline{J}_h)}{\mathrm{d}\overline{J}_h} \right|_{\overline{J}_h = \frac{\mathrm{vol}(\tau)}{\mathrm{vol}(\tau_0)}},$$

with the scalar variable $\overline{p}$, such that $\overline{p} = p$ is satisfied in a weak sense.

Example 5.2. *With a function $U(J)$ as defined in* (3.56) *we get for the hydrostatic pressure in an arbitrary element τ_0*

$$\overline{p}_h = \kappa \left(\frac{\mathrm{vol}(\tau)}{\mathrm{vol}(\tau_0)} - 1 \right) .$$

These piecewise constant volumetric variables are incorporated in the discrete version of the decoupled variational formulation, see Sect. 5.3. This leads to a Q_p–P_0–element for hexahedrons and a P_p–P_0–element for tetrahedrons. Here p is the order of the base functions for the displacement field. It is known that linear finite elements are very prone to volumetric locking. Hence for nearly incompressible materials piecewise quadratic elements ($p = 2$) are a better choice. The resulting P_2–P_0–element for tetrahedrons was also the choice to model nearly incompressible arterial material in [84, Klawonn and Rheinbach (2010)].

5.2. Inexact Newton Methods

In the case of the numerical solution of nonlinear elasticity problems we have to take function and derivative approximations into account. Hence we have to study inexact Newton methods of the kind

$$F'(x^k)\delta x^k = -F(x^k) + r^k, \quad x^{k+1} = x^k + \delta x^k, \tag{5.13}$$

with the inexact Newton corrections δx^k. Equivalently, using (4.28), this can be written as

$$F'(x^k)(\delta x^k - \Delta x^k) = r^k, \quad x^{k+1} = x^k + \delta x^k,$$

where Δx^k are the exact Newton corrections. In this thesis we use Galerkin methods as a dicretization technique. Thus we focus on *local Newton-Galerkin methods*, e.g., cf. [35, Deuflhard (2004)], as described in the following. For $x^k \in W^{1,p}$ we have the scheme

$$x^{k+1} = x^k + \delta x^k, \tag{5.14}$$

where the inexact Newton corrections δx^k have to satisfy

$$\langle x^k, F'(x^k)(\delta x^k - \Delta x^k)\rangle = \langle \delta x^k, r^k\rangle \ . \tag{5.15}$$

As a theoretical framework to the convergence properties of the above Newton–Galerkin method we formulate the following Newton–Mysovskikh type theorem.

Theorem 5.2 (Newton–Mysovskikh). *Let $D \subset W^{1,p}$ be an open and convex subset equipped with the norm $\|\bullet\|_D$. Let $f : D \to \mathbb{R}$ be a twice continuously differentiable functional which is minimized over D. Let $F'(x) = f''(x)$ such that it is strictly positive and fulfills the affine conjugate Lipschitz condition*

$$\|F'(z)^{-1/2}(F'(y) - F'(x))v\|_D \leq \omega \|F'(x)^{-1/2}(y-x)\|_D \dot{\|} F'(x)^{1/2} v\|_D,$$

with $0 \leq \omega < \infty$ and collinear $x, y, z \in D$. We consider a Newton–Galerkin method satisfying (5.15) *with*

$$\delta_k := \frac{\|F'(x^k)^{1/2}(\delta x^k - \Delta x^k)\|_D}{\|F'(x^k)^{1/2}\delta x^k\|_D}$$

the approximation errors. Define the so-called Kantorovich quantities

$$\eta_k := \omega \|F'(x^k)^{1/2}\Delta x^k\|_D, \quad \eta_k^\delta := \omega \|F'(x^k)^{1/2}\delta x^k\|_D = \frac{\eta_k}{\sqrt{1+\delta_k^2}}$$

for any well-defined iterate x^k. Assume that for an initial guess $x^0 \in D$ the level set

$$\mathcal{L} := \left\{ x \in D : f(x) \leq f(x^0) \right\} \neq \emptyset$$

is bounded and closed. Then it holds:

1. (Linear convergence) *Let the initial guess x_0 satisfy for a constant $\Theta < 1$*

$$\eta_0 \leq 2\Theta < 2 \tag{5.16}$$

and assume that $\delta_{k+1} \geq \delta_k$ for all k. Let the Galerkin approximation be such that

$$\frac{\eta_k^\delta + \delta_k\left(\eta_k^\delta + \sqrt{4 + (\eta_k^\delta)^2}\right)}{2\sqrt{1+\delta_k^2}} \leq \Theta.$$

Then we have a minimizing point $x^* \in \mathcal{L}_0$ such that the iterates $x^k \in \mathcal{L}_0$ converge to x^* at least linearly, i.e.

$$\eta_{k+1} \leq \Theta \eta_k \text{ and } \eta_{k+1}^\delta \leq \Theta \eta_k^\delta.$$

2. (Quadratic convergence) *Let the initial guess x_0 satisfy for a constant $\theta > 0$*

$$\eta_0 < \frac{2}{1+\theta} \tag{5.17}$$

and let the Galerkin approximation be such that

$$\delta_k \leq \frac{\theta \eta_k^\delta}{\eta_k^\delta + \sqrt{4 + (\eta_k^\delta)^2}}.$$

Then $x^k \in \mathcal{L}_0$ converge quadratically to the minimizing point $x^* \in \mathcal{L}_0$, i.e.

$$\eta_{k+1} \leq \frac{(1+\theta)}{2}(\eta_k)^2 \text{ and } \eta_{k+1}^\delta \leq \frac{(1+\theta)}{2}(\eta_k^\delta)^2.$$

Proof. For more information and the proof see [35, Deuflhard (2004), Sect. 2.3 and Sect. 8.3]. □

In our case the assumptions of Theorem 5.2 are satisfied due to the properties of the strain energy function, see Remark 3.8.3 (Normalization Conditions), and the equivalence to the minimization problem (4.39). Using Eq. (4.28) we can write η_0 in Eqs. (5.16) and (5.17) as

$$\eta_0 = \omega \|F'(x^0)^{1/2} \Delta x^0\|_{H^1(\Omega)} = \omega \|F'(x^0)^{-1/2} F(x^0)\|_{H^1(\Omega)}.$$

In the case of nonlinear elasticity we have with the definitions and assumptions in Sect. 4.4

$$\eta_0 = \|(\boldsymbol{\Delta u}, A'(\boldsymbol{u}^0)\boldsymbol{v})^{-1/2}(\langle \boldsymbol{f}, \boldsymbol{v}\rangle - (A(\boldsymbol{u}^0), \boldsymbol{v}))\|_{H^1(\Omega)}.$$

Hence the convergence rate is dependent on the initial solution $\boldsymbol{u}_0$, on the parameters used in the model and on the inhomogeneous Dirichlet and Neumann boundary conditions which influence $\langle \boldsymbol{f}, \boldsymbol{v}\rangle$. An appropriate choice for the initial solution $\boldsymbol{u}_0$ could be the solution of a simplified problem, like the linear elasticity or the Neo-Hooke model, or the solution of a modified nonlinear elasticity problem. The latter comprises the solution of the same nonlinear model with modified parameters, e.g. a reduced bulk modulus κ, or modified boundary conditions, e.g. a reduced pressure on the surface.

We write for the Newton method used in our numerical simulations

$$(\boldsymbol{\delta u}_h, A'(\boldsymbol{u}_h^k)\boldsymbol{v}_h) = \langle \boldsymbol{f}, \boldsymbol{v}_h\rangle - \langle A(\boldsymbol{u}_h^k), \boldsymbol{v}_h\rangle, \quad \boldsymbol{u}_h^{k+1} = \boldsymbol{u}_h^k + \boldsymbol{\delta u}_h. \tag{5.18}$$

Using the equivalent linear system of equations we have to solve

$$\mathsf{K}'(\underline{u}^k)\,\underline{\delta u} = \underline{f} - K(\underline{u}^k), \quad \underline{u}^{k+1} = \underline{u}^k + \underline{\delta u} \tag{5.19}$$

with the tangent stiffness matrix

$$\mathsf{K}'(\underline{u}^k)[i,j] := (\varphi_j, A'(\boldsymbol{u}_h^k)\,\varphi_i)$$

and the right hand sides

$$\underline{f}[i] := \langle \boldsymbol{f}, \varphi_i \rangle \quad \text{and} \quad \underline{K}(\underline{u}^k)[i] := (A(\boldsymbol{u}_h^k), \varphi_i).$$

5.3. Assembling of the Stiffness Matrices

In this section we will give a short overview to the assembling of the element stiffness matrices using the discretized and linearized variational equations for the elasticity models. Using standard methods these element stiffness matrix are assembled to global stiffness matrix, e.g., cf. [77, Jung and Langer (2001)].

For linear elasticity we have the discretized bilinear form

$$a(\boldsymbol{u}_h, \boldsymbol{v}_h) = \int_\Omega \mathbb{C}\,\varepsilon(\boldsymbol{u}_h, \boldsymbol{x}) : \varepsilon(\boldsymbol{v}_h, \boldsymbol{x})\,\mathrm{d}\boldsymbol{x}, \tag{5.20}$$

For this we obtain the 3×3 entries in the element stiffness matrix for each degree of freedom by

$$\mathsf{K}_{(\tau)}[i,j] = a'(\varphi_j, \varphi_i) = \int_\tau \mathcal{B}_i^\top\,\mathcal{C}\,\mathcal{B}_j\,\mathrm{d}\boldsymbol{x} \quad \text{for } i,j = 1,\ldots,\hat{N}, \tag{5.21}$$

with $\mathcal{C}$ the elasticity tensor in Voigt notation and

$$\mathcal{B}_i^\top = \begin{pmatrix} \frac{\partial\varphi_i}{\partial x_1} & 0 & 0 & \frac{\partial\varphi_i}{\partial x_2} & 0 & \frac{\partial\varphi_i}{\partial x_3} \\ 0 & \frac{\partial\varphi_i}{\partial x_2} & 0 & \frac{\partial\varphi_i}{\partial x_1} & \frac{\partial\varphi_i}{\partial x_3} & 0 \\ 0 & 0 & \frac{\partial\varphi_i}{\partial x_3} & 0 & \frac{\partial\varphi_i}{\partial x_2} & \frac{\partial\varphi_i}{\partial x_1} \end{pmatrix} \tag{5.22}$$

In the case of nonlinear elasticity we show the assembling of the stiffness matrices in the current configuration. A similar procedure in the reference configuration is obtained using the corresponding pull-back operations. For the first summand in Eq. (4.34) we have the discretized form

$$a'_{\mathrm{geo}}(\boldsymbol{\delta u}_h, \boldsymbol{v}_h) := (\boldsymbol{\delta u}_h, A'_{\mathrm{geo}}(\boldsymbol{u}_h^k), \boldsymbol{v}_h) = \int_\Omega \mathrm{grad}(\boldsymbol{\delta u}_h)\,\sigma(\boldsymbol{u}_h^k) : \mathrm{grad}\,\boldsymbol{v}_h\,\mathrm{d}\boldsymbol{x}.$$

Applying the ansatz functions component-wise yields the so-called geometrical part of the tangent element stiffness matrix $\mathsf{K}_{\text{geo}}^{\prime(\tau)}(\underline{u}^k)$

$$\mathsf{K}_{\text{geo}}^{\prime(\tau)}[i,j] = a'_{\text{geo}}(\varphi_j,\varphi_i) = \mathsf{I}\int_\tau (\operatorname{grad}\varphi_j)^\top \sigma(\boldsymbol{u}_h^k)\operatorname{grad}\varphi_i \,\mathrm{d}\boldsymbol{x} \quad \text{for } i,j=1,\dots,\hat{N}. \tag{5.23}$$

For the decoupled representation (4.37) we have, with the element-wise constant volumetric variable $\overline{p}_h$, see Example 5.2, and $\overline{\sigma}_{ij}$ the components of $\overline{\sigma}(u_h^k)$, for the stress tensor

$$\sigma(\boldsymbol{u}_h^k) = \begin{pmatrix} \overline{p}_h & 0 & 0 \\ 0 & \overline{p}_h & 0 \\ 0 & 0 & \overline{p}_h \end{pmatrix} + \begin{pmatrix} \overline{\sigma}_{11} & \overline{\sigma}_{12} & \overline{\sigma}_{13} \\ . & \overline{\sigma}_{22} & \overline{\sigma}_{23} \\ \text{sym.} & . & \overline{\sigma}_{33} \end{pmatrix} \tag{5.24}$$

Similar to linear elasticity we get for the second summand in Eq. (4.34), the so-called material part of the element tangent stiffness matrix $\mathsf{K}_{\text{mat}}^{\prime(\tau)}(\underline{u}^k)$

$$\mathsf{K}_{\text{mat}}^{\prime(\tau)}[i,j] = a'_{\text{mat}}(\varphi_j,\varphi_i) = \int_\tau \mathcal{B}_j^\top \mathcal{C}(\boldsymbol{u}_h^k)\,\mathcal{B}_i \,\mathrm{d}\boldsymbol{x} \quad \text{for } i,j=1,\dots,\hat{N}. \tag{5.25}$$

with $\mathcal{C}(\boldsymbol{u}_h^k)$ the elasticity tensor in Voigt notation and $\mathcal{B}$ from Eq. (5.22). In the case of the decoupled formulation we can write

$$\mathcal{C} = \begin{pmatrix} c_{1111} & c_{1122} & c_{1133} & c_{1112} & c_{1123} & c_{1113} \\ . & c_{2222} & c_{2233} & c_{2212} & c_{2223} & c_{2213} \\ . & . & c_{3333} & c_{3312} & c_{3323} & c_{3313} \\ . & . & . & c_{1212} & c_{1223} & c_{1213} \\ . & \text{sym.} & . & . & c_{2323} & c_{2313} \\ . & . & . & . & . & c_{1313} \end{pmatrix} - \begin{pmatrix} \overline{p}_h & -\overline{p}_h & -\overline{p}_h & & & \\ -\overline{p}_h & \overline{p}_h & -\overline{p}_h & & & \\ -\overline{p}_h & -\overline{p}_h & \overline{p}_h & & & \\ & & & \overline{p}_h & & \\ & & & & \overline{p}_h & \\ & & & & & \overline{p}_h \end{pmatrix},$$

where c_{ijkl} are the components of the isochoric part of the elasticity tensor $\mathbb{C}_{\text{iso}}(\boldsymbol{u}_h^k)$ and $\overline{p}_h$ is the element-wise constant hydrostatic pressure.

Finally, for the decoupled model, we deal with the pressure contribution

$$a'_{\text{pre}}(\boldsymbol{\delta u}_h,\boldsymbol{v}_h) := (\boldsymbol{\delta u}_h, A'_{\text{pre}}(\boldsymbol{u}_h^k),\boldsymbol{v}_h) = \int_\Omega \left.\frac{\partial^2 U(J)}{\partial J^2}\right|_{J=J_h} \operatorname{div}(\boldsymbol{\delta u}_h)\operatorname{div}(\boldsymbol{v}_h)\,\mathrm{d}\boldsymbol{x}, \tag{5.26}$$

with the volumetric function $U(J)$. A component-wise application of the ansatz functions yields for the 3×3 entries of the pressure part of the tangent element stiffness matrix $\mathsf{K}_{\text{pre}}^{\prime(\tau)}(\underline{u}^k)$

$$\mathsf{K}_{\text{pre}}^{\prime(\tau)}[i,j] = a'_{\text{pre}}(\varphi_j,\varphi_i) = \int_\tau \left.\frac{\partial^2 U(J)}{\partial J^2}\right|_{J=\overline{J}} \operatorname{grad}\varphi_j(\operatorname{grad}\varphi_i)^\top \,\mathrm{d}\boldsymbol{x} \quad \text{for } i,j=1,\dots,\hat{N}. \tag{5.27}$$

Example 5.3. *For the volumetric function* (3.56)

$$U(J) = \frac{\kappa}{2}(J-1)^2$$

we get

$$\left.\frac{\partial^2 U(J)}{\partial J^2}\right|_{J=\overline{J}} = \kappa \frac{\mathrm{vol}(\tau)}{\mathrm{vol}(\tau_0)}.$$

The construction of the global tangent stiffness matrix follows the standard assembly procedure of element stiffness matrices

$$\mathsf{K}'(\underline{u}^k) = \sum_{\tau \in \Omega_h} \mathsf{A}_\tau^\top \left(\mathsf{K}'^{(\tau)}_{\mathrm{geo}}(\underline{u}^k) + \mathsf{K}'^{(\tau)}_{\mathrm{pre}}(\underline{u}^k) + \mathsf{K}'^{(\tau)}_{\mathrm{mat}}(\underline{u}^k) \right) \mathsf{A}_\tau$$

with A_τ connectivity matrices. Due to the self-adjointness (cf. Remark 4.4.2) and the X–ellipticity (cf. Sect. 4.4.5) of the operator A', the stiffness matrix $\mathsf{K}'(\underline{u}^k)$ is symmetric and positive definite in the case of the Eulerian formulation.

The linearized systems in the Lagrangian formulation, Eqs. (4.33) and (4.36), lead to a tangent stiffness matrix that is not necessarily symmetric. Since we have also shown X–ellipticity it is at least positive definite.

5.4. Time Stepping Schemes and Assembling of the Right Hand Side

Following cf. [154, Whiteley and al. (2007)] we can neglect the derivative with respect to time in Cauchy's equation of motion (3.23) and use the quasi-static formulation (3.30) as a starting point for our time stepping scheme. Hence we have to solve

$$\begin{aligned} -\operatorname{div} \sigma(\boldsymbol{u}, \boldsymbol{x}, t) &= \boldsymbol{0} && \text{in } \Omega_t \ , \\ \boldsymbol{u}(\boldsymbol{x}, t) &= \boldsymbol{u}_D(\boldsymbol{x}, t) && \text{on } \Gamma_{t,D} \ , \\ \sigma(\boldsymbol{u}, \boldsymbol{x}, t)\boldsymbol{n}(\boldsymbol{x}) &= \boldsymbol{t}_N(\boldsymbol{x}, t) && \text{on } \Gamma_{t,N} \end{aligned}$$

or the equivalent formulation in the reference configuration, respectively.

In terms of Newton's method, see Eq. (5.19), we have to solve the linearized system of equations

$$\mathsf{K}'(\underline{u}^k_{n+1})\, \underline{\delta u} = \underline{f} - \underline{K}(\underline{u}^k_{n+1}), \quad \underline{u}^{k+1}_{n+1} = \underline{u}^k_{n+1} + \underline{\delta u} \tag{5.28}$$

to obtain the equilibrium state at time t_{n+1}.

Total and updated Lagrangian formulation As we have seen in Sect. 4.2 we can express the variational formulation in terms of variables in the original and undeformed reference configuration. A term often used in this context are *material variables*. Another way is to express the variables in the current or deformed configuration; such variables are referred to as *spatial variables*.

The *total Lagrangian scheme* is characterized by using the formulation with material variables and the differentiations and integrations are carried out with respect to the domain Ω_0 and the Lagrangian coordinates $\boldsymbol{X}$.

On the other hand for the *updated Lagrangian scheme* we use spatial variables and the differentiation and integration procedures are carried out within Eulerian coordinates $\boldsymbol{x}$. With a coordinate transformation one can show that both formulations are equivalent.

One very important difference between the two formulations is the treatment of displacement dependent traction forces on the surface like pressure, see Sect. 3.6. In the updated Lagrangian scheme we incorporate a pressure load ϕ in the opposite direction of the outward normal $\boldsymbol{n}(\boldsymbol{x})$, using the variational formulation of the right hand side (4.15), by

$$\langle \boldsymbol{f}, \boldsymbol{v} \rangle = - \int_{\Gamma_N} \phi(\boldsymbol{x}, t) \boldsymbol{n}(\boldsymbol{x}, t) \cdot \boldsymbol{v}(\boldsymbol{x}) \, \mathrm{d}s_{\boldsymbol{x}}. \tag{5.29}$$

Here Γ_N is the Neumann boundary of the domain in the current configuration Ω. The discretized version of (5.29) reads

$$\langle \boldsymbol{f}, \boldsymbol{v}_h \rangle = - \int_{\Gamma_N} \phi(\boldsymbol{x}, t) \boldsymbol{n}(\boldsymbol{x}, t) \cdot \boldsymbol{v}_h(\boldsymbol{x}) \, \mathrm{d}s_{\boldsymbol{x}}$$

and hence we get for the entries for an element τ

$$\underline{f}[3i + k] = \langle \boldsymbol{f}, \varphi_i \rangle = - \int_{\Gamma_N \cap \partial\tau} \phi_{n+1} n_k \varphi_i \, \mathrm{d}s_{\boldsymbol{x}}, \qquad \text{for } k = 1, 2, 3; \; i = 1, \ldots, \hat{N},$$

with ϕ_{n+1} the pressure applied at time step t_{n+1} and n_k the k-th component of the normal vector $\boldsymbol{n}(\boldsymbol{x}, t)$. We note that pressure loads are dependent on the normal direction $\boldsymbol{n}(\boldsymbol{x}, t)$ and the surface area $\mathrm{d}s_{\boldsymbol{x}}$. We transform (5.29), using Nanson's formula (Theorem 3.1) to the formulation in terms of the reference configuration

$$\langle \boldsymbol{f}(\boldsymbol{U}^k, t), \boldsymbol{V} \rangle = - \int_{\partial\Gamma_{0,N}} \phi(\boldsymbol{X}, t) \, J(\boldsymbol{U}^k, t) \, \mathsf{F}^{-\top}(\boldsymbol{U}^k, t) \boldsymbol{N}(\boldsymbol{X}) \cdot \boldsymbol{V}(\boldsymbol{X}) \, \mathrm{d}S_{\boldsymbol{X}}, \tag{5.30}$$

with $\Gamma_{0,N}$ the Neumann boundary in the reference configuration. With the discretization

$$\langle \boldsymbol{f}(\boldsymbol{U}_h^k, t), \boldsymbol{V}_h \rangle = - \int_{\partial\Gamma_{0,N}} \phi(\boldsymbol{X}, t) \; J(\boldsymbol{U}_h^k, t) \, \mathsf{F}^{-\top}(\boldsymbol{U}_h^k, t) \boldsymbol{N}(\boldsymbol{X}) \cdot \boldsymbol{V}_h(\boldsymbol{X}) \, \mathrm{d}S_{\boldsymbol{X}},$$

we get the vector entries corresponding to Eq. (5.28)

$$\underline{f}(\underline{U}_{n+1}^k)[3i+k] = \langle \boldsymbol{f}(\boldsymbol{U}_{n+1}^k), \varphi_i \rangle = - \int\limits_{\Gamma_{0,N} \cap \partial\tau} \phi_{n+1}\; J(\boldsymbol{U}_{n+1}^k)\, \mathsf{F}^{-\top}(\boldsymbol{U}_{n+1}^k) N_k \varphi_i \, \mathrm{d}S_{\boldsymbol{X}},$$

for $k = 1, 2, 3;\ i = 1, \ldots, \hat{N}$ and ϕ_{n+1} the pressure applied at time step t_{n+1}.

In Sect. 4.4.3 and Sect. 4.4.4 we considered the loads as independent of the deformation. In the case of the Lagrangian formulation and pressure loads this assumption yields an approximation of the tangent stiffness matrix since there is a certain dependency on the displacement. An entirely correct formulation includes the Fréchet derivation of the right hand side (5.30) which is

$$\begin{aligned}(\boldsymbol{\Delta U}, \boldsymbol{f}'(\boldsymbol{U}^k)\boldsymbol{V}) = - \int\limits_{\partial\Gamma_{0,N}} \phi(\boldsymbol{X}, t) \Big\{ & [J(\boldsymbol{U}^k)\mathsf{F}^{-\top}(\boldsymbol{U}^k) : \mathrm{Grad}(\boldsymbol{\Delta U})]\mathsf{F}^{-\top}(\boldsymbol{U}^k) \\ & + J(\boldsymbol{U}^k) \frac{\partial \mathsf{F}^{-\top}(\boldsymbol{U}^k)}{\partial \mathsf{F}} \mathrm{Grad}(\boldsymbol{\Delta U}) \Big\} \boldsymbol{N}(\boldsymbol{X}) \cdot \boldsymbol{V}(\boldsymbol{X}) \, \mathrm{d}S_{\boldsymbol{X}}\end{aligned} \tag{5.31}$$

using observations and denotations from the Sections 4.4.3 and 4.4.4. A discretization approach leads to the additional non-symmetric stiffness matrix

$$\mathsf{M}'(\underline{U}_{n+1}^k)[i,j] = (\varphi_j, \boldsymbol{f}'(\boldsymbol{U}_h^k)\, \varphi_i)$$

and we have to solve the linearized system

$$\Big[\mathsf{K}'(\underline{U}_{n+1}^k) + \mathsf{M}'(\underline{U}_{n+1}^k)\Big]\, \underline{\delta U} = \underline{f}(\underline{U}_{n+1}^k) - \underline{K}(\underline{U}_{n+1}^k), \quad \underline{U}_{n+1}^{k+1} = \underline{U}_{n+1}^k + \underline{\delta U} \tag{5.32}$$

to obtain the equilibrium state at time t_{n+1}. It is obvious that this is an non-symmetric system of equations. Nonetheless the total Lagrangian scheme has the advantage that it is always based on the reference configuration Ω_0. Hence we do not have to update the coordinates of our underlying mesh. In contrast to that the updated Lagrangian scheme uses an updated reference geometry. In our case, this is the last equilibrium state of the problem, which is the situation at the end of the previous time step. Thus, we have to update our coordinates after each time step and take the resulting configuration as new reference configuration. For nonlinear problems it is important to mention that the coordinates are not changed within the Newton steps.

The total Lagrangian and the updated Lagrangian time stepping methods are most common within the field of solid mechanics. Another way would be the *Eulerian scheme* which is mainly used in fluid mechanics. The basis of a finite element approach in this scheme is that the finite elements are fixed in space and do not deform as in the case of the two Lagrangian schemes as mentioned above.

For more information on this topic e.g. cf. [138, Shabana (2008)].

5.5. Solving a Linear System of Equations

The finite element method, discussed in Section 5.1, leads to linear systems of equations with – in many cases – a very large number of degrees of freedom. One possibility to solve such systems are direct methods, cf. Section 5.5.1, such as the very well known Gaussian elimination. For many practical applications, for instance modeling biological tissues, direct solvers reach their limits concerning runtime and memory use. Hence for larger systems iterative solvers become important, see Section 5.5.2.

5.5.1. Direct Solvers

The very simplest method to solve a linear system of equations in the form $\mathsf{A}\underline{x} = \underline{f}$ with $\mathsf{A} \in \mathbb{R}^{m \times m}$ is the Gaussian elimination, which needs $\mathcal{O}(m^3)$ operations. To improve this cubic order there are many different approaches and strategies, e.g. a smart re-ordering of the matrix A.

Stiffness matrices arising from the finite element method are generally sparse, since the support of the basis functions of the FE spaces is local. In this case, given optimal orderings, the computational costs may be reduced to $\mathcal{O}(m^{3/2})$ in 2D and $\mathcal{O}(m^2)$ in 3D. The sparsity of the FE stiffness matrices also allows us to reduce memory costs, since only nonzero entries have to be stored.

There are many software packages available to solve linear systems of equations directly. Two of them are MUMPS [1,2, Amestoy et al.] and UMFPACK [31,32, Davis], which are both available in source code. Another direct solver, which showed some advantages in computational speed but needs a licence and is not available in source code, is PARDISO [131, 132, Schenk and Gärtner].

5.5.2. Iterative Solvers

We will concentrate on the special case of *Krylov subspace methods* to solve the linear system $\mathsf{A}\underline{x} = \underline{f}$. For a general theory and introduction to iterative solvers refer to [147, Steinbach (2008)], [55, Hackbusch (1991)], [6, Axelsson (1994)], [50, Greenbaum (1997)], and many others.

Software packages that deal with highly scalable iterative solving on massively parallel computers are for example *Hypre* (http://acts.nersc.gov/hypre/), *PETSc* (http://www-unix.mcs.anl.gov/petsc/petsc-as/) and *DUNE* (http://www.dune-project.org/).

In the case of finite element methods, an elliptic variational problem results in a symmetric and positive definite stiffness matrix. Here we can apply the preconditioned conjugate gradient method.

Preconditioned Conjugate Gradient Method (PCGM)

Let $\mathsf{C_A} \in \mathbb{R}^{m\times m}$ be a symmetric and positive definite matrix. Then Algorithm 1 describes the PCG-method to solve the linear system $\mathsf{A}\underline{x} = \underline{f}$.

Algorithm 1 Preconditioned conjugate gradient method (PCGM)

Initialize:
$\underline{r}^0 := \mathsf{A}\underline{x}^0 - f,\ v^0 := \mathsf{C_A}^{-1}\underline{r}^0,\ \underline{p}^0 = \underline{v}_0,\ \rho_0 := \langle \underline{v}^0, \underline{r}^0\rangle$

Iterate:
for $k = 0, \dots, m-1$ **do**
  $\underline{s}^k := \mathsf{A}\underline{p}^k,\ \sigma_k := \langle \underline{s}^k, \underline{p}^k\rangle,\ \alpha_k := \rho_k/\sigma_k$
  $\underline{x}^{k+1} := \underline{x}^k - \alpha_k\underline{p}^k,\ \underline{r}^{k+1} := \underline{r}^k - \alpha_k\underline{s}^k$
  $\underline{v}^{k+1} := \mathsf{C_A}^{-1}\underline{r}^{k+1},\ \rho_{k+1} := \langle \underline{v}^{k+1}, \underline{r}^{k+1}\rangle$
  if $\rho_{k+1} < \varepsilon\rho_0$ **then** {breaking condition for given $\varepsilon > 0$}
    break
  else {find new conjugate direction}
    $\beta_k := \rho_{k+1}/\rho_k,\ \underline{p}^{k+1} := \underline{v}^{k+1} + \beta_k\underline{p}^k$
  end if
end for

Proposition 5.3 (Error estimate for the PCGM). *Let $\mathsf{A} \in \mathbb{R}^{m\times m}$ be a symmetric and positive definite matrix and $\underline{x}^* \in \mathbb{R}^m$ be the exact solution of the system of linear equations $\mathsf{A}\underline{x} = \underline{f}$. Then the PCGM (Algorithm 1) converges for every initial value $\underline{u}_0 \in \mathbb{R}^m$ to the exact solution $\underline{x}^*$ and the following error estimate holds*

$$\|\underline{x}^k - \underline{x}^*\|_{\mathsf{A}} \le \frac{2q}{1+q^{2k}}\|\underline{x}^0 - \underline{x}^*\|_{\mathsf{A}}\,, \quad \text{with } q = \frac{\sqrt{\kappa(\mathsf{C_A}^{-1}\mathsf{A})}+1}{\sqrt{\kappa(\mathsf{C_A}^{-1}\mathsf{A})}-1}\,,$$

with $\kappa = \lambda_{max}(\mathsf{C_A}^{-1}\mathsf{A})/\lambda_{min}(\mathsf{C_A}^{-1}\mathsf{A})$ the condition number.

Proof. Cf. [55, Hackbusch (1991)]. □

Preconditioned Conjugate Residual Method (PCG)

A generalization of the CG method for symmetric and indefinite problems is the preconditioned conjugate residual method, cf. [5, Ashby et al. (1990)] or [55, Hackbusch (1991)]. This method is very closely related to the CG method and has similar convergence properties.

Generalized Minimal Residual Method (GMRES)

For a non-symmetric linear system of equations

$$\mathsf{A}\underline{x} = \underline{f},$$

the conjugate gradient method is not applicable. In the field of elasticity, displacement dependent pressure loads, see eq. 3.31, may lead to a non-symmetric load stiffness matrix, see 5.4 and [137, Schweizerhof and Ramm (1984)].

In this case the Generalized Minimal Residual (GMRES) method [128, Saad and Schultz (1986)] is one way to solve the non-symmetric system of equations. The main idea of this method is to minimize the residual over some certain Krylov subspace. For error estimates of GMRES we refer to [50, Greenbaum (1997)] and [145, Starke (1997)].

Remark 5.5.1 (Jacobi preconditioner)**.** *Assuming $A_{ii} \neq 0$ for all i, then one possible choice for the preconditioner C_A is the so-called Jacobi preconditioner*

$$\mathsf{C}_\mathsf{A} = \mathrm{diag}(\mathsf{A}).$$

The Jacobi preconditioner is a very simple form of preconditioning, but shows good results for diagonal dominant matrices A. More efficient possibilities for preconditioning are multilevel preconditioners such as the BPX-preconditioner [15, Bramble, Pasciak, Xu (1990)] or multigrid methods [54, Hackbusch (1985)]. An algebraic multigrid software package, suitable for efficient preconditioning, is *BoomerAMG* included in the *hypre* project.

6. Domain Decomposition Methods

Due to the fine structure of biological tissue and its anisotropic behavior, the numerical simulation of the elastic response of such materials evokes some numerical problems. The discretization needed for the finite element method, discussed in Section 5.1, results in very fine meshes and hence in a very large number of degrees of freedom. Moreover, we are faced with multi-layer materials and therefore we have to treat jumping coefficients, i.e. different material parameters in each layer.

For such complex problems the application of direct solvers results in non-optimal efficiency and high memory usage. Typically, we cannot solve these problems sufficiently fast and accurate on one processor. A possible treatment are iterative solvers and here especially parallelized iterative solvers. In the latter field, domain decomposition (DD) methods are proven to be a very useful and efficient parallel solution strategy. These techniques offer the possibility to distribute the calculations to many computers with relatively low communication between the processors. Furthermore, domain decomposition methods provide a natural way to treat jumping coefficients.

The basic principle of DD methods is the decomposition of the original domain into several overlapping or non-overlapping subdomains. They go back to the Alternating Schwarz Method, introduced in [136, H.A. Schwarz (1870)]; see Fig. 6.1. For a detailed

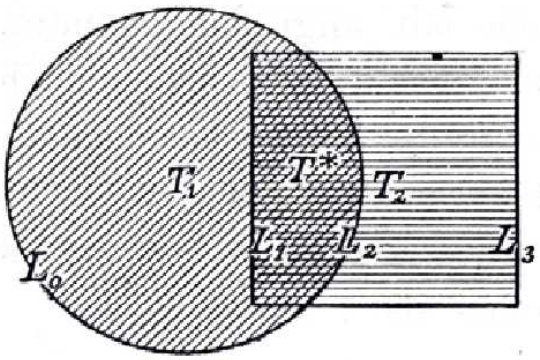

Figure 6.1. – Picture in [136, H.A. Schwarz (1870)] to illustrate the Alternating Schwarz Method.

discussion on domain decomposition methods, including overlapping as well as non-overlapping methods, the interested reader is referred to the monograph [148, Toselli and Widlund (2005)]. See also [142, Smith, Bjøerstad and Gropp (1996)], [117, Quarteroni and Valli (1999)] and [53, Haase (1999)].

In the following, we will concentrate on non-overlapping domain decomposition methods and later on one specific approach: the finite element tearing and interconnecting (FETI) method.

6.1. Basic Principles of Domain Decomposition Methods

Let $\Omega \in \mathbb{R}^3$ be a bounded Lipschitz domain. As mentioned before the underlying principle of DD methods is the partition of the domain Ω into p non-overlapping subdomains

$$\overline{\Omega} = \bigcup_{i=1}^{p} \overline{\Omega}_i \ , \quad \text{with} \quad \Omega_i \cap \Omega_j = \emptyset \text{ for } i \neq j, \tag{6.1}$$

where Ω_i are as well Lipschitz domains. With $\Gamma_i := \partial\Omega_i$ we denote the boundary of one specific subdomain. The local interface is given by $\Gamma_{ij} := \Gamma_i \cap \Gamma_j$ for all $i \neq j$. The global interface Γ_C and the skeleton Γ_S of the domain decomposition are denoted as

$$\Gamma_C := \bigcup_{i \neq j} \Gamma_{ij}, \quad \Gamma_S := \bigcup_{i=1}^{p} \Gamma_i.$$

We denote the typical diameter of the subdomains as

$$H := \max_{i \in \mathcal{I}} \{\operatorname{diam} \Omega_i\}, \quad \text{with the index set } \mathcal{I} := \{1, \ldots, p\}; \tag{6.2}$$

bear in mind that the typical diameter of a finite element is h.

A decomposition of a given global mesh into local submeshes can be generated using a mesh partitioner like METIS (cf. [79, 80, Karypis and Kumar (1998)]). Academic examples, like a decomposition of a cube in several subcubes, can easily be created by simple algorithms. An example for a partitioning generated by METIS is shown in Fig. 6.2. Attention should be paid to the not admissible decomposition as illustrated in Fig. 6.2 (b). For arborescent global meshes it can happen that the METIS algorithm produces subdomains that have more than one component. To avoid problems we eliminate such situations with a simple check for connectivity. Hence, in the following, we treat each Ω_i as a connected subdomain with Lipschitz boundary.

For matters of simplicity, we derive the domain decomposition formulation of a boundary value problem first for the example of the *scalar potential equation*

$$\begin{aligned} -\operatorname{div}[\alpha(\boldsymbol{x})\nabla u(\boldsymbol{x})] &= f(\boldsymbol{x}) \qquad \text{for } \boldsymbol{x} \in \Omega \ , \\ \gamma_0^{\text{int}} u(\boldsymbol{x}) &= g_D(\boldsymbol{x}) \quad \text{for } \boldsymbol{x} \in \Gamma_D \ , \\ \gamma_1^{\text{int}} u(\boldsymbol{x}) &= g_N(\boldsymbol{x}) \quad \text{for } \boldsymbol{x} \in \Gamma_N \ , \end{aligned} \tag{6.3}$$

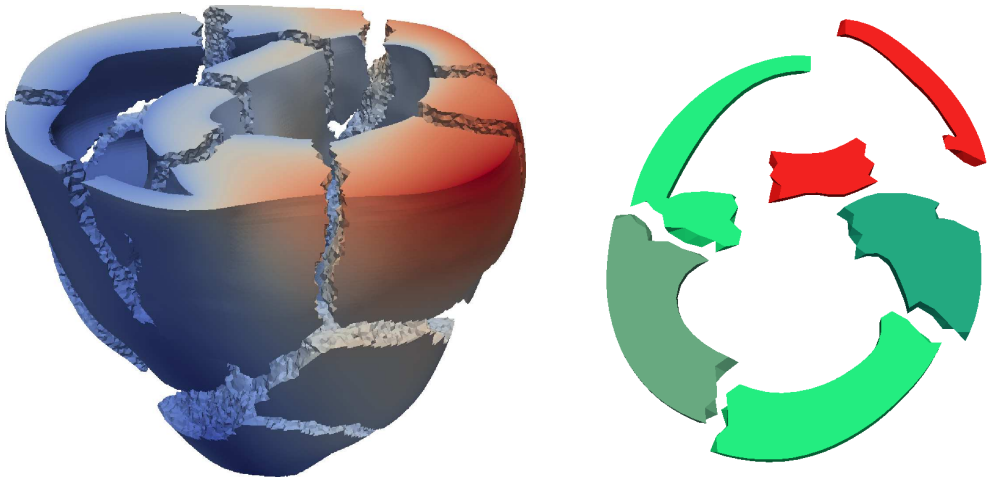

Figure 6.2. – Decomposition of the mesh of a rabbit heart in subdomains via METIS:
(left) Decomposition of the whole heart into 16 connected subdomains; the colors show the displacement of a Dirichlet boundary value problem.
(right) Decomposition of the cross section of the heart in five subdomains; note that the algorithm generated four connected subdomains (green) and one that has two components (red); both meshes from G. Plank and A. Prassl, Institut für Biophysik, Medizinische Universität Graz.

where γ_0^{int} is the Dirichlet trace operator, γ_1^{int} the Neumann trace operator and $\alpha(\boldsymbol{x})$ is a piecewise constant coefficient, i.e.

$$\alpha(\boldsymbol{x}) = \alpha_i \quad \text{for } \boldsymbol{x} \in \Omega_i \ , \quad i = 1, \cdots, p. \tag{6.4}$$

The variational formulation of this problem reads: find $u \in H^1(\Omega)$ with $u = g_D$ on Γ_D such that

$$\int_\Omega \alpha \nabla u \cdot \nabla v \, \mathrm{d}\boldsymbol{x} = \int_\Omega f v \, \mathrm{d}\boldsymbol{x} + \int_{\Gamma_N} g_N v \, \mathrm{d}s_{\boldsymbol{x}}, \quad \text{for all } v \in H_0^1(\Omega, \Gamma_D). \tag{6.5}$$

In accordance with (6.1) and (6.4) we can rewrite this variational formulation for the simple case of two subdomains: find $u \in H^1(\Omega)$ with $u = g_D$ on Γ_D such that

$$\alpha_1 \int_{\Omega_1} \nabla u \cdot \nabla v \, \mathrm{d}\boldsymbol{x} + \alpha_2 \int_{\Omega_2} \nabla u \cdot \nabla v \, \mathrm{d}\boldsymbol{x} = \int_\Omega f v \, \mathrm{d}\boldsymbol{x} + \int_{\Gamma_N} g_N v \, \mathrm{d}s_{\boldsymbol{x}},$$

for all test functions $v \in H_0^1(\Omega, \Gamma_D)$. By integration by parts (Green's formula) we obtain

$$\sum_{i=1,2} \left[-\alpha_i \int_{\Omega_i} \Delta u v \, \mathrm{d}\boldsymbol{x} - \alpha_i \int_{\Gamma_i} \frac{\partial u}{\partial n_i} v \, \mathrm{d}s_x \right] = \int_\Omega f v \, \mathrm{d}\boldsymbol{x} + \int_{\Gamma_N} g_N v \, \mathrm{d}s_{\boldsymbol{x}},$$

for all $v \in H_0^1(\Omega, \Gamma_D)$, where n_i is the exterior normal vector of the domain Ω_i. Hence

$$\sum_{i=1,2} \alpha_i \int_{\Omega_i} -\Delta u \; v \, \mathrm{d}\boldsymbol{x} - \int_{\Gamma_i} \sum_{i=1,2} \left(\alpha_i \frac{\partial u}{\partial n_i} \right) v \, \mathrm{d}s_{\boldsymbol{x}} = \int_{\Omega} f v \, \mathrm{d}\boldsymbol{x} + \int_{\Gamma_N} g_N v \, \mathrm{d}s_{\boldsymbol{x}}.$$

We define the conormal derivatives

$$t_i := \alpha_i \frac{\partial u_i}{\partial n_i}, \quad i = 1, 2. \tag{6.6}$$

With this and density and extension arguments, see, e.g. [117, Quarteroni and Valli (1999)], we may formulate the following boundary value problem which is equivalent to (6.3)

$$\begin{aligned} -\alpha_i \Delta u_i(\boldsymbol{x}) &= f(\boldsymbol{x}) && \text{for } \boldsymbol{x} \in \Omega_i, \\ u_i(\boldsymbol{x}) &= g_D && \text{for } \boldsymbol{x} \in \Gamma_D \cap \Gamma_i, \\ \alpha_i \frac{\partial}{\partial n_i} u_i(\boldsymbol{x}) &= g_N && \text{for } \boldsymbol{x} \in \Gamma_N \cap \Gamma_i, \end{aligned}$$

where $u_i = u|_{\Omega_i}$, $\Gamma_i = \partial\Omega_i$, $i = 1, 2$ and the so-called *transmission conditions*

$$\begin{aligned} t_1(\boldsymbol{x}) + t_2(\boldsymbol{x}) &= 0 && \text{for } \boldsymbol{x} \in \Gamma_{12}, \\ u_1(\boldsymbol{x}) &= u_2(\boldsymbol{x}) && \text{for } \boldsymbol{x} \in \Gamma_{12}. \end{aligned}$$

The above ideas are valid for any elliptic partial differential equation, hence they may be applied to the elasticity problem (3.30). Generalizing for an arbitrary amount of p subdomains we can formulate the coupled boundary value problem for elasticity: find $\boldsymbol{u} \in [H^1(\Omega)]^3$ with $\boldsymbol{u} = \boldsymbol{u}_D$ on Γ_D such that

$$\begin{aligned} -\operatorname{div} \sigma(\boldsymbol{u}_i, \boldsymbol{x}) &= \boldsymbol{f}(\boldsymbol{x}) && \text{for } \boldsymbol{x} \in \Omega_i, \\ \boldsymbol{u}_i(\boldsymbol{x}) &= \boldsymbol{u}_D(\boldsymbol{x}) && \text{for } \boldsymbol{x} \in \Gamma_D \cap \Gamma_i, \\ \sigma(\boldsymbol{u}_i, \boldsymbol{x})\, \boldsymbol{n}_i(\boldsymbol{x}) &= \boldsymbol{t}_N(\boldsymbol{x}) && \text{for } x \in \Gamma_N \cap \Gamma_i, \\ \boldsymbol{u}_i(\boldsymbol{x}) &= \boldsymbol{u}_j(\boldsymbol{x}) && \text{for } \boldsymbol{x} \in \Gamma_{ij}, \\ \boldsymbol{t}_i(\boldsymbol{x}) + \boldsymbol{t}_j(\boldsymbol{x}) &= \boldsymbol{0} && \text{for } \boldsymbol{x} \in \Gamma_{ij}, \end{aligned} \tag{6.7}$$

with $\boldsymbol{u}_i = \boldsymbol{u}|_{\Omega_i} \in [H^1(\Omega_i)]^3$. The boundary stresses are defined as

$$\boldsymbol{t}_i(\boldsymbol{x}) := \sigma(\boldsymbol{u}_i, \boldsymbol{x}) \boldsymbol{n}_i(\boldsymbol{x}). \tag{6.8}$$

In the absence of volume forces, i.e. $\boldsymbol{f}(\boldsymbol{x}) = \boldsymbol{0}$ and using the *Steklov–Poincaré operator* $S_i^{\mathrm{int}} : H^{1/2}(\Gamma_i) \to H^{-1/2}(\Gamma_i)$ we can describe the *Dirichlet to Neumann map*

$$\boldsymbol{t}_i(\boldsymbol{x}) = \gamma_1^{\mathrm{int}} \boldsymbol{u}_i(\boldsymbol{x}) = (S_i^{\mathrm{int}} \gamma_0^{\mathrm{int}}) \boldsymbol{u}_i(\boldsymbol{x}) \quad \text{for } \boldsymbol{x} \in \Gamma_i, \tag{6.9}$$

e.g., cf. [147, Steinbach (2008), Sect. 6.6]. Note that in the case of linear elasticity we have $\sigma(\boldsymbol{u}_i) = \mathbb{C}_i \varepsilon(\boldsymbol{u}_i)$ with the constant forth-order tensor

$$\mathbb{C}_i = \mathbb{C}|_{\Omega_i}, \quad \text{for all } i \in \mathcal{I}. \tag{6.10}$$

Concerning the nonlinear elasticity problem we have the constitutive equation

$$\sigma(\boldsymbol{u}_i) = 2J^{-1}(\boldsymbol{u}_i)\mathsf{F}(\boldsymbol{u}_i)\frac{\partial \Psi_i(\mathsf{C})}{\partial \mathsf{C}}\mathsf{F}^{\top}(\boldsymbol{u}_i) \tag{6.11}$$

where Ψ_i is the strain energy function in Ω_i. Hence the local stress tensors $\sigma(\boldsymbol{u}_i)$ are defined locally by using the strain energy function Ψ_i as introduced in the material models, and by using localized parameter sets and fiber directions, e.g. for the artery we have $\kappa_i, k_{1,i}, k_{2,i}, c_i$ and directions $\beta_{1,i}$, $\beta_{2,i}$ for $i \in \mathcal{I}$.

6.2. Standard one-level FETI methods

First ideas of this domain decomposition method can be found in the early work [49, Glowinski and Wheeler (1988)], but the classical one-level FETI method was introduced by [41,42, Farhat and Roux (1991,1994)]. Since then these techniques got very popular and are widely used in scientific computing. Our presentation is based on the explanations of [148, Toselli and Widlund (2005), Ch. 6.3] and [91, Steinbach and Langer (2003)]. Other contributions are the works of [96, Mandel and Tezaur], publishing a first convergence proof of these methods in the non-redundant case, [86, 87, Klawonn and Widlund (2000,2001)], doing the same for a redundant formulation, and [91,92, Langer and Steinbach (2003)] where the authors enhanced the method to boundary element methods and present a coupling of finite and boundary element domain decomposition methods.

To apply the finite element method to domain decomposition problems we introduce for each subdomain the finite element spaces V_i and the trace spaces W_i by

$$V_i := V_h(\Omega_i) \quad \text{for } i \in \mathcal{I} \quad \text{and} \quad W_i := V_h(\Omega_i)|_{\Gamma_i} \quad \text{for } i \in \mathcal{I}. \tag{6.12}$$

Furthermore we define the product spaces

$$V := \prod_{i=1}^{p} V_i \quad \text{and} \quad W := \prod_{i=1}^{p} W_i. \tag{6.13}$$

Using this we introduce the separate discrete displacement unknowns $\boldsymbol{u}_{i,h}$ for the solution $\boldsymbol{u}_h$ in the subdomains by

$$\boldsymbol{u}_{i,h} \in V_i, \quad \boldsymbol{u}_h := [\boldsymbol{u}_{i,h}]_{i\in\mathcal{I}} \in V \tag{6.14}$$

As in Section 5.1 we introduce the basis representation for the local solution vectors $\boldsymbol{u}_{i,h} = \sum_i \boldsymbol{u}_i\varphi_i$ and denote by $\underline{u}_i \in \mathbb{R}^{m_i}$ the vector consisting of the coefficients $\boldsymbol{u}_i$.

Hence, by reordering the degrees of freedom, the linear system of equations (5.10) can be written as

$$\begin{pmatrix} \mathsf{K}_{11} & & & \mathsf{K}_{1C}\mathsf{A}_1 \\ & \ddots & & \vdots \\ & & \mathsf{K}_{pp} & \mathsf{K}_{pC}\mathsf{A}_p \\ \mathsf{A}_1^\top\mathsf{K}_{C1} & \cdots & \mathsf{A}_p^\top\mathsf{K}_{Cp} & \sum_{i=1}^{p}\mathsf{A}_i^\top\mathsf{K}_{CC,i}\mathsf{A}_i \end{pmatrix} \begin{pmatrix} \underline{u}_{1,I} \\ \vdots \\ \underline{u}_{p,I} \\ \underline{u}_C \end{pmatrix} = \begin{pmatrix} \underline{b}_1 \\ \vdots \\ \underline{b}_p \\ \sum_{i=1}^{p}\mathsf{A}_i^\top\underline{b}_{C,i} \end{pmatrix},$$

and the linearized system of equations (5.19) can be written as

$$\begin{pmatrix} \mathsf{K}'_{11}(\underline{u}_1^k) & & & \mathsf{K}'_{1C}(\underline{u}_1^k)\mathsf{A}_1 \\ & \ddots & & \vdots \\ & & \mathsf{K}'_{pp}(\underline{u}_p^k) & \mathsf{K}'_{pC}(\underline{u}_p^k)\mathsf{A}_p \\ \mathsf{A}_1^\top\mathsf{K}'_{C1}(\underline{u}_1^k) & \cdots & \mathsf{A}_p^\top\mathsf{K}'_{Cp}(\underline{u}_p^k) & \sum_{i=1}^{p}\mathsf{A}_i^\top\mathsf{K}'_{CC,i}(\underline{u}_i^k)\mathsf{A}_i \end{pmatrix} \begin{pmatrix} \underline{\delta u}_{1,I} \\ \vdots \\ \underline{\delta u}_{p,I} \\ \underline{\delta u}_C \end{pmatrix} = \begin{pmatrix} \underline{b}_1(\underline{u}_1^k) \\ \vdots \\ \underline{b}_p(\underline{u}_p^k) \\ \sum_{i=1}^{p}\mathsf{A}_i^\top\underline{b}_{C,i}(\underline{u}_i^k) \end{pmatrix},$$

where $\underline{u}_{i,I}$ and the increments $\underline{\delta u}_{i,I}$ correspond to the local degrees of freedom within the subdomain Ω_i, and $\underline{u}_C$ and $\underline{\delta u}_C^k$ are related to all global degrees of freedom on the coupling boundary Γ_C and $\underline{b}_i(\underline{u}_i^k) = \underline{f}_i - \underline{K}_i(\underline{u}_i^k)$.

We introduce the tearing for linear elasticity

$$\underline{u}_i = \begin{pmatrix} \underline{u}_{i,I} \\ \mathsf{A}_i\underline{u}_C \end{pmatrix},\ \mathsf{K}_i = \begin{pmatrix} \mathsf{K}_{ii} & \mathsf{K}_{iC} \\ \mathsf{K}_{Ci} & \mathsf{K}_{CC,i} \end{pmatrix},\ \underline{f}_i = \begin{pmatrix} \underline{b}_i \\ \underline{b}_{C,i} \end{pmatrix},$$

and for nonlinear elasticity

$$\underline{\delta u}_i = \begin{pmatrix} \underline{\delta u}_{i,I}^k \\ \mathsf{A}_i\underline{\delta u}_C^k \end{pmatrix},\ \mathsf{K}'_i(\underline{u}_i^k) = \begin{pmatrix} \mathsf{K}'_{ii}(\underline{u}_i^k) & \mathsf{K}'_{iC}(\underline{u}_i^k) \\ \mathsf{K}'_{Ci}(\underline{u}_i^k) & \mathsf{K}'_{CC,i}(\underline{u}_i^k) \end{pmatrix},\ \underline{f}(\underline{u}_i^k) = \begin{pmatrix} \underline{b}_i(\underline{u}_i^k) \\ \underline{b}_{C,i}(\underline{u}_i^k) \end{pmatrix}.$$

As the unknowns $\underline{u}_i$ and $\underline{u}_i^{k+1} = \underline{u}_i^k + \underline{\delta u}_i$ are typically not continuous over the interfaces we have to ensure the continuity of the solution by the constraints

$$\underline{u}_i = \underline{u}_j \quad \text{and} \quad \underline{\delta u}_i = \underline{\delta u}_j \quad \text{on } \Gamma_{ij},\ i,j \in \mathcal{I}. \tag{6.15}$$

For coupling nodes which appear on more than two subdomains there are two different schemes how to implement these constraints: a non-redundant (cf. Fig. 6.3 (a) and [148, Toselli and Widlund (2005), Ch. 6.3.2]) and a fully redundant case (cf. Fig. 6.3 (b) and [148, Toselli and Widlund (2005), Ch. 6.3.3]). In case of elasticity the constraints have to be fulfilled for each component; i.e. in the 3D case for all three components.

In our implementation we concentrate on the fully redundant case since it is easier to implement and showed advantages due to the full symmetry. The drawback is the larger amount of constraints in contrast to the non-redundant formulation.

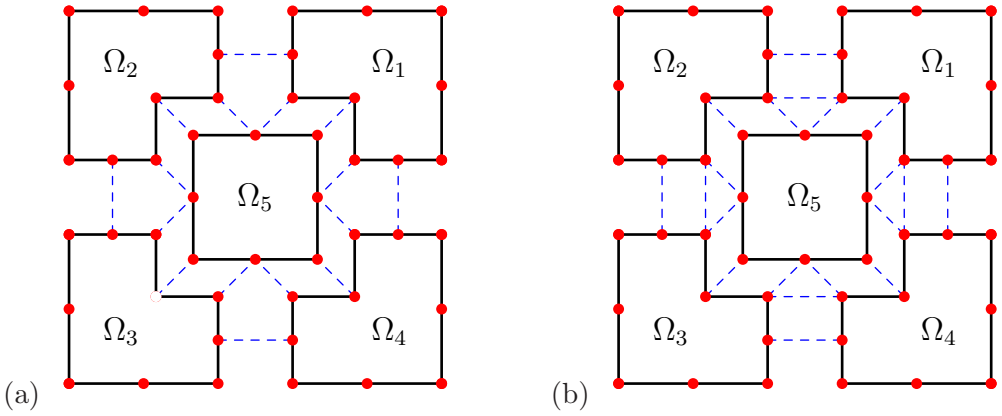

Figure 6.3. – (a) non-redundant case: the number of necessary constraints is minimized; (b) fully redundant constraints

We can write the constraints in compact form for linear elasticity as

$$\sum_{i=1}^{p} \mathsf{B}_i \underline{u}_i = \underline{0} \quad \text{or} \quad \mathsf{B}\underline{u} = \underline{0} \,. \tag{6.16}$$

The so-called *jump operators* B_i are signed boolean matrices. The most entries equal zero since we get 1 or -1 entries only for coupling nodes, i.e. for neighboring subdomains. We denote by m the total number of constraints. Let m_i be the number of degrees of freedom of a specific domain Ω_i, then we can state that

$$\mathsf{B}_i \in \mathbb{R}^{m \times m_i} \quad \text{and} \quad \mathsf{B}_i : \mathbb{R}^{m_i} \to \mathbb{R}^m \tag{6.17}$$

for each $i \in \mathcal{I}$. To fulfill the constraints in (6.15), the jump operators are defined such that

$$\left(\mathsf{B}_i \boldsymbol{u}_i\right)_{jk}(\boldsymbol{x}) = \begin{cases} \underline{u}_i(\boldsymbol{x}) & \text{if } i = j \\ -\underline{u}_i(\boldsymbol{x}) & \text{if } i = k \\ \underline{0} & \text{else} \end{cases} \tag{6.18}$$

for $\boldsymbol{x} \in \Gamma_{jk}$ and per definition $j > k$. By construction it holds

$$\langle \mathsf{B}\underline{u}, \underline{\mu} \rangle = \sum_{i=1}^{p} \langle \mathsf{B}_i \underline{u}_i, \underline{\mu} \rangle \quad \text{for all } \underline{\mu} \in \mathbb{R}^m \tag{6.19}$$

Note that the construction of the jump operators B_i is exactly the same for nonlinear elasticity.

To enforce the constraints of the continuitiy of the solution (6.16) and using (6.19), we introduce the vector of Lagrange multipliers $\underline{\lambda}$ and get the saddle point system: find

$(\underline{u}_i, \underline{\lambda}) \in \mathbb{R}^{m_i} \times \mathbb{R}^m$ such that

$$\begin{pmatrix} \mathsf{K}_1 & & & \mathsf{B}_1^\top \\ & \ddots & & \vdots \\ & & \mathsf{K}_p & \mathsf{B}_p^\top \\ \mathsf{B}_1 & \dots & \mathsf{B}_p & \end{pmatrix} \begin{pmatrix} \underline{u}_1 \\ \vdots \\ \underline{u}_p \\ \underline{\lambda} \end{pmatrix} = \begin{pmatrix} \underline{f}_1 \\ \vdots \\ \underline{f}_p \\ \underline{0} \end{pmatrix}. \tag{6.20}$$

Correspondingly, for the nonlinear elasticity case, cf. (5.19), we get the linearized system of equations

$$\begin{pmatrix} \mathsf{K}_1'(\underline{u}_i^k) & & & \mathsf{B}_1^\top \\ & \ddots & & \vdots \\ & & \mathsf{K}_p'(\underline{u}_i^k) & \mathsf{B}_p^\top \\ \mathsf{B}_1 & \dots & \mathsf{B}_p & \end{pmatrix} \begin{pmatrix} \underline{\delta u}_1 \\ \vdots \\ \underline{\delta u}_p \\ \underline{\lambda} \end{pmatrix} = \begin{pmatrix} \widetilde{\underline{f}}_1(\underline{u}_i^k) \\ \vdots \\ \widetilde{\underline{f}}_p(\underline{u}_i^k) \\ \underline{0} \end{pmatrix}. \tag{6.21}$$

An identical representation can be retrieved using the transmission conditions with the Dirichlet to Neumann mapping (6.9). From this derivation of the FETI method we see that the Lagrange multipliers λ may be interpreted as boundary stresses. For more information on this derivation of the FETI formulation see, e.g., [113, Pechstein (2008)], [124, Rixen and Farhat (1999)] or [148, Toselli and Widlund (2005)].

Note that the problems (6.20) and (6.21) are uniquely solvable given that

$$\ker \mathsf{K}_i \cap \ker \mathsf{B}_i = \emptyset, \quad \ker \mathsf{K}_i'(\underline{u}_i^k) \cap \ker \mathsf{B}_i = \emptyset \quad \text{for all } i \in \mathcal{I}, \tag{6.22}$$

e.g., cf. [19, Brezzi and Fortin (1991)]. For linear and nonlinear elasticity problems condition (6.22) is fulfilled for subdomains Ω_i with a Dirichlet boundary, i.e. $\Gamma_i \cap \Gamma_D \neq \emptyset$. For such a subdomain it holds that $\ker \mathsf{K}_i = \emptyset$ and $\ker \mathsf{K}_i'(\underline{u}_i^k) = \emptyset$, respectively. For Neumann subdomains, typically referred to as *floating subdomains*, we additionally require the solvability conditions

$$(\underline{f}_i - \mathsf{B}_i^\top \underline{\lambda}, \underline{r}_{k,i}) = 0 \text{ and } (\widetilde{\underline{f}}_i(\underline{u}_i^k) - \mathsf{B}_i^\top \underline{\lambda}, \underline{r}_{k,i}) = 0 \text{ for } k = 1, \dots, 6;\ i \in \mathcal{I}_{\text{floating}}, \tag{6.23}$$

where $\underline{r}_{k,i} \in \ker \mathsf{K}_i'$ correspond to the rigid body motions of elasticity, cf. Remark 4.2.1, and $\mathcal{I}_{\text{floating}}$ is the index set of all floating subdomains.

In the following, we will concentrate on the nonlinear elasticity problem, since linear elasticity is just a special case and works the same. For matters of simplicity, we denote by $\mathsf{K}_i' := \mathsf{K}_i'(\underline{u}_i^k)$ the local tangent stiffness matrices and by $\widetilde{\underline{f}}_i := \widetilde{\underline{f}}_i(\underline{u}_i^k)$ the local right hand sides.

Starting from (6.21) we follow the standard approach of tearing and interconnecting methods in eliminating the local degrees of freedom $\underline{\delta u}_i$. In the case of a floating

subdomain Ω_i, i.e. $\Gamma_i \cap \Gamma_D = \emptyset$, the local matrices K_i' are not invertible. Hence we introduce the Moore–Penrose pseudo inverse $\mathsf{K}_i^\dagger$ to represent the local solutions as

$$\underline{\delta u}_i = \mathsf{K}_i^\dagger(\widetilde{\underline{f}}_i - \mathsf{B}_i^\top \underline{\lambda}) + \sum_{k=1}^{6} \gamma_{k,i} \underline{r}_{k,i}, \tag{6.24}$$

where $\gamma_{k,i}$ are unknown constants. In the case of a non-floating subdomain, i.e. $\ker \mathsf{K}_i = \emptyset$, we may set $\mathsf{K}_i^\dagger = \mathsf{K}_i^{-1}$. As in Section 6.2.1 we may also consider an all-floating approach where also Dirichlet boundary conditions are incorporated by using discrete Lagrange multipliers.

In general, we consider the Schur complement system of (6.21) to obtain

$$\sum_{i=1}^{p} \mathsf{B}_i \mathsf{K}_i^\dagger \mathsf{B}_i^\top \underline{\lambda} - \sum_{i=1}^{p} \sum_{k=1}^{6} \gamma_{k,i} \mathsf{B}_i \underline{v}_{k,i} = \sum_{i=1}^{p} \mathsf{B}_i \mathsf{K}_i^\dagger \widetilde{\underline{f}}_i, \quad (\widetilde{\underline{f}}_i - \mathsf{B}_i^\top \underline{\lambda}, \underline{r}_{k,i}) = 0,$$

which can be written as

$$\begin{pmatrix} \mathsf{F} & -\mathsf{G} \\ \mathsf{G}^\top & \end{pmatrix} \begin{pmatrix} \underline{\lambda} \\ \underline{\gamma} \end{pmatrix} = \begin{pmatrix} \underline{d} \\ \underline{e} \end{pmatrix} \tag{6.25}$$

with the denotations

$$\mathsf{F} := \sum_{i=1}^{p} \mathsf{B}_i \mathsf{K}_i^\dagger \mathsf{B}_i^\top, \ \mathsf{G} := \sum_{i=1}^{p} \sum_{k=1}^{6} \mathsf{B}_i \underline{r}_{k,i}, \ \underline{d} =: \sum_{i=1}^{p} \mathsf{B}_i \mathsf{K}_i^\dagger \widetilde{\underline{f}}_i, \ e_{k,i} := (\widetilde{\underline{f}}_i, \underline{r}_{k,i}). \tag{6.26}$$

Denote by X the space

$$X := \ker(\mathsf{G}^\top) = \{\underline{\lambda} \in \mathbb{R}^m : \langle \mathsf{B}_i \underline{r}, \underline{\lambda} \rangle = 0 \text{ for all } \underline{r}_{k,i} \in \ker \mathsf{K}_i', \ k = 1, \ldots, 6; i \in \mathcal{I}\}.$$

For the solution of the linear system (6.25) we introduce the projection $\mathsf{P} : \mathbb{R}^m \to X$ by

$$\mathsf{P}^\top := \mathsf{I} - \mathsf{G} \left(\mathsf{G}^\top \mathsf{G}\right)^{-1} \mathsf{G}^\top \tag{6.27}$$

and it remains to consider the projected system

$$\mathsf{P}^\top \mathsf{F} \underline{\lambda} = \mathsf{P}^\top \underline{d} \tag{6.28}$$

which can be solved by using a parallel iterative Krylov subspace method with suitable preconditioning, cf. Section 6.2.2. Note that the initial approximate solution $\underline{\lambda}_0$ has to satisfy the compatibility condition $\mathsf{G}^\top \underline{\lambda}^0 = \underline{e}$. A possible choice would be

$$\underline{\lambda}^0 = \mathsf{G} \left(\mathsf{G}^\top \mathsf{G}\right)^{-1} \underline{e}.$$

In a post processing we finally recover the vector of constants

$$\underline{\gamma} = \left(\mathsf{G}^\top \mathsf{G}\right)^{-1} \mathsf{G}^\top (\mathsf{F}\underline{\lambda} - \underline{d})$$

and subsequently the desired solution by (6.24).

Remark 6.2.1. *Due to the construction of* F*, see* (6.26)*, and the projection* P*, see* (6.27)*, the system* (6.28) *is symmetric given that the local stiffness matrices* K_i' *are symmetric. This is the case for the formulation of the nonlinear elasticity problem in Euler coordinates and the linear elasticity problem, cf. Sect. 5.3.*

Remark 6.2.2. *With the positive definiteness of the local tangent stiffness matrices* K_i' *and the definitions of* F *and* P *it holds for all* $\underline{\lambda} \in X$*,* $\underline{\lambda} \notin \ker \mathsf{B}_i^\top$ *for all* $i \in \mathcal{I}$ *and* $\underline{\lambda} \neq 0$

$$\langle \mathsf{P}^\top \mathsf{F}\lambda, \lambda\rangle = \langle \mathsf{F}\underline{\lambda}, \mathsf{P}\underline{\lambda}\rangle = \langle \mathsf{F}\underline{\lambda}, \underline{\lambda}\rangle = \langle \sum_{i=1}^{p} \mathsf{B}_i \mathsf{K}_i^\dagger \mathsf{B}_i^\top \ \underline{\lambda}, \underline{\lambda}\rangle = \sum_{i=1}^{p} \langle \mathsf{K}_i^\dagger \mathsf{B}_i^\top \underline{\lambda}, \mathsf{B}_i^\top \underline{\lambda}\rangle > 0,$$

which shows the positive definiteness of the system (6.28) *on* $X \setminus \ker \mathsf{B}^\top$ *for the considered linear and nonlinear elasticity problems.*

6.2.1. All-floating FETI methods

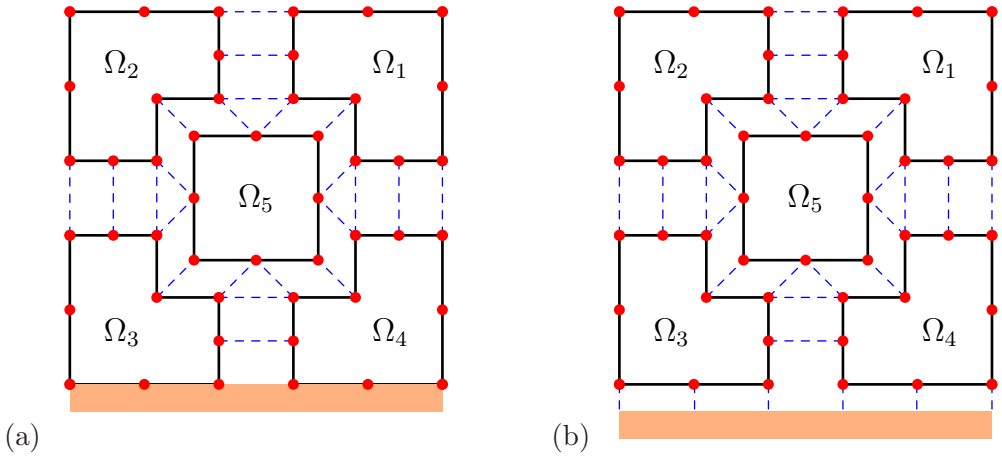

Figure 6.4. – classical FETI (a) and all-floating FETI (b) formulation

The idea of this special FETI method is to treat all subdomains as floating subdomains, i.e. domains with no Dirichlet boundary conditions, see Fig. 6.4. In addition to the standard procedure of gluing the subregions along the auxiliary interfaces, the Lagrange multipliers are now used for the implementation of the Dirichlet boundary conditions as well. This eases the implementation of the FETI procedure, since it is possible to treat all subdomains the same way. Further to that, some tests (cf. Chapter 7) showed more efficiency than the classical FETI method and the asymptotic behavior improved, see also [111, Of and Steinbach (2009)]. The drawback is an increasing number of degrees of freedom and Lagrange multipliers. More information on all-floating FETI one may find in [109, Of (2006)], [111, Of and Steinbach (2009)] and on the related Total–FETI (TFETI) method in [37, Dostál et al. (2006)].

If all regions are treated as floating subdomains the conformance of the Dirichlet boundary conditions is not given. So they have to be enhanced in the system of constraints in the following way:

$$\sum_{i=1}^{p} \widetilde{\mathsf{B}}_i \underline{u}_i = \underline{b}$$

where $\widetilde{\mathsf{B}}_i$ and $\underline{b}$ are given such that

$$\left(\widetilde{\mathsf{B}}_i \underline{u}_i\right)_{jk}(\boldsymbol{x}) = \begin{cases} \underline{u}_i(\boldsymbol{x}) & \text{if } i = j,\ \boldsymbol{x} \in \Gamma_{jk},\ j > k, \\ -\underline{u}_i(\boldsymbol{x}) & \text{if } i = k,\ \boldsymbol{x} \in \Gamma_{jk},\ j > k, \\ \underline{u}_i(\boldsymbol{x}) & \text{if } \boldsymbol{x} \in \Gamma_j \cap \Gamma_D, \\ \underline{0} & \text{else} \end{cases} \tag{6.29}$$

and

$$\underline{b}_{jk}(\boldsymbol{x}) = \begin{cases} \underline{0} & \text{if } \boldsymbol{x} \in \Gamma_{jk}, \\ \underline{u}_D(\boldsymbol{x}) & \text{if } \boldsymbol{x} \in \Gamma_j \cap \Gamma_D. \end{cases}$$

In the case of elasticity all subdomain stiffness matrices will have the same and known defect

$$\operatorname{def}(K_i) = \#(\text{rigid body motions}) = 6 \quad \text{in 3D}$$

which eases the calculation of a Moore–Penrose generalized inverse matrix $\mathsf{K}^{\dagger}$, see Sect. 6.2.3.

6.2.2. Preconditioning

In order to give suitable preconditioners for the described FETI methods we first introduce a weighting function known from balancing Neumann-Neumann methods, see [148, Toselli and Widlund (2005), Sect. 6.2] and [109, Of (2006), Sect. 5.5.2],

$$\delta_i^{\dagger}(\boldsymbol{x}) := \frac{\alpha_i^{\gamma}}{\sum_k^n \alpha_k^{\gamma}}, \quad \boldsymbol{x} \in \Gamma_i,\ i \in \mathcal{I}$$

with $\gamma \in [0.5, \infty]$, n the number of subdomains which share the coupling node x and α_i a coefficient depending on the material parameters. In the case of linear elasticity we choose $\alpha_i = E_i/(1+\nu_i)$ with Young's modulus E_i and Poisson's ratio ν_i in Ω_i, cf. [88, Klawonn and Widlund (2005)]. For the Neo–Hooke and the artery model we choose $\alpha_i = c_i/2$ and for the myocardium model $\alpha_i = a_i/2$, $i \in \mathcal{I}$. Using this scaling factor we can define the scaled jump operators B_D as

$$\mathsf{B}_{\mathsf{D},i} := \mathsf{D}_i \mathsf{B}_i$$

with $\mathsf{D}_i = \operatorname{diag}(\delta_i^{\dagger}(\boldsymbol{x}))$, $\boldsymbol{x} \in \Gamma_i$.

Note that all preconditioners for the FETI method have the form

$$\mathsf{M}^{-1} := \sum_{i=1}^{p} \mathsf{B}_{\mathrm{D},i} \mathsf{Y}_i \mathsf{B}_{\mathrm{D},i}^{\top}, \tag{6.30}$$

with a matrix $\mathsf{Y}_i \in \mathbb{R}^{m_i \times m_i}$.

Definition 6.1 (Lumped preconditioner). *Following [40, Farhat et al. (1994)] we define the lumped preconditioner as*

$$\mathsf{M}_{\mathrm{l}}^{-1} := \sum_{i=1}^{p} \mathsf{B}_{\mathrm{D},i} \mathsf{A}_i \mathsf{B}_{\mathrm{D},i}^{\top}, \tag{6.31}$$

with A_i the local stiffness matrix K_i for linear elasticity or the local tangent stiffness matrix $\mathsf{K}_i'(u_{i,h}^k)$ for nonlinear elasticity, respectively.

Definition 6.2 (Dirichlet preconditioner). *An optimal domain decomposition preconditioner is the Dirichlet preconditioner, cf. [40, Farhat et al. (1994)],*

$$\mathsf{M}_{\mathrm{D}}^{-1} := \sum_{i=1}^{p} \mathsf{B}_i \begin{pmatrix} 0 & 0 \\ 0 & \mathsf{S}_i \end{pmatrix} \mathsf{B}_i^{\top}, \tag{6.32}$$

where

$$\mathsf{S}_i = \mathsf{K}_{CC}'(\underline{u}_i^k) - \mathsf{K}_{Ci}'(\underline{u}_i^k)\mathsf{K}_{ii}'^{-1}(\underline{u}_i^k)\mathsf{K}_{iC}'(\underline{u}_i^k)$$

is the Schur complement of the local tangent finite element matrices $\mathsf{K}_i'(\underline{u}_{i,h}^k)$ in the case of nonlinear elasticity. Note that for FETI this Schur complement is the discrete version of the Steklov–Poincaré operator $S_i^{int} : H^{1/2}(\Gamma_i) \to H^{-1/2}(\Gamma_i)$ described in (6.9).

Due to the optimality of the Dirichlet preconditioner it shows the best results concerning the condition number of the FETI system (6.28) and hence also the number of iterations of the Krylov solver, see Chapter 7.

Nonetheless, the formation of the Dirichlet preconditioner needs an additional inversion to calculate the Schur complement. To avoid local iterative solving which would have to be executed in each global Krylov solver step and hence decreases the computational performance significantly for most problems, we use a direct solver package, cf. Sect. 5.5.1, to compute the needed factorization. For large subdomains this may be very time and memory consuming. Since the building happens locally the burden of more computational complexity is not as serious as the supplemental storage requirements. As illustrated in Chapter 7 some problems are not solvable due to depleting memory.

In contrast, the lumped preconditioner is more economical and needs no additional storage or computation. Thus this type of preconditioning outperforms the more sophisticated Dirichlet preconditioner for certain numerical experiments. On the other

hand we encountered experiments where the global Krylov method was not converging within a commensurate amount of iterations, see Chapter 7.

Alternatively, we also use a scaled hypersingular boundary integral operator preconditioner as proposed in [91, Langer and Steinbach (2003)]. Following [147, Steinbach (2008)], we introduce the *hypersingular boundary integral operators* $D_i : [H^{1/2}(\Gamma_i)]^3 \to [H^{-1/2}(\Gamma_i)]^3$ as

$$(\mathsf{D}_i\, \boldsymbol{u}_i)(\boldsymbol{x}) = -\gamma_{1,x}^{i,\mathrm{int}} \int_{\Gamma_i} \left(\gamma_{1,y}^{i,\mathrm{int}} \mathsf{U}^*(\boldsymbol{x},\boldsymbol{y})\right)^\top \boldsymbol{u}_i(\boldsymbol{y})\, \mathrm{d}s_{\boldsymbol{y}}, \tag{6.33}$$

with the fundamental solution of linear elasticity, *Kelvin's tensor*,

$$\mathsf{U}^*_{kl}(\boldsymbol{x},\boldsymbol{y}) = \frac{1}{8\pi}\frac{1}{E}\frac{1+\nu}{1-\nu}\left[(3-4\nu)\frac{\delta_{kl}}{|\boldsymbol{x}-\boldsymbol{y}|} + \frac{(x_k-y_k)(x_l-y_l)}{|\boldsymbol{x}-\boldsymbol{y}|^3}\right], \quad k,l=1,2,3, \tag{6.34}$$

and $\gamma_{1,(\bullet)}^{i,\mathrm{int}}$ the Neumann trace operator for $\boldsymbol{x},\boldsymbol{y} \in \Gamma_i$.

Definition 6.3 (BETI preconditioner)**.** *On the basis of [91, Langer and Steinbach (2003)] we define the BETI preconditioner for linear and nonlinear elasticity problems as*

$$\mathsf{M}_{\mathrm{BETI}}^{-1} := \sum_{i=1}^{p} \mathsf{B}_i \begin{pmatrix} 0 & 0 \\ 0 & \mathsf{D}_{i,h} \end{pmatrix} \mathsf{B}_i^\top, \tag{6.35}$$

with $\mathsf{D}_{i,h}$ the discretized version of the hypersingular boundary integral operator introduced in (6.33)*.*

Lemma 6.4. *For linear elasticity problems, when the Dirichlet preconditioner is employed, the condition number of the preconditioned FETI problem satisfies*

$$\kappa(\mathsf{P}\mathsf{M}_{\mathrm{D}}^{-1}\mathsf{P}^\top\mathsf{F}) = c\left(1+\log\left(\frac{H}{h}\right)\right)^2, \tag{6.36}$$

with the positive constant c which is independent of h, H, p and the values of the coefficients E_i and ν_i.

Proof. For the proof cf. [85, Klawonn and Widlund (2001)] building on results of [96, Mandel and Tezaur (1996)] and also [114, Pechstein and Scheichl (2008)]. □

Lemma 6.5. *The condition number of the preconditioned linear elasticity FETI problem with the BETI preconditioner $\mathsf{M}_{\mathrm{BETI}}^{-1}$ satisfies*

$$\kappa(\mathsf{P}\mathsf{M}_{\mathrm{BETI}}^{-1}\mathsf{P}^\top\mathsf{F}) = c\left(1+\log\left(\frac{H}{h}\right)\right)^2, \tag{6.37}$$

with the positive constant c which is independent of h, H, p and the values of the coefficients E_i and ν_i.

Proof. This was proved in [91, Langer and Steinbach (2003)] by showing the spectral equivalence of $\mathsf{M}_{\mathrm{BETI}}^{-1}$ and $\mathsf{M}_{\mathrm{D}}^{-1}$ and using Lemma 6.4. □

6.2.3. Computing the Moore–Penrose Generalized Inverse

In order to set up the projected FETI system (6.28) we need to compute the local pseudo inverse matrices $\mathsf{K}_i^\dagger$. In this thesis we will concentrate on local direct solvers, see Sect. 5.5.1. The alternative, local iterative solving, shows advantages in storage consumption but may have certain drawbacks in the computational performance. This is due to the fact that for every global Krylov solver iteration we have several local iterations, while in using direct solvers we just have to factorize the local stiffness matrix once and subsequently compute a matrix vector multiplication in each global step. Note that for large subdomains and problems with storage restrictions an iterative strategy for the local inversion may be advantageous.

As mentioned before, for non-floating subdomains the pseudo-inverse matrix $\mathsf{K}_i^\dagger$ is simply the inverse matrix K_i^{-1}. For floating subdomains we need to compute a Moore–Penrose pseudoinverse such that

$$\mathsf{K}_i \mathsf{K}_i^\dagger \mathsf{K}_i = \mathsf{K}_i, \quad \text{for } i \in \mathcal{I}_{\text{floating}}.$$

Given the local stiffness matrix K_i and $\underline{u}, \underline{v} \in \mathbb{R}^{m_i}$ this can be achieved as follows. With $k_i = \dim(\ker(\mathsf{K}_i))$ we write

$$(\widetilde{\mathsf{K}}_i \underline{u}, \underline{v}) := (\mathsf{K}_i \underline{u}, \underline{v}) + \sum_{j=1}^{k_i} \beta_k \, (\underline{u}, \boldsymbol{r}_j^{(i)})_{\mathcal{R}_i} \, (\underline{v}, \underline{r}_j^{(i)})_{\mathcal{R}_i},$$

where $(\cdot,\cdot)_{\mathcal{R}_i}$ is a bilinear form that is coercive and bounded on $\ker \mathsf{K}_i$ and $\{\underline{r}_j^{(i)}\}_{j=1,\dots,k_i}$ is a set of vectors spanning $\ker \mathsf{K}_i$. In the case of elasticity these are the rigid body motions. We set

$$\mathsf{K}_i^\dagger := (\widetilde{\mathsf{K}}_i)^{-1}.$$

For $\underline{f} \in \operatorname{range}(\mathsf{K}_i)$ we then have $(\mathsf{K}_i^\dagger \underline{f}, \underline{r}_j^{(i)})_{\mathcal{R}_i} = 0$ for all $j = 1, \dots, k_i$. This implies

$$\mathsf{K}_i^\dagger \underline{f} \perp_{\mathcal{R}_i} \ker \mathsf{K}_i.$$

Thus $\mathsf{K}_i^\dagger$ is a Moore–Penrose inverse with respect to a special inner product. In order to preserve the sparsity of the stiffness matrix, a requirement to use a direct solver, we choose the scalar product

$$(\underline{u}, \underline{v})_{\mathcal{R}_i} := \int_{\omega_i} \underline{u} \cdot \underline{w} \, \mathrm{d}X_i,$$

where ω_i is a subset of Ω_i, or a submanifold in Ω_i. This can be a set of points, edges or faces.

For elasticity we choose the scalar product as follows: Let Ω_i be some subdomain with a point set $\mathcal{P}$ containing at least three points $p^{(1)}$, $p^{(2)}$ and $p^{(3)}$ that are not collinear,

see Fig. 6.5 . We then use

$$(\underline{v}, \underline{w})_{\mathcal{R}_i} := \sum_{m=1}^{n_p} \underline{v}(p^{(m)}) \cdot \underline{w}(p^{(m)})$$

where $\underline{v}(p^{(\bullet)})$ and $\underline{w}(p^{(\bullet)})$ are the point evaluations of the vectors $\boldsymbol{v}$ and $\boldsymbol{w}$ at the point $p^{(\bullet)}$ and n_p is the number of regularization points. The kernel $\ker \mathsf{K}_i$ for linear elasticity and the kernel $\ker \mathsf{K}_i'$ for nonlinear elasticity are spanned by $\boldsymbol{r}_j^{(i)}$, the rigid body modes. Let k_m^* denote the node index of vertex $p^{(m)}$. All basis functions vanish at the point

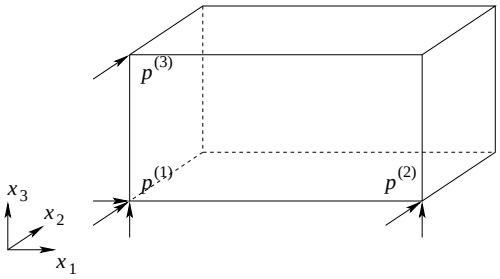

Figure 6.5. – One possibility to fix the six rigid body motions of a Neumann subdomain with three non-collinear points.

$p^{(m)}$ except for those associated to it. In addition just one component of the point realizes as 1 as we apply the basis function. Hence the regularization with n_p points in 3D results in

$$\widetilde{\mathsf{K}}_i[j,k] = \mathsf{K}_i[j,k] + \sum_{l=1}^{k_i} \sum_{m=1}^{n_p} \sum_{d=1}^{3} \beta_l \, \delta_{j(3k_m^*+d)} r_l(p^{(m)}) \cdot \delta_{k(3k_m^*+d)} r_l(p^{(m)})$$

For the choice of the constants β_l we take a look at the condition number of the regularized elasticity matrix.

Condition Number of the Regularized Elasticity Matrix Let H be the typical subdomain diameter, see (6.2) and let us assume a quasi-uniform triangulation of Ω with mesh size h. In the following we concentrate on the linear elasticity case but the estimates also hold true for nonlinear elasticity. For $\underline{v}$, $\underline{w} \in \mathbb{R}^{m_i}$ we set

$$(\widetilde{\mathsf{K}}\underline{v}, \underline{w}) = (\mathsf{K}\underline{v}, \underline{w}) + \sum_{l=1}^{6} \sum_{m=1}^{n_p} \beta_l \underline{v}(p^{(m)}) \underline{w}(p^{(m)})$$

for a vertex p and K the stiffness matrix arising from the linear elasticity problem. From the inverse inequality and the usual reference element transformation, we get that

$$\begin{aligned}(\mathsf{K}\underline{v}, \underline{v}) &\leq \frac{2E}{1-2\nu} |\boldsymbol{v}_h|^2_{[H^1(\Omega_i)]^3} = \frac{2E}{1-2\nu} \|\nabla \boldsymbol{v}_h\|^2_{[L_2(\Omega_i)]^3} \leq \widetilde{C} \, \frac{2E}{1-2\nu} h^{-2} \|\boldsymbol{v}_h\|^2_{[L_2(\Omega_i)]^3} \\ &\leq \widetilde{C} \, \frac{2E}{1-2\nu} h^{-2} h^3 \|\underline{v}\|_2^2 = C \, h \, \|\underline{v}\|_2^2.\end{aligned}$$

Hence with $\beta_{\max} = \max \beta_l$, $l = 1, \ldots, 6$,

$$(\widetilde{\mathsf{K}}\underline{v}, \underline{v}) \leq (C\,h + 6\,\beta_{\max})\ \|\underline{v}\|_2^2.$$

For the lower bound we use with $\beta_{\min} = \min \beta_l$, $l = 1, \ldots, 6$,

$$(\widetilde{\mathsf{K}}\underline{v}, \underline{v}) \geq |\boldsymbol{v}_h|^2_{[H^1(\Omega)]^3} + \beta_{\min} \sum_{m=1}^{n_p} |\underline{v}(p^{(m)})|^2$$

We now use the discrete Poincaré–Friedrich inequality, cf. [148, Toselli and Widlund (2005), Sect. 4.6]

$$\|\boldsymbol{v}_h - \overline{v}(\epsilon))\|^2_{L^2(\Omega_i)} \leq C\,H^2\,(H/h)|\boldsymbol{v}_h|^2_{H^1(\Omega_i)} \qquad \forall \boldsymbol{v}_h \in V_h(\Omega_i)\,,$$

for ϵ and edge, a face or a wire basket.

From this inequality and the Cauchy–Schwarz inequality we can conclude that

$$\begin{aligned}\|\boldsymbol{v}_h\|^2_{L^2(\Omega_i)} &\leq 2\,C\,H^2\,(H/h)\,|\boldsymbol{v}_h|^2_{H^1(\Omega_i)} + 2\,|\Omega_i|\,|v(\epsilon)|^2 \\ &\leq\ C\,H^2\,\max\left(H/h,\,\frac{|\Omega_i|}{\beta_{\min}\,H^2}\right)\,(\widetilde{\mathsf{K}}\boldsymbol{v},\,\boldsymbol{v})\end{aligned}$$

Finally,

$$\|\boldsymbol{v}_h\|^2_{L^2(\Omega_i)}\ \geq\ C\,h^3\,\|\underline{v}\|_2^2.$$

Summarizing,

$$\kappa(\widetilde{\mathsf{K}})\ \leq\ C\,H^2\,\max(h,\,6\,\beta_{\max})\,\max\left(H/h,\frac{|\Omega_i|}{\beta_{\min}\,H^2}\right)$$

which suggests to choose

$$\beta_l \in \left[\frac{|\Omega_i|}{H^2\,(H/h)},\,\frac{1}{6\,h}\right], \quad \text{for } l = 1, \ldots, 6.$$

This is satisfied, e.g., for $\beta = 1$. Then,

$$\kappa(\widetilde{\mathsf{K}}) = \mathcal{O}((H/h)^2(H/h)).$$

The extra factor of (H/h) is unavoidable and there is no better choice of β to get a better result than $\kappa(\widetilde{\mathsf{K}}) = \mathcal{O}((H/h)^3)$ in comparison to $\kappa(\mathsf{K}) = \mathcal{O}((H/h)^2)$. The only way to improve the condition number is to choose a different inner product $\mathcal{R}_i$ which then affects the sparsity of the regularized stiffness matrix $\widetilde{\mathsf{K}}$. Since we are using direct solvers the higher condition number will create almost no problems: all that is affected by the condition number itself is the rounding error, which means, that we only loose a bit of accuracy.

7. Numerical Examples

In this chapter we give numerical examples for the finite element tearing and interconnecting approach for linear and nonlinear elasticity problems. In Section 7.1 we test the FETI implementation for the linear elasticity case. Here we are able to compare the computed results to a given exact solution. This enables us to show the correctness of our implementation and to show the convergence rates as predicted from the theory. We compare the different preconditioning techniques and present differences between the classical FETI and the all-floating FETI approach. Following to this in Section 7.2 we apply the FETI approach to nonlinear elasticity problems. In this thesis we concentrate on the artery and the myocardium model as described in Chapter 3. As in the linear case we compare the different preconditioning techniques as well as all-floating FETI and the classical FETI method for simple geometries. At the end we present examples using more realistic triangulations. We apply the anisotropic artery model to a tube consisting of two materials, i.e. the media and the adventitia, and the orthotropic myocardium model to the myocardium of the ventricles of a rabbit heart.

The calculations were done using the *GHOST*-cluster (ghost.tugraz.at) located at the Graz University of Technology and the *VSC2*-cluster (http://vsc.ac.at/) in Vienna.

GHOST is a Linux-cluster consisting of two nodes, each with eight Quad-Core AMD Opteron 8356 Barcelona processors and a memory of 252.48 GB RAM. The AMD processors run with a clockrate of 2.3 GHz. The The Linux-cluster *VSC2* features 1314 compute nodes, each with two AMD Opteron Magny Cours 6132HE (8 Cores, 2.2 GHz) processors and 8 x 4 RAM. This yields the total number of 21 024 available processor cores.

We implemented the mechanics and the FETI framework in coorporation with Clemens Pechstein from the Johannes Kepler University in Linz, using the C++ template software package ParMax[1].

As local direct solver we use PARDISO [131, 132, Schenk and Gärtner] on *GHOST* and UMFPACK [31, 32] on the *VSC2* cluster.

[1] http://www.numa.uni-linz.ac.at/P19255/software.shtml, Clemens Pechstein and others.

7.1. Linear Elasticity

In this first section of numerical examples we consider linear elasticity problems with the academical example of a unit cube which is decomposed into a certain number of subcubes. Dirichlet boundary conditions are imposed all over the surface $\Gamma_D = \partial\Omega$, see Fig. 7.1. The calculated solution is compared to the exact solution

$$\mathsf{U}^*_{1l}(\boldsymbol{x}, \boldsymbol{x}^*) = \frac{1}{8\pi}\frac{1}{E}\frac{1+\nu}{1-\nu}\left[(3-4\nu)\frac{\delta_{1l}}{|\boldsymbol{x}-\boldsymbol{x}^*|} + \frac{(x_1 - x_1^*)(x_l - x_l^*)}{|\boldsymbol{x}-\boldsymbol{x}^*|^3}\right], \quad l = 1, 2, 3. \quad (7.1)$$

We compare the different strategies of preconditioning and all-floating and classical FETI. As the global iterative method we use the conjugate gradient method with a relative error reduction of 1.e-08.

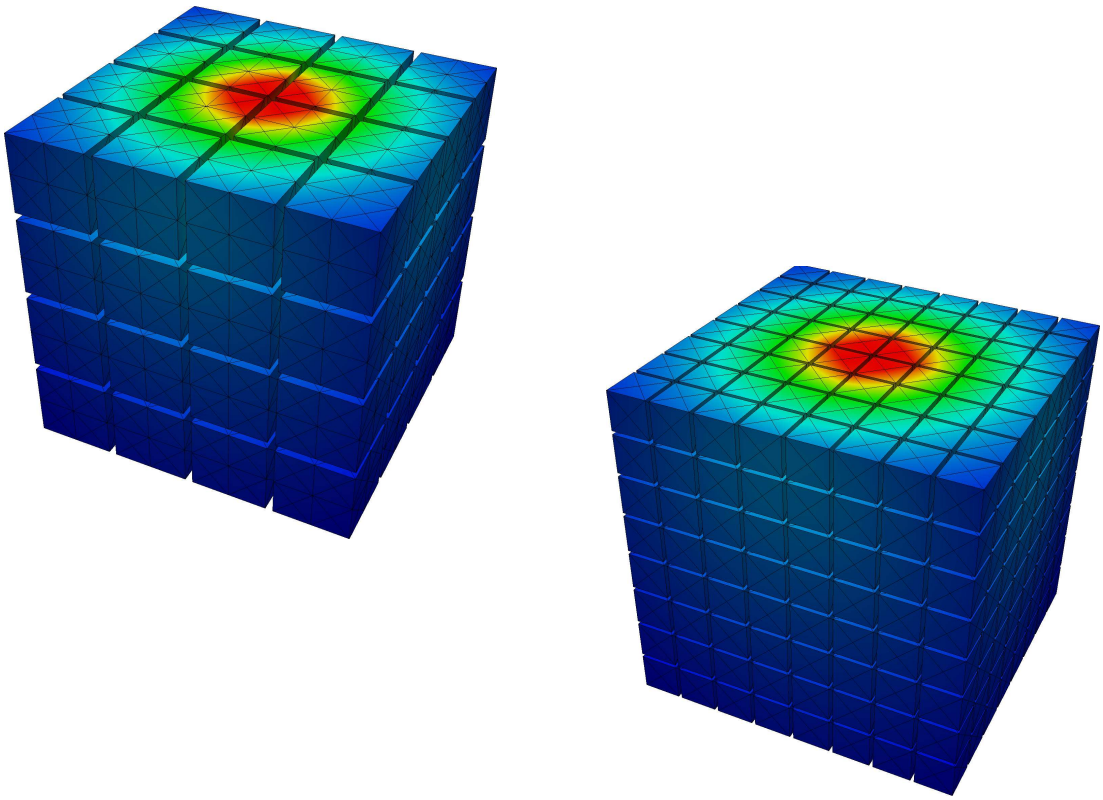

Figure 7.1. – Unit cube decomposed in 64 subdomains, level 2 (left) and decomposed in 512 subdomains, level 1 (right). Colors show fundamental solution (7.1)

7.1.1. Linear Elements

We consider a linear elasticity problem using linear tetrahedral elements ($\mathcal{P}_1$–element) given a cube with 512 subdomains and a cube with 64 subdomains. The parameters are

$E = 210.$ and $\nu = 0.3$. Note at first that for all examined settings, the L2 error and the estimated order of convergence (eoc) behave as expected from the theory. For both mesh settings, the cube subdivided into 512 subdomains and the cube subdivided into 64 subdomains, we get similar results if we compare the iteration numbers of the global CG method subject to the preconditioning techniques. We get the least iteration numbers for the optimal Dirichlet preconditioner. Given a large enough size of the subcubes, the application of the BEM preconditioner results in better iteration numbers than the lumped preconditioner and the very simple preconditioning technique, using the identity matrix for Y_i in (6.30), leads to the most iteration numbers. In fact for all-floating FETI this preconditioning techinique shows almost no reduction of the condition numbers. Nonetheless, since we need no additional time to compute the lumped preconditioner, in contrast to the Dirichlet and the BEM preconditioner, this type of preconditioning yields the best computational time for the problem with the largest amount of DOF (level 5). For the numbers in the tables Tab. 7.1 and Tab. 7.2 the underlying mesh is a

			Preconditioning			
l	DOF	Lagr.	identity	lumped	Dirichl.	BEM
all-floating						
1	9 981	38 052	35 (16.2)	16 (3.9)	13 (3.1)	33 (15.8)
2	62 397	84 276	47 (28.5)	23 (7.3)	18 (4.7)	30 (11.8)
3	480 573	238 932	61 (50.2)	28 (10.3)	21 (6.0)	32 (14.3)
4	3 860 541	797 076	83 (100.2)	43 (25.3)	26 (8.7)	37 (19.4)
5	31 116 861	2 908 692	113 (199.2)	63 (59.6)	31 (12.0)	44 (26.3)
classical						
1	6 621	38 388	50 (33.2)	23 (6.3)	19 (4.7)	49 (44.3)
2	56 349	77 700	77 (78.7)	39 (18.6)	28 (10.0)	49 (44.2)
3	469 149	204 708	104 (154.8)	61 (49.6)	37 (17.0)	57 (45.8)
4	3 838 365	652 260	141 (297.8)	90 (115.4)	45 (25.0)	66 (60.6)
5	31 073 181	2 321 508	187 (576.5)	123 (248.9)	52 (33.5)	77 (79.9)

Table 7.1. – Table shows iteration numbers and condition numbers (in brackets) for the different preconditioning techniques. Mesh: Cube with 512 subdomains.

cube with 512 subdomains and we used 512 processing units on the *VSC2* cluster to do our computations. We observe that all-floating FETI yields better condition numbers (in brackets) for all preconditioners and hence as well better convergence rates of the global conjugate gradient method, cf. Tab. 7.1. Although the global iterative method converges in less iterations for the all-floating approach, we achieve lower computation times for the classical FETI method for the first four levels, cf. Tab. 7.2. This is mainly due to the larger expenditure of time to set up the all-floating FETI system (i.e. set up the jump operators (6.29)). In level 5 the global system gets large enough that all-floating FETI outperforms the classical approach in computational time. That means that the lower amount of iteration numbers overbalances the higher setup times

			Preconditioning			
l	L2 error	eoc	identity	lumped	Dirichl.	BEM
all-floating						
1	9.60e-05	-	23.33 s	19.26 s	19.66 s	20.55 s
2	2.52e-05	1.98	22.06 s	19.76 s	19.50 s	19.86 s
3	6.41e-06	1.98	22.59 s	21.13 s	21.15 s	23.13 s
4	1.62e-06	1.99	33.61 s	28.89 s	28.09 s	46.09 s
5	4.08e-07	1.99	187.81 s	143.26 s	174.80 s	321.66 s
classical						
1	1.01e-04	-	6.32 s	6.55 s	5.93 s	6.46 s
2	2.54e-05	1.98	6.82 s	7.06 s	6.18 s	6.71 s
3	6.42e-06	1.98	8.94 s	7.43 s	8.18 s	10.28 s
4	1.62e-06	1.99	18.72 s	15.66 s	13.90 s	37.84 s
5	4.08e-07	1.99	207.73 s	158.00 s	173.50 s	341.81 s

Table 7.2. – Computation times for the different preconditioning techniques achieved with 512 processing units on *VSC2*. The underlying mesh is a cube with 512 subdomains.

for this case. From level 4, with a maximum of 8 907 local degrees of freedom, to level 5, with a maximum of 66 195 local degrees of freedom, we observe an increase in local assembling and factorization time from approximately 2 seconds up to about 66 seconds for the Dirichlet precnditioner. This is mainly due to the higher memory requirements of the direct solver. To some extend this also explains the higher numbers of the BEM preconditioner, but for sure we need to invest additional time in improving the implementation of the hypersingular operators to be competitive with the sophisticated direct solver packages.

For the examples summarized in Tab. 7.3 and Tab. 7.4 a cube with 64 subdomains was considered. For the computation we used 32 processing units on *GHOST*. Note that the higher levels of this calculation are inexecutable on the larger *VSC2* cluster, since there each processor has only a limited amount of private memory and there is no global shared memory. That means that the memory consuming factorization of the local stiffness matrices by the direct solver is unfeasible, if the number of local degrees of freedom gets too large. On the other hand on the *GHOST* cluster we have additional global shared memory. Here we have the drawback that the communication between this shared memory and the processing units is comparatively slow. This explains the high computation times for level 6 in Tab. 7.4. Moreover, the larger memory requirements of the Dirichlet and the BEM preconditioning technique lead to an out of memory (OOM) error for the highest level (i.e. 31 million DOF). We see very clearly, that in this case the FETI method with direct local solving is not really practicable. A possibility to overcome this performance problem would be the usage of fast local iterative solvers, e.g. the CG method with a multigrid or a BPX preconditioner.

As in the previous case with 512 subdomains we observe better iteration numbers for the all-floating FETI method, cf. Tab. 7.3. Again, given large enough local subdomains, the all-floating approach outperforms classical FETI, cf. Tab. 7.4. Summing up it seems, at least for this example of a unit cube, that all-floating FETI is more feasible for larger subdomains, while classical FETI shows advantages for many smaller subdomains. Moreover the simple lumped preconditioner appears to be favorable for this academical example with very structured subdomains.

			Preconditioning			
l	DOF	Lagr.	identity	lumped	Dirichl.	BEM
all-floating						
1	1 733	3 876	35 (16.7)	15 (3.8)	12 (2.8)	33 (15.9)
2	9 212	9 708	46 (28.8)	21 (7.4)	17 (4.5)	30 (12.0)
3	64 874	30 012	59 (50.8)	28 (10.5)	20 (5.6)	31 (13.7)
4	500 293	105 180	80 (101.8)	42 (25.5)	25 (8.3)	36 (18.8)
5	3 957 756	393 756	109 (202.3)	62 (60.3)	30 (11.5)	42 (25.8)
6	31 541 098	1 523 868	148 (399.3)	89 (130.7)	OOM	OOM
classical						
1	1 049	3 780	44 (30.4)	19 (6.0)	17 (4.7)	44 (31.6)
2	7 984	7 884	63 (72.6)	33 (17.0)	24 (9.6)	43 (30.5)
3	62 557	21 276	83 (143.2)	47 (44.1)	31 (16.2)	52 (43.6)
4	495 801	68 796	113 (273.3)	68 (101.7)	37 (23.5)	59 (58.7)
5	3 948 912	246 780	151 (527.4)	95 (218.4)	43 (31.7)	68 (78.4)
6	31 523 549	934 524	202 (1031.8)	131 (452.6)	OOM	OOM

Table 7.3. – Iteration numbers and condition numbers (in brackets) of the global CG Method for the different preconditioning techniques. Mesh: Cube with 64 subdomains.

all-floating / time			Preconditioning			
l	L2 error	eoc	none	lumped	Dirichl.	BEM
all-floating						
1	1.40e-04	-	0.92 s	0.99 s	0.88 s	3.41 s
2	3.95e-05	1.96	1.16 s	0.87 s	0.98 s	4.37 s
3	9.95e-06	2.00	2.33 s	2.30 s	2.67 s	9.16 s
4	2.51e-06	1.99	35.62 s	26.57 s	35.61 s	80.71 s
5	6.34e-07	1.99	712.20 s	516.91 s	691.84 s	1113. s
6	1.59e-07	1.99	16123. s	11850. s	OOM	OOM
classical						
1	1.54e-04	-	0.31 s	0.22 s	0.24 s	2.80 s
2	3.98e-05	1.96	0.47 s	0.33 s	0.52 s	3.75 s
3	9.96e-06	2.00	1.64 s	1.53 s	2.22 s	10.32 s
4	2.51e-06	1.99	38.53 s	29.69 s	38.57 s	83.31 s
5	6.34e-07	1.99	799.87 s	582.30 s	726.70 s	1277. s
6	1.59e-07	1.99	19341. s	14496. s	OOM	OOM

Table 7.4. – Computation times (in seconds) for the different preconditioning techniques and a cube with 64 subdomains. The times were achieved with 32 processing units of the *GHOST* cluster.

7.1.2. Quadratic Elements

In this section we consider a linear elasticity problem using tetrahedral elements and quadratic ansatz functions, i.e. $\mathcal{P}_2$–elements. The parameters are $E = 210.$ and $\nu = 0.49$. Note that for all preconditioning types as well as for all-floating and classical FETI the L2 error compared to the fundamental solution behaves as expected from the theory and hence we get a cubic convergence rate (eoc), see Tab. 7.6.

First, we look at a cube with 64 subdomains. For reasons of memory limits this example was computed on the *GHOST* cluster. As for the case of linear ansatz functions, see Section 7.1.1, we get the lowest condition numbers of the global system and thus the least iteration numbers of the global CG method using the optimal Dirichlet preconditioner. The highest iteration numbers we observe with the simple identity preconditioning technique, using the identity matrix for Y_i in (6.30). We did not implement the BEM preconditioner for quadratic ansatz functions. For all-floating FETI we have the very interesting case that the global CG iteration numbers stay almost constant for the lumped preconditioner and even seem to decay for the identity and the Dirichlet preconditioner, if we increase the local degrees of freedom, i.e. increase the level l, see Tab. 7.5.

For the classical FETI approach the iteration numbers stay almost constant for the

		Preconditioning		
l	DOF	identity	lumped	Dirichl.
all-floating				
1	8 060	199 (2284.24)	134 (289.98)	69 (103.17)
2	55 658	183 (1590.10)	137 (314.29)	63 (78.10)
3	426 565	171 (979.22)	134 (295.44)	53 (48.08)
4	3 367 932	160 (581.40)	133 (272.79)	45 (30.11)
classical				
1	6 832	161 (1481.74)	107 (183.65)	55 (50.82)
2	53 341	170 (1152.87)	113 (229.75)	54 (52.65)
3	422 073	174 (932.99)	141 (428.24)	54 (51.12)
4	3 359 088	201 (1053.93)	188 (935.79)	55 (57.05)

Table 7.5. – Table shows iteration numbers and condition numbers (in brackets) for the different preconditioning techniques using quadratic ansatz functions. Mesh: Cube with 64 subdomains.

				Preconditioning		
l	L2 error	eoc	DOF	identity	lumped	Dirichl.
all-floating						
1	1.04e-01	-	8 060	1.63 s	1.66 s	1.67 s
2	1.36e-02	2.96	55 658	5.86 s	5.84 s	6.43 s
3	1.78e-03	2.94	426 565	72.87 s	66.62 s	60.80 s
4	2.22e-04	3.01	3 367 932	997.18 s	927.67 s	766.68 s
classical						
1	1.06e-01	-	6 832	0.80 s	0.62 s	0.73 s
2	1.37e-02	2.96	53 341	4.34 s	4.13 s	4.84 s
3	1.78e-03	2.94	422 073	68.21 s	65.73 s	57.79 s
4	2.22e-04	3.01	3 359 088	1123.47 s	1124.93 s	807.45 s

Table 7.6. – Computation times for the different preconditioning techniques using quadratic ansatz functions. Mesh: Cube with 64 subdomains.

Dirichlet preconditioner and increase slightly for the other two preconditioning techniques, see Tab. 7.5.

Given a high enough number of local degrees of freedom, in this example level $l = 4$, the all-floating FETI method outperforms the classical approach regarding the computation times for all preconditioners. This characteristic was also observed with linear ansatz functions, see Section 7.1.1. In contrast to the formulation with $\mathcal{P}_1$-elements, the optimal Dirichlet preconditioner now shows a noticeable advantage to the other two preconditioners. As in Section 7.1.1, the significantly higher computation times in level 4 compared to level 3 are mainly due to high memory requirements of the direct solver in this case.

In the following we deal with at a cube with 512 subdomains and again use quadratic ansatz functions on tetrahedral elements. Now the computations were done on the *VSC2* cluster. We investigate iteration numbers and computation times depending on Poisson's ratio ν, i.e. $E = 210.$ and $\nu \in \{0.3, 0.49, 0.4999\}$. With the iteration number > 1000 we indicate that the global conjugate gradient method did not converge within 1000 iterations to reach the relative error reduction of 1.e-08. In all the examples the estimated order of convergence behaves as expected, i.e. we get a cubic convergence rate, for all examples where the global CG method converged. Again we observe that for almost every case the iteration numbers for all-floating FETI improve with a higher level. This can be seen especially for the simple identity preconditioner and the Dirichlet preconditioner for materials with almost incompressible behavior. Note that the lumped preconditioner does not seem to work very well for quadratic elements and a nearly incompressible material, i.e. $\nu = 0.4999$. This behavior can be explained with the very ill-conditioned local stiffness matrices that result from dealing with almost incompressible materials, see Section. 4.3.1. In fact all preconditioners show high iteration numbers for almost incompressible materials and the FETI methods seems to be unstable. A possibility to overcome these locking effects is the usage of $\mathcal{P}_2$–$\mathcal{P}_0$–elements, see Section 5.1.3. In this thesis we will not deal with $\mathcal{P}_2$–$\mathcal{P}_0$–elements and linear elasticity since we will concentrate on nearly incompressible nonlinear materials in Section 7.2. For numerical examples that examine the behavior of the FETI-DP method given nearly incompressible linear materials see for instance [83, Klawonn and Rheinbach (2006)].

In Tab. 7.8 we outline the computation times for quadratic ansatz functions. For this special example with a very structures subdomain grid it seems that for a Poisson's ratio ν close to 0.5 the preconditioning technique with $\mathsf{Y}_i = \mathsf{I}$ in (6.30) is the best choice concerning the computation time.

			Preconditioning		
l	DOF	Lagr. Mult.	identity	lumped	Dirichl.
all-floating					
1	53 181	84 276	102 / 199 / 878	44 / 148 / >1000	32 / 90 / 796
2	406 845	238 932	89 / 181 / 754	47 / 153 / >1000	31 / 80 / 703
3	3 270 717	797 076	82 / 169 / 662	45 / 147 / >1000	27 / 64 / 535
4	26 398 269	2 908 692	77 / 160 / 584	45 / 138 / >1000	24 / 50 / 404
classical					
1	47 133	77 700	92 / 178 / 672	40 / 133 / >1000	27 / 79 / 696
2	395 421	204 708	85 / 181 / 662	44 / 140 / >1000	29 / 76 / 663
3	3 248 541	652 260	88 /195 / 656	64 / 182 / >1000	36 / 73 / 603
4	26 354 589	2 321 508	108 / 216 / 716	89 / 205 / >1000	42 / 75 / 575

Table 7.7. – Iteration numbers for the different preconditioning techniques depending on Poisson's ratio ν using $\mathcal{P}_2$–elements. Parameter setting: $E = 210.$, $\nu = 0.3$ (left), $E = 210.$, $\nu = 0.49$ (middle), $E = 210.$, $\nu = 0.4999$ (right), Mesh: Cube with 512 subdomains. Calculated on *VSC2* with 512 cores.

	Preconditioning		
l	none	lumped	Dirichl.
all-floating			
1	27.9 s / 30.2 s / 74.9 s	22.5 s / 28.4 s / -	20.6 s / 25.8 s / 86.2s
2	25.5 s / 30.6 s / 74,2 s	22.9 s / 30.9 s / -	21.2 s / 26.3 s / 77.0 s
3	34.6 s / 44.3 s / 99.6 s	29.6 s / 46.3 s / -	29.2 s / 35.9 s / 118.4 s
4	239.0 s / 417.8 s / 853.9 s	220.3 s / 390.5 s / -	299.4 s / 346.0 s / 968.4 s
classical			
1	7.7 s / 9.6 s / 23.9 s	7.9 s / 9.1 s / -	7.6 s / 9.6 s / 24.3 s
2	8.4 s / 10.2 s / 27.7 s	7.2 s / 10.8 s / -	6.6 s / 8.8 s / 29.0 s
3	16.1 s / 25.2 / 62.4 s	14.3 s / 24.7 s / -	14.9 s / 19.7 s / 93.6
4	233.1 s / 421.4 s / 772.2	219.4 s / 370.9 s / -	292.0 s / 350.2 s / 1269.7

Table 7.8. – Computation times for the different preconditioning techniques depending on Poisson's ratio ν using $\mathcal{P}_2$–elements. Parameter setting: $E = 210.$, $\nu = 0.3$ (left), $E = 210.$, $\nu = 0.49$ (middle), $E = 210.$, $\nu = 0.4999$ (right). Mesh: Cube with 512 subdomains. Calculated on *VSC2* with 512 cores.

7.1.3. Scaling for Linear Elasticity

We consider a unit cube that is subdivided into 512 subcubes with inhomogeneous Dirichlet boundary conditions all over the boundary. With linear ansatz functions this leads to a linear elasticity problem with approximately 3.9 million total DOF. We apply the all-floating FETI approach with the lumped preconditioner. The global FETI system has 797 096 Lagrange multipliers and was solved using the CG method with a varying amount of processing units p on the *VSC*-cluster. In all cases the global iterative method converged within 45 iterations and the estimated condition number for the system is 26.86.

As expected the local time, i.e. the assembling of the stiffness matrices and the factorization of the local problems with the direct solver package UMFPACK [31, 32], scales almost perfectly. This is not surprising, since we do not need any communication between the processing units for these operations. The efficiency for the solving time of the global conjugate gradient method and the efficiency of the total time is good up to 64 processing units and then decays to 55% and 38%. This is due to the communication within the iterative method and within the setup of the FETI method and the realization of the coarse system $(\mathsf{G}^\top \mathsf{G})^{-1}$, see (6.27). Possiblities to overcome this lower scaling with a large amount of processors are perhaps the usage of parallel solver packages as *hypre* and a more efficient assembling of the coarse system. It also needs some tricks with MPI and memory management. It is obvious that a longer lasting assembling procedure effects the scaling in a positive way. Hence with nonlinear elasticity we expect a better parallel efficiency.

p	local time	efficiency	global CG time	efficiency	total time	efficiency
16	46.00 s	-	50.12 s	-	179.76 s	-
32	23.18 s	.9921	26.42 s	.9485	99.11 s	.9068
64	11.61 s	.9906	14.56 s	.8607	59.40 s	.7565
128	5.84 s	.9853	8.47 s	.7393	37.47 s	.5997
256	2.95 s	.9754	5.65 s	.5539	29.24 s	.3843

Table 7.9. – Computation times (in seconds) and efficiency for a linear elasticity problem using a varying number of processing units p.

7.2. Nonlinear Elasticity

In this section we will apply the FETI method to nonlinear elasticity problems, i.e. the nonlinear artery model, see Section 3.12, and the nonlinear myocardium model, see Section 3.13. The computations in this chapter are all done using the *VSC2*-cluster and UMFPACK as direct local solver.

For most examples in this section we will apply a rather low pressure to the nonlinear materials to have a converging Newton scheme. Nonetheless, the material model as used is orthotropic. To simulate a higher pressure, an appropriate time stepping scheme has to be used. However, this does not affect the number of local iterations significantly.

$\kappa = 3333.33$ [kPa],	$a = 0.33445$ [kPa],	$b = 9.242$ [-],
$a_f = 18.535$ [kPa],	$b_s = 10.446$ [-],	$b_f = 15.972$ [-],
$a_{fs} = 0.417$ [kPa]	$a_s = 2.564$ [kPa],	$b_{fs} = 11.602$ [-].

Table 7.10. – Material parameters for the myocardium from [38, Eriksson et al. (2012)] where they use an adaptation from [65, Holzapfel and Ogden (2009)].

Media	**Adventitia**
$c_M = 3.0$ [kPa]	$c_A = 0.3000$ [kPa],
$k_{1M} = 2.3632$ [kPa],	$k_{1A} = 0.5620$ [kPa],
$k_{2M} = 0.8393$ [-],	$k_{2A} = 0.7112$ [-].

Table 7.11. – Material parameters for an arterial material, from [63, Holzapfel et al. (2000)], see Fig. 3.3.

7.2.1. Academic Example

At first, we will do the computations on a simple unit cube that is subdivided in 512 subcubes with a tetrahedral triangulation. We will use the following boundary conditions: one face ($y = 0$) is fixed with homogneous Dirichlet boundary conditions, on one face ($y = 1$) we apply a tensile stress of 1 mmHg, on the other four faces we have homogeneous Neumann boundary conditions. With linear ansatz functions and the FETI approach this yields a system with a total number of approximately 3.9 million DOF and 652 260 Lagrange multipliers. This example was calculated on 64 processing units on *VSC2*. We use the myocardium model (3.117) and the parameters as indicated in Tab. 7.10. The results of these calculations can be found in Tab. 7.12. The Newton scheme needed 3 to 4 Newton steps to reach the stopping criterion. The stopping criterion is an absolute residual norm of 1.e-06, as also used in [16, Brands et al. (2008)]. We observe that for the proposed setting of $\kappa = 3333$ kPa only the

κ	prec.	it. p.N.s	time p.N.s.	$J_{\min}$	$J_{\max}$
0.833	identity	80 / 143	34 s / 34 s	1.000000	1.004886
	Dirichlet	25 / 44	28 s / 27 s		
	lumped	41 / 91	30 s / 33 s		
	BEM	36 / 63	34 s / 37 s		
3.333	identity	114 / 194	36 s / 38 s	1.000000	1.002257
	Dirichlet	31 / 52	31 s / 28 s		
	lumped	59 / 127	33 s / 31 s		
	BEM	53 / 88	41 s / 42 s		
33.33	identity	276 / 442	54 s / 58 s	0.999939	1.000302
	Dirichlet	71 / 105	36 s / 36 s		
	lumped	149 / 301	39 s / 48 s		
	BEM	173 / 214	74 s / 74 s		
333.3	identity	734 / >1000	90 s / -	0.999992	1.000037
	Dirichlet	203 / 293	52 s / 57 s		
	lumped	408 / 808	64 s / 96 s		
	BEM	>1000 / 603	- / 169 s		
3333.	identity	>1000 / >1000	- / -	0.999998	1.000001
	Dirichlet	592 / 867	101 s / 134 s		
	lumped	>1000 / >1000	- / -		
	BEM	>1000 / >1000	- / -		

Table 7.12. – Iteration numbers (it. p.N.s) and computation times per Newton step (it. p.N.s.) for all-floating FETI (left) and classical FETI (right) with **linear** ansatz functions. κ gives the setting of the bulk modulus, prec. the preconditioner applied. $J_{\min}$ and $J_{\max}$ give the mininal and the maximal volume ratio change of the tetrahedral elements. The underlying mesh is a cube with 512 subdomains.

Dirichlet preconditioner yields iteration numbers of the global iterative method below 1000 iterations. This preconditioning technique seems to be a good choice for all other settings as well. In this example all-floating FETI yields better iteration numbers than the classical approach. With the BEM preconditioner we achieve in most cases better iteration numbers than with the lumped preconditioner, although it is built with the hypersingular operators for linear elasticity and we had to fit the nonlinear parameters to it.

Using quadratic ansatz functions we get a system with a total number of 26 488 475 degrees of freedom and 2 420 142 Lagrange multipliers. For the parameter setting as given in Tab. 7.10, the global iterative method only converged within 1000 iterations using the Dirichlet preconditioner: 506 iterations for the all-floating and 701 iterations for the classical approach. The computation times per Newton step (assembling and solving) was 1275 seconds for all-floating and 1623 seconds for classical FETI.

7.2.2. Examples with Realistic Geometries

In this section we present some examples to show the applicability of the FETI approach for the simulation of the myocardium and the artery on realistic geometries.

First, we look at a mesh of the left and the right ventricle of a rabbit heart with given fiber and sheet directions, see Fig. 7.2, (left), which is decomposed into a certain number of subdomains, e.g. 256 subdomains in Fig. 7.2, (right). To describe the anisotropic and nonlinear cardiac tissue, we use the material model (3.117) with the parameters given in table 7.10. Dirichlet boundary conditions are imposed on the top of the myocardium mesh. The interior wall of the right ventricle is exposed to the pressure of 1 mmHg which is modeled with Neumann boundary conditions. The local Moore–Penrose pseudoinverse matrices are realized with a sparsity preserving regularization and the direct solver package UMFPACK [31, 32]. The global nonlinear finite element system with 1 643 040 degrees of freedom is solved by a Newton scheme, where the FETI approach is used in each Newton step. For this specific example the Newton scheme needed four to six iterations. Due to the non-uniformity of the subdomains the efficiency of a global preconditioner becomes more important. The vast differences between the all-floating and the classical FETI approach in Tab. 7.13 are explained with the characteristic of the decomposition where some subdomains only have very few or even only one point located at the Dirichlet boundary, see Fig. 7.2.

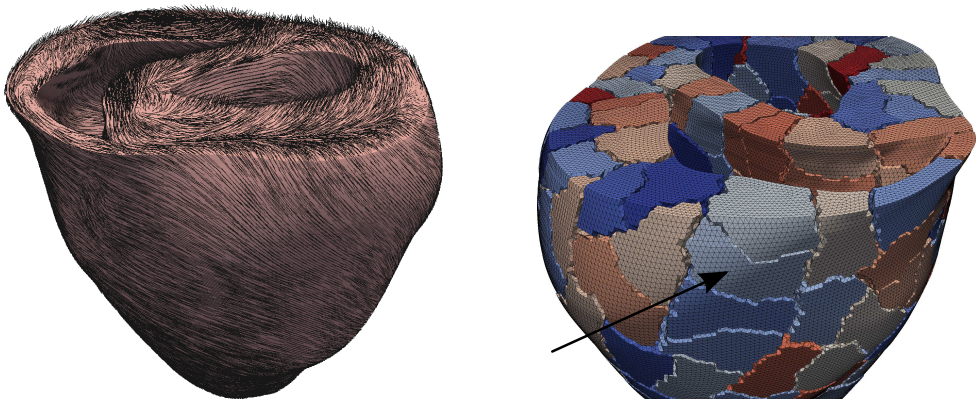

Figure 7.2. – Left and right ventricle of the rabbit heart. Mesh consists of 3 073 529 tetrahedrons and 547 680 vertices. Point of view is from above showing the interior of the left and right ventricle Black lines on the left picture indicate fiber directions $\boldsymbol{f}_0$. Some decompositions, here into 256 subdomains, (right picture) lead to subdomains that have only a few or even only only one point on the dirichlet boundary (indicated by the black arrow). This yields problems with classical FETI.

As for the academic example in Section 7.2.1 the sophisticated Dirichlet preconditioner and all-floating FETI seem to be the best choice to solve the system. For the proposed parameter setting with $\kappa = 3333$. the GMRES method needed 910 iterations and

κ	prec.	it. p.N.s.	times p.N.s.	$J_{\min}$	$J_{\max}$
0.8333	identity	261 / 868	100 s / 256 s	0.9972	1.000102
	Dirichlet	63 / 239	61 s / 139 s		
	lumped	113 / 470	59 s / 154 s		
	BEM	106 / 393	63 s / 206 s		
3.333	identity	368 / >1000	136 s / -	0.998876	1.000066
	Dirichlet	80 / 275	70 s / 157 s		
	lumped	162 / 628	74 s / 198 s		
	BEM	150 / 542	85 s / 282 s		
33.33	identity	944 / >1000	296 s / -	0.999952	1.000044
	Dirichlet	162 / 486	110 s / 231 s		
	lumped	387 / >1000	140 s / -		
	BEM	432 / >1000	225 s / -		
333.3	identity	>1000 / >1000	- / -	0.999966	1.000028
	Dirichlet	351 / 933	202 s / 470 s		
	lumped	870 / >1000	287 s / -		
	BEM	>1000 / >1000	- / -		
3333.	identity	>1000 / >1000	- / -	0.999987	1.000010
	Dirichlet	910 / >1000	474 s / -		
	lumped	>1000 / >1000	- / -		
	BEM	>1000 / >1000	- / -		

Table 7.13. – Iteration numbers per Newton step (it. p.N.s) and computation times per Newton step (it. p.N.s.) in seconds for the all-floating (left) and the classical FETI approach (right) with **linear** ansatz functions. The column κ gives the setting of the bulk modulus κ and the column prec. the preconditioner applied. $J_{\min}$ and $J_{\max}$ give the mininal and the maximal volume ratio change of the tetrahedral elements.
Mesh: rabbit heart subdivided in 256 subdomains, calculated with 256 cores.

the solving time of one Newton step (assembling and solving) lasted 474 seconds, see Tab. 7.13.

Using quadratic ansatz functions we have a total number of 12 188 296 degrees of freedom. In order to not infringe the memory limitations on the *VSC2* cluster we have to use a decomposition into 480 subdomains, see Fig. 7.3. Using all-floating FETI and the Dirichlet preconditioner we needed 862 iterations for the global GMRES method and a total solving time of 986 seconds per Newton step, see Tab. 7.14. By comparing $J_{\min}$ and $J_{\max}$ from this table to Tab. 7.13, we can clearly see that quadratic ansatz functions resolve the incompressible elastic behavior much better than linear ansatz functions, see also Sect. 5.1.4. Hence a much lower κ than the proposed value of 3333 kPa should be sufficient to simulate the nearly incompressible behavior of the myocardium. Nonetheless, the numbers in this table show as well, that the convergence of the GMRES method within the FETI approaches chosen in this simulation, is still dependent on the bulk modulus κ.

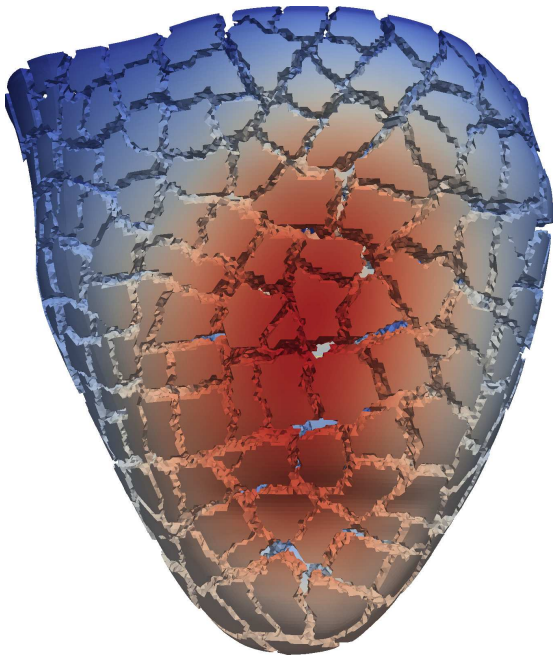

Figure 7.3. – The picture shows the displacement field of the rabbit heart with pressure applied in the right ventricle and the decomposition in 480 subdomains. Point of view is from below showing the apex of the heart at the bottom. Red colors indicate high, blue colors indicate low displacement.

As an abstraction of an artery we consider a tube consisting of two materials, the media and the adventitia, on which we apply the arterial model with parameters given in Tab. 7.11. We apply a pressure of 10 mmHg to the interior wall. For linear ansatz function we decompose the tube in 512 subdomains, see Fig. 7.5, and we end up with 3 655 642 degrees of freedom. Again the Dirichlet preconditioner is the best choice for

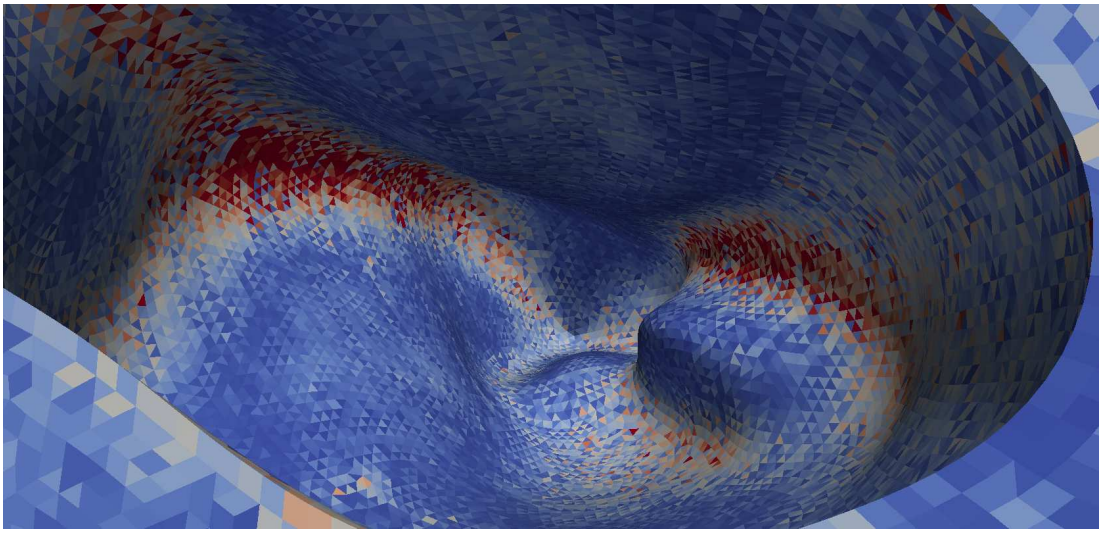

Figure 7.4. – Von Mises stress in the right ventricle. Point of view is from above looking inside the right ventricler; values of high von Mises stress in red and of low stress in blue.

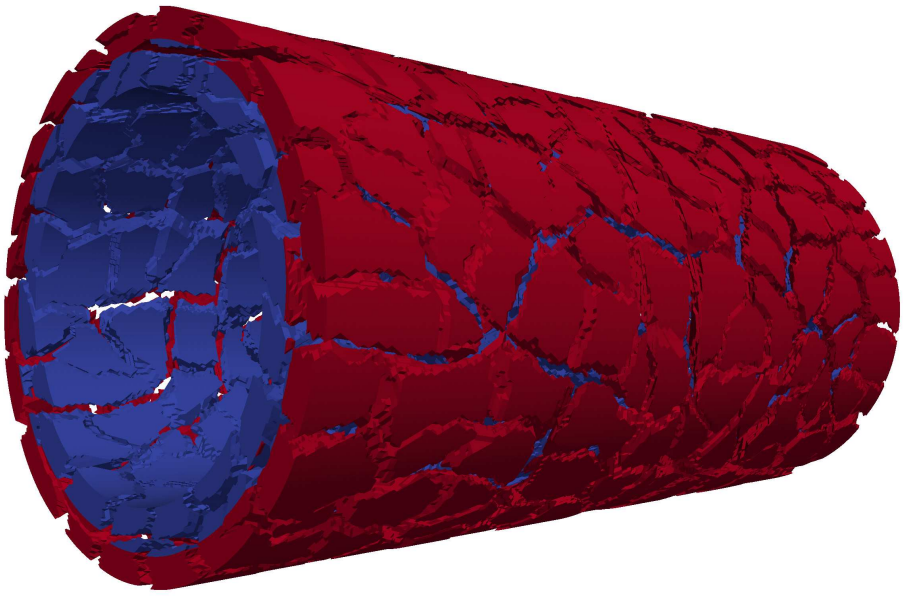

Figure 7.5. – Abstraction of the artery with a tube mesh;
the blue color indicates the media and the red color the adventitia.

κ	prec.	it. p.N.s.	times p.N.s.	$J_{\min}$	$J_{\max}$
0.8333	identity	229 / 407	253 s / 360 s	0.999882	1.000047
	Dirichlet	65 / 134	232 s / 309 s		
	lumped	112 / 265	185 s / 275 s		
3.333	identity	266 / 483	275 s / 420 s	0.999968	1.000014
	Dirichlet	68 / 149	237 s / 325 s		
	lumped	155 / 366	209 s / 345 s		
33.33	identity	535 / 941	452 s / 705 s	0.999997	1.000002
	Dirichlet	108 / 215	282 s / 406 s		
	lumped	401 / 916	375 s / 709 s		
333.3	identity	>1000 / >1000	- / -	1.000000	1.000000
	Dirichlet	300 / 455	527 s / 684 s		
	lumped	>1000 / >1000	- / -		
3333.	identity	>1000 / >1000	- / -	1.000000	1.000000
	Dirichlet	862 / >1000	986 s / -		
	lumped	>1000 / >1000	- / -		

Table 7.14. – Iteration numbers per Newton step (it. p.N.s) and computation times per Newton step (it. p.N.s.) in seconds for the all-floating (left) and the classical FETI approach (right) with **quadratic** ansatz functions. The column κ gives the setting of the bulk modulus and the column prec. the preconditioner applied. $J_{\min}$ and $J_{\max}$ give the mininal and the maximal volume ratio change of the tetrahedral elements.
Mesh: rabbit heart, subdivided in 480 subdomains, calculated with 480 cores.

this problem, see Tab. 7.15. The Newton method converged within 4 and 7 steps.

κ	prec.	it. p.N.s.	times p.N.s.	$J_{\min}$	$J_{\max}$
0.833	identity	>1000 / >1000	- / -	1.000000	1.001111
	Dirichlet	148 / 319	289 s / 504 s		
	lumped	265 / 643	289 s / 580 s		
3.333	identity	>1000 / >1000	- / -	1.000000	1.000290
	Dirichlet	170 / 361	316 s / 557 s		
	lumped	310 / 910	323 s / 862 s		
33.33	identity	>1000 / >1000	- / -	1.000000	1.000041
	Dirichlet	312 / 627	498 s / 898 s		
	lumped	612 / >1000	563 s / -		
333.3	identity	>1000 / >1000	- / -	0.999995	1.000010
	Dirichlet	705 / >1000	999 s / -		
	lumped	897 / >1000	1249 s / -		
3333.	identity	>2000 / >2000	- / -	0.999999	1.000001
	Dirichlet	1877 / >2000	2502 s / -		
	lumped	>2000 / >2000	- / -		

Table 7.15. – Iteration numbers per Newton step (it. p.N.s) and computation times per Newton step (it. p.N.s.) in seconds for the all-floating (left) and the classical FETI approach (right) with **linear** ansatz functions. The column κ gives the setting of the bulk modulus and the column prec. the preconditioner applied. $J_{\min}$ and $J_{\max}$ give the mininal and the maximal volume ratio change of the tetrahedral elements.
Mesh: tube mesh with 2 materials; 10 mmHg applied to the interior wall.

For quadratic ansatz functions we get a system with 28 183 189 total degrees of freedom. For the parameter setting as given in Tab. 7.11 and $\kappa = 3333.$ we needed about 1500 iterations and approximately 45 minutes for each Newton step on 1024 cores.

7.2.3. Scaling for Nonlinear Elasticity

We consider a unit cube that is subdivided into 512 subcubes with homogeneous Dirichlet boundary conditions and a traction force that is applied to one face of the cube. We apply the myocardium model with the parameters from Tab. 7.10 and $\kappa = 33.33$ using all-floating FETI with a Dirichlet preconditioner. With linear ansatz functions this leads to a nonlinear elasticity problem with approximately 3.95 million total DOF. We apply the all-floating FETI approach with the lumped preconditioner. The global FETI system has 676 782 Lagrange multipliers and was solved using the CG method

(since we used the symmetric system arising from the Euler description) with a varying amount of processing units p on the *VSC*-cluster. In all cases and each Newton step the global iterative method converged within 70 iterations and the estimated condition number for the system is about 64.48. We needed one initial linear elasticity step and then 3 further nonlinear Newton steps, i.e. four solution steps, to reach an absolute error of <1.e-06.

In Tab. 7.16 we present the following numbers: the *local time* is the sum of all assembling and local factorization times during the four solution steps. The factorization of the local problems was done with the direct solver package UMFPACK [31, 32]. With this value we observe in most cases a super linear speedup and hence an efficiency greater than 1. This is due to memory issues, mainly the so-called *cache effect*. The *global CG time* is the duration of all four CG solution steps together. We see that this value scales very good up to 256 cores, due to possible cache effects also in some cases super linear. The *total time* is the total computation time. It also scales admissibly well up to 256 processing units. From 256 to 512 cores the speedup is rather low. Possibilities to increase the efficiency with a higher amount of cores were already explained in Sect. 7.1.3.

As expected, the nonlinear elasticity case scales better than the linear case, compare Tab. 7.9. Note that using a larger amount of subdomains or a larger amount of local degrees of freedom improves the scaling properties of the problem. This is again due to memory issues and cache effects. Unfortunately, due to the memory restrictions on *VSC2*, larger problems are not taken into account; they are no longer solvable using $p = 16$ cores.

p	local time	efficiency	global CG time	efficiency	total time	efficiency
16	396.2035 s	-	726.3933 s	-	1532.8520 s	-
32	197.7438 s	1.0018	305.4898 s	1.1889	700.9290 s	1.0934
64	99.6202 s	0.9943	162.6970 s	1.1162	394.3193 s	0.9718
128	48.7876 s	1.0151	91.6482 s	0.9907	233.9563 s	0.8190
256	24.4350 s	1.0134	54.7808 s	0.8286	159.1056 s	0.6021
512	12.3342 s	1.0038	37.5423 s	0.6046	130.7105 s	0.3665

Table 7.16. – Computation times (in seconds) and efficiency for a nonlinear elasticity problem using a varying number of processing units p.

8. Conclusions and Outlook

We have shown the application of the finite element tearing and interconnecting method to elasticity problems, in particular to the simulation of the nonlinear elastic behavior of biological tissues, such as the myocardium and the artery. The models to simulate these materials were described in detail. Furthermore, we presented the requirements for the existence of a solution of the nonlinear equations and outlined convergence properties of the necessary Newton method. The main ideas of domain decomposition methods were summarized and the classical and the all-floating FETI approach were discussed in detail.

Illustrated by numerical examples we have shown certain advantages of the all-floating FETI method compared to the classical FETI approach. To the best of our knowledge the application of the all-floating approach to nonlinear orthotropic elasticity problems is not yet to be found in literature. For sure the mentioned advantages are influenced by the mesh structure and the choice of the boundary conditions and hence the method to choose depends on the specific problem.

We have presented and compared different techniques of preconditioning: the lumped preconditioner, the optimal Dirichlet preconditioner and a, in such applications, new BEM-preconditioner (to the best of our knowledge), which is based on the hypersingular integral operators. We have shown that the iteration numbers of the global iterative method behave like expected from the theory: due to the spectral equivalence of the local hypersingular operators to the local Steklov–Poincaré operators, the BEM preconditioner yields iteration numbers that lie in between the numbers obtained with the optimal Dirichlet preconditioner and the numbers obtained with the simple lumped preconditioner. Nonetheless, the numerical examples show that the implementation of the hypersingular operator still needs some work and improvements to achieve competitive or even better computational times compared to the sophisticated direct solver packages.

Furthermore, the numerical examples exposed some instabilities of the global iterative method for incompressible material parameters, i.e. for a very large bulk modulus κ. These problems were resolved in the past for linear elasticity problems but to the best of our knowledge are still an open task in nonlinear elasticity. Here we were able to present, like it was also shown in earlier contributions, that quadratic ansatz functions resolve the incompressible elastic behavior much better than linear ansatz functions.

Future work may include the coupling of the nonlinear elasticity problem with fluid dynamics to simulate the blood flow through cardiovascular vessels. Other interesting

topics are the coupling of the electric activity in the heart with the mechanical behavior of the myocardium or contact problems, which occur while simulating certain surgery techniques such as artery stenting. FETI methods for such coupled problems are very demanding and hence still in their infancy. But beyond doubt these topics deserve closer attention.

A. Appendix

A.1. Tensor Calculus

This section treats the calculus of vectors, matrices and tensors in general. Basic relations are omitted, for a general introduction to tensor calculus confer [30, Danielson (2003)]. A good compendium of formulas including derivations of tensors and many identities can be found in [115, Petersen and Pedersen (2008)]. Many formulas needed in the modeling of nonlinear elasticity are given in the first chapter of the book [59, Holzapfel (2000)].

A tensor of order n is defined by

$$\mathsf{A}_{i_1 i_2 \ldots i_n} \mathsf{e}_{i_1} \otimes \mathsf{e}_{i_2} \otimes \cdots \otimes \mathsf{e}_{i_n}, \tag{A.1}$$

with an orthonormal basis $\{\boldsymbol{e}_{i_j}\}, . = 1, \cdots, n$.

The **double contraction** of two second-order tensors A and B, characterized by two dots, yields a scalar and is defined as

$$\mathsf{A} : \mathsf{B} = \operatorname{tr}(\mathsf{A}^\top \mathsf{B}) = \operatorname{tr}(\mathsf{B}^\top \mathsf{A}) = \mathsf{B} : \mathsf{A} = A_{ij} B_{ij}. \tag{A.2}$$

The **tensor product** or **dyadic product** of two vectors $\boldsymbol{u}$ and $\boldsymbol{v}$, each having the same dimension, is denoted by $\mathsf{A} = \boldsymbol{u} \otimes \boldsymbol{v}$. It results in a tensor of order two and rank one. The components A_{ij} of the dyadic product may be defined as

$$A_{ij} = (\boldsymbol{u} \otimes \boldsymbol{v})_{ij} = u_i v_j. \tag{A.3}$$

The following identities are a direct consequence of the definition of the dyadic product and properties of the orthonormal basis vectors $\{\boldsymbol{e}_i\}$

$$\begin{aligned} (\boldsymbol{u} \otimes \boldsymbol{v})\boldsymbol{w} &= \boldsymbol{u}(\boldsymbol{v} \cdot \boldsymbol{w}) = (\boldsymbol{v} \cdot \boldsymbol{w})\boldsymbol{u}, \\ \mathsf{A} &= A_{ij} \boldsymbol{e}_i \otimes \boldsymbol{e}_j, \\ \mathsf{I} &= \boldsymbol{e}_j \otimes \boldsymbol{e}_j. \end{aligned}$$

The *dyadic product* of two second-order tensors results in a tensor of forth-order

$$\mathbb{D} = \mathsf{A} \otimes \mathsf{B}, \quad D_{ijkl} = A_{ij} B_{kl}. \tag{A.4}$$

The product of a forth-order tensor with a second order tensor is defined as

$$\mathsf{B} = \mathbb{D}\mathsf{A}, \quad B_{ij} = \sum_{k,l} D_{ijkl} A_{kl}. \tag{A.5}$$

Every second-order tensor A can be decomposed into its so-called **spherical** and its **deviatoric part** by

$$\mathsf{A} = \frac{1}{3}\operatorname{tr}(\mathsf{A})\mathsf{I} + \operatorname{dev}\mathsf{A},$$

with the deviatoric operator

$$\operatorname{dev}(\bullet) = (\bullet) - \frac{1}{3}\operatorname{tr}(\bullet)\mathsf{I}. \tag{A.6}$$

The deviatoric operator in the Lagrangian description reads

$$\operatorname{Dev}(\bullet) = (\bullet) - \frac{1}{3}\left[(\bullet) : \mathsf{C}\right]\mathsf{C}^{-1}, \tag{A.7}$$

with the right Cauchy-Green tensor $\mathsf{C} = \mathsf{F}^{\top}\mathsf{F}$.

Two important properties of the deviatoric operator are

$$\operatorname{tr}(\operatorname{dev}\mathsf{A}) = 0, \tag{A.8}$$

$$\operatorname{dev}\mathsf{A} = (\mathbb{I} - \frac{1}{3}\mathsf{I}\otimes\mathsf{I}) : \mathsf{A}, \tag{A.9}$$

where $\mathbb{I}$, the forth-order unit tensor is defined by

$$(\mathbb{I})_{ijkl} = \delta_{ik}\delta_{jl}. \tag{A.10}$$

The unique transpose of a forth-order tensor $\mathbb{A}$ is denoted by $\mathbb{A}^{\top}$ and defined by

$$\left(\mathbb{A}^{\top}\right)_{ijkl} = A_{klij}, \tag{A.11}$$

with A_{ijkl} the components of the forth-order tensor $\mathbb{A} = A_{ijkl}\boldsymbol{e}_i \otimes \boldsymbol{e}_j \otimes \boldsymbol{e}_k \otimes \boldsymbol{e}_l$.

Lemma A.1 (Important Identities). *Given the second-order tensors* $\mathsf{A}, \mathsf{B}, \mathsf{C}, \mathsf{D}$*, we can state*

$$(\mathsf{A}\otimes\mathsf{B}) : \mathsf{C} = \mathsf{A}(\mathsf{B} : \mathsf{C}) = (\mathsf{B} : \mathsf{C})\mathsf{A}\ , \tag{A.12}$$

$$\mathsf{A}(\mathsf{B}\otimes\mathsf{C})\mathsf{D} = (\mathsf{A}\mathsf{B})\otimes(\mathsf{C}\mathsf{D}), \tag{A.13}$$

$$(\mathsf{A}\otimes\mathsf{B})^{\top} = \mathsf{B}\otimes\mathsf{A}. \tag{A.14}$$

For the forth-order tensor $\mathbb{A}$ *and the forth-order unit tensor* $\mathbb{I}$ *it holds*

$$\mathbb{A} = \left(\mathbb{A}^{\top}\right)^{\top}, \tag{A.15}$$

$$\mathsf{A} = \mathbb{I} : \mathsf{A} = \mathsf{A} : \mathbb{I}, \tag{A.16}$$

$$\mathbb{A} : \mathsf{B} = \mathsf{B} : \mathbb{A}^{\top}, \tag{A.17}$$

$$\mathsf{B} : \mathbb{A}^{\top} : \mathsf{C} = \mathsf{C} : \mathbb{A} : \mathsf{B} = (\mathbb{A} : \mathsf{B}) : \mathsf{C}. \tag{A.18}$$

Proof. For the proof we need the following identities, cf. the first chapter of the book [59, Holzapfel (2000)],

$$\begin{aligned}(\boldsymbol{u}\otimes\boldsymbol{v}\otimes\boldsymbol{w}\otimes\boldsymbol{x}):(\boldsymbol{y}\otimes\boldsymbol{z}) &= (\boldsymbol{w}\cdot\boldsymbol{y})(\boldsymbol{x}\cdot\boldsymbol{z})(\boldsymbol{u}\otimes\boldsymbol{v})\\ (\boldsymbol{u}\otimes\boldsymbol{v}):(\boldsymbol{w}\otimes\boldsymbol{x}\otimes\boldsymbol{y}\otimes\boldsymbol{z}) &= (\boldsymbol{u}\cdot\boldsymbol{w})(\boldsymbol{v}\cdot\boldsymbol{x})(\boldsymbol{y}\otimes\boldsymbol{z})\\ (\boldsymbol{u}\otimes\boldsymbol{v})\otimes(\boldsymbol{w}\otimes\boldsymbol{x}) &= \boldsymbol{u}\otimes\boldsymbol{v}\otimes\boldsymbol{w}\otimes\boldsymbol{x}.\end{aligned}$$

With this we obtain

$$\begin{aligned}(\mathsf{A}\otimes\mathsf{B}):\mathsf{C} &= A_{ij}B_{kl}C_{mn}(\boldsymbol{e}_i\otimes\boldsymbol{e}_j)\otimes(\boldsymbol{e}_k\otimes\boldsymbol{e}_l):(\boldsymbol{e}_m\otimes\boldsymbol{e}_n)\\ &= A_{ij}B_{kl}C_{mn}(\boldsymbol{e}_k\cdot\boldsymbol{e}_m)(\boldsymbol{e}_l\cdot\boldsymbol{e}_n)(\boldsymbol{e}_i\otimes\boldsymbol{e}_j)\\ &= A_{ij}B_{kl}C_{kl}(\boldsymbol{e}_i\otimes\boldsymbol{e}_j).\end{aligned}$$

By using the representation $\mathsf{A} = A_{ij}\boldsymbol{e}_i\otimes\boldsymbol{e}_j$ and the definition of the double contraction (A.2) we get (A.12).

$$\begin{aligned}\mathsf{A}(\mathsf{B}\otimes\mathsf{C})\mathsf{D} &= A_{ij}B_{kl}C_{mn}D_{rs}(\boldsymbol{e}_i\otimes\boldsymbol{e}_j)\left((\boldsymbol{e}_k\otimes\boldsymbol{e}_l)\otimes(\boldsymbol{e}_m\otimes\boldsymbol{e}_n)\right)(\boldsymbol{e}_r\otimes\boldsymbol{e}_s)\\ &= A_{ij}B_{kl}C_{mn}D_{rs}\left((\boldsymbol{e}_i\otimes\boldsymbol{e}_j)(\boldsymbol{e}_k\otimes\boldsymbol{e}_l)\right)\otimes\left((\boldsymbol{e}_m\otimes\boldsymbol{e}_n)(\boldsymbol{e}_r\otimes\boldsymbol{e}_s)\right)\\ &= (\mathsf{AB})\otimes(\mathsf{CD}).\end{aligned}$$

This proves (A.13).

The definition of the transposed of a forth-order tensor (A.11) yields (A.14):

$$\begin{aligned}(\mathsf{A}\otimes\mathsf{B})^{\top} &= A_{ij}B_{kl}(\boldsymbol{e}_i\otimes\boldsymbol{e}_j\otimes\boldsymbol{e}_k\otimes\boldsymbol{e}_l)^{\top}\\ &= B_{kl}A_{ij}(\boldsymbol{e}_k\otimes\boldsymbol{e}_l\otimes\boldsymbol{e}_i\otimes\boldsymbol{e}_j)\\ &= \mathsf{B}\otimes\mathsf{A}.\end{aligned}$$

(A.15) follows immediately from the definition of the transposed of a forth-order tensor (A.11).

For (A.16) we calculate

$$\begin{aligned}\mathbb{I}:\mathsf{A} &= I_{ijkl}A_{mn}(\boldsymbol{e}_i\otimes\boldsymbol{e}_j\otimes\boldsymbol{e}_k\otimes\boldsymbol{e}_l):(\boldsymbol{e}_m\otimes\boldsymbol{e}_n)\\ &= \delta_{ik}\delta_{jl}A_{mn}(\boldsymbol{e}_k\cdot\boldsymbol{e}_m)(\boldsymbol{e}_l\cdot\boldsymbol{e}_n)(\boldsymbol{e}_i\otimes\boldsymbol{e}_j)\\ &= \delta_{ik}\delta_{jl}A_{mn}\delta_{km}\delta_{ln}(\boldsymbol{e}_i\otimes\boldsymbol{e}_j)\\ &= A_{ij}(\boldsymbol{e}_i\otimes\boldsymbol{e}_j) = \mathsf{A}\end{aligned}$$

and

$$\begin{aligned}\mathsf{A}:\mathbb{I} &= A_{ij}I_{klmn}(\boldsymbol{e}_i\otimes\boldsymbol{e}_j):(\boldsymbol{e}_k\otimes\boldsymbol{e}_l\otimes\boldsymbol{e}_m\otimes\boldsymbol{e}_n)\\ &= A_{ij}\delta_{km}\delta_{ln}(\boldsymbol{e}_i\cdot\boldsymbol{e}_k)(\boldsymbol{e}_j\cdot\boldsymbol{e}_l)(\boldsymbol{e}_m\otimes\boldsymbol{e}_n)\\ &= A_{ij}\delta_{ik}\delta_{jl}(\boldsymbol{e}_k\otimes\boldsymbol{e}_l)\\ &= A_{ij}(\boldsymbol{e}_i\otimes\boldsymbol{e}_j) = \mathsf{A}.\end{aligned}$$

With the definition of the transposed of a forth-order tensor we obtain

$$\begin{aligned}(\mathbb{A} : \mathsf{B}) &= A_{ijkl}B_{mn}(\boldsymbol{e}_i \otimes \boldsymbol{e}_j \otimes \boldsymbol{e}_k \otimes \boldsymbol{e}_l) : (\boldsymbol{e}_m \otimes \boldsymbol{e}_n) \\ &= A_{ijkl}B_{mn}\delta_{km}\delta_{ln}(\boldsymbol{e}_i \otimes \boldsymbol{e}_j) \\ &= A_{ijkl}B_{kl}(\boldsymbol{e}_i \otimes \boldsymbol{e}_j) \\ &= B_{mn}A_{ijkl}\delta_{mk}\delta nl(\boldsymbol{e}_i \otimes \boldsymbol{e}_j) \\ &= B_{mn}A_{ijkl}(\boldsymbol{e}_m \otimes \boldsymbol{e}_n) : (\boldsymbol{e}_k \otimes \boldsymbol{e}_l \otimes \boldsymbol{e}_i \otimes \boldsymbol{e}_j) \\ &= B_{mn}A_{ijkl}(\boldsymbol{e}_m \otimes \boldsymbol{e}_n) : (\boldsymbol{e}_i \otimes \boldsymbol{e}_j \otimes \boldsymbol{e}_k \otimes \boldsymbol{e}_l)^\top \\ &= B : \mathbb{A}^\top\end{aligned}$$

which proves (A.17). Finally with

$$\begin{aligned}(\mathbb{A} : \mathsf{B}) : \mathsf{C} &= A_{ijkl}B_{mn}C_{rs}((\boldsymbol{e}_i \otimes \boldsymbol{e}_j \otimes \boldsymbol{e}_k \otimes \boldsymbol{e}_l) : (\boldsymbol{e}_m \otimes \boldsymbol{e}_n)) : (\boldsymbol{e}_r \otimes \boldsymbol{e}_s) \\ &= A_{ijkl}B_{mn}C_{rs}\delta_{km}\delta_{ln}(\boldsymbol{e}_i \otimes \boldsymbol{e}_j) : (\boldsymbol{e}_r \otimes \boldsymbol{e}_s) \\ &= A_{ijkl}B_{kl}C_{rs}\delta_{ir}\delta_{js} \\ &= A_{ijkl}B_{kl}C_{ij}\end{aligned}$$

and

$$\begin{aligned}\mathsf{B} : \mathbb{A}^\top : \mathsf{C} &= B_{ij}A_{klmn}C_{rs}((\boldsymbol{e}_i \otimes \boldsymbol{e}_j) : (\boldsymbol{e}_k \otimes \boldsymbol{e}_l \otimes \boldsymbol{e}_m \otimes \boldsymbol{e}_n)^\top) : (\boldsymbol{e}_r \otimes \boldsymbol{e}_s) \\ &= B_{ij}A_{klmn}C_{rs}((\boldsymbol{e}_i \otimes \boldsymbol{e}_j) : (\boldsymbol{e}_m \otimes \boldsymbol{e}_n \otimes \boldsymbol{e}_k \otimes \boldsymbol{e}_l)) : (\boldsymbol{e}_r \otimes \boldsymbol{e}_s) \\ &= B_{mn}A_{klmn}C_{rs}\delta_{im}\delta_{jn}(\boldsymbol{e}_k \otimes \boldsymbol{e}_l) : (\boldsymbol{e}_r \otimes \boldsymbol{e}_s) \\ &= A_{klmn}B_{mn}C_{rs}\delta_{kr}\delta_{ls} \\ &= A_{klmn}B_{mn}C_{kl}\end{aligned}$$

and

$$\begin{aligned}\mathsf{C} : \mathbb{A} : \mathsf{B} &= C_{ij}A_{klmn}B_{rs}((\boldsymbol{e}_i \otimes \boldsymbol{e}_j) : (\boldsymbol{e}_k \otimes \boldsymbol{e}_l \otimes \boldsymbol{e}_m \otimes \boldsymbol{e}_n)) : (\boldsymbol{e}_r \otimes \boldsymbol{e}_s) \\ &= C_{ij}A_{klmn}B_{rs}\delta_{ik}\delta_{jl}(\boldsymbol{e}_m \otimes \boldsymbol{e}_n) : (\boldsymbol{e}_r \otimes \boldsymbol{e}_s) \\ &= C_{ij}A_{ijmn}B_{rs}\delta_{mr}\delta_{ns} \\ &= A_{ijmn}B_{mn}C_{ij}\end{aligned}$$

we get with a renumbering the desired result (A.18) and hence the proof of the whole lemma. □

Lemma A.2.

$$(\mathsf{A}^\top\mathsf{B}) : (\boldsymbol{a} \otimes \boldsymbol{b}) = \boldsymbol{a} \cdot (\mathsf{A}^\top\mathsf{B}\boldsymbol{b}) = (\mathsf{A}\boldsymbol{a}) \cdot (\mathsf{B}\boldsymbol{b})$$

Proof.

$$\begin{aligned}\mathsf{A}^\top\mathsf{B} : (\boldsymbol{a} \otimes \boldsymbol{b}) &= A_{ki}B_{kj}a_ib_j = a_iA_{ki}B_{kj}b_j = a_i(\mathsf{A}^\top\mathsf{B}\boldsymbol{b})_i = \boldsymbol{a} \cdot (\mathsf{A}^\top\mathsf{B}\boldsymbol{b}) \\ \mathsf{A}^\top\mathsf{B} : (\boldsymbol{a} \otimes \boldsymbol{b}) &= A_{ki}B_{kj}a_ib_j = A_{ki}a_iB_{kj}b_j = (\mathsf{A}\boldsymbol{a})_k(\mathsf{B}\boldsymbol{b})_k = (\mathsf{A}\boldsymbol{a}) \cdot (\mathsf{B}\boldsymbol{b})\end{aligned}$$

□

A.1.1. Derivatives

The derivative of a function $\mathsf{F} : \mathbb{R} \to \mathbb{R}^{n\times m}$ with respect to a scalar t is defined as

$$\frac{\partial F}{\partial t} = \begin{bmatrix} \frac{\partial F_{11}}{\partial t} & \cdots & \frac{\partial F_{1m}}{\partial t} \\ \vdots & \ddots & \vdots \\ \frac{\partial F_{n1}}{\partial t} & \cdots & \frac{\partial F_{nm}}{\partial t} \end{bmatrix}, \quad \left(\frac{\partial F}{\partial t}\right)_{ij} = \frac{\partial F_{ij}}{\partial t}. \tag{A.19}$$

The derivative of the scalar function $f : \mathbb{R}^{n\times m} \to \mathbb{R}$ with respect to a tensor $\mathsf{X} \in \mathbb{R}^{n\times m}$ is defined by convention as

$$\frac{\partial f}{\partial \mathsf{X}} = \begin{bmatrix} \frac{\partial f}{\partial X_{11}} & \cdots & \frac{\partial f}{\partial X_{1m}} \\ \vdots & \ddots & \vdots \\ \frac{\partial f}{\partial X_{n1}} & \cdots & \frac{\partial f}{\partial X_{nm}} \end{bmatrix}, \quad \left(\frac{\partial f}{\partial \mathsf{X}}\right)_{ij} = \frac{\partial f}{\partial X_{ij}}. \tag{A.20}$$

The derivative of a second-order tensor valued function $\mathsf{F} : \mathbb{R}^{n\times m} \to \mathbb{R}^{p\times q}$ with respect to a second-order tensor is a tensor of forth order, i.e. a $n \times m$ matrix whose entries are $k \times l$ matrices. In accordance with (A.19) and (A.20) it is defined by

$$\frac{\partial \mathsf{F}}{\partial \mathsf{X}} = \begin{bmatrix} \frac{\partial \mathsf{F}}{\partial X_{11}} & \cdots & \frac{\partial \mathsf{F}}{\partial X_{1m}} \\ \vdots & \ddots & \vdots \\ \frac{\partial \mathsf{F}}{\partial X_{n1}} & \cdots & \frac{\partial \mathsf{F}}{\partial X_{nm}} \end{bmatrix}, \quad \left(\frac{\partial \mathsf{F}}{\partial \mathsf{X}}\right)_{ijkl} = \frac{\partial F_{kl}}{\partial X_{ij}}. \tag{A.21}$$

Using (A.20) and (A.21) we get for the second order derivative

$$\left[\frac{\partial^2 f}{\partial \mathsf{X}^2}\right]_{ijkl} = \frac{\partial^2 f}{\partial X_{ij} \partial X_{kl}}. \tag{A.22}$$

In the following corollaries we treat some special derivations.

Corollary A.1. *Let A be a second-order tensor. Then*

$$\frac{\partial \mathsf{A}}{\partial \mathsf{A}} = \mathbb{I}. \tag{A.23}$$

Proof. Following (A.21) we obtain

$$\left(\frac{\partial \mathsf{A}}{\partial \mathsf{A}}\right)_{ijkl} = \frac{\partial A_{kl}}{\partial A_{ij}} = \delta_{ik}\delta_{jl}.$$

The latter is the definition of $\mathbb{I}$, cf. (A.10). □

Corollary A.2. *Let A be an invertible $n \times n$ matrix. Then the derivation of the determinant of A with respect to A is*

$$\frac{\partial \det \mathsf{A}}{\partial \mathsf{A}} = \det(\mathsf{A})\mathsf{A}^{-\top}.$$

Proof. Using Laplace's formula for the determinant of an $n \times n$ matrix and Jacobi's formula of matrix calculus we can write

$$\frac{\mathrm{d}\det(\mathsf{A})}{\mathrm{d}x} = \det(\mathsf{A})\,\mathrm{tr}\left(\mathsf{A}^{-1}\frac{\mathrm{d}\mathsf{A}}{\mathrm{d}x}\right).$$

From this it follows with (A.20), (A.19) and properties of the trace that

$$\begin{aligned}\left(\frac{\partial\det(\mathsf{A})}{\partial\mathsf{A}}\right)_{ij} &= \frac{\partial\det(\mathsf{A})}{\partial\mathsf{A}_{ji}} = \det(\mathsf{A})\,\mathrm{tr}\left(\mathsf{A}^{-1}\frac{\partial\mathsf{A}}{\partial A_{ji}}\right)\\ &= \det(\mathsf{A})\frac{\partial A_{ij}}{\partial A_{ji}}\left(\mathsf{A}^{-1}\right)_{ji} = \det(\mathsf{A})\mathsf{A}^{-\top}.\end{aligned}$$

□

Corollary A.3. *Let A be an invertible $n \times n$ matrix. Then the derivation of the inverse of A with respect to A is*

$$\left[\frac{\partial\mathsf{A}^{-1}}{\partial\mathsf{A}}\right]_{ijkl} = -\frac{1}{2}(A^{-1}_{ik}A^{-1}_{lj} + A^{-1}_{il}A^{-1}_{kj}).$$

For symmetric tensors A *we get with definition* (3.132)

$$\frac{\partial\mathsf{A}^{-1}}{\partial\mathsf{A}} = -\mathsf{A}^{-1}\odot\mathsf{A}^{-1}.$$

Proof. cf. [59, Holzapfel (2000), Ch. 1.7]. □

Corollary A.4 (Chain rules in tensor calculus)**.** *For the second-order tensors* $\mathsf{A},\mathsf{B},\mathsf{C}$ *and the scalar valued function f the following chain rules hold*

$$\frac{\partial f}{\partial\mathsf{A}} = \frac{\partial f}{\partial\mathsf{B}} : \frac{\partial\mathsf{B}}{\partial\mathsf{A}}, \tag{A.24}$$

$$\frac{\partial\phi\mathsf{A}}{\partial\mathsf{C}} = \mathsf{A}\otimes\frac{\partial\phi}{\partial\mathsf{C}} + \phi\frac{\partial\mathsf{A}}{\partial\mathsf{C}}, \tag{A.25}$$

$$\frac{\partial(\mathsf{A}:\mathsf{B})}{\partial\mathsf{C}} = \mathsf{A} : \frac{\partial\mathsf{B}}{\partial\mathsf{C}} = \mathsf{B} : \frac{\partial\mathsf{A}}{\partial\mathsf{C}}. \tag{A.26}$$

Proof. see [59, Holzapfel (2000), Ch. 1.7]. □

Corollary A.5 (Derivation of Traces)**.** *For the second-order tensors* $\mathsf{A},\mathsf{B},\mathsf{C}$ *we obtain*

$$\frac{\partial\mathrm{tr}(\mathsf{A})}{\partial\mathsf{A}} = \mathsf{I}, \quad \frac{\partial\mathrm{tr}(\mathsf{A}^2)}{\partial\mathsf{A}} = 2\mathsf{A}^{\top}. \tag{A.27}$$

Proof. First part follows immediately form (A.26), cf. Holzapfel 1.252 for the second. □

A.1.2. Special Derivatives in Mechanics

In the following let F be the deformation gradient, $J = \det(\mathsf{F})$ the Jacobian, $\mathsf{C} = \mathsf{F}^\top\mathsf{F}$ the right Cauchy-Green tensor.

Corollary A.6.

$$\frac{\partial J}{\partial \mathsf{C}} = \frac{J}{2}\mathsf{C}^{-1} \quad , \quad \frac{\partial J^{-2/3}}{\partial \mathsf{C}} = -\frac{1}{3}J^{-2/3}\mathsf{C}^{-1}. \tag{A.28}$$

Proof. With $\det(\mathsf{C}) = \det(\mathsf{F}^\top)\det(\mathsf{F}) = J^2$, Cor. A.2 and the symmetry of C we obtain

$$\frac{\partial J^2}{\partial \mathsf{C}} = \frac{\partial \det \mathsf{C}}{\mathsf{C}} = \det(\mathsf{C})\mathsf{C}^{-\top} = J^2\mathsf{C}^{-1}.$$

Using the chain rule we get

$$\frac{\partial J^2}{\partial \mathsf{C}} = 2J\frac{\partial J}{\partial \mathsf{C}}.$$

Hence we may conclude

$$2J\frac{\partial J}{\partial \mathsf{C}} = J^2\mathsf{C}^{-1}.$$

With this result we obtain

$$\frac{\partial J^{-2/3}}{\partial \mathsf{C}} = -\frac{2}{3}J^{-5/3}\frac{\partial J}{\partial \mathsf{C}} = -\frac{1}{3}J^{-2/3}\mathsf{C}^{-1},$$

which concludes the proof. □

In accordance with (3.53) let $\overline{\mathsf{F}} = J^{-1/3}\mathsf{F}$ and $\overline{\mathsf{C}} = J^{-2/3}\mathsf{C}$.

Corollary A.7. *With the projection tensor introduced in* (3.131) *it holds that*

$$\frac{\partial \overline{\mathsf{C}}}{\partial \mathsf{C}} = J^{-2/3}\mathbb{P}^\top. \tag{A.29}$$

Proof. With (A.25) and $(\text{A.28})_2$ we get

$$\frac{\partial \overline{\mathsf{C}}}{\partial \mathsf{C}} = \frac{\partial J^{-2/3}\mathsf{C}}{\partial \mathsf{C}} = J^{-2/3}\frac{\partial \mathsf{C}}{\partial \mathsf{C}} + \mathsf{C} \otimes \frac{\partial J^{-2/3}}{\partial \mathsf{C}} = J^{-2/3}\mathbb{I} - \mathsf{C} \otimes \frac{1}{3}J^{-2/3}\mathsf{C}^{-1}.$$

□

Corollary A.8. *The transpose of the projection tensor is*

$$\mathbb{P} = \mathbb{I} - \frac{1}{3}\mathsf{C}^{-1} \otimes \mathsf{C}. \tag{A.30}$$

Proof. With the equations (A.14) and (A.15) we obtain

$$\mathbb{P} = \left(\mathbb{P}^{\top}\right)^{\top} = \left(\mathbb{I} - \frac{1}{3}\mathsf{C} \otimes \mathsf{C}^{-1}\right)^{\top} = \mathbb{I} - \frac{1}{3}(\mathsf{C} \otimes \mathsf{C}^{-1})^{\top} = \mathbb{I} - \frac{1}{3}\mathsf{C}^{-1} \otimes \mathsf{C}.$$

□

Corollary A.9 (Derivation of Invariants)**.** *Let A be a second-order tensor. Then for the invariants defined in 3.4 it holds*

$$\frac{\partial I_1}{\partial \mathsf{A}} = \mathsf{I}, \quad \frac{\partial I_2}{\partial \mathsf{A}} = I_1\mathsf{I} - \mathsf{A}^{\top}, \quad \frac{\partial I_3}{\partial \mathsf{A}} = I_3\mathsf{A}^{-\top}. \tag{A.31}$$

Proof. The derivative of the first invariant gives with A.26

$$\frac{\partial I_1}{\partial \mathsf{A}} = \frac{\partial \operatorname{tr}\mathsf{A}}{\partial \mathsf{A}} = \frac{\partial(\mathsf{I} : \mathsf{A})}{\partial \mathsf{A}} = \mathsf{I}.$$

By means of (A.27) we get for the derivative of the second invariant

$$\frac{\partial I_2}{\partial \mathsf{A}} = \frac{1}{2}\frac{\partial(\operatorname{tr}(\mathsf{A})^2 - \operatorname{tr}(\mathsf{A}^2)}{\partial \mathsf{A}} = \frac{1}{2}\left(2\operatorname{tr}\mathsf{A}\frac{\partial \operatorname{tr}(\mathsf{A})}{\partial \mathsf{A}} - (2\mathsf{A}^{\top})\right).I_1\mathsf{I} - \mathsf{A}^{\top}.$$

The third part follows immediately from Cor. A.2. □

A.2. Numerical Derivatives

Especially the computation of the isochoric part of the elasticity tensor may be very time consuming, since it involves a lot of matrix manipulations, cf. Cor. 3.6. This tensor is needed for the material part of the stress contribution, see (4.36) and (4.37). To improve the computational performance we can think about other possibilities to compute the elasticity tensor and one of them is the idea of numerical derivatives. In the following we will outline the basic concepts of this topic. For more information and error estimates confer [116, Press et al. (2007)] and [34, Dennis and Schnabel (1983)].

Starting point is the symmetrized form of the differential quotient

$$f'(x) \approx \frac{f(x+h) - f(x-h)}{2h}.$$

Since this is no exact computation two sources of errors have to be taken into consideration. First we notice a *truncation error* e_t which results from higher terms in the Taylor series expansion of the function $f(x \pm h)$. We can state that $e_t \sim h^2 f'''$. The other error is the so-called *roundoff error* e_r. It may be estimated by $e_r \sim \epsilon_f |f(x)/h|$, where ϵ_f is the accuracy with which f is computed. Hence the choice of h is very

important. As an optimal choice for h, in order to minimize the total error $e_r + e_t$, we have

$$h \sim \left(\frac{\epsilon_f f}{f'''}\right)^{1/3} \sim \epsilon_f^{1/3} x_c.$$

Here we denote by $x_c = (f/f'')^{1/2}$ a measure of the curvature of the function f.

One can easily compute other derivations, e.g. the mixed derivative formula for a function of two dimensions,

$$\frac{\partial^2 f}{\partial x \partial y} \approx \frac{[f(x+h, y+h) - f(x+h, y-h)] - [f(x-h, y+h) - f(x-h, y-h)]}{4h^2}. \tag{A.32}$$

The optimal scaling in this case is

$$h \sim {\epsilon_f}^{1/4} x_c.$$

This leads us now to the case of the scalar-valued energy function Ψ and its derivative with respect to a tensor. Following (A.20) we can state

$$\left[\frac{\partial \Psi(\mathsf{C})}{\partial \mathsf{C}}\right]_{ij} = \frac{\partial \Psi(\mathsf{C})}{\partial C_{ji}} = \frac{\partial \Psi(\mathsf{C})}{\partial C_{ij}}.$$

Hence we get for the numerical derivation

$$\left[\frac{\partial \Psi(\mathsf{C})}{\partial \mathsf{C}}\right]_{ij} \approx \frac{\Psi(\mathsf{C}^{ij}_{+h}) - \Psi(\mathsf{C}^{ij}_{-h})}{2h}, \tag{A.33}$$

where the second order tensor C^{ij}_a is defined as

$$\left[\mathsf{C}^{ij}_a\right]_{kl} = \begin{cases} \mathsf{C}_{kl} & \text{for } kl \neq ij \\ \mathsf{C}_{kl} + a & \text{for } kl = ij \end{cases}.$$

With (A.33) we may calculate, using formulas (3.45) and (3.46), an approximate of the stress tensors in the reference and current configuration, respectively.

The second derivative of the energy function with respect to the tensor C yields a forth-order tensor. Using (A.22) we get for the entries of this value

$$\left[\frac{\partial^2 \Psi(\mathsf{C})}{\partial \mathsf{C}^2}\right]_{ijkl} = \frac{\partial^2 \Psi(\mathsf{C})}{\partial C_{ij} \partial C_{kl}}.$$

The numerical derivation is obtained in an analogous way as (A.32) and yields for the entries of the forth-order tensor

$$\left[\frac{\partial^2 \Psi(\mathsf{C})}{\partial \mathsf{C}^2}\right]_{ijkl} = \frac{(\Psi({}^{kl}_{+h}\mathsf{C}^{ij}_{+h}) - \Psi({}^{kl}_{+h}\mathsf{C}^{ij}_{-h})) - (\Psi({}^{kl}_{-h}\mathsf{C}^{ij}_{+h}) - \Psi({}^{kl}_{-h}\mathsf{C}^{ij}_{-h}))}{4h^2}. \tag{A.34}$$

Bibliography

[1] P.R. Amestoy, I.S. Duff, J. Koster, and J.-Y. L'Excellent. A fully asynchronous multifrontal solver using distributed dynamic scheduling. *SIAM Journal on Matrix Analysis and Applications*, 23(1):15–41, 2001.

[2] P.R. Amestoy, A. Guermouche, J.-Y. L'Excellent, and S. Pralet. Hybrid scheduling for the parallel solution of linear systems. *Parallel Computing*, 32(2):136–156, 2006.

[3] S.S. Antman. The eversion of thick spherical shells. *Arch. Rational Mech. Anal.*, 70(2):113–123, 1979.

[4] D.N. Arnold. Discretization by finite elements of a model parameter dependent problem. *Numer. Math.*, 37(3):405–421, 1981.

[5] S.F. Ashby, T.A. Manteuffel, and P.E. Saylor. A taxonomy for conjugate gradient methods. *SIAM J. Numer. Anal.*, 27(6):1542–1568, 1990.

[6] O. Axelsson. *Iterative solution methods*. Cambridge University Press, Cambridge, 1994.

[7] I. Babuška. The finite element method with Lagrangian multipliers. *Numer. Math.*, 20:179–192, 1972/73.

[8] I. Babuška and M. Suri. Locking effects in the finite element approximation of elasticity problems. *Numer. Math.*, 62(4):439–463, 1992.

[9] J.M. Ball. Convexity conditions and existence theorems in nonlinear elasticity. *Arch. Rational Mech. Anal.*, 63(4):337–403, 1976/77.

[10] J.M. Ball. Constitutive inequalities and existence theorems in nonlinear elastostatics. In *Nonlinear analysis and mechanics: Heriot-Watt Symposium (Edinburgh, 1976), Vol. I*, pages 187–241. Res. Notes in Math., No. 17. Pitman, London, 1977.

[11] D. Balzani, P. Neff, J. Schröder, and G.A. Holzapfel. A polyconvex framework for soft biological tissues. adjustment to experimental data. *Int. J. of Solids and Structures*, 43:6052–6070, 2006.

[12] H. Benhassine and A. Bendali. A non-overlapping domain decomposition method for continuous-pressure mixed finite element approximations of the Stokes problem. *ESAIM Math. Model. Numer. Anal.*, 45(4):675–696, 2011.

[13] C. Bernardi, Y. Maday, and A.T. Patera. A new nonconforming approach to domain decomposition: the mortar element method. In *Nonlinear partial differential equations and their applications. Collège de France Seminar, Vol. XI (Paris, 1989–1991)*, volume 299 of *Pitman Res. Notes Math. Ser.*, pages 13–51. Longman Sci. Tech., Harlow, 1994.

[14] D. Braess. *Finite Elemente - Theorie, schnelle Löser und Anwendungen in der Elastizitätstheorie*. Springer, Berlin-Heidelberg, forth edition, 2007.

[15] J.H. Bramble, J.E. Pasciak, and J. Xu. Parallel multilevel preconditioners. In *Numerical analysis 1989 (Dundee, 1989)*, volume 228 of *Pitman Res. Notes Math. Ser.*, pages 23–39. Longman Sci. Tech., Harlow, 1990.

[16] D. Brands, A. Klawonn, O. Rheinbach, and J. Schröder. Modeling and convergence in arterial wall simulations using a parallel feti solution strategy. *Computer Methods in Biomechanics and Biomedical Engineering*, 11(5):569–583, 2008.

[17] S.C. Brenner and L.R. Scott. *The mathematical theory of finite element methods*, volume 15 of *Texts in Applied Mathematics*. Springer-Verlag, New York, 1994.

[18] F. Brezzi. On the existence, uniqueness and approximation of saddle-point problems arising from Lagrangian multipliers. *Rev. Française Automat. Informat. Recherche Opérationnelle Sér. Rouge*, 8(R-2):129–151, 1974.

[19] F. Brezzi and M. Fortin. *Mixed and hybrid finite element methods*, volume 15 of *Springer Series in Computational Mathematics*. Springer-Verlag, New York, 1991.

[20] R. Bustamante and G.A. Holzapfel. Methods to compute 3D residual stress distributions in hyperelastic tubes with application to arterial walls. *Internat. J. Engrg. Sci.*, 48(11):1066–1082, 2010.

[21] C. Calgaro and J. Laminie. On the domain decomposition method for the generalized Stokes problem with continuous pressure. *Numer. Methods Partial Differential Equations*, 16(1):84–106, 2000.

[22] P. Charrier, B. Dacorogna, B. Hanouzet, and P. Laborde. An existence theorem for slightly compressible materials in nonlinear elasticity. *SIAM J. Math. Anal.*, 19(1):70–85, 1988.

[23] C.J. Chuong and Y.C. Fung. Three-dimensional stress distribution in arteries. *J. Biomech. Engr.*, 105:268–274, 1983.

[24] P.G. Ciarlet. *The finite element method for elliptic problems*. North-Holland Publishing Co., Amsterdam, 1978. Studies in Mathematics and its Applications, Vol. 4.

[25] P.G. Ciarlet. *Mathematical elasticity. Vol. I*, volume 20 of *Studies in Mathematics and its Applications*. North-Holland Publishing Co., Amsterdam, 1988. Three-dimensional elasticity.

[26] K.D. Costa, J.W. Holmes, and A.D. McCulloch. Modeling cardiac mechanical properties in three dimensions. *Phil. Trans. R. Soc. Lond. A*, 359:1233–1250, 2001.

[27] M. Crouzeix and P.-A. Raviart. Conforming and nonconforming finite element methods for solving the stationary Stokes equations. I. *Rev. Française Automat. Informat. Recherche Opérationnelle Sér. Rouge*, 7(R-3):33–75, 1973.

[28] B. Dacorogna. *Direct methods in the calculus of variations*, volume 78 of *Applied Mathematical Sciences*. Springer-Verlag, Berlin, 1989.

[29] B. Dacorogna. *Direct methods in the calculus of variations*, volume 78 of *Applied Mathematical Sciences*. Springer, New York, second edition, 2008.

[30] D. A. Danielson. *Vectors and tensors in engineering and physics*. Westview Press, Boulder, CO, second edition, 2003.

[31] T.A. Davis. Algorithm 832: UMFPACK V4.3—an unsymmetric-pattern multifrontal method. *ACM Trans. Math. Software*, 30(2):196–199, 2004.

[32] T.A. Davis. A column pre-ordering strategy for the unsymmetric-pattern multifrontal method. *ACM Trans. Math. Software*, 30(2):167–195, 2004.

[33] H. Demiray. A note on the elasticity of soft biological tissues. *J. Biomech.*, 5:309–311, 1972.

[34] J.E. Dennis, Jr. and R.B. Schnabel. *Numerical methods for unconstrained optimization and nonlinear equations*. Prentice Hall Series in Computational Mathematics. Prentice Hall Inc., Englewood Cliffs, NJ, 1983.

[35] P. Deuflhard. *Newton methods for nonlinear problems*, volume 35 of *Springer Series in Computational Mathematics*. Springer-Verlag, Berlin, 2004. Affine invariance and adaptive algorithms.

[36] S. Dokos, B.H. Smaill, A.A. Young, and I.J. LeGrice. Shear properties of passive ventricular myocardium. *Am. J. Physiol. Heart Circ. Physiol.*, 283:H2650–H2659, 2002.

[37] Z. Dostál, D. Horák, and R. Kučera. Total feti - an easier implementable variant of the feti method for numerical solution of elliptic pde. *Comm. Numer. Methods Engrg.*, 22:1155–1162, 2006.

[38] T.S.E. Eriksson, Prassl A.J., Plank G., and Holzapfel G.A. Modelling the electromechanically coupled orthotropic structure of myocardium. *submitted to Elsevier*, 2012.

[39] C. Farhat, M. Lesoinne, P. LeTallec, K. Pierson, and D. Rixen. FETI-DP: a dual-primal unified FETI method. I. A faster alternative to the two-level FETI method. *Internat. J. Numer. Methods Engrg.*, 50(7):1523–1544, 2001.

[40] C. Farhat, J. Mandel, and F. X. Roux. Optimal convergence properties of the feti domain decomposition method. *Comput. Methods Appl. Mech. Engrg.*, 115:365–385, 1994.

[41] C. Farhat and F. X. Roux. A method of finite element tearing and interconnecting and its parallel solution algorithm. *Internat. J. Numer. Methods Engrg.*, 32:1205–1227, 1991.

[42] C. Farhat and F. X. Roux. Implicit parallel processing in structural mechanics. *Comput. Mech. Adv.*, 2(1):124, 1994.

[43] P.J. Flory. Thermodynamic relations for high elastic materials. *Trans. Faraday Soc.*, 57:829–838, 1961.

[44] Y.C. Fung. Elasticity of soft tissues in simple elongation. *American Journal of Physiology*, 213:1532–1544, 1967.

[45] Y.C. Fung. Stress-strain-history relations of soft tissues in simple elongation. In Y.C. Fung, N. Perrone, and M. Anliker, editors, *Biomechanics: Its Foundations and Objectives*, chapter 7, pages 181–208. New Jersey: Prentice-Hall, Inc., Englewood Cliffs., 1971.

[46] B.G. Galerkin. Series solution of some problems of elastic equilibrium of rods and plates. *Vest. Inzh. Tech.*, 19:897–908, 1915.

[47] T.C. Gasser, R.W. Ogden, and G.A. Holzapfel. Hyperelastic modelling of arterial layers with distibuted collagen fibre orientations. *J. R. Soc. Interface*, 3:15–35, 2006.

[48] V. Girault and P.-A. Raviart. *Finite element methods for Navier-Stokes equations*, volume 5 of *Springer Series in Computational Mathematics*. Springer-Verlag, Berlin, 1986. Theory and algorithms.

[49] R. Glowinski and M. F. Wheeler. Domain decomposition and mixed finite element methods for elliptic problems. In *First International Symposium on Domain Decomposition Methods for Partial Differential Equations (Paris, 1987)*, pages 144–172. SIAM, Philadelphia, PA, 1988.

[50] A. Greenbaum. *Iterative methods for solving linear systems*, volume 17 of *Frontiers in Applied Mathematics*. Society for Industrial and Applied Mathematics (SIAM), Philadelphia, PA, 1997.

[51] M.E. Gurtin. The linear theory of elasticity. In S. Flügge and C. Truesdell, editors, *Handbuch der Physik*, volume VIa/2, pages 1–295. Springer, Berlin, 1972.

[52] M.E. Gurtin. *An introduction to continuum mechanics*, volume 158 of *Mathematics in Science and Engineering*. Academic Press Inc. [Harcourt Brace Jovanovich Publishers], New York, 1981.

[53] G. Haase. *Parallelisierung numerischer Algorithmen für partielle Differentialgleichungen*. B. G. Teubner, Stuttgart, 1999.

[54] W. Hackbusch. *Multigrid methods and applications*, volume 4 of *Springer Series in Computational Mathematics*. Springer-Verlag, Berlin, 1985.

[55] W. Hackbusch. *Iterative Lösung großer schwachbesetzter Gleichungssysteme*, volume 69 of *Leitfäden der Angewandten Mathematik und Mechanik [Guides to Applied Mathematics and Mechanics]*. B. G. Teubner, Stuttgart, 1991. Teubner Studienbücher Mathematik. [Teubner Mathematical Textbooks].

[56] H. Heuser. *Lehrbuch der Analysis. Teil 2*. Vieweg+Teubner, Wiesbaden, 14 edition, 2008.

[57] I. Hlaváček and J. Nečas. On inequalities of Korn's type. I. Boundary-value problems for elliptic system of partial differential equations. *Arch. Rational Mech. Anal.*, 36:305–311, 1970.

[58] I. Hlaváček and J. Nečas. On inequalities of Korn's type. II. Applications to linear elasticity. *Arch. Rational Mech. Anal.*, 36:312–334, 1970.

[59] G.A. Holzapfel. *Nonlinear Solid Mechanics. A Continuum Approach for Engineering*. John Wiley & Sons Ltd, Chichester, 2000.

[60] G.A. Holzapfel. Structural and Numerical Models for the (Visco)elastic Response of Arterial Walls with Residual Stresses. In G.A. Holzapfel and R.W. Ogden, editors, *Biomechanics of Soft Tissue in Cardiovascular Systems*. Springer, Wien, New York, 2003.

[61] G.A. Holzapfel. Determination of material models for arterial walls from uniaxial extension tests and histological structure. *J. Theoret. Biol.*, 238(2):290–302, 2006.

[62] G.A. Holzapfel. Collagen in arterial walls: Biomechanical aspects. In P. Fratzl, editor, *Collagen. Structure and Mechanics*, chapter 11, pages 285–324. Springer-Verlag, 2008.

[63] G.A. Holzapfel, T.C. Gasser, and R.W. Ogden. A new constitutive framework for arterial wall mechanics and a comparative study of material models. *J. Elasticity*, 61:1–48, 2000. Soft tissue mechanics.

[64] G.A. Holzapfel, T.C. Gasser, and R.W. Ogden. Comparison of a multi-layer structural model for arterial walls with a fung-type model, and issues of material stability. *J. Biomech. Eng.*, 126:264–275, 2004.

[65] G.A. Holzapfel and R.W. Ogden. Constitutive modelling of passive myocardium: a structurally based framework for material characterization. *Philos. Trans. R. Soc. Lond. Ser. A Math. Phys. Eng. Sci.*, 367(1902):3445–3475, 2009.

[66] G.A. Holzapfel and R.W. Ogden. Constitutive modelling of arteries. *Proc. R. Soc. Lond. Ser. A Math. Phys. Eng. Sci.*, 466(2118):1551–1596, 2010.

[67] G.A. Holzapfel and R.W. Ogden. Modelling the layer-specific 3d residual stresses in arteries, with an application to the human aorta. *Journal of the Royal Society Interface*, 7:787–799, 2010.

[68] G.A. Holzapfel, G. Sommer, M. Auer, P. Regitnig, and R.W. Ogden. Layer-specific 3d residual deformations of human aortas with non-atherosclerotic intimal thickening. *Annals of Biomedical Engineering*, 35:530–545, 2007.

[69] G.A. Holzapfel and H.W. Weizsäcker. Biomechanical behavior of the arterial wall and its numerical characterization. *Comp. Biol. Med.*, 28:377–392, 1998.

[70] G.C. Hsiao and W.L. Wendland. *Boundary integral equations*, volume 164 of *Applied Mathematical Sciences*. Springer-Verlag, Berlin, 2008.

[71] T.J.R. Hughes. *The Finite Element Method: Linear Static and Dynamic Finite Element Analysis*. Dover, New York, 2000.

[72] J.D. Humphrey. Mechanics of the arterial wall: review and directions. *Critical Reviews in Biomed. Engr.*, 23:1–162, 1995.

[73] J.D. Humphrey. An evaluation of pseudoelastic descriptors used in arterial mechanics. *J. Biomech. Engr.*, 121:259–262, 1999.

[74] J.D. Humphrey. *Cardiovascular Solid Mechanics. Cells, Tissues, and Organs.* Springer-Verlag, New York, 2002.

[75] J.D. Humphrey and F.C.P. Yin. On constitutive relations and finite deformations of passive cardiac tissue. part i. a pseudo-strain energy function. *J. Biomech. Eng.*, 109:298–304, 1987.

[76] A. D. Ioffe and V. M. Tihomirov. *Theory of extremal problems*, volume 6 of *Studies in Mathematics and its Applications*. North-Holland Publishing Co., Amsterdam, 1979. Translated from the Russian by Karol Makowski.

[77] M. Jung and U. Langer. *Methode der finiten Elemente für Ingenieure*. Teubner, Stuttgart, Leipzig, Wiesbaden, 2001.

[78] L. Kantorovich. On newton's method for functional equations. *Dokl. Akad. Nauk SSSR*, 59:1237–1249, 1948.

[79] G. Karypis and V. Kumar. A fast and high quality multilevel scheme for partitioning irregular graphs. *SIAM J. Sci. Comput.*, 20(1):359–392 (electronic), 1998.

[80] G. Karypis and V. Kumar. *METIS: A Software Package for Partitioning Unstructured Graphs, Partitioning Meshes, and Computing Fill-Reducing Orderings of Sparse Matrices; Version 4.0*. University of Minnesota, Department of Computer Science / Army HPC Research Center, Minneapolis, MN 55455, September 1998.

[81] N. Kechkar and D. Silvester. Analysis of locally stabilized mixed finite element methods for the Stokes problem. *Math. Comp.*, 58(197):1–10, 1992.

[82] A. Klawonn and L.F Pavarino. Overlapping Schwarz methods for mixed linear elasticity and Stokes problems. *Comput. Methods Appl. Mech. Engrg.*, 165(1-4):233–245, 1998.

[83] A. Klawonn and O. Rheinbach. A parallel implementation of dual-primal FETI methods for three-dimensional linear elasticity using a transformation of basis. *SIAM J. Sci. Comput.*, 28(5):1886–1906 (electronic), 2006.

[84] A. Klawonn and O. Rheinbach. Highly scalable parallel domain decomposition methods with an application to biomechanics. *ZAMM Z. Angew. Math. Mech.*, 90(1):5–32, 2010.

[85] A. Klawonn and O. B. Widlund. FETI and Neumann-Neumann iterative substructuring methods: connections and new results. *Comm. Pure Appl. Math.*, 54(1):57–90, 2001.

[86] A. Klawonn and O.B. Widlund. A domain decomposition method with Lagrange multipliers and inexact solvers for linear elasticity. *SIAM J. Sci. Comput.*, 22(4):1199–1219, 2000.

[87] A. Klawonn and O.B. Widlund. Dual and dual-primal FETI methods for elliptic problems with discontinuous coefficients in three dimensions. In *Domain decomposition methods in sciences and engineering (Chiba, 1999)*, pages 29–39 (electronic). DDM.org, Augsburg, 2001.

[88] A. Klawonn and O.B. Widlund. Selecting constraints in dual-primal FETI methods for elasticity in three dimensions. In *Domain decomposition methods in science and engineering*, volume 40 of *Lect. Notes Comput. Sci. Eng.*, pages 67–81. Springer, Berlin, 2005.

[89] A. Korn. Über einige Ungleichungen, welche in der Theorie der elastischen und elektrischen Schwingungen eine Rolle spielen. *Bull. Intern. Cracovie Akad. Umiejet, Classe des Sciences Math, et Naturelles*, pages 705–724, 1909.

[90] O.A. Ladyzhenskaya. *The mathematical theory of viscous incompressible flow.* Second English edition, revised and enlarged. Translated from the Russian by Richard A. Silverman and John Chu. Mathematics and its Applications, Vol. 2. Gordon and Breach Science Publishers, New York, 1969.

[91] U. Langer and O. Steinbach. Boundary element tearing and interconnecting methods. *Computing*, 71(3):205–228, 2003.

[92] U. Langer and O. Steinbach. Coupled finite and boundary element domain decomposition methods. In *Boundary element analysis*, volume 29 of *Lect. Notes Appl. Comput. Mech.*, pages 61–95. Springer, Berlin, 2007.

[93] I.J. LeGrice, P.J. Hunter, and B.H. Smaill. Laminar structure of the heart: a mathematical model. *Am. J. Physiol. Heart Circ. Physiol.*, 272:H2466–H2476, 1997.

[94] I.J. LeGrice, B.H. Smaill, L.Z. Chai, S.G. Edgar, J.B. Gavin, and P.J. Hunter. Laminar structure of the heart: ventricular myocyte arrangement and connective

tissue architecture in the dog. *Am. J. Physiol. Heart Circ. Physiol.*, 269:H571–H582, 1995.

[95] Y. Maday, C. Mavriplis, and A.T. Patera. Nonconforming mortar element methods: application to spectral discretizations. In *Domain decomposition methods (Los Angeles, CA, 1988)*, pages 392–418. SIAM, Philadelphia, PA, 1989.

[96] J. Mandel and R. Tezaur. Convergence of a substructuring method with Lagrange multipliers. *Numer. Math.*, 73(4):473–487, 1996.

[97] J.E. Marsden and Hughes T.J.R. *Mathematical Foundations of Elasticity*. Dover, New York, 1994.

[98] W. McLean. *Strongly elliptic systems and boundary integral equations*. Cambridge University Press, Cambridge, 2000.

[99] S. Mendis, P. Puska, and B. Norrving, editors. *Global Atlas on cardiovascular disease prevention and control*. World Health Organization, 2011.

[100] N.G. Meyers. Quasi-convexity and lower semi-continuity of multiple variational integrals of any order. *Trans. Amer. Math. Soc.*, 119:125–149, 1965.

[101] C. Miehe. Aspects of the formulation and finite element implementation of large strain isotropic elasticity. *Internat. J. Numer. Methods Engrg.*, 37(12):1981–2004, 1994.

[102] C. Miehe and E. Stein. A canonical model of multiplicative elasto-plasticity. formulation and aspects of the numerical implementation. *European Journal of Mechanics A/Solids*, 11:25–43, 1992.

[103] M. Mooney. A theory of large elastic deformation. *Journal of Applied Physics*, 11:582–592, 1940.

[104] C.B. Morrey, Jr. Quasi-convexity and the lower semicontinuity of multiple integrals. *Pacific J. Math.*, 2:25–53, 1952.

[105] C.B. Morrey, Jr. *Multiple integrals in the calculus of variations*. Die Grundlehren der mathematischen Wissenschaften, Band 130. Springer-Verlag New York, Inc., New York, 1966.

[106] J.C. Nagtegaal, D.M. Parks, and J.R. Rice. On numerically accurate finite element solutions in the fully plastic range. *Comput. Methods Appl. Mech. Engrg.*, 4(2):153–177, 1974.

[107] J. Nečas and I. Hlaváček. *Mathematical theory of elastic and elasto-plastic bodies: an introduction*, volume 3 of *Studies in Applied Mechanics*. Elsevier Scientific Publishing Co., Amsterdam, 1980.

[108] J.A. Nitsche. On Korn's second inequality. *RAIRO Anal. Numér.*, 15(3):237–248, 1981.

[109] G. Of. *BETI-Gebietszerlegungsmethoden mit schnellen Randelementverfahren und Anwendungen*. PhD thesis, Universität Stuttgart, 2006.

[110] G. Of. The all-floating BETI method: numerical results. In *Domain decomposition methods in science and engineering XVII*, volume 60 of *Lect. Notes Comput. Sci. Eng.*, pages 295–302. Springer, Berlin, 2008.

[111] G. Of and O. Steinbach. The all-floating boundary element tearing and interconnecting method. *J. Numer. Math.*, 17(4):277–298, 2009.

[112] R.W. Ogden. *Non-linear Elastic Deformations*. Dover, New York, 1997.

[113] C. Pechstein. *Finite and Boundary Element Tearing and Interconnecting Methods for Multiscale Elliptic Partial Differential Equations*. PhD thesis, Universität Linz, 2008.

[114] C. Pechstein and R. Scheichl. Analysis of FETI methods for multiscale PDEs. *Numer. Math.*, 111(2):293–333, 2008.

[115] K. B. Petersen and M. S. Pedersen. The matrix cookbook, oct 2008. Version 20081110.

[116] W.H. Press, S.A. Teukolsky, W.T. Vetterling, and B.P. Flannery. *Numerical recipes*. Cambridge University Press, Cambridge, third edition, 2007. The art of scientific computing.

[117] A. Quarteroni and A. Valli. *Domain decomposition methods for partial differential equations*. Numerical Mathematics and Scientific Computation. The Clarendon Press Oxford University Press, New York, 1999. Oxford Science Publications.

[118] O. Rheinbach. Parallel iterative substructuring in structural mechanics. *Arch. Comput. Methods Eng.*, 16(4):425–463, 2009.

[119] W. Ritz. Über eine neue methode zu lösung gewisser variationsprobleme der mathematischen physik. *J. reine angew. Math.*, 135:1–61, 1908.

[120] R.S. Rivlin. Large elastic deformations of isotropic materials. I. Fundamental concepts. *Philos. Trans. Roy. Soc. London. Ser. A.*, 240:459–490, 1948.

[121] R.S. Rivlin. Large elastic deformations of isotropic materials. IV. Further developments of the general theory. *Philos. Trans. Roy. Soc. London. Ser. A.*, 241:379–397, 1948.

[122] R.S. Rivlin. Large elastic deformations of isotropic materials. V. The problem of flexure. *Proc. Roy. Soc. London. Ser. A.*, 195:463–473, 1949.

[123] R.S. Rivlin. Large elastic deformations of isotropic materials. VI. Further results in the theory of torsion, shear and flexure. *Philos. Trans. Roy. Soc. London. Ser. A.*, 242:173–195, 1949.

[124] D.J. Rixen and C. Farhat. A simple and efficient extension of a class of substructure based preconditioners to heterogeneous structural mechanics problems. *Internat. J. Numer. Methods Engrg.*, 44(4):489–516, 1999.

[125] M.R. Roach and A.C. Burton. The reason for the shape of the distensibility curve of arteries. *Canad. J. Biochem. Physiol.*, 35:681–690, 1957.

[126] T.R. Rockafellar. *Convex Analysis*. Princeton Univ. Press, Princeton, NJ, 1972.

[127] J. Rodin. The architecture of the vessel wall. In D.F. Bohr, A.D. Somlyo, and H.V. Sparks, editors, *Handbook of Physiology*, volume 2, pages 1–31. American Physiological Society, Bethesda, 1980.

[128] Y. Saad and M.H. Schultz. GMRES: a generalized minimal residual algorithm for solving nonsymmetric linear systems. *SIAM J. Sci. Statist. Comput.*, 7(3):856–869, 1986.

[129] G.B. Sands, D.A. Gerneke, D.A. Hooks, C.R. Green, B.H. Smaill, and I.J. LeGrice. Automated imaging of extended tissue volumes using confocal microscopy. *Microsc. Res. Tech.*, 67:227–239, 2005.

[130] K. Schellbach. Probleme der variationsrechnung. *J. reine angew. Math.*, 41:293–363, 1851.

[131] O. Schenk and K. Gärtner. Solving unsymmetric sparse systems of linear equations with PARDISO. *Journal of Future Generation Computer Systems*, 20(3):475–487, 2004.

[132] O. Schenk and K. Gärtner. On fast factorization pivoting methods for sparse symmetric indefinite systems. *Elec. Trans. Numer. Anal*, 23:158–179, 2006.

[133] H. Schmid, M.P. Nash, A.A. Young, and P.J. Hunter. Myocardial material parameter estimation—a comparative study for simple shear. *J. Biomech. Eng.*, 128:742–750, 2006.

[134] H. Schmid, P. O'Callaghan, M.P. Nash, W. Lin, I.J. LeGrice, B.H. Smaill, A.A. Young, and P.J. Hunter. Myocardial material parameter estimation: a non-homogeneous finite element study from simple shear tests. *Biomech. Model. Mechanobiol.*, 7:161–173, 2008.

[135] C.A.J. Schulze-Bauer, P. Regitnig, and G.A. Holzapfel. Mechanics of the human femoral adventitia including high-pressure response. *Am. J. Physiol. Heart Circ. Physiol.*, 282, 2002.

[136] H.A. Schwarz. II. Über einen Grenzübergang durch alternierendes Verfahren. *Vierteljahrsschrift der Naturforschenden Gesellschaft in Zürich*, 1870.

[137] K. Schweizerhof and E. Ramm. Displacement dependent pressure loads in non-linear finite element analyses. *Computers & Structures*, 18:1099–1114, 1984.

[138] A.A. Shabana. *Computational continuum mechanics*. Cambridge University Press, Cambridge, 2008.

[139] J.C. Simo. Numerical analysis and simulation of plasticity. In *Handbook of numerical analysis, Vol. VI*, Handb. Numer. Anal., VI, pages 183–499. North-Holland, Amsterdam, 1998.

[140] J.C. Simo, R.L. Taylor, and K.S. Pister. Variational and projection methods for the volume constraint in finite deformation elasto-plasticity. *Comput. Methods Appl. Mech. Engrg.*, 51(1-3):177–208, 1985. FENOMECH '84, Part I, II (Stuttgart, 1984).

[141] J. Šístek, Sousedik B., Burda P., Mandel J., and Novotny J. Application of the parallel bDDC preconditioner to the stokes flow. *Comput. Fluids*, 46(6):429–435, 2011.

[142] B.F. Smith, P.E. Bjørstad, and W.D. Gropp. *Domain decomposition*. Cambridge University Press, Cambridge, 1996. Parallel multilevel methods for elliptic partial differential equations.

[143] A.J.M. Spencer. Theory of invariants. In A.C. Eringen, editor, *Continuum Physics*, volume I. Academic Press, 1971.

[144] A.J.M. Spencer. Constitutive theory for strongly anisotropic solids. In A.J.M.

Spencer, editor, *Continuum Theory of the Mechanics of Fibre-Reinforced Composites*, volume 282, pages 1–32. Springer, 1984.

[145] G. Starke. Field-of-values analysis of preconditioned iterative methods for nonsymmetric elliptic problems. *Numer. Math.*, 78(1):103–117, 1997.

[146] O. Steinbach. *Stability estimates for hybrid coupled domain decomposition methods*, volume 1809 of *Lecture Notes in Mathematics*. Springer-Verlag, Berlin, 2003.

[147] O. Steinbach. *Numerical approximation methods for elliptic boundary value problems*. Springer, New York, 2008. Finite and boundary elements, Translated from the 2003 German original.

[148] A. Toselli and O. Widlund. *Domain decomposition methods—algorithms and theory*, volume 34 of *Springer Series in Computational Mathematics*. Springer-Verlag, Berlin, 2005.

[149] F. Tröltzsch. *Optimal control of partial differential equations*, volume 112 of *Graduate Studies in Mathematics*. American Mathematical Society, Providence, RI, 2010. Theory, methods and applications, Translated from the 2005 German original by Jürgen Sprekels.

[150] C. Truesdell. Some challenges offered to analysis by rational thermomechanics. In *Contemporary developments in continuum mechanics and partial differential equations (Proc. Internat. Sympos., Inst. Mat., Univ. Fed. Rio de Janeiro, Rio de Jane)*, volume 30 of *North-Holland Math. Stud.*, pages 495–603. North-Holland, Amsterdam, 1978.

[151] C. Truesdell and W. Noll. *The nonlinear field theories of mechanics*. Springer-Verlag, Berlin, second edition, 1992.

[152] R. Verfürth. Error estimates for a mixed finite element approximation of the Stokes equations. *RAIRO Anal. Numér.*, 18(2):175–182, 1984.

[153] J. Vossoughi, R.N. Vaishnav, and D.J. Patel. Compressibility of the myocardial tissue. In Van C. Mow, editor, *Advances in bioengineering*, pages 45–48. American Society of Mechanical Engineers, New York, 1980.

[154] J.P. Whiteley, M.J. Bishop, and D.J. Gavaghan. Soft tissue modelling of cardiac fibres for use in coupled mechano-electric simulations. *Bulletin of Mathematical Biology*, 69:2199–2225, 2007.

[155] B.I. Wohlmuth. A mortar finite element method using dual spaces for the Lagrange multiplier. *SIAM J. Numer. Anal.*, 38(3):989–1012, 2000.

[156] F.C.P. Yin. Ventricular wall stress. *Circ. Res.*, 49:829–842, 1981.

[157] K. Yosida. *Functional analysis*, volume 123 of *Grundlehren der Mathematischen Wissenschaften [Fundamental Principles of Mathematical Sciences]*. Springer-Verlag, Berlin, sixth edition, 1980.

[158] A.A. Young, I.J. LeGrice, M.A. Young, and B.H. Smaill. Extended confocal microscopy of myocardial laminae and collagen network. *J Microsc.*, 192:139–150, 1998.

[159] O.C. Zienkiewicz. *The finite element method in engineering science*. McGraw-Hill, London, 1971. The second, expanded and revised, edition of ıt The finite element method in structural and continuum mechanics.